A geophysical study of volcanic processes at a persistently active volcano and at two calderas in a state of unrest

A thesis presented for the degree of
Doctor of Philosophy

By

Elske de Zeeuw-van Dalfsen
M.Sc. Vrije Universiteit, Amsterdam, NL

Department of Earth Sciences
The Open University

November 2004

Abstract

With the ever increasing world population, more and more people live in the vicinity of a potentially active volcano. At any given time, around 20 of those are erupting. In the past decades advances have been made in forecasting volcanic eruptions. This work shows that by combining established monitoring techniques, more can be learnt about the ongoing volcanic processes at active volcanoes.

Volcanic processes vary from very fast persistent activity to extremely slow caldera unrest. Here, volcanoes at both ends of the spectrum were studied using micro-gravity techniques in combination with at least one other technique. Askja and Krafla caldera in Iceland represented the slow processes while Stromboli in Italy symbolized the processes in the faster part of the range.

At the rapidly deflating Askja caldera in Iceland, conventional micro-gravity techniques show a net micro-gravity decrease in the centre during 1988-2003. This net micro-gravity decrease is most likely caused by a combination of cooling and contraction of the shallow magma reservoir and magma drainage. Mogi point-source models are used to calculate an ongoing magma drainage rate of 0.125 m^3/s from 1988 to 2003. Tectonic forces are inferred to generate space in the ductile part of the crust allowing magma to drain to deeper levels.

InSAR data of Krafla caldera in Iceland (1993-1999) reveal, apart from the previously described rift zone and small concentric deflating features, a broad inflating signature 15 km north of Krafa mountain. This signal is, after extensive modelling, interpreted as magma accumulation at 21 km depth, close to the crust-mantle boundary. It is a revelation that the effect of such a deep source can be observed at the surface using modern monitoring techniques. When magma in this reservoir reaches a critical

pressure it will migrate to the shallow magma chamber from where it eventually may erupt. This agrees with the long periods of dormancy between rifting episodes.

Geodetic data from Krafla confirm that the area is still deflating. Interpretation of micro-gravity surveys is hampered by a geothermal power plant within the caldera whose operation effects the water mass balance. For the first time, micro-gravity data have been corrected for these effects and results show a net micro-gravity decrease from 1990 to 2003. This mass decrease is interpreted as a result of magma draining at a rate of 0.23 m^3/s.

Observations at Askja and Krafla volcano suggest they each have a draining shallow magma chamber connected to a deeper magma reservoir. Analysis of InSAR data suggest the deeper Krafla reservoir is inflating. It is possible a pressure-link between these volcanoes exists along the ductile crust in Iceland.

Continuous micro-gravity may be used as a tool to understand conduit processes at persistently active volcanoes, such as Stromboli in Italy. My data show Low Frequency Oscillations possibly related to column height changes and High Frequency Oscillations related to volcanic vibrations caused by degassing events. However, more extensive data are needed to correct for instrumental drift.

Micro-gravity has proved to be a valuable tool in monitoring active volcanoes at either the slow or the fast ends of the spectrum. Micro-gravity data become even more powerful when combined with other techniques, which is feasible with the use of modern equipment.

Acknowledgements

I would first like to thank my supervisors, Hazel Rymer, Dave Rothery, Glyn Williams-Jones and Freysteinn Sigmundsson, for their help and support during the past three years. It wasn't always easy to put up with four supervisors, but after I learnt to 'manage' them well, things became a lot easier and I think it worked out fine. Thanks also to my examiners, Steve Blake and Giovanna Berrino, for their helpful comments and suggestions.

This project would not have been possible without the support of several sources of funding: the Department of Earth Sciences of the Open University, The Geological Society, The MinSoc, VMSG, The Peter Francis Travel Bursery, GDR-strainsar and ridge 2000. They enabled me to finance fieldwork and attend workshops and conferences.

The project also relied on collaboration with a large group of people. In Italy, I am grateful to Maurizio Ripepe and Emanuelle Marchetti especially for their help with instrument setup and logistics, Pasquale Pogi for programming, and 'Zaza' for helping to build the instrument box at the summit. In Iceland, fieldwork would have been impossible without Erik Sturkell and Haldor Olafsson. I thank Rikke Pedersen for her patience while I was trying to get to grips with the DIAPASON software and Carolina Pagli for her suggestions concerning InSAR. I would also like to thank the whole NVI staff who took me in during my visits there, it was greatly appreciated.

The InSAR work would have been extremely difficult without the head-start I was given by Jean-Luc Froger, the on-line help from Nadine Pourtier and the suggestions from Kurt Feigl.

At the OU, I am greatful to my office mates Anne Jay and Kirti Sharma for putting up with me (and the baby!!) and always being there. Thanks also to the lunch crew (Andrew Ball, who doubled as field assistant, Martin Towner and Axel Hagermann), Eliza Calder (Stromboli fieldwork) and Caco Cortez, Dave Wallis (python), Jo Gottsmann (Stromboli fieldwork), Dick Carlton (computer stuff), Andy Lloyd and John Taylor (Figure preparation), Nico Fournier (Stromboli Fieldwork), Ashea Tambe and all the other people of the VDG.

I am indebted to Jim Kauaikaua and Toti Corpuz for rousing my interest in volcanology and for giving me the opportunity to work with them. They have inspired me more than they can imagine.

I would like to express my gratitude to Ton de zeeuw for his interest, support, and help in the field and also for moving to the UK. I was also delighted that Tim de Zeeuw let me finish on time! But most of all I thank my parents, Joop and Irène van Dalfsen, who stimulated me to improve my English at a time when I needed it most. This is for them.

Table of contents

List of Figures

List of Tables

Chapter 1: Introduction

1.1 Introduction to this work

Volcanic processes have been studied for centuries. The oldest (surviving) eyewitness account of a volcanic eruption was written by Pliny the Younger who observed the devastating eruption of Vesuvius, in A.D. 79 (Pliny, 80). The improvement of technical equipment (e.g. computers, radio-transmission) as well as the development of new monitoring techniques (InSAR, GPS, seismic tomography) has increased our understanding of these processes, but crucial aspects still remain unclear. A volcanic eruption or even just volcanic unrest can have significant effect on local population, culminating in damage to the environment and/or property and casualties in the worst cases. Increasing the understanding of the processes involved will help us to improve our perception of the volcanic system as a whole and is important for eruption forecasting and hazard mitigation. Furthermore, research in this field may give us valuable insights into how the planet we live on actually works.

The purpose of this particular work is to investigate volcanic processes using geophysical techniques. The study can be divided into clearly defined sub-projects but all incorporate the same theme: volcanic processes. The rates of volcanic processes vary tremendously. Persistently active volcanoes, such as Stromboli in Italy and Villarrica in Chile, are examples of volcanoes exhibiting fast rates of volcanic processes. Caldera unrest, like at the Campi Flegrei in Italy or at Askja in Iceland, exemplifies volcanic processes in the slower part of the spectrum. Here, I have studied volcanoes on both sides of the range by applying micro-gravity techniques in combination with appropriate and available data of other sorts.

1.2 Geophysical techniques

1.2.1 Micro-gravity

In recent decades, micro-gravity has become increasingly recognised as a valuable tool for studying volcanoes (Gottsmann and Rymer, 2002; Williams-Jones and Rymer, 2002). Gravity variations are measured in Gals where 1 Gal equals 1 cms^{-2}. Modern instruments can measure up to 10^{-9} Gal but generally variations are on the order of 100 times this value. Therefore micro-gravity measurements are expressed in micro-Gal (μGal), hence the term micro-gravity (Rymer, 1996).

Micro-gravity techniques can be used, in combination with geodetic measurements, to constrain and quantify sub-surface mass and or density changes through time at volcanoes (Rymer et al., 1998a; Rymer and Tryggvason, 1993; Williams-Jones et al., 2003). Resulting models are, however, non-unique, as precise geometry and absolute values for the mass and or density change can not be fully constrained. Micro-gravity theory and field-practice have been widely documented and described e.g. (Rymer, 1996) and are therefore only summarized in this thesis (see APPENDIX B).

There are three types of gravity surveys: i) the static Bouguer survey, ii) the dynamic survey and iii) the continuous survey. The first two techniques are well established (Brown et al., 1991; Rymer et al., 1998a; Rymer and Tryggvason, 1993; Williams-Jones et al., 2003) while the third type of survey is still developing (Andò and Carbone, 2001; Berrino et al., 2000; Carbone et al., 2003; Jousset et al., 2000). The first two techniques are surveys whereby the micro-gravity instrument is moved from point to point whereas the third type of survey uses measurements taken at a single location.

A static Bouguer survey is used to investigate sub-surface density structures and determine the gross sub-surface volcanic structure of the volcano. In volcanic regions,

these density anomalies typically have a wavelength of several kilometres and gravity varies by tens to hundreds of milliGals (Locke et al., 2003). For example, the Bouguer map for Askja in Iceland (Brown et al., 1991) covers an area of ~300 km^2 and is characterised by a 2 mGal positive anomaly within a broader 8 mGal negative anomaly.

During a conventional dynamic survey, changes in the value of gravity relative to a reference point are measured over time. These changes are much smaller than those measured during a static survey, typically on the order of tens to hundreds of μGal per year (Locke et al., 2003). This technique is used to quantify sub-surface mass or density changes through time (Rymer et al., 1998a) which are of great interest, especially during periods of inflation and deflation. Data can be used to recognize inflow of magma into the volcanic system before the onset of an eruption and can therefore enhance hazard mitigation.

Continuous micro-gravity surveys have been attempted at Vesuvius (Berrino et al., 2000) and Etna (Carbone et al., 2003) in Italy. The technique still suffers from temperature and pressure correction problems and is far from established, but can possibly be used to identify magma movement in shallow open conduit systems.

For the purpose of this study, dynamic surveys were conducted at Askja (Chapter 2) and Krafla volcano (Chapter 4) in Iceland in 2002 and 2003 and a continuous gravity survey (Chapter 5) was set-up at Stromboli in Italy in 2003.

1.2.2 InSAR

InSAR stands for Interferometric Synthetic Aperture Radar. It is a remote sensing technique that uses radar satellite images acquired by satellites such as ERS1, ERS2 and Radarsat. The technique can be used to monitor ground deformation (Massonnet and Feigl, 1998) and has been applied in this thesis (Chapter 3) to analyse

volcanic deformation at Krafla (de Zeeuw-van Dalfsen et al., 2004a). The technique is described in more detail in APPENDIX D.

1.3 Geological settings

1.3.1 Iceland

The combination of a divergent plate boundary and a 'hot-spot' makes Iceland a special place to study active volcanism (Gudmundsson, 2000). Iceland is located between the Kolbeinsey Mid Oceanic Ridge (MOR) in the north and the Reykjanes MOR in the south (Figure 1-1). The surface expression of the MOR in Iceland is the zone of active volcanism, the neovolcanic zone, with an average total spreading rate of 1.8 cm/year in the direction N105E. The zone has three main segments: the North Volcanic Zone (NVZ), the West Volcanic Zone (WVZ) and the East Volcanic Zone (EVZ). The volcanic zones are connected to the oceanic ridges by complex fracture zones. The Tjornes fracture zone in north Iceland is a transform fault zone connecting the plate boundary of the Kolbeinsey MOR with the NVZ. The Husavik-Flatey fault, a major dextral strike slip fault, forms the main part of the fracture zone. The south Iceland seismic zone (SISZ) is a zone of complex faulting located between the WVZ and the EVZ. At the Reykjanes peninsula the WVZ joins the Reykjanes MOR.

According to seismic surveys, the Icelandic crust may be as thick as 15-45 km (Allen et al., 2002) but is thinnest beneath the currently active Holocene volcanic systems. Scientists agree that a low velocity anomaly, observed with seismic techniques exists (Allen et al., 1999; Foulger et al., 2000; Shen et al., 2002; Zhao, 2001). Some (Allen et al., 2002; Shen et al., 2002; Zhao, 2001) call this anomaly a mantle plume (Morgan, 1971): a hot up-welling of relatively primordial material which rises from the deep mantle and feeds the surface 'hot-spots'. Such plumes rise because of thermal buoyancy and originate at a thermal boundary layer. The only such layer known to exist

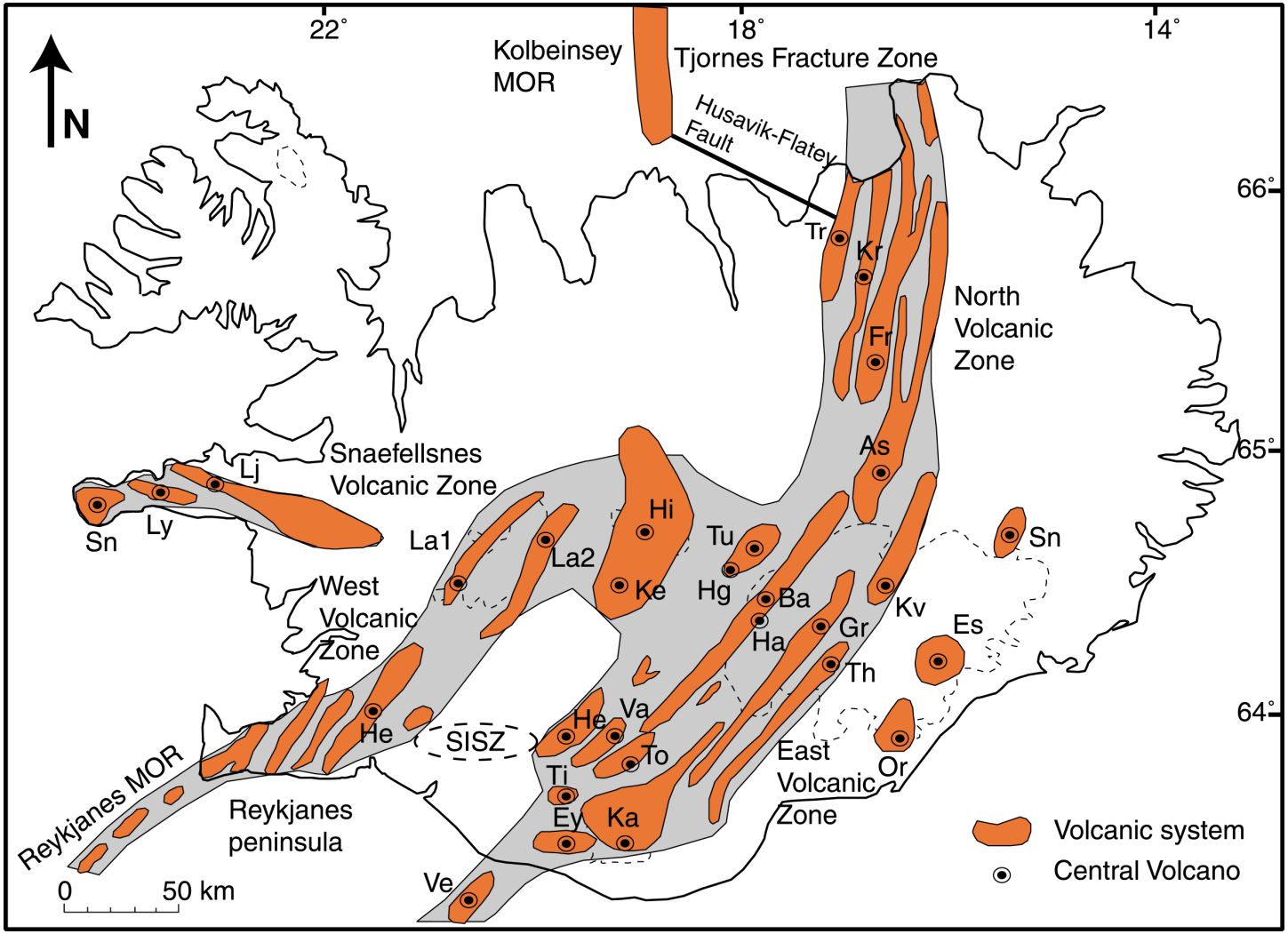

Figure 1-1 Overview of the volcanic systems of Iceland. The neovolcanic zone or zone of active volcanism, is depicted in light-grey. Locations of some of the main glaciers are shown with a dashed line. Key: As for Askja, Kr for Krafla, Tr for Theystareykir, Fr for Fremri-Namur, Kv for Kverkfjoll, Th for Thordarhyrna, Gr for Grimsvotn, Ha for Hamarinn, Ba for Bardarbunga, Tu for Tungnafellsjokull, Hg for Hagongur, Ka for Katla, Ey for Eyjafjallajokull, Ve for Vestmannaeyjar, Ti for Tindfjallajokull, Va for Vatnafjoll, He for Hekla, Hj for Hofsjokull, Ke for Kerlingarfjoll, La1&2 for Langjokull, He for Hengill, Sn for Sneafellsjokull, Ly for Lysuskard, Lj for Ljosufjoll, Or for Oraefajokull, Es for Esjufjoll and Sn for Snaefell. Adapted from Gudmundsson (2000).

in the deep mantle is the core-mantle boundary and thus plumes are assumed to rise from there. The existence of this plume is thought to have contributed significantly to Icelandic volcanism. Others (Anderson, 2000; Foulger et al., 2003; Foulger et al., 2000; Foulger et al., 1992; Keller et al., 2000) suggest a different source, such as the subducted Iapetus ocean, for the tremendous amount of basaltic magma which formed Iceland. These different views may stem from the fact that hot-spots may have different sources in the mantle (Courtillot et al., 2002) or from the fact that the plume model has become so flexible that it can not be tested properly (Foulger et al., 2000) nor can it be rejected. Foulger et al. (2000) reported that the Icelandic plume does not originate from the lower mantle while Courtillot et al. (2002) classifies the Icelandic hotspot as a potential primary plume with a lower mantle origin, based on the appearance of a 'hot-spot' track, an accompanying flood basalt, a large buoyancy flux, high ratios of $^{3}He/^{4}He$ and a low shear wave velocity in the underlying mantle. It seems that both groups agree on the existence of a low velocity upwelling beneath Iceland, but not on the origin of its source. It is not the purpose of this work to establish this, nor to decide who is right or wrong. Therefore in the following we refer to 'the low velocity zone' beneath Iceland instead of a mantle plume or 'hot-spot'.

The volcanic zones in Iceland are dynamic systems, which migrate through time. One of the primary driving forces for shifting and re-location of the volcanic zones is the overall westward movement of the plate boundary relative to the centre of the Icelandic low velocity zone. Volcano-tectonic activity takes place in around 30 volcanic systems, characterised by 5-20 km wide and 40-100 km long swarms of tension fractures, normal faults and volcanic fissures (Gudmundsson, 1995). Apart from basaltic crater rows and shield volcanoes, many have a central volcano, some of which have developed a caldera. The frequently erupting large central volcanoes are mostly fed by a shallow crustal magma chambers, and produce intermediate and acid rocks as a result.

The Icelandic low velocity zone provides magma that is erupted in the volcanic systems (Gudmundsson, 2000). The magma is divided between the systems by fluid-dynamic processes which are partly controlled by plate movements and associated stresses. The magma then accumulates in a reservoir (Figure 1-2) at the boundary between the upper mantle and the crust or in the lower crust (around 15-30 km for Icelandic volcanoes). The existence of such reservoirs was previously suggested following tilt data (Tryggvason, 1986) and is now evident from GPS for Askja (Sturkell et al., 2004 - submitted) and InSAR data for Krafla (de Zeeuw-van Dalfsen et al., 2004a). The reservoir will gradually become stratified. At the initial stage all intrusions and eruptions are fed directly from the magma reservoir. Later (see Figure 1-2) a shallow chamber may form (at a few km depth), which acts as a sink for magma injections from the deeper reservoir as well as a source for magma injection and eruptions in the central volcano. The shallow chamber depends on the reservoir as a source and becomes extinct when that source no longer exists. Plate movements in Iceland may transport a chamber, with a life time of 0.5-1 Ma, laterally by 10-20 km. If the source reservoir remains stationary, progressively fewer dikes will reach the chamber resulting in it gradually becoming extinct (Gudmundsson, 2000).

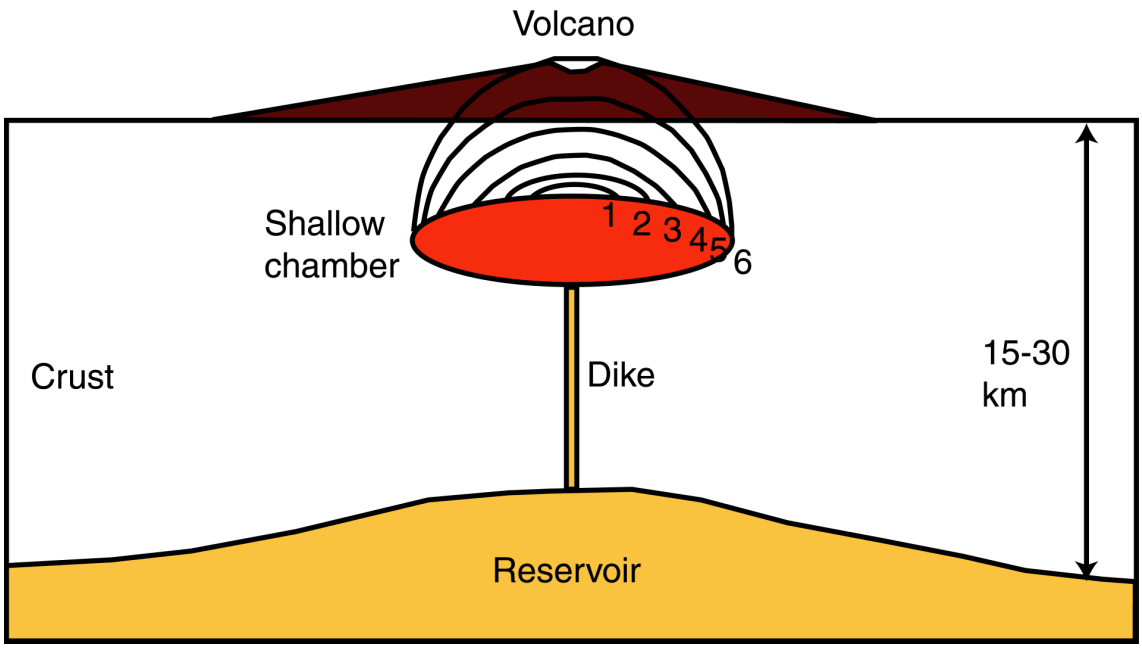

Figure 1-2 Schematic diagram (not drawn to scale) after Gudmundsson (2000) showing the formation of a central volcano in an Icelandic volcanic zone. Numbers refer to the different levels (1-5) at which sheet injections may be terminated.

1.3.1.1 Askja

Caldera unrest, often caused by processes in a several km deep magma chamber, is a volcanic process which takes decades or longer. Askja caldera has been in a state of unrest for the past decades and was therefore chosen as a suitable area for this study. It is located in the Dyngjufjöll central volcano (see Figure 2-1), situated in a 10-15 km wide fissure system, extending 100 km north from the northern margin of the Vatnajökull icecap (Sigvaldason, 2002). Volcanic activity is associated with two fissure swarms, with slightly different strikes (N05°E, N20°E). The volcanic centre hosts three calderas. The largest one, 8 km across and 200-300 m deep, is the circular Askja caldera. Along the northern ridge is an almost completely filled and less pronounced older caldera. The youngest caldera, with a diameter of 4.5 km, was formed in 1875 and hosts lake Öskjuvatn. Geothermal activity is found along the east and southern edge of the 1875 caldera, at the Víti crater (Figure 2-2), and at the 1922 and 1923 eruption sites (Sturkell and Sigmundsson, 2000).

A Plinian rhyolitic eruption, dated at about 10 ka, left a pumice deposit which now serves as a marker horizon (Sigvaldason, 2002). According to Sigvaldason (2002) the Plinian eruption was probably triggered by pressure release caused by glacier melting and volatile supersaturation. The vent location for the 10-ka Plinian eruption has been destroyed by later events but the suggested location, possibly supported by a gravity survey, lies in the central part of the Dyngjufjöll volcanic centre. The eruption formed a subsidence structure, presently seen as an embayment in the hyaloclastite mountain block (Thorvaldsfjall) in the southern part of the Askja caldera. A model is proposed involving uplift of tectonically well-defined crustal blocks to the north and west of the Askja caldera, combined with down-sagging caused by voluminous outpouring of basaltic lava. The southern and eastern borders of the caldera are

remnants of a subsidence following the 10-ka Plinian eruption, partly reactivated by the 1875 AD Plinian eruption.

A major rifting event took place in 1874-1875. It included series of dyke injections, basaltic fissure eruptions and the explosive rhyolite eruption that formed the youngest caldera. The main fissure eruption occurred in the northern part of the swarm (Sveinagjá graben). It has been suggested that magma drained laterally from a reservoir beneath Askja caldera and erupted in the Sveinagjá graben (Sigurdsson and Sparks, 1978), and this may have induced the caldera collapse. A reconstruction of the caldera formation is shown in Figure 1-3 (Jónsson, 1942). The next eruptive period took place 1921-29, during which a fissure eruption occurred south of the Dyngjufjöll mountains and several minor eruptions occurred at the 1875 rim. The most recent eruption began October 1961 and continued into early December. An E-W trending fissure opened close to the main caldera rim and lava flowed through the Öskjuop pass onto the plain east of the Dyngjufjöll mountains.

Excluding erupting volcanoes, Askja has displayed a significantly higher rate of ground deformation, i.e., deflation, since 1983, than anywhere else in Iceland (Tryggvason, 1989a). There are at least three possible explanations for this observed deflation: i) cooling/contraction of magma in a shallow (~3 km) magma chamber (Rymer and Tryggvason, 1993); ii) void compaction of the underlying material and iii) magma drainage from a shallow magma chamber. In this work, I investigate which of the above mentioned explanation is most likely.

1.3.1.2 Krafla

Krafla like Askja, is located in an actively spreading regime and has also been in a state of unrest for the past two decades. The Krafla fissure swarm (Figure 4-1) is 80 km long and 4-10 km wide and consists of more than 1000 tectonic fractures

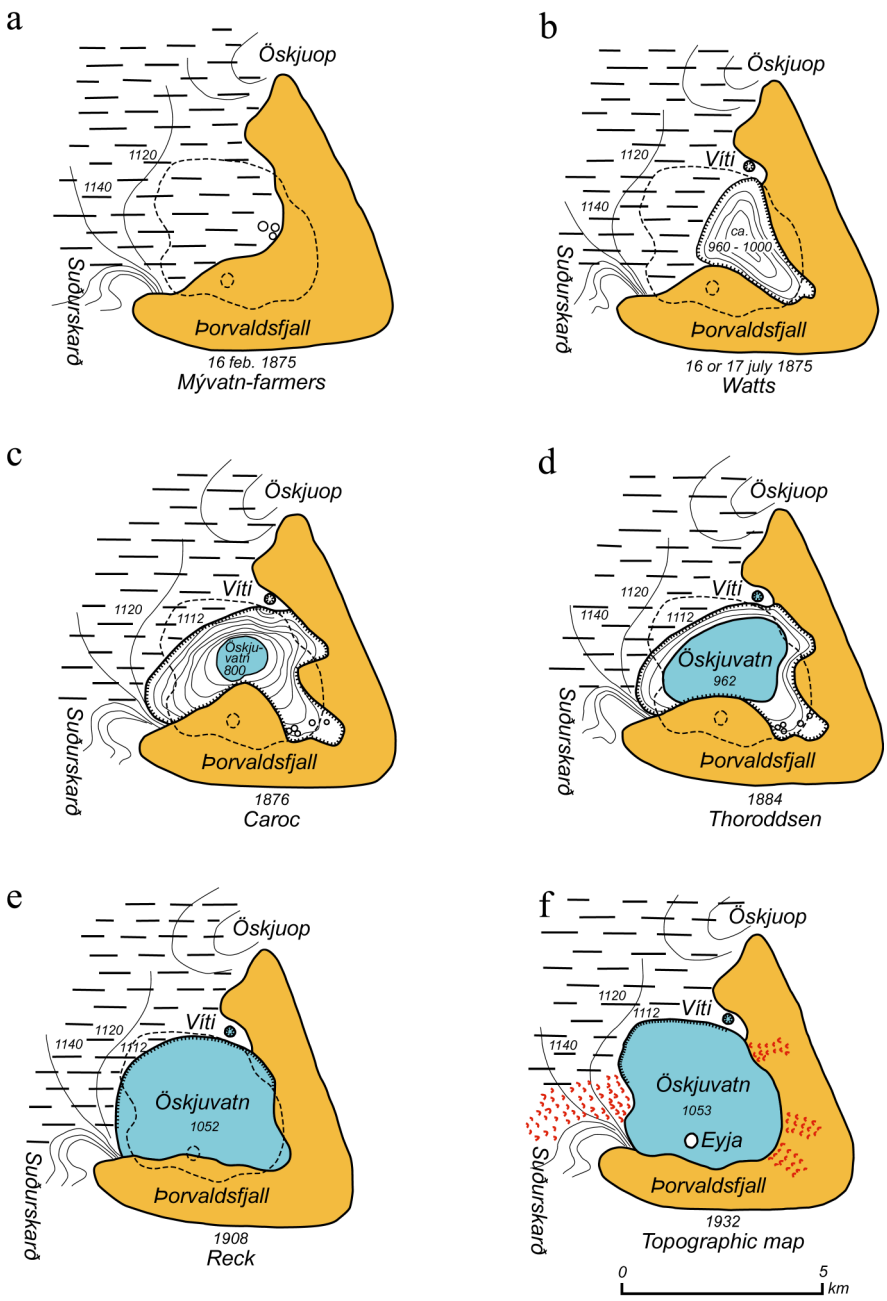

Figure 1-3 Reconstruction of the Öskjuvatn caldera formation following the Plinian eruption of 1875, compiled by Ólafur Jónsson (1942) after descriptions from: a) the farmers from the Mývatn area, 16 February 1875; b) Watts, 16 or 17 July 1875; c) Caroc, the summer of 1876; d) Thoroddsen, 1884; e) Reck, 1908 and f) the topographic map, 1932. The formation of the caldera was almost complete in 1908, when Hans Reck visited Askja.

(Opheim and Gudmundsson, 1989). The Krafla central volcano forms a low, broad shield ~ 25 km in diameter with a central caldera. The caldera has an elliptical shape and stretches 10 km in the east-west direction and 8 km north-south (Opheim and Gudmundsson, 1989). It formed during an explosive eruption in the last interglacial period about 0.1 Ma ago, and has since been almost completely filled by lavas. A high temperature geothermal field lies within the caldera and has been exploited for the past several years producing about 30MW of electrical power (Nielsen et al., 2000).

In post glacial times some 18 eruptions have occurred in the Krafla caldera. Activity is characterised by rifting episodes separated by long periods of dormancy. Two historical rifting episodes, the Mývatn and Krafla fires, occured from 1724 to 1729 and 1975 to 1984, respectively. During the Krafla fires (Árnadóttir et al., 1998; Rymer et al., 1998a; Tryggvason, 1986; Tryggvason, 1994), 9 out of 20 deflation and inflation cycles were accompanied by basaltic fissure eruptions in the Krafla fissure swarm. Cumulative widening in the repeated diking events reached up to 9 m, averaging at about 5 m (Tryggvason, 1986). The total area covered by lavas amounted to 36 km^3 (Rossi, 1997).

Detailed seismic studies have been conducted in the Krafla area by Brandsdóttir et al. (1997) and Menke et al. (1998). Strong seismic reflection occurs at the Moho discontinuity. The crust-mantle boundary beneath Krafla has an asymmetric dome shape as established by E-W (Brandsdóttir et al., 1997) and N-S (Menke et al., 1998) seismic profiles. The minimum boundary depth of ~18.5 km is reached 5 km east of the centre of the caldera. This depth increases assymetrically in all directions and reaches ~26 km at a distance of ~60 km to the east and west and ~23 km at a distance of ~40 km to the north and south.

Krafla has been deflating since at least 1989 but at a much smaller rate than Askja. Is it feasible to distinguish between the possible sources of this deflation? How

much influence does the water extraction by the geothermal power plant have? These questions can possibly be answered by combining new and existing micro-gravity data with InSAR and other geodetic data.

1.3.2 Italy

Italy is often called "the cradle of volcanology". A title it deserves as the Italian volcanoes were among the first to be observed (Pliny, 80) and are still the subject of extensive research and monitoring. Italy (Figure 1-4) is the location of some of the world famous volcanoes: Etna, Vesuvius, Vulcano and Stromboli. Etna has the highest number of historically documented eruptions while Vesuvius is regarded as one of the most dangerous volcanoes in the world. The term ‘plinian eruption’, used to describe explosive activity, was derived from the first description of Plinian activity of Vesuvius by Pliny the Younger. The term ‘volcano’ is derived from the volcano ‘Vulcano’ which was named after the Roman god of fire ‘Vulcan’. Stromboli is one of the few volcanoes in the world that erupts many times a day and the activity it displays is now a generic name: Strombolian activity.

About half of the ~23 known sub-aerial volcanoes in Italy have been active in historic times (Figure 1-4). Their existence is principally linked to 5 different tectonic environments: subduction, back-arc rifting, continental rifting, sea-floor spreading, and a fifth one that is very poorly understood but may involve a ‘hot-spot’. Generally, Italy's volcanism is a result of the collision of two lithospheric plates (Bonaccorso, 2002) - the African plate to the south, and the European (or Eurasian) plate to the north. This collision is confused by the complex physical characteristics of the colliding plate margins - rather than being homogeneous over a wide area, these are extremely heterogeneous.

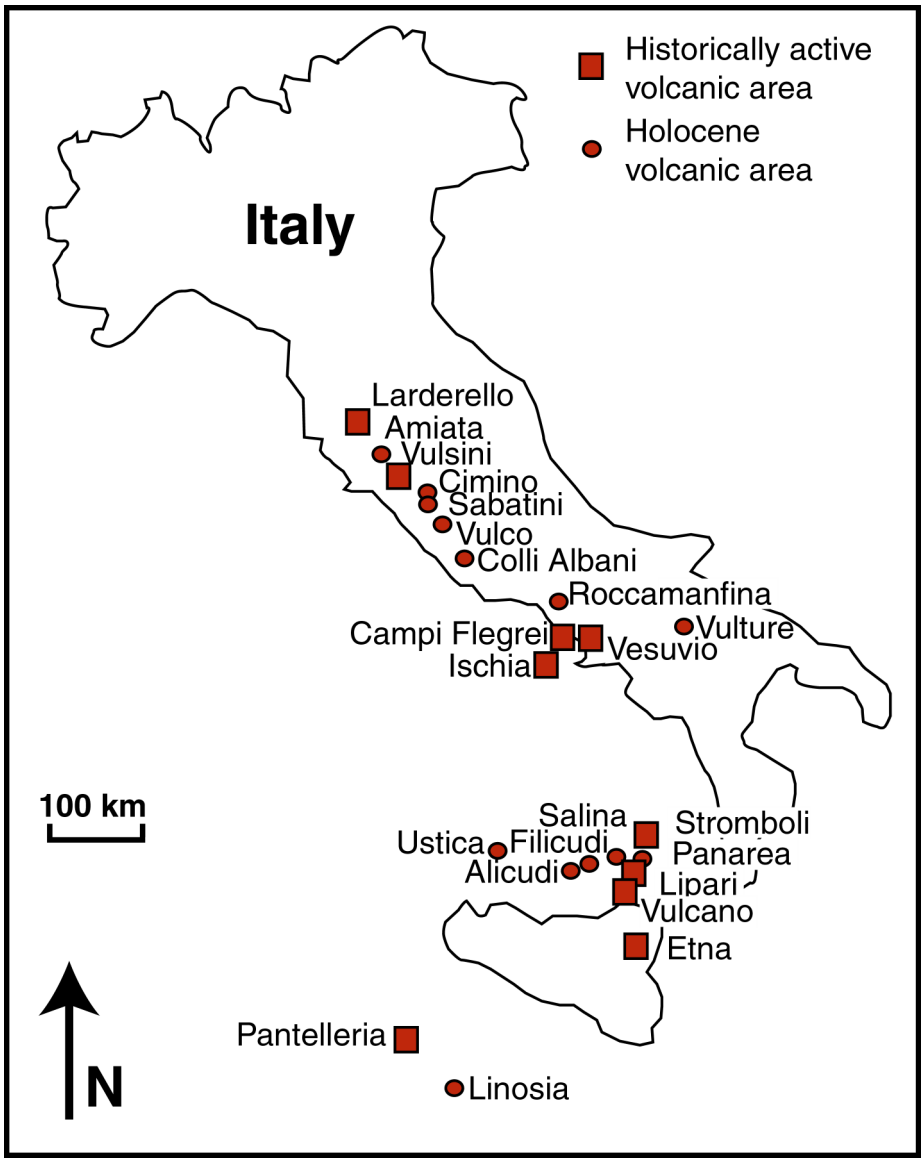

Figure 1-4 Overview of volcanoes in Italy which were historically active (square) or active during the Holocene (circle).

1.3.2.1 Stromboli

Shallow conduit processes, like the persistent activity at Stromboli (Ripepe and Gordeev, 1999) occur over only minutes to days. This activity represents the other (fast) side of the spectrum of the rates of volcanic processes, compared to the (slow) caldera unrest in Iceland. Stromboli has therefore been chosen as area for this study.

Stromboli (see Figure 5-2), the northernmost volcanic island of the Aeolian archipelago in the Tyrrenian sea, has been active for at least 2000 years. The persistent activity is characterised by permanent degassing and mild explosions emitting ejecta up to heights of 300 m. Data can be collected safely from the rim 150 m above the crater complex.

The island of Stromboli was formed by several cycles of volcanic edifice build up followed by partial collapses. Several stages of this process are still recognisable in exposures on the island today. The complete evolution of the geology is displayed in Figure 1-5.

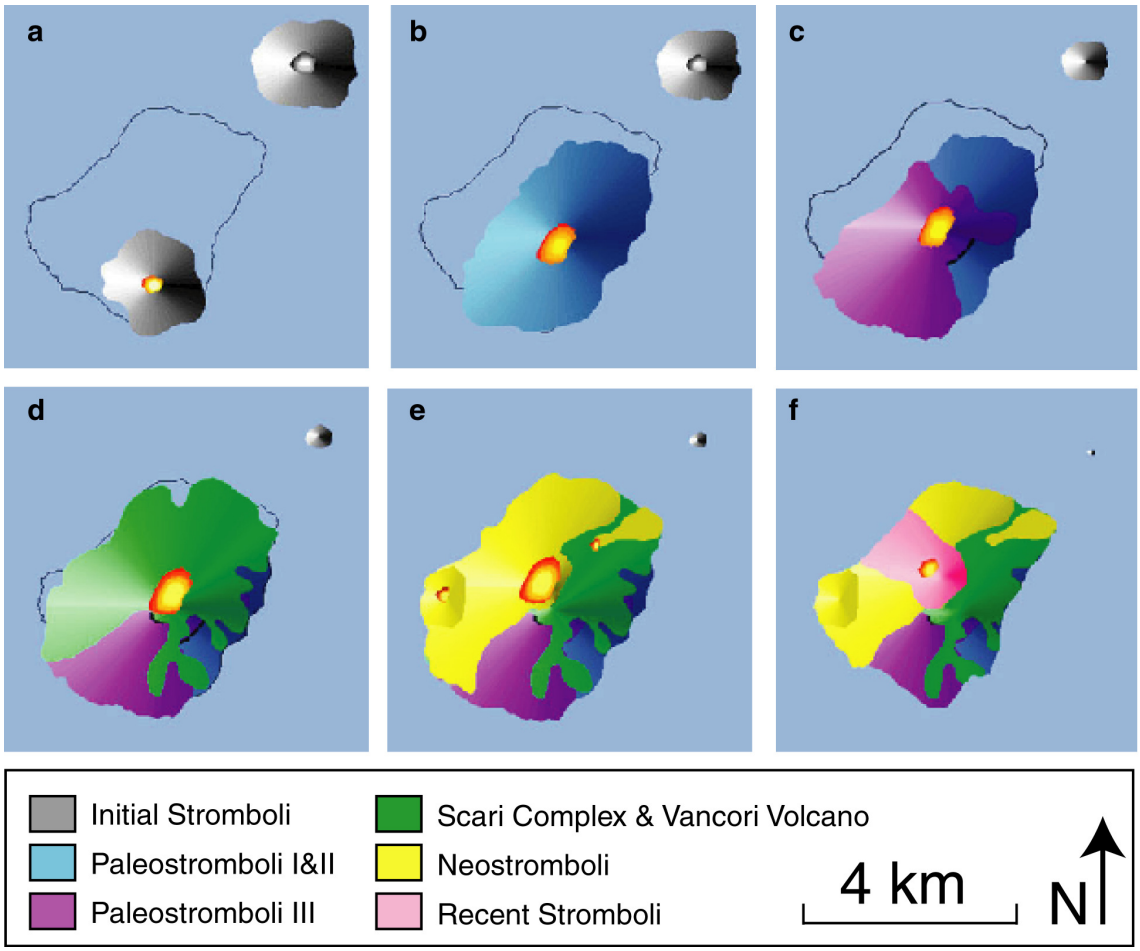

Figure 1-5 Geological evolution of Stromboli. a) 1.6 Ma B.P: Stromboli emerged from the sea in the southern part of todays island. Strombolicchio to the NE had already started eroding. b) Paleostromboli I&II: lava flows and pyroclastics built up a stratovolcano. c) Paleostromboli III: activity shifts slightly to the NW, the cone builds up to 700 m a.s.l. d) Scari Complex and Vancori Volcano: bombs, lahars and pyroclastic sequences are covered by basaltic lava flows building up the ever growing cone. W/NW part of the volcano collapses. e) Neostromboli: crater in the N fills in the collapsed area; secondary craters are active in Ginostra and San Bertolo. f) Recent Stromboli: NW slope collapses forming the Sciara del Fuoco; pyroclastic and lava flows rebuilt part of the collapsed area.

1.4 Previous studies

1.4.1 Askja

Ground deformation measurements at Askja started in 1966 (Tryggvason, 1989b) with the installation of a precise levelling line. Two years later, the line was expanded and lake level benchmarks were installed. From 1966 to 1972, alternating periods of subsidence and uplift were observed. No measurements were made in the 1973 to 1982 period but monitoring resumed in 1983. New techniques, such as Electronic Distance Measurements (EDM), dry tilt and GPS have since been used (Camitz et al., 1995; Rymer and Tryggvason, 1993; Tryggvason, 1989a; Tryggvason, 1989b). Deformation data show that Askja has been deflating at least since 1983 (Sturkell and Sigmundsson, 2000).

The first micro-gravity data at Askja were measured with LaCoste & Romberg gravity meters in 1988 (Rymer and Tryggvason, 1993). Measurements of the Free Air Gradient (FAG) at Askja range from -240 μGal/m in the southeast, to -360 μGal/m in the centre and have a standard deviation of 12 μGal/m at each site. These deviations from the theoretical value (-308.6 μGal/m) are due to the caldera-centred Bouguer negative gravity anomaly (Brown et al., 1991), and a positive anomaly in the east associated with a fissure swarm (Rymer and Tryggvason, 1993). Interpretation of micro-gravity results should only be attempted if accurate geodetic data are available (see APPENDIX B). Further detailed analysis of the 1988 to 1991 deformation data set shows that the deflation reported by Rymer and Trygvasson (1993) was underestimated for the central and south-eastern stations and overestimated for the northern stations. Micro-gravity data for this period are therefore recalculated in Chapter 2.

1.4.2 Krafla

Geodetic measurements for the purpose of investigating tectonic movements were first made at Krafla in 1938. No significant changes were observed over the 1938-1965 period (Björnsson et al., 1979). Deflation was observed from 1965 to 1971 followed by extension and uplift from 1970 to 1975. During the Krafla fires, deformation was monitored extensively using a wide range of geodetic techniques such as EDM, precise levelling, tilt and lake level observations (Allard et al., 1994; Björnsson, 1985; Ewart et al., 1991; Tryggvason, 1986; Tryggvason, 1994). Ground deformation was characterised by repeated cycles of steady inflation followed by rapid subsidence. From 1985 to 1989, slow inflation occurred followed by an ever decreasing subsidence since then (Rymer et al., 1998a).

Micro-gravity measurements started at Krafla with surveys in 1965, 1970 and 1975. Data taken during the Krafla fires (1975-1984) correlate well with geodetic data of this period (Björnsson et al., 1979; Johnsen et al., 1980). Since 1990, micro-gravity measurements have been made on a regular basis using LaCoste & Romberg instruments (Rymer et al., 1998a). Data acquired during this last period have also been used in this study and the results are described in Chapter 4.

Analysis of InSAR images aquired by the ERS1 and ERS2 satellites, has proven a valuable tool when studying the ongoing deformation at Krafla (de Zeeuw-van Dalfsen et al., 2004a; Henriot et al., 2001; Sigmundsson et al., 1997). Interferograms have been produced for the Krafla area with images from 1992 to 1998 (Henriot et al., 2001; Sigmundsson et al., 1997). The topographic fringes were removed from all interferograms using a Digital Elevation Model (DEM) from the Icelandic geodetic survey. Orbital corrections were done using the post-computed orbits from the European Space Agency. By using pair-wise discrimination, different groups all observed a circular pattern of subsidence near the centre of the Krafla system, above the inferred

magma chamber. They also reported an increase in range along the rift axis. Different models were suggested by the different teams to explain the observations. Sigmundsson et al. (1997) modelled the magma chamber as a Mogi point source (Mogi, 1958) at 3 km depth in an elastic halfspace, and the along-rift change by an infinite line source. They estimated a volume decrease of 0.9 x 10^6 m^3/y from 1992 to 1995. They considered solidification and cooling the most likely process responsible although according to them, drainage of magma into the rift zone can not be excluded. In contrast, Henriot et al. (2001) modelled their results by three horizontal planar structures of which the central one is comparable to the magma chamber of Sigmundsson et al. (1997). The two other structures are finite elements; a 4 km wide sill at 3 km depth to the south, and a 100 m wide sill at 1.5 km depth to the north. They interpreted the models with a steady volume decrease of the magma chamber from 1992 to 1998 of 0.52 x 10^6 m^3/y which they interpreted as due to thermal contraction.

1.4.3 Stromboli

A team of scientists, mainly from the University of Florence, the University of Hawaii, the Alaska Volcano Observatory and the Open University set up a collaborative experiment in 1999 collecting seismic, infrasonic, thermal, meteorological and continuous gravity data (Harris and Stevenson, 1997; Ripepe and Gordeev, 1999; Ripepe et al., 2002; Ripepe and Marchetti, 2002). The purpose of the project was to improve the understanding of the dynamics of persistently active volcanism. A more detailed description of their and my achievements can be found in Chapter 5.

1.5 Outline of the present work

This thesis expands upon the research of Rymer et al. (1998) and Rymer and Tryggvasson (1993) to further investigate the processes responsible for caldera deflation at Askja and Krafla. It develops upon the research of Sigmundsson et al. (1997) and

Henriot et al. (2001) to further explore the deformation at Krafla with the use of InSAR techniques. And finally it builds on the work of Ripepe et al. (2002) to try and achieve better constraints on shallow conduit processes at the persistently active volcano of Stromboli. The main objective of this study is to investigate the mechanisms responsible for caldera unrest at Askja and Krafla and those accountable for persistent activity at Stromboli through the application of micro-gravity and deformation (precise levelling, GPS and InSAR) measurements. Specifically addressed questions are:

1) Which process is responsible for the faster than average deflation observed at Askja? What implications does that have for the plumbing system?

2) Does the analysis of InSAR data of Krafla reveal features previously unaccounted for? How can these features be interpreted and modelled and what consequences do their existence have for the plumbing system at Krafla?

3) Is it possible to distinguish between the several explanations for deflation at Krafla, taking into account the extensive geothermal exploitation?

4) Is it possible to observe magma column or foam height changes in the open conduit system of Stromboli volcano with the use of continuous micro-gravity techniques?

5) What are the implications of all above observations for the volcanic processes at Icelandic volcanoes?

Three of the main chapters are written in article format, and therefore some repetition is inevitable. Chapter 3 has been published in Geophysical Research letters, Chapter 2 has been accepted for publication in Journal of Volcanology and Geothermal Research and Chapter 4 has been submitted to Bulletin of Volcanology.

Chapter 2 investigates the cause of deflation at Askja in Iceland and answers question 1. Chapter 3 describes the analysis of newly acquired InSAR images of Krafla,

revealing a striking new feature previously not described, and answers question 2. Chapter 4 combines micro-gravity data with a model for all available geodetic data at Krafla, taking into account water extraction from the geothermal power plant. This allows for better understanding of the processes involved in the ongoing deflation and answers question 3. Chapter 5 assesses the use of continuous micro-gravity as a tool to understand conduit processes at Stromboli and answers question 4. Finally, in chapter 6, all observations are integrated to try and improve our understanding of volcanic processes while answering question 5.

Fieldwork and discussion for this thesis was undertaken in collaboration with a number of colleagues from Iceland: Freysteinn Sigmundsson, Rikke Pedersen and Carolina Pagli from the Nordic Volcanological Institute, Pall Einarsson from the Science Institute, Erik Sturkell from the Icelandic Meteorological Office and Eysteinn Tryggvasson from the National Energy Authority, Italy: Maurizio Ripepe, Emanuele Marchetti and Pasquale Poggi from the University of Florence, and Hawaii: Andy Harris from UH-Manoa. Micro-gravity data from 2002 and 2003 were collected by myself with aid of my supervisor, Hazel Rymer and field assistants. InSAR data were generated and analysed by myself with help of my supervisor, Freysteinn Sigmundsson, Jean-Luc Froger and Rikke Pedersen. Bearing all this in mind, >80% of this thesis is my own work.

Chapter 2: Net gravity decrease at Askja volcano, Iceland: Constraints on processes responsible for continuous caldera deflation, 1988-2003.

This Chapter was published in the Journal of Volcanology and Geothermal Reasearch, Volume 139, issues 3-4 in January 2005. It discusses the results of analysis of newly acquired micro-gravity data (2002 and 2003) as well as the re-interpretation of previously published micro-gravity data (1988-1997) in combination with a new geodetic model developed by Erik Sturkell. The location of the stations is described in Appendix A and the original data are displayed in Appendix C.

2.1 Abstract

Askja caldera in northeast Iceland has been in a state of unrest for decades. Ground-deformation surveys show that the rate of deformation i.e., deflation, is much higher then observed at any other dormant volcano in Iceland. This work presents the results from micro-gravity and deformation studies at Askja from 1988 to 2003. The deflation reaches a maximum of -0.46 m in the centre of the caldera, relative to a station outside the caldera, during the study period. The source of deformation is inferred to be at ~3 km depth and a recent study infers a second deeper source at ~16 km depth. The deflation is consistent with a sub-surface volume change of -0.018 km^3. We find a net micro-gravity decrease of 115 μGal in the centre of the caldera relative to the same station. This corresponds to a sub-surface mass decrease of 1.6 $x10^{11}$ kg between 1988 and 2003 based on the use of a point source model. A combination of magma drainage and cooling and contraction of the shallow magma reservoir at 3 km depth is our favoured model, consistent with the integrated observations. We suggest that

extensional tectonic forces generate space in the ductile part of the crust to accommodate on-going magma drainage from the shallow magma chamber.

2.2 Introduction

Caldera unrest may last for decades or longer, and can pose a significant hazard for local populations e.g., Campi Flegrei 1975 and onwards (Gottsmann et al., 2003). Unrest is often associated with gradual and persistent uplift or deflation (Newhall and Dzurisin, 1988) and is usually thought to be caused by magmatic processes. Combined micro-gravity and deformation studies can improve our understanding of these processes and thus of the volcanic caldera system as a whole (Gottsmann et al., 2003; Rymer and Williams-Jones, 2000). Askja caldera in northeast Iceland (Figure 2-1) has been in a state of unrest for many years (Sturkell and Sigmundsson, 2000) and references therein), and has therefore been chosen as the area for this study.

Askja caldera in the Dyngjufjöll central volcano (Figure 2-1) is situated in a 10-15 km wide fissure system, extending 100 km north from the Vatnajokull icecap. Volcanic activity is associated with two fissure swarms, with slightly different strikes (Sigvaldason, 2002). The volcanic centre hosts three calderas (Figure 2-1) The largest one, 8 km across and 200-300 m deep, is the circular Askja caldera. North of it is an almost completely filled and less pronounced older caldera. The youngest caldera, with a diameter of 4.5 km, was formed in 1875 and is occupied by lake Öskjuvatn (Sturkell and Sigmundsson, 2000). It is nested within a parabolic embayment which cuts into the hyaloclastite Thorvaldsfjall block.

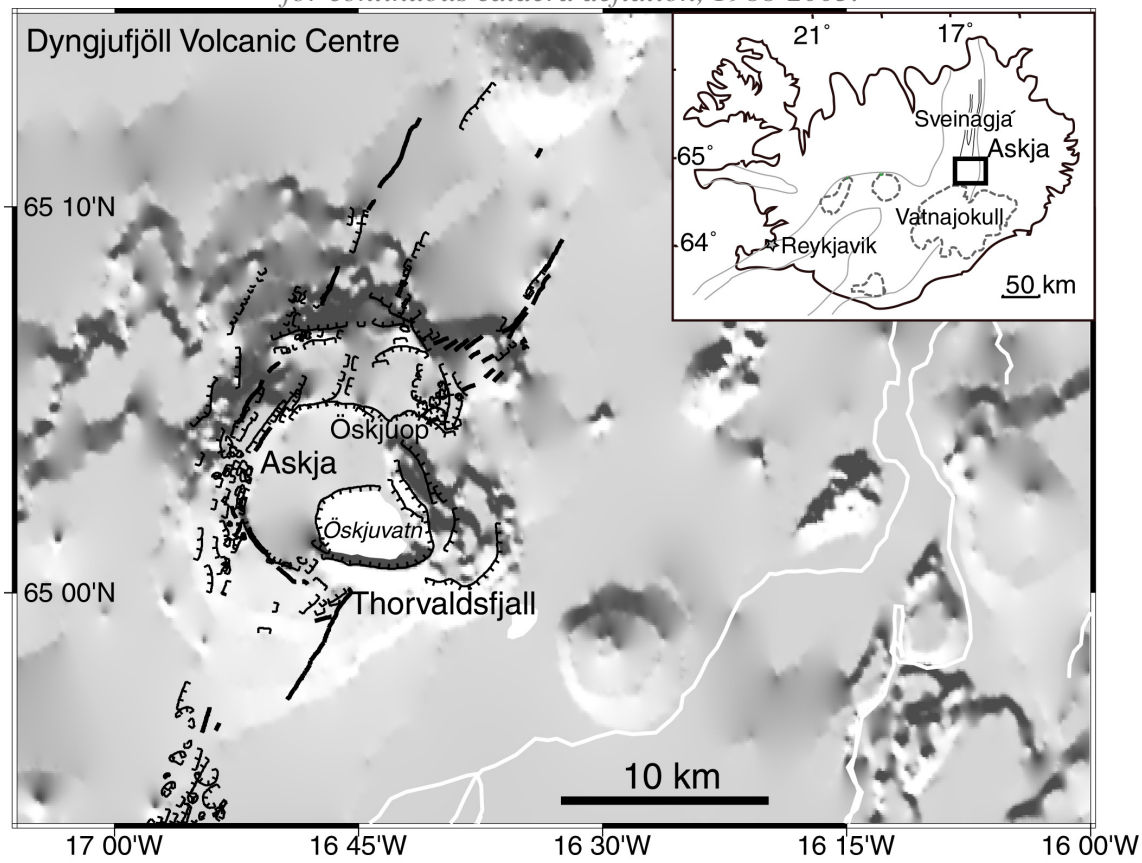

Figure 2-1 Overview of the Dyngjufjöll volcanic centre. Inset shows location of Askja caldera in Iceland. Note the location of the Vatnajökull glacier to the south, and the Sveinagjá graben to the north of Askja. Öskjuvatn is the lake filling the smallest caldera which cuts into the Thorvaldsfjall block. The 1961 lava flowed out of the Askja caldera through the Öskjuop opening. The white lines depict the rivers, shaded background indicates topography. Figure is adapted after Strukell and sigmundsson (2000).

The Holocene eruption history of Askja, includes a Plinian rhyolitic eruption, dated at ~10 ka. This eruption left a pumice deposit which now serves as a marker horizon in NE Iceland (Sigvaldason, 2002). A major rifting event occurred from 1874 to 1876 and included a series of dyke injections, basaltic fissure eruptions and the explosive rhyolite eruption associated with formation of the youngest caldera. The main fissure eruption occurred 40-70 km north of Askja, in the northern part of the fissure swarm (Sveinagjá graben, Figure 2-1-inset). It has been suggested (Sigurdsson and Sparks, 1978) that lateral magma drainage from a reservoir beneath Askja caldera induced the caldera collapse. The next eruptive period took place from 1921 to 1929, continuing with a small eruption in the beginning of the 1930s. During this episode, a fissure eruption opened to the south of the Dyngjufjöll mountains and several minor effusive eruptions occurred around the 1875 caldera margin. The most recent eruption began in October 1961 and continued into early December of the same year. An E-W trending fissure opened close to the northern rim of the main caldera and lava flowed through the Öskjuop pass onto the plain east of the Dyngjufjöll mountains.

Excluding erupting volcanoes, Askja has displayed a significantly higher rate of ground deformation i.e., deflation, during the past decades, than anywhere else in Iceland (Tryggvason, 1989a). There are at least three possible explanations for this observed deflation: i) cooling/contraction of magma in a shallow (~3 km) magma chamber (Rymer and Tryggvason, 1993); ii) void compaction of the underlying material and iii) magma drainage from a shallow magma chamber. Here, micro-gravity and ground-deformation data from 1988 to 2003 inclusive are presented. Joint interpretation of these data removes some of the ambiguities concerning the cause of deflation and allows an estimate of any sub-surface mass change to be made. Mass change (ΔM) within a spherical (point source) body, whose depth is much greater than its radius, causes a gravitational effect (Δg) given by:

$$\Delta M = \frac{\Delta g (r^2 + d^2)^{3/2}}{Gd} \qquad \text{(eq. 2-1)}$$

where G is the Universal gravitational constant: 6.67 x 10^{-11} Nm^2/kg^2, d is the depth to the point source, and r is the horizontal distance to it.

2.3 Ground deformation data

A 1.7-km long levelling line (Figure 2-2) with 12 benchmarks was installed by Eysteinn Tryggvason and colleagues in 1966, followed in 1968 by the addition of 18 benchmarks to the line and the installation of 20 benchmarks around the shores of lake Öskjuvatn. Precision levelling, lake level, EDM, dry tilt and GPS observations have been made at Askja since then (Rymer and Tryggvason, 1993; Sturkell and Sigmundsson, 2000; Tryggvason, 1989a; Tryggvason, 1989b). While no levelling was conducted at Askja between 1973 and 1982 annual levelling surveys recommenced in 1983 and continue to present. From 1966 to 1972, these measurements show alternating periods of subsidence and uplift of the caldera floor. Since 1983, there has been consistent subsidence towards the central part of the caldera (Sturkell and Sigmundsson, 2000). Combining all the available ground deformation data from 1988 to 1991, Rymer and Tryggvason (1993) found that 80% of the deformation could be explained by a point source at 2.8 km depth, located to the north of the lake. More recently, using a data set running from 1983 to 1998, Sturkell and Sigmundsson (2000) found that the majority of the deformation was caused by a source under the central part of the main caldera, only 1 km SW of the location suggested by Rymer and Tryggvason (1993). Sturkell and Sigmundsson (2000) also noted that the rate of deflation decreased slightly in the past decade.

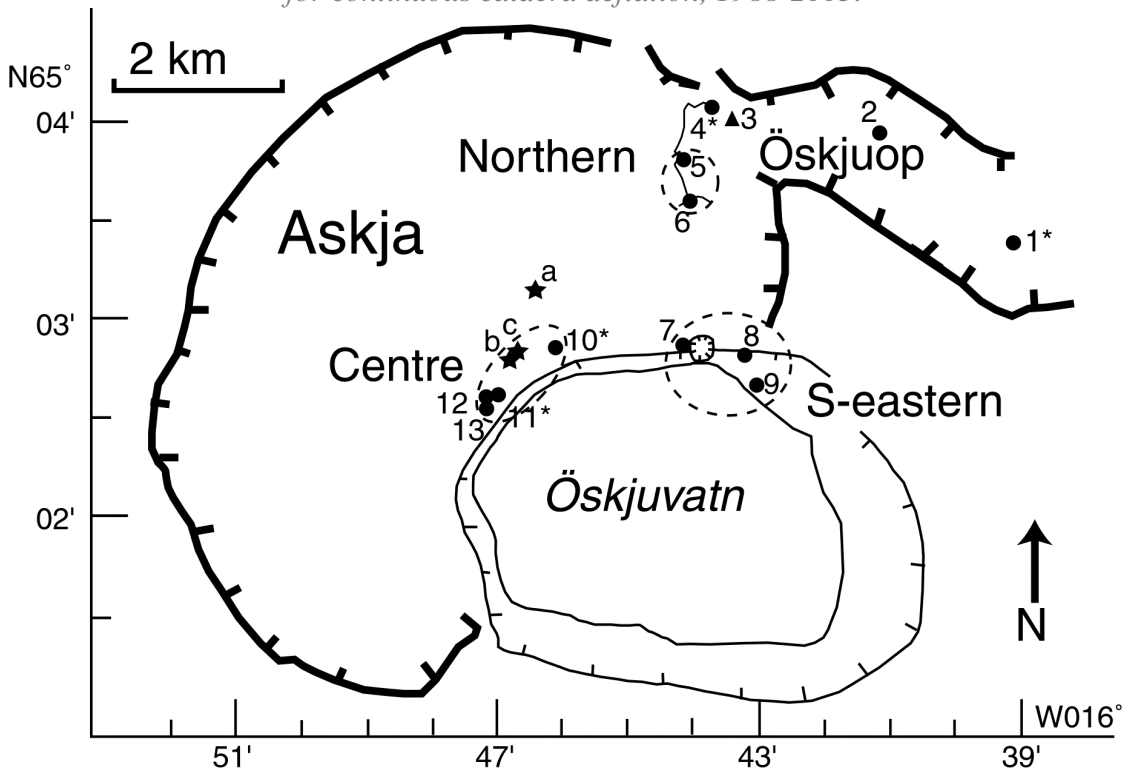

Figure 2-2 Locations of gravity stations in Askja caldera modified after Rymer and Trygvasson (1993). Dots represent the stations (numbered 1 to 13, see Table 2-4) which are divided into three groups (dashed ellipses): the Northern, South-eastern and Centre. 1 is DYNG, 2 is 83009, 3 is 83001, 4 is 430, 5 is 412, 6 is 405, 7 is Von Knebel, 8 is IV16, 9 is D-18, 10 is NE2002005, 11 is NE2002006,12 is NE82005 and 13 is D-19. Stations set-up or first measured in 2002 are marked with a *. In the future, station 1* may serve as a base station, station 4* will strengthen observations at location 3 and stations 10* and 11* will be added to the centre station group. The extent of the main caldera is shown by the thick outer curve. Lake Öskjuvatn is located within a second, smaller caldera within the first. The small, round, steep-sided feature, north of the lake (next to station 7) is the Víti explosion crater. The three stars show the location of the point sources as suggested in Table 2-1. The levelling line is indicated by the thin solid line going through stations 4, 5 and 6.

Several authors (Rymer and Tryggvason, 1993; Sturkell and Sigmundsson, 2000) have estimated the location of a point source which can account for the observed deformation. The parameters of these Mogi sources (Table 2-1) are consistent and the models explain most of the observed deformation. Recently, however, an improved model, featuring two Mogi Sources at the same horizontal position but at different depths (3.0 and 16.2 km), has been suggested by Sturkell et al. (2004-submitted). The shallow point source is responsible for 80 % of the vertical displacement, with the remaining 20% being contributed by the deeper point source.

To compare the ground-deformation data with the micro-gravity data, it is necessary to re-calculate the vertical changes with respect to the micro-gravity base station (i.e., 83001, #3 in Figure 2-2). This is done using the newest model for surface deformation (Sturkell et al., 2004 - submitted) which is based on GPS-measurements from 1993 to 1998 and yearly levelling data (Table 2-2).

2.4 Micro-gravity data

Micro-gravity measurements have been made at Askja since 1988 using LaCoste & Romberg meters (Rymer and Tryggvason, 1993). Askja is one of the few calderas in the world (others include Krafla in Iceland (Rymer et al., 1998a); Masaya in Nicaragua (Rymer et al., 1998b; Williams-Jones et al., 2003); and Campi Flegrei in Italy (Berrino, 1994; Gottsmann et al., 2003) with such an extensive (i.e., 15 year) micro-gravity data set. The nine micro-gravity stations at Askja (extended to thirteen in 2002) are grouped

Table 2-1 Parameters of the three available deformation models used for modelling the deformation data at Askja. h_0 is the absolute total subsidence directly above the point source in cm/yr.

Parameters of Mogi Source	Rymer & Trygvasson (1993), a in Fig. 2	Sturkell & Sigmundsson (2000), b in Fig. 2	Sturkell et al. (2004-submitted.), c in Fig. 2
Latitude	N 65º 03′ 11.5″	N 65º 02′ 41.3″	N 65º 02′ 44.2″
Longitude	W 016º 46′ 05.9″	W 016º 46′ 49.8″	W 016º 46′ 48.7″
Depth (*km*)	2.8	2.8	3.0 and 16.2
h_0 (*cm/yr*)	4.2 (‘88-‘91)	5 (‘93-‘98)	5.2 (‘93-‘98)
Data input	Optical levelling tilt, precise levelling.	Optical levelling tilt, precise levelling, GPS.	GPS, precise levelling

Table 2-2 Total vertical displacement in m calculated for each year using the two point Mogi model suggested by Sturkell et al. (2004). The bottom row shows the cumulative volume decrease of the Mogi source for each year in percentage from 1988. The rate is the same for both sources. All values with respect to base station 83001, which lies within the deformation field.

	Station	1989	1990	1991	1992	1993	1994	1995	1996	1997	1998	1999	2000	2001	2002	2003
1	DYNG	0.010	0.010	0.009	0.009	0.009	0.009	0.009	0.008	0.008	0.008	0.008	0.007	0.007	0.007	0.007
2	83009	0.007	0.006	0.006	0.006	0.006	0.006	0.006	0.006	0.005	0.005	0.005	0.005	0.005	0.005	0.005
3	83001	0.000	0.000	0.000	0.000	0.000	0.000	0.000	0.000	0.000	0.000	0.000	0.000	0.000	0.000	0.000
4	430	0.000	0.000	0.000	0.000	0.000	0.000	0.000	0.000	0.000	0.000	0.000	0.000	0.000	0.000	0.000
5	412	-0.006	-0.006	-0.006	-0.005	-0.005	-0.005	-0.005	-0.005	-0.005	-0.005	-0.005	-0.004	-0.004	-0.004	-0.004
6	405	-0.007	-0.007	-0.007	-0.007	-0.007	-0.006	-0.006	-0.006	-0.006	-0.006	-0.006	-0.006	-0.005	-0.005	-0.005
7	Von Knebel	-0.012	-0.012	-0.012	-0.012	-0.011	-0.011	-0.011	-0.010	-0.010	-0.010	-0.010	-0.009	-0.009	-0.009	-0.009
8	IV16	-0.006	-0.006	-0.006	-0.006	-0.006	-0.006	-0.005	-0.005	-0.005	-0.005	-0.005	-0.005	-0.005	-0.004	-0.004
9	D-18	-0.006	-0.006	-0.006	-0.005	-0.005	-0.005	-0.005	-0.005	-0.005	-0.005	-0.005	-0.004	-0.004	-0.004	-0.004
10	NE2002005	-0.034	-0.033	-0.032	-0.032	-0.031	-0.030	-0.029	-0.028	-0.028	-0.027	-0.026	-0.026	-0.025	-0.024	-0.024
11	NE2002006	-0.037	-0.036	-0.035	-0.034	-0.033	-0.033	-0.032	-0.031	-0.030	-0.029	-0.029	-0.028	-0.027	-0.027	-0.026
12	NE82005	-0.037	-0.036	-0.035	-0.034	-0.033	-0.032	-0.032	-0.031	-0.030	-0.029	-0.029	-0.028	-0.027	-0.026	-0.026
13	D-19	-0.036	-0.035	-0.035	-0.034	-0.033	-0.032	-0.031	-0.030	-0.030	-0.029	-0.028	-0.028	-0.027	-0.026	-0.025
Cum. V decr. (%)		2.5	5.0	7.4	9.7	12.0	14.2	16.4	18.5	20.5	22.5	24.5	26.4	28.2	30.1	32.0

according to location: caldera centre, northern, and south-eastern stations (Figure 2-2). The caldera centre stations are located in the region of maximum deflation, while the other stations are situated closer to the edge of the deformation zone. It is therefore expected that any gravity anomaly directly related to this deformation will be best recorded by the central stations. Within each group of stations, data would be expected to be consistent to within error, although some deviations do still occur. Such deviations can be caused by local meteorological disturbances. The uncertainty expected for this type of survey considering the climate, time delay between readings, and jolting of the instruments during transport is 10-15 μGal (Rymer, 1989).

2.4.1 Previous work

Rymer and Trygvasson (1993) integrated micro-gravity and deformation data sets from 1988 to 1991 and found negligible net gravity increases at the northern and central stations. Rymer and Trygvasson (1993) concluded that 80% of the deformation from 1988 to 1991 occurred without a sub-surface mass-change and that deflation was primarily due to relaxation of the caldera. However, they found a net gravity increase at the SE station group which was modelled in terms of a dyke intrusion with a width of 1 m reaching between 10-100 m beneath the surface. Furthermore they calculated that if a mass change greater than 10^9 kg were to occur, it would be clearly measurable in terms of gravity at the surface.

Further detailed analysis of the 1988 to 1991 deformation data set shows that the deflation reported by Rymer and Trygvasson (1993) was underestimated for the central and south-eastern stations and overestimated for the northern stations. Using the latest two point source Mogi model proposed by Sturkell et al. (2004-submitted), the corrected value for the deformation at the central stations is -0.107 m from 1988 to 1991 with respect to base station 83001 (see Table 2-3), instead of the -0.047 m reported by Rymer and Trygvasson (1993). Their interpretation is therefore revised in two ways: i)

the insignificant net gravity increase at the centre becomes a slight net gravity decrease of 13 ± 9 μGal (Table 2-3) and ii) the mass increase at the south-eastern group of stations becomes insignificant over the period 1988 to 1991 (Table 2-3). Following eq. 2-1 and assuming the center of the magmatic body is located 406 m horizontally away from the centre stations at a depth of 3000 m, the net gravity decrease in the centre can now be interpreted as a sub-surface mass decrease of 1.8×10^{10} kg in the 1988-1991 period.

2.4.2 New data

During the summers of 1992, 1994, 1995, 1997, 2002 and 2003, micro-gravity surveys were performed at Askja while deformation measurements were repeated annually. LaCoste & Romberg meter G-513 has been used for all surveys since 1988 and its calibration characteristics are well known (Carbone and Rymer, 1999); another meter, G-403, has been used in addition since 1997. In 2002, the micro-gravity network was extended along the north-western shore line of lake Öskjuvatn in order to fill in the gap between the central and south-eastern stations (two new stations, # 10 & 11 in Figure 2-2 and Table 2-4). Furthermore, the northern-end station of the precise levelling line (430) and the GPS base station (DYNG) were also added to the micro-gravity network in 2002 (# 1 & 4 in Figure 2-2 and Table 2-4). The deformation network has been using station DYNG as a reference station since 1993 while the micro-gravity is referred to 83001 (#3 in Figure 2-2 and Table 2-4). The addition of station DYNG to the micro-gravity network will solve the problem of different reference points during future campaigns. It should be noted however, that even station DYNG lies within the deformation field of Askja. It must be kept in mind that the quoted gravity and height changes are measured relative to their reference points and they do not represent absolute change.

Table 2-3 Calculation of net gravity for the periods 1988 to 1991 inclusive, 1992 to 2003 inclusive and 1988 to 2003 inclusive.

Time	**Station group**	**Δh (m)**	**$\Delta g_{measured}$ (μGal)**	**FAG** (μGal/m)	**$\Delta g_{theoretical}$ (μGal)**	**Δg_{net} (μGal)**
1988 - 1991	centre	-0.107	26 (9)	-360	39	-13 ± 9
	northern	-0.020	13 (9)	-310	5	+8 ± 9
	s-eastern	-0.024	17 (9)	-240	6	+11 ± 9
1992 - 2003	centre	-0.349	24 (9)	-360	126	-102 ± 9
	northern	-0.064	10 (9)	-310	20	-10 ± 9
	s-eastern	-0.079	25 (9)	-240	19	+6 ± 9
1988 - 2003	centre	-0.456	50 (9)	-360	165	-115 ± 9
	northern	-0.084	23 (9)	-310	25	-2 ± 9
	s-eastern	-0.103	42 (9)	-240	25	+17 ± 9

During the 2002 and 2003 field campaigns, the majority of the stations were measured at least three times with meter G-513 and most were measured twice with meter G-403. The average standard deviation was 16 and 6 μGal in 2002 and 20 and 7 μGal in 2003 (Table 2-4), for meter G-403 and meter G-513 respectively. This is within range of the uncertainty expected during this type of survey (Rymer and Tryggvason, 1993). In this study, station 83001 has been used as a reference for both the gravity and deformation data, in order to compare the results with previously published work (Rymer and Tryggvason, 1993). Comparing the 2002 and 2003 surveys with earlier surveys (Figure 2-3 and Table 2-3) reveals that there has been a micro-gravity increase at all stations from 1988 to 2003. The south-eastern, northern and centre stations show a total micro-gravity increase of 42, 23 and 50 μGal, respectively, from 1988 to 2003. A trend-line representing the average rate of change of micro-gravity change with time is shown to enhance visual interpretation (solid line in Figure 2-3). All data plot within error bar range from the trend-line and it is therefore not possible to draw conclusions about any variations in the rate of change through time. However, on a year to year basis, the central and northern stations appear to follow the same trend (e.g., either decreasing or increasing gravity compared with the previous year) while the south-eastern stations appear to do the opposite (Figure 2-3). The average rate of change ranges from 1.5 to 3.3 μGal/yr, depending on the location. This is too small to detect yearly and shows the importance of a long term data set (Locke et al., 2003). Because of this, we suggest that a micro-gravity survey, carried out once every two or three years, is appropriate for Askja while the current style of deformation continues.

2.4.3 Interpretation

To interpret the data in terms of mass changes, the net micro-gravity changes must be calculated. This is done by correcting for the change of gravity with height above ground level using the measured Free Air Gradient (FAG,Table 2-3). The use of a

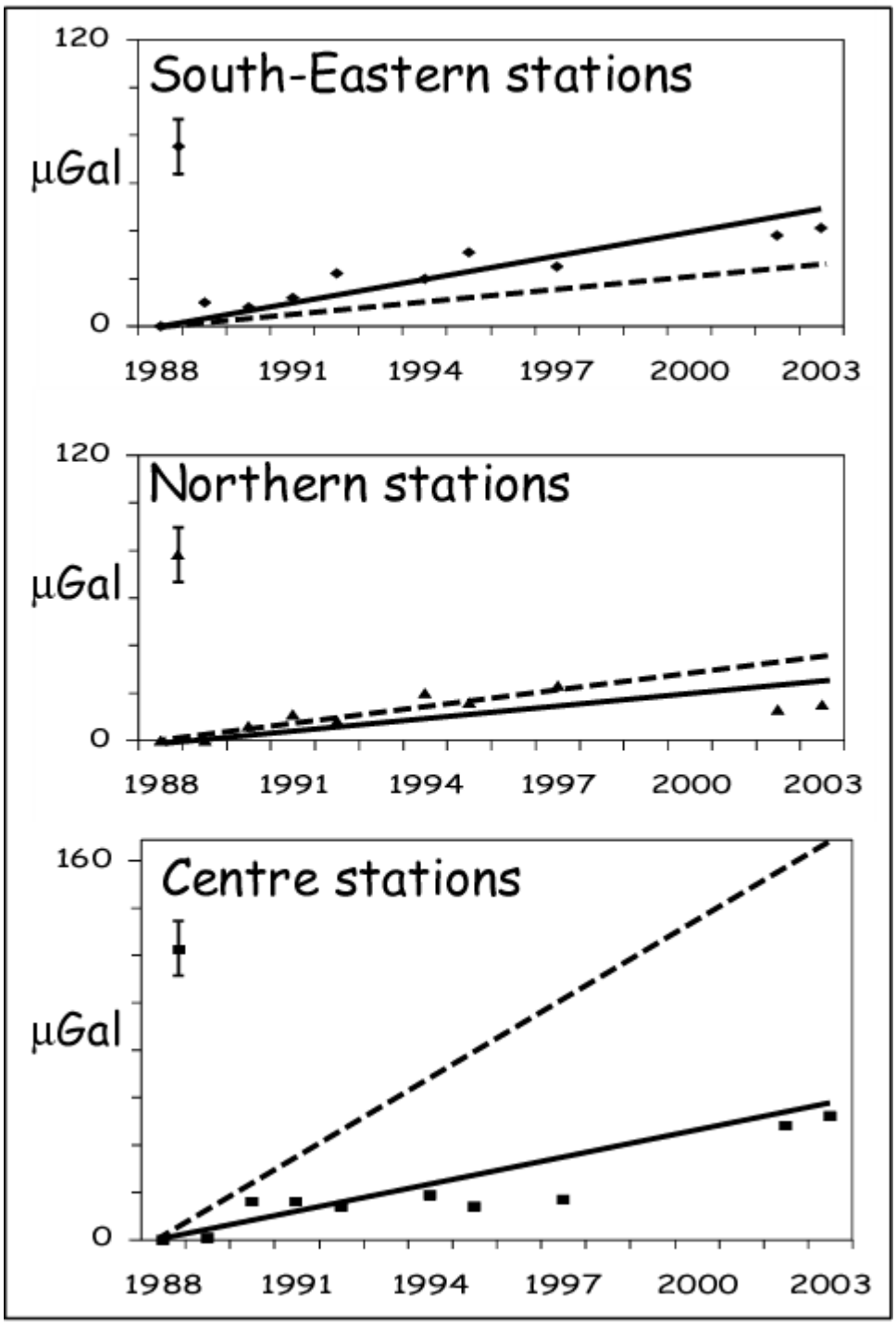

Figure 2-3 Micro-gravity data from 1988 to 2003. Symbols represent average yearly gravity changes in µGal with respect to station 83001 and referred to 1988. Solid lines show the data trend, dashed lines show expected micro-gravity calculated using the observed deformation and measured FAG (see Table 2-4). If the data trend is higher then the expected micro-gravity, as for the south-eastern stations, this implies a net micro-gravity increase. If the data trend is less then expected, as for the centre stations, there is a net micro-gravity decrease. Vertical bars show average error on the data.

measured FAG (Rymer, 1996) is more accurate then the use of the theoretical value for the FAG (-308.6 μGal/m) and is therefore favoured. Measurements of the FAG at Askja range from -240 μGal/m in the southeast, to -360 μGal/m in the centre and have a standard deviation of 12 μGal/m at each site. These deviations from the theoretical value are due to the caldera-centred Bouguer negative gravity anomaly (Brown et al., 1991), and a positive anomaly in the east associated with a fissure swarm (Rymer and Tryggvason, 1993). The difference between measured and theoretical Free-Air Gradient at Askja therefore amounts to ± 50 μGal/m, which if unaccounted for, would add an uncertainty of 0.5 μGal for every centimetre of deformation (at the central stations using the theoretical value would therefore result in a net gravity change of -84 μGal instead of -102 μGal between 1992 and 2003).

The base station used in the micro-gravity surveys (83001, #3 in Figure 2-2 and Table 2-4) is located on the 1961 lava flow just outside the north-eastern side of the caldera rim and is actually located within the deformation zone. Deformation surveys (Sturkell and Sigmundsson, 2000) show that it moves vertically with ~1 cm/yr and that the total area of deformation extends to all sides beyond the micro-gravity network. Because the total area of deformation is larger than that covered by either of the networks, any estimates for mass quantities or volumes following from this work are necessarily minimum values. To be able to interpret the data in this paper, the deformation data have also been referred to 83001.

The total deformation at the centre stations from 1988 to 2003, relative to the base station, is -0.46 m. Multiplication by the measured FAG value of -360 μGal/m, gives an expected micro-gravity increase of 165 μGal. Subtraction from the measured micro-gravity increase of 50 μGal leaves a significant net micro-gravity decrease of 115 ± 9 μGal from 1988 to 2003 at the centre of the caldera. This change can only be explained by a sub-surface mass decrease. A sub-surface mass decrease could be caused

by drainage of magma or a fall in the water table or a combination of these (Rymer and Williams-Jones, 2000; Williams-Jones and Rymer, 2002). For an unconfined aquifer approximated by an infinite slab, the gravity change, Δg_{wt}, expected as a result of water table and lake level movements, δz, is calculated as (Battaglia et al., 2003):

$$\Delta g_{wt} = 2\pi G \phi_e \rho_w \delta z \qquad \text{(eq. 2-2)}$$

For an effective porosity, ϕ_e, of 17% (Franzson et al., 2001) a one-meter fall in water table would lead to a gravity increase of 7 μGal. Alternatively, to explain the totality of the net gravity decrease of 115 μGal, the water level would need to have fallen by approximately 16 metres. On the contrary, the water level of lake Öskjuvatn is known to be slowly increasing. From 1986 to 1993, lake level observation at a station at the Northeast shore of lake Öskjuvatn shows an increase in water height of 76 cm. Furthermore, since stations undergoing net gravity increase are close to those experiencing net gravity decrease and both are within a few hundred metres of the lake, water level change is an unlikely explanation for more then a very minor component of the observed mass decrease. Hydrothermal activity has been cited as the cause of elevation change during recent activity at the Campi Flegrei (Bonafede and Mazzanti, 1998). A different study suggests, however, that overpressures required within the system are unrealistically large if hydrothermal activity is the explanation (Gottsmann et al., 2003). For this reason, and because hydrothermal activity at Askja is significantly less extensive than at Campi Flegrei, the causative mechanism at Askja is considered to be more likely magmatic in origin.

To quantify the overall mass decrease from 1988 to 2003, a spherical body whose depth is much greater than its radius, is modelled as the source of the change using eq. 2-1. Crustal deformation due to such a source is well known and described by the "Mogi model" for a point source of pressure in an elastic halfspace (Mogi, 1958).

Table 2-4 Latitude and Longitude of the gravity stations at Askja (numbers 1-13 refer to those in Figure 2-2) and gravity data (in mGal) from the 2002 and 2003 surveys at Askja, referred to station 83001. Distance to Mogi Source from Sturkell et al. (2004). Four letter codes refer to GPS station names. Stations set-up or first measured in 2002 are marked with a *. For location of the stations see Figure 2-2. The 2002 and 2003 averages are with respect to 1988 values, averaged for each group (e.g., Northern, South-eastern or Central, Figure 2-3).Values in brackets are standard deviations. They are slightly higher then expected for this type of survey for instrument G-403 which is due to a smaller number of measurements.

					2002				2003	
	Station name	**Distance to Mogi Source**	**Latitude**	**Longitude**	**Meter G-403**	**Meter G-513**			**Meter G-403**	**Meter G-513**
					Campaign 1	Campaign 1	Campaign 2	Avg. G-513		
1	NE84011 = DYNG *	6.220 km	N65º03′22.84″	W016º39′05.79″	23.539 (21)	23.579 (-)	23.600 (4)	23.589 (15)	23.567 (-)	23.584 (6)
2	83/009	5.029 km	N65º03′56.5″	W016º41′07.7″	14.124 (-)	14.142 (-)	14.167 (4)	14.155 (18)	14.125 (-)	14.142 (9)
3	83001=VIKR	3.681 km	N65º04′05.8″	W016º43′26.7″	0.000 (-)	0.000 (-)	0.000 (-)		0.000 (-)	0.000 (-)
4	430 * (on levelling line)	3.631 km	N65º04′08.9″	W016º43′39.2″			0.692 (2)	0.692 (-)	0.637 (31)	0.650 (9)
5	412 (on levelling line)	2.942 km	N65º03′48.6″	W016º44′06.1″	-3.535 (-)	-3.556 (-)	-3.565 (2)	-3.560 (6)	-3.548 (4)	-3.547 (1)
6	405 (on levelling line)	2.799 km	N65º03′35.6″	W016º43′55.8″	-3.476 (5)	-3.505 (5)	-3.502 (16)	-3.503 (1)	-3.480 (37)	-3.491 (2)
7	V. Knebel (no pin)	2.332 km	N65º02′47.3″	W016º43′54.7″	-9.127 (8)	-9.150 (3)	-9.137 (10)	-9.144 (9)	-9.120 (1)	-9.103 (3)
8	IV-16 (no pin)	2.907 km	N65º02′49.4″	W016º43′10.9″			-3.035 (7)	-3.035 (-)	-3.059 (-)	-3.015 (8)
9	D-18 = BATS	2.941 km	N65º02′36.9″	W016º43′08.8″	-0.207 (-)	-0.170 (-)	-0.180 (15)	-0.175 (7)	-0.235 (-)	-0.174 (8)
10	NE02005 = MASK *	0.721 km	N65º02′48.2″	W016º45′58.4″	-14.707 (32)	-14.755 (11)	-14.757 (7)	-14.756 (1)	-14.757 (13)	-14.779 (7)
11	NE02006 *	0.370 km	N65º02′32.9″	W016º46′52.6″	-15.455 (48)	-15.478 (10)	-15.478 (16)	-15.478 (0)	-15.466 (37)	-15.490 (9)
12	NE82005 = OLAF	0.385 km	N65º02′32.6″	W016º46′58.1″	-15.391 (-)	-15.430 (14)	-15.439 (9)	-15.434 (6)	-15.400 (5)	-15.432 (6)
13	D-19	0.455 km	N65º02′30.3″	W016º46′58.0″	-15.185 (11)	-15.217 (7)	-15.207 (12)	-15.212 (8)	-15.173 (1)	-15.209 (7)
				Avg.STD	(20)			(7)	(16)	(6)

We choose to use a spherical source, rather then for instance an ellipsoid model (Battaglia et al., 2003), as it fits well the geodetic data. More complicated models have not been tested. For a net gravity change of -115 μGal at the centre of the caldera (r = 406 m) and a source depth of 3000 m, the minimum net mass decrease is 1.6 x 10^{11} kg.

Utilisation of the Mogi model allows estimation of several volumes. The first is the integrated volume of vertical surface displacement or the volume change of the volcanic edifice, ΔV_e. Then there is the volume change of the underlying magma chamber, or the volume change of the Mogi source itself, ΔV_{ch}. If we assume a Poisson's ratio of 0.25, then ΔV_e = (3/2) x ΔV_{ch}. The volume of magma flowing to or from a magma chamber, ΔV_m, is not necessarily the same as ΔV_{ch} because of inelastic effects in the magma chamber. For example, if magma leaves a magma chamber, then magma remaining in it can expand to accommodate some of the magma removal. These effects and volume relations are discussed by Delany and McTigue (1994) and Johnson et al. (2000).

The volume change of the volcanic edifice (integrated surface subsidence), ΔV_e, can be calculated from the deformation data assuming a Mogi model (Mogi, 1958) :

$$\Delta V_e = 2\pi\Delta h \frac{(r^2 + d^2)^{3/2}}{d} \qquad \text{(eq. 2-3)}$$

where Δh is the total subsidence at the central stations from 1988 to 2003 relative to station 83001 (-0.46 m), d is the depth to the source (3000 m) and r is the horizontal distance to the source (406 m). ΔV_e is therefore calculated to be -0.027 km^3. The corresponding sub-surface geometric volume change of the Mogi source (ΔV_{ch}) is then two thirds of the surface deflation volume, which is -0.018 km^3. The volume change can be explained by cooling and solidification and/or magma drainage although it is impossible to distinguish between the two on the basis of deformation data alone. If magma drainage is the only process, then the volume of magma flowing from the

shallow chamber can be larger than 0.018 km^3, because of inelastic effects in the magma chamber. The micro-gravity data (using equation 2-1 and our observations) constrain the net mass decrease to be 1.6 x 10^{11} kg from 1988 to 2003. Since the geometric volume change of the Mogi Source (ΔV_{ch}) is caused by a combination of at least two processes, cooling/contraction and magma drainage, a simple relationship between the calculated mass and volume change does not exist.

Assuming a density of 2700 kg/m^3 for the subsurface magma body, the mass decrease would coincide with a change in magma volume (ΔV_m) of -0.06 km^3 (volume of magma flowing away from the magma chamber). Comparing this value with the calculated geometric volume change of the Mogi source (ΔV_{ch}) we find that the magma drainage volume is actually three times larger than the Mogi source volume. The variation in chamber pressure accompanying magma drainage e.g. depressurization, produces volumetric decompression of stored magma in the Mogi source (Johnson, 1992; Johnson et al., 2000). The cumulative effect of this decompression amounts to a significant net volume change of the stored magma. Drainage of magma, ΔV_m, is accommodated by a combination of reduction of the chamber size, ΔV_{ch}, and decompression of the stored magma. The observed ΔV_{ch} to ΔV_m ratio of 0.3 indicates that 30% of the volume of magma drained from the chamber is accommodated by magma chamber reduction measurable as deflation at the surface while the remaining 70% is accommodated by decompression of stored reservoir magma. These values compare well to those reported by Johnson (1992) for Pu'u 'Ō'ō on Kilauea.

There is a net micro-gravity increase at the south-eastern stations of 17 ± 9 μGal from 1988 to 2003 (Table 2-3). This could reflect a sub-surface mass increase that was modelled by Rymer and Trygvasson (1993) as a dyke intrusion for the period 1988-1991. From the gravity data trends, it is clear that the south-eastern stations are influenced by processes which do not affect the rest of the caldera. Deformation data

from InSAR and GPS, show a similar anomaly in this area (C. Pagli, E. Sturkell personal communication 2004). The area is subject to hydrothermal activity e.g., in the proximity of Víti crater, which is filled with warm water.

For the northern stations, there is no significant net micro-gravity change for the period 1988-2003. The northern stations are located close to the reference station 83001, which also lies in the deformation zone. This means that if micro-gravity changes occur at the northern stations they will be masked by deformation at the reference station. The observed net micro-gravity decrease of 2 μGal falls within error boundaries. It may be that there is a real (minor) gravity increase at these stations, but more data are required to evaluate this fully.

2.5 Gravity gradients

A plot of gravity versus height change data, for calderas in a state of unrest, shows an inverse correlation (Rymer, 1996). The measured Free-Air Gradient at Askja ranges from -240 to -360 μGal/m. The Bouguer Corrected Free Air Gradient (BCFAG) ranges from -181 to -272 μGal/m for a point source and from -127 to -247 μGal/m for a slab source, assuming an average density of 2700 kg/m^3 and the measured range of the FAG (Gottsmann and Rymer, 2002). It is important to use an accurate estimate for the source density in the calculation. The source density for Askja caldera was re-calculated following the method described in Gottsmann and Rymer (2003) but results were comparable to the previously used (Rymer and Tryggvason, 1993) values of 2700 kg/m^3.

Deviations of data points from the gradients can be interpreted in terms of subsurface processes. Magma intrusion/drainage, (de)vesiculation or void filling/creation can cause changes in density. Magma intrusion/drainage, (de)vesiculation or rise/fall in water table can explain changes in mass. Of most interest

is the area between the FAG and the BCFAG, where there is a mass decrease and density increase during deflation (Williams-Jones and Rymer, 2002).

Gottsmann and Rymer (2002) interpreted gravity-height data from Askja caldera with the use of a $\Delta g/\Delta h$ diagram (Figure 2-4). Since they used the underestimated deformation values from Rymer and Trygvasson (1993), we have recalculated the gradients here using the revised deformation values. Gradients for the central area plot below, instead of above, the BCFAG after re-calculation (Figure 2-4). Data plotting in this part of the diagram imply sub-surface mass decrease which we interpret as magma drainage. The data from the south-eastern stations can not be interpreted using a $\Delta g/\Delta h$ diagram because accurate deformation data for the area do not exist. At the northern stations, the small magnitude of deformation limits the use of a $\Delta g/\Delta h$ diagram (Gottsmann et al., 2003).

None of the data plot within the critical region between the FAG and the BCFAG. Following the roof collapse theory proposed by Gottsmann et al. (2002), this implies there is no immediate danger for another caldera collapse.

2.6 Discussion

Extensive ground-deformation monitoring shows that Askja has been deflating since at least 1983. In the following, we will incorporate the micro-gravity data and discuss the possible sources and processes responsible for this deflation.

Cooling and contraction can cause deflation as a result of degassing and crystallisation of the magma (Sigmundsson et al., 1997). Historic lavas at Askja, however, have all been aphyric (Óskarsson et al., 1982) suggesting that there is no large volume of ponded magma crystallising prior to an eruption. Nevertheless, some crystallisation may occur in the shallow chamber and this might be responsible for a small part of the deflation. Cooling and contraction are processes which do not involve

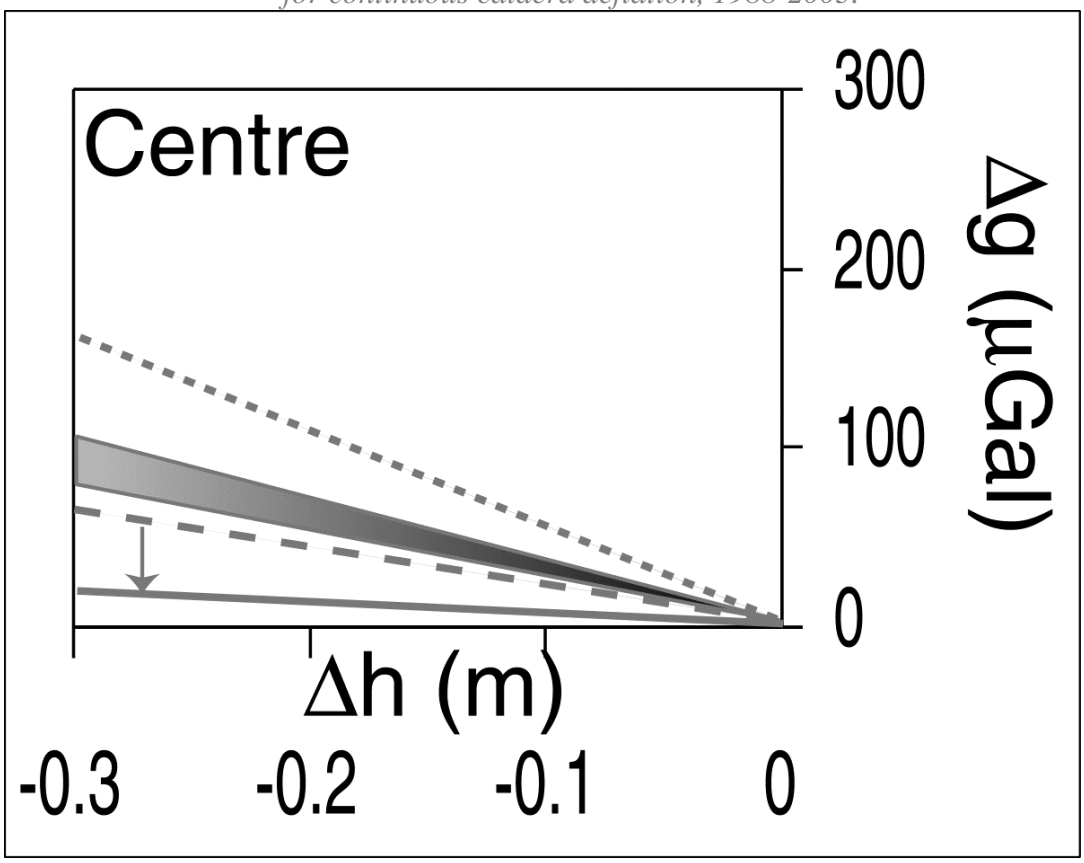

Figure 2-4 Gravity/height gradients at Askja, displayed in a Δg/Δh diagram. Deformation data show the area has been deflating (negative Δh), while the gravity has increased (positive Δg). The shaded area depicts the area between the FAG (upper boundary) and the BCFAG (lower boundary). Values for the FAG have been measured in the field. The dotted line depicts the gradient presented by Gottsmann and Rymer (2002), the dashed line the re-calculated value for the period 1988-91. The solid line shows the value calculated for the period 1988-2003. See text for discussion.

mass changes, only volume changes, thus if they were the only processes responsible for deflation, the micro-gravity data would follow the trend predicted with the measured FAG, e.g., the net gravity would be zero. While it is likely that cooling and contraction occurs, there must be another significant process to explain the observed deflation.

Part of the deformation network is located on the 1961 lava flow. Lava flows can continue to compact for tens of years after they have been erupted (Briole et al., 1997) and compaction of the flow could therefore have been partly responsible for the observed deflation. However, caldera unrest and lava flow compaction should not be confused. The levelling line is situated on the 1961 lava flow, and some deformation was expected due to the cooling of that flow. Levelling results show that the source of deformation is much deeper than just within the new lava and that deflation is therefore not caused by compaction (Tryggvason, 1989b). Furthermore, alternating periods of deflation and inflation from 1966 to 1972 indicate there must be a different mechanism that, unlike compaction, is reversible.

Magma movement can explain part of the observed deflation. The process of magma movement does involve a mass change which fits well with the gravity data. We have calculated that a minimum mass decrease of 1.6×10^{11} kg occurred beneath the central part of the caldera between 1988 and 2003. Assuming a magma density of 2700 kg/m^3, and assuming that the mass decrease is a constant ongoing process, 0.125 m^3/s (1 m^3 per 8 seconds) must have drained from 1988 to 2003. The question remains: where does this magma go? Magma can rise to the surface where it is likely to erupt; it can drain laterally into the volcanic rift zone or perhaps even drain to deeper levels.

As there has not been an eruption at Askja since 1961, the magma has clearly not reached the surface. Part of it may have entered into a shallow dyke system. A conventional idea is that magma drains into the rift zone, more specifically into the fissures in the brittle part of the crust. However if this were the case, one would expect

to see some sign of this in the form of seismic tremors, earthquake swarms, a rapid change in deflation rate or surface fractures. Lack of these suggests that the drained magma may not be moving in the brittle crust of the Askja fissure swarm (Sturkell and Sigmundsson, 2000). Rather un-degassed magma may be draining to deeper levels.

Askja is located above an extensional regime with an average full spreading rate of ~1.97 cm/yr (Camitz et al., 1995; DeMets et al., 1994). The extension of the ductile part of the crust will facilitate drainage from the shallow magma chamber to deeper levels. Modelling of GPS, levelling and tilt data suggest the existence of a deeper magma source at ~16.2 km (Sturkell et al., 2004-submitted). The crust beneath Askja is approximately 30 km thick and the brittle-ductile transition is thought to be at ~7 km (Foulger et al., 2003). This suggests that the shallow magma chamber is situated in the brittle part of the crust and the deeper seated magma chamber in the ductile part. At present it is difficult to constrain the diverse models further, but further observations may lead to more refined interpretation in the future.

Evolution of the gradients can give considerable information about future activity (Gottsmann and Rymer, 2002; Rymer and Williams-Jones, 2000). The centre stations measured at Askja show a change from a steeper gradient to a less steep gradient (Figure 2-4), suggesting more sub-surface mass changes with time, since the gradient is moving away from the FAG and BCFAG. This may be interpreted in terms of an increasing rate of drainage. The rate of deflation, however, is decreasing according to the levelling data (Sturkell and Sigmundsson, 2000). This highlights the observation made earlier, that there is not a simple relationship between the observed ground deformation at the surface and the mass decrease estimated from the micro-gravity data as the latter suggests the underlying processes are continuing. We envisage the drainage as an ongoing continuous process, with a variable rate through time, which is

superimposed on other processes, such as insignificant water table variations and cooling and contraction within the magma chamber.

Clearly a more detailed interpretation is possible when integrated micro-gravity and high quality deformation data are used, as opposed to either technique used in isolation.

2.7 Conclusions

The micro-gravity and ground-deformation data used in this study result from extensive surveys conducted between 1988 and 2003. Even though the use of micro-gravity surveys is sometimes thought of as controversial because of the low signal to noise, e.g., error ratio, this study has shown that its interpretation, together with geodetic crustal deformation studies, can be crucial to the understanding of a volcanic system.

Previously, analysis of deformation data (GPS, precise levelling, dry tilt) at Askja led to the conclusion that the volcano is subsiding, but the exact cause of the subsidence remained uncertain. By combining micro-gravity data with ground-deformation data we can determine the most likely cause. Our data show a net micro-gravity decrease of 115 μGal from 1988 to 2003 in the centre of the caldera, which can only be interpreted as a sub-surface mass decrease. Integration of the micro-gravity data results in a minimum value for this mass decrease of 1.6×10^{11} kg. Surface deformation at Askja caldera can therefore no longer solely be attributed to cooling and contraction as we now know a process involving mass change is responsible for surface deformation.

The most likely explanation for this mass decrease is magma drainage. Recent geodetic modelling shows a Mogi model with two point sources at 3 and 16.2 km depth fits the data best. We envisage that extension of the ductile part of the crust facilitates drainage from the shallow magma chamber to the deeper levels. We conclude that the

surface deformation observed at Askja results from a combination of cooling and contraction and drainage of magma. The potential of the study of gravity–height gradients in volcanology has only just begun to be realised and we anticipate a wealth of new information will arise in the near future with this approach.

2.8 Acknowledgements

This work was supported by The Geological Society, London and an Open University studentship. H.R.'s work on this project was supported by the Royal Society. We would like to thank all the people that have participated in collection of data and discussions, especially Halldór Ólafsson, Corinne Locke, John Cassidy and Andrew J. Ball. F.S.'s work on this project has been supported by the Retina project (EVG1-CT-00046). The geodetic work on this project was supported by a grant from the Icelandic Research Council RANNÍS. An earlier version of the manuscript was greatly improved by discussion with Glyn Williams-Jones. We thank Maurizio Bonafede and an anonymous referee for useful reviews.

2.9 References

Battaglia, M., Segall, P. and Roberts, C., 2003. The mechanics of unrest at Long Valley caldera, California. 2. Constraining the nature of the source using geodetic and micro-gravity data. Journal of Volcanology and Geothermal Research, 127: 219-245.

Berrino, G., 1994. Gravity changes induced by height-mass variations at the Campi Flegrei caldera. Journal of Volcanology and Geothermal Research, 61(3-4): 293-309.

Bonafede, M. and Mazzanti, M., 1998. Modelling gravity variations consistent with ground deformation in the Campi Flegrei caldera (Italy). Journal of Volcanology and Geothermal Research, 81(1-2): 137-157.

Briole, P., Massonnet, D. and Delacourt, C., 1997. Post-eruptive deformation associated with the 1986-87 and 1989 lava flows of Etna detected by radar interferometry. Geophysical Research Letters, 24(1): 37-40.

Brown, G.C., Everett, S.P., Rymer, H., McGarvie, D.W. and Foster, I., 1991. New Light on Caldera Evolution - Askja, Iceland. Geology, 19(4): 352-355.

Camitz, J. et al., 1995. Plate boundary deformation and continuing deflation of the Askja volcano, North Iceland, determined with GPS, 1987-1993. Bulletin of Volcanology, 57(2): 136-145.

Carbone, D. and Rymer, H., 1999. Calibration shifts in a LaCoste-and-Romberg gravimeter: comparison with a Scintrex CG-3M. Geophysical Prospecting, 47(1): 73-83.

Delany, P.T. and McTigue, D.F., 1994. Volume of magma accumulation or withdrawal estimated from surface uplift or subsidence, with application to the 1960 collapse of Kilauea volcano, Bull. Volcanol., 56, 417-424

DeMets, C., Gordon, R.G., Argus, D.F. and Stein, S., 1994. Effect of recent revisions to the geomagnetic reversal time scale on estimates of current plate motions. Geophysical Research Letters, 21(20): 2191-2194.

Foulger, G., Du, Z. and Julian, B.R., 2003. Icelandic-type crust. Geophysical Journal International, 155: 567-590.

Franzson, H., Gudlaugsson, S. and Fridleifsson, G., 2001. Petrophysical properties of Icelandic Rocks. Proceedings of the 6th Nordic Symposium on Petrophysics, Trondheim, Norway.

Gottsmann, J., Berrino, G., Rymer, H. and Williams-Jones, G., 2003. Hazard assessment during caldera unrest at the Campi Flegrei, Italy: a contribution from gravity-height gradients. Earth and Planetary Science Letters, 211: 295-309.

Gottsmann, J. and Rymer, H., 2002. Deflation during caldera unrest: constraints on subsurface processes and hazard prediction from gravity -height data. Bulletin of Volcanology, 64(5): 338-348.

Johnson, D., 1987. Chapter 47: Elastic and inelastic magma storage at Kilauea volcano. Volcanism in Hawaii, 2, 1297-1306 pp.

Johnson, D.J., 1992. Dynamics of magma storage in the summit reservoir of Kilauea volcano, Hawaii. Journal of Geophysical Research, 97(B2): 1807-1820.

Johnson, D.J., Sigmundsson, F. and Delaney, P.T., 2000. Comment on 'Volume of magma accumulation or withdrawal estimated from surface uplift or subsidence, with application to the 1960 collapse of Kilauea volcano' by P.T. Delaney and D.F. McTigue. Bulletin of Volcanology, 61: 491-493.

Locke, C.A., Rymer, H. and Cassidy, J., 2003. Magma transfer processes at persistently active volcanoes: insights from gravity observations. Journal of Volcanology and Geothermal Research, 127: 73-86.

Mogi, K., 1958. Relations between the eruptions of various volcanoes and the deformations of the ground surfaces around them. Bulletin of the earthquake research institute, 36: 99-134.

Newhall, C.G. and Dzurisin, D., 1988. Historical unrest at large calderas of the world. U.S. Geol.Surv. Bull. US Geol Surv, Reston, Virginia, 1855 pp.

Óskarsson, N., Sigvaldason, G.E. and Steinthórsson, S., 1982. A dynamic model of rift zone petrogenesis and the regional petrology of Iceland. Journal of Petrology, 23(1): 28-74.

Rymer, H., 1989. A contribution to precision microgravity data-analysis using Lacoste and Romberg gravity meters. Geophysical Journal, 97(2): 311-322.

Rymer, H., 1996. Microgravity monitoring. Monitoring and mitigation of volcano hazards. Springer-Verslag, Berlin, 169-198 pp.

Rymer, H., Cassidy, J., Locke, C.A. and Sigmundsson, F., 1998a. Post-eruptive gravity changes from 1990 to 1996 at Krafla volcano, Iceland. Journal of Volcanology and Geothermal Research, 87(1-4): 141-149.

Rymer, H., de Vries, B.V., Stix, J. and Williams-Jones, G., 1998b. Pit crater structure and processes governing persistent activity at Masaya Volcano, Nicaragua. Bulletin of Volcanology, 59(5): 345-355.

Rymer, H. and Tryggvason, E., 1993. Gravity and elevation changes at Askja, Iceland. Bulletin of Volcanology, 55(5): 362-371.

Rymer, H. and Williams-Jones, G., 2000. Volcanic eruption prediction: Magma chamber physics from gravity and deformation measurements. Geophysical Research Letters, 27(16): 2389-2392.

Sigmundsson, F., Vadon, H. and Massonnet, D., 1997. Readjustment of the Krafla spreading segment to crustal rifting measured by satellite radar interferometry. Geophysical Research Letters, 24(15): 1843-1846.

Sigurdsson, H. and Sparks, R.S.J., 1978. Rifting episode in north Iceland in 1874-1875 and the eruption of Askja and Sveinagja. Bulletin of Volcanology, 41: 149-167.

Sigvaldason, G.E., 2002. Volcanic and tectonic processes coinciding with glaciation and crustal rebound: an early Holocene rhyolitic eruption in the Dyngjufjoll volcanic centre and the formation of the Askja caldera, north Iceland. Bulletin of Volcanology, 64(3-4): 192-205.

Sturkell, E. and Sigmundsson, F., 2000. Continuous deflation of the Askja caldera, Iceland, during the 1983-1998 noneruptive period. Journal of Geophysical Research-Solid Earth, 105(B11): 25671-25684.

Sturkell, E., Sigmundsson, F. and Slunga, R., 2004 – submitted to Bulletin of Volcanology. 1983-2003 decaying rate of deflation at Askja caldera: Pressure decrease in an extensive magma plumbing system at a spreading plate boundary.

Tryggvason, E., 1989a. Ground deformation in Askja, Iceland: its source and possible relation to flow of the mantle plume. Journal of Volcanology and Geothermal Research, 39: 61-71.

Tryggvason, E., 1989b. Measurement of ground deformation in Askja 1966 to 1989. Nordic Volcanological Institute Report 8904.

Williams-Jones, G. and Rymer, H., 2002. Detecting volcanic eruption precursors: a new method using gravity and deformation measurements. Journal of Volcanology and Geothermal Research, 113: 379-389.

Williams-Jones, G., Rymer, H. and Rothery, D.A., 2003. Gravity changes and passive SO_2 degassing at the Masaya caldera complex, Nicaragua. Journal of Volcanology and Geothermal Research, 123: 137-160.

Chapter 3: Satellite Radar Interferometry 1993-1999 suggests deep accumulation of magma near the crust-mantle boundary at the Krafla volcanic system, Iceland

This Chapter was published in Geophysical Research Letters, volume 31, issue 13, July 2004. For discussion of the DIAPASON software used during the processing of the InSAR images and a full list of image combinations acquired see Appendix D.

3.1 Abstract

Deep magma accumulation near the crust-mantle boundary (21 km depth) at the Krafla volcanic system is suggested from InSAR observations. A best fit model, applied to four interferograms covering 1993-1999, comprises an opening dike, representing plate spreading and post-rifting deformation, and two Mogi sources. A Mogi source deflating at a rate of ~ 0.3 x 10^6 m^3/yr coincides with the shallow Krafla magma chamber while a deeper inflating Mogi source, further north, at 21 km depth, inflates at a rate of ~ 26 x 10^6 m^3/yr. The inflating source is at or near the crust-mantle boundary as identified by seismic studies and is interpreted as accumulating magma.

3.2 Introduction

Magma accumulation beneath volcanic areas has been studied extensively with various geodetic techniques. Most of these studies locate magma sources at depths within the brittle crust. Only few studies discuss the existence of deeper magma reservoirs. For Krafla volcano, Tryggvason (1986) concluded, from geodetic data spanning the 1984 eruption, that a vertically stacked series of chambers exists at depths of 2.6 km, less than 10 km and deeper than 20 km. At Askja volcano, N-Iceland, 1993-

1998 GPS data has been used to infer the location of two magma sources, at 3 and 16 km depth (Sturkell et al., submitted, 2004). In this paper we discuss new analysis of Interferometric Synthetic Aperture Radar (InSAR) images from the Krafla area that can be interpreted in terms of magma accumulation at the crust-mantle boundary at 21 km depth.

The Krafla volcanic system in N-Iceland (Figure 3-1) consists of a central volcano which encompasses a 10 by 7 km wide caldera, mostly filled by younger lavas. The system is transected by an approximately 100 km long fissure swarm striking N010°E. Detailed seismic studies have been conducted in the Krafla area, e.g. by Brandsdóttir et al. (1997) and Menke et al. (1998). The crust-mantle boundary underneath Krafla has an asymmetric dome shape. Good seismic reflection originates at the Moho discontinuity. The minimum boundary depth of ~19 km is reached 5 km east of the caldera centre. This depth increases asymmetrically in all directions, at a rate of 1-2 km for each 10 km distance on a north-south profile next to the caldera. Activity at the Krafla volcanic system is characterised by rifting episodes separated by long periods of dormancy. Two historical rifting episodes occurred in 1724-1729 and 1975-1984. During the most recent episode, 9 of 20 deflation/inflation cycles were accompanied by basaltic fissure eruptions in the Krafla fissure swarm.

Geodetic data show that the area around the central volcano was deflating at 5 cm/yr in the 1989-1992 period (Tryggvason, 1994) decaying to 2.4 cm/yr from 1992 to 1995 (Sigmundsson et al., 1997). A shallow Mogi point source can explain this deflation and its location has been well constrained by several studies at 65.72°N, 16.80°W and 2.7 km depth (Árnadóttir et al., 1998; Sigmundsson et al., 1997; Tryggvason, 1986; Tryggvason, 1994). Krafla is located on the Mid-Atlantic Ridge where the average full spreading rate is ~1.9 cm/yr. GPS measurements in north Iceland have, however, revealed a full spreading rate of 6 cm/yr from 1987 to 1990 in the Krafla

area, decaying to 4 cm/yr from 1990 to 1992. This higher rate is attributed to post-rifting relaxation of stresses in the crust after the 1975-1984 rifting episode, and has been modelled e.g. by Foulger et al. (1992) and Pollitz and Sacks (1996).

Analysis of InSAR images acquired by ERS1 and ERS2, has proven a valuable tool when studying the ongoing deformation at Krafla (Henriot et al., 2001; Sigmundsson et al., 1997). Previous work concentrated on the readjustment of the Krafla spreading segment e.g., crustal deformation after the last rifting episode. In this paper we analyse interferograms covering the Krafla region from 1993 to 1999. A signal previously unaccounted for, associated with small but widespread uplift, is attributed to deep accumulation of magma. An alternative model, attributing the signal to post-rifting relaxation is considered less likely.

3.3 Radar interferometric data

To calculate interferometric images, we used the PRISME/DIAPASON software developed by CNES. Twelve SAR images from ERS1 and ERS2, track 9, frame 2277 acquired in the period 1993-2000, allowed the formation of twelve interferograms, with reasonable coherence. Four of these, spanning from 2 to 6 years, were selected for modelling (Table 3-1 and Figure 3-2). A Digital Elevation Map from the Icelandic Land Survey and postcomputed orbits from the European Space Agency were used to correct for topographic effects. Residual orbital fringes were removed by subtracting linear range-change gradients.

Four interferograms (Table 3-1, Figure 3-2 a-d) are analysed here. Pair-wise comparison (Massonnet and Feigl, 1998) was used to confirm deformation signals and discriminate them from atmospheric and topographic artifacts. Three different deformation signals can be distinguished: a linear fringe pattern aligned along the rift

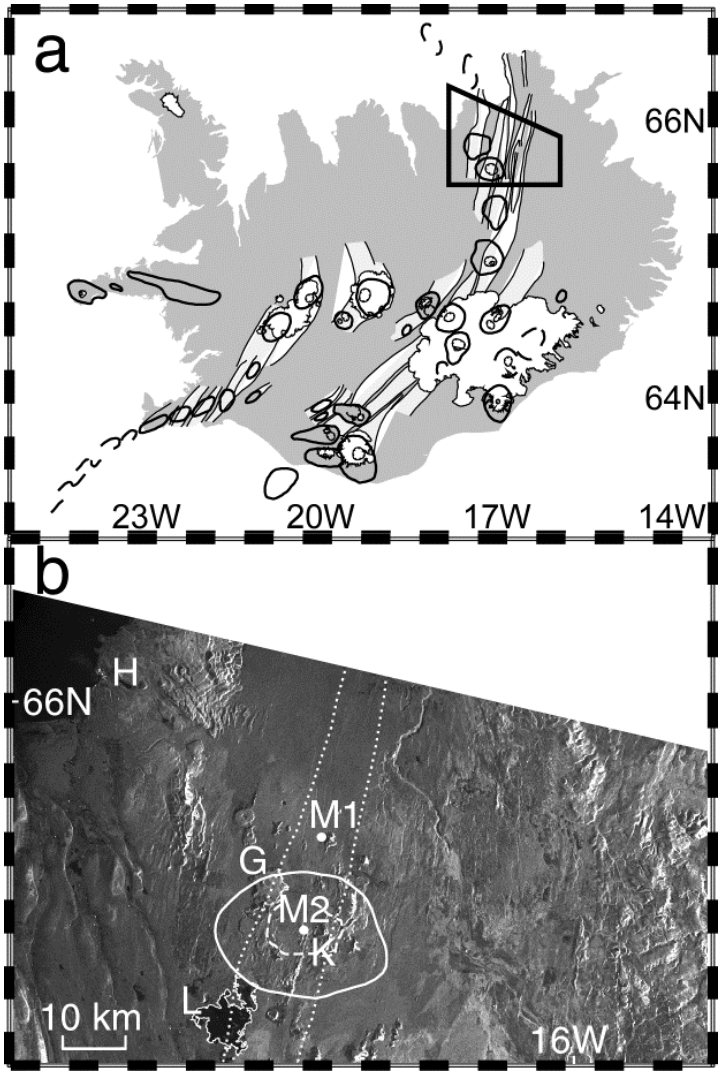

Figure 3-1 a) Location of the Krafla area in Iceland. Overview map shows volcanic systems, plate boundary, calderas and icecaps (Einarsson, 1991). The studied area, track 9, frame 2277 is outlined in black. b) A SAR amplitude image of frame 2277 showing the town of Husavik (H), lake Mývatn (L), the Krafla Rift Zone (dotted), the outline of the Krafla central volcano (solid white line), the caldera (white dashed line) and the location of the model sources (M1&M2).

axis, localized concentric fringes in the centre of the Krafla caldera and a widespread concentric fringe pattern centered 15 km north of Krafla. Each phase fringe represents a range change of 28 mm. Small atmospheric artifacts are present in the upper left corner of Figure 3-2d.

The linear fringe pattern is at least 20 km long, striking N10°E and most likely shows the combined effect of plate spreading and post-rifting relaxation. The concentric fringes in the centre of the caldera cover an area 3 km across. The increase in range suggests deflation in this area, amounting to ~5 cm in the 1993-1999 interferogram. Both these features have been previously described (Henriot et al., 2001; Sigmundsson et al., 1997). The widespread concentric fringes 15 km north of the Krafla centre (8 cm in the 1993-1999 interferogram) have, however, not been identified before. The signal shows a decrease in range, representing inflation, and covers a roughly circular area 50 km across.

3.4 Modelling

Processes contributing to the widespread uplift signal may include post-rifting stress relaxation and/or deep accumulation of magma. To evaluate the effect of post-rifting relaxation, the models of Pollitz and Sacks (1996) were considered. The average 1992-2000 velocity field was calculated (F. Pollitz, pers. comm., 2004) using an earth model with one of the "acceptable" viscosity structures of Pollitz and Sacks (1996) (with $\eta_c = 2\times10^{19}$ Pa s, and $\eta_m = 4\times10^{18}$ Pa s), and considering rifting along their south and central Krafla segments (see their Figure 10). The results predict horizontal postrifting opening rates of ~1cm/yr on both sides of the rift and a maximum uplift of ~2 mm/yr (F. Pollitz, pers. comm., 2004). It represents only ~15% of the observed inflation rate and this model can therefore not entirely explain the InSAR observations. Utilizing elastic deformation models, we explore whether the widespread uplift can be

Table 3-1 Best fit model parameters of displayed interferograms. The M1 Mogi source is located at 65.83ºN, 16.73ºW at 21 km depth, M2 is located at 65.72ºN, 16.78ºW at 2.4 km depth. The modelled dislocation has a length of 53 km and a width of 85 km; the strike is N11ºE and the dip 78ºW. The centre of the upper edge of the dislocation is located at 65.64ºN, 16.84 ºW at 4.6 km depth. Strike-slip and dip-slip components are fixed at 0 cm. h_a is the altitude of ambiguity of the interferograms.

					Dislocation		Inflating Mogi (M1)		Deflating Mogi (M2)	
Interferogram	h_a [m]	Timespan [year]	Timespan [days]	RMS [cm]	Total opening [cm]	Opening [cm/yr]	Volume [$10^6 m^3$]	Volume [$10^6 m^3$/yr]	Volume [$10^6 m^3$]	Volume [$10^6 m^3$/yr]
11677_22408	-369	93-99	2190	0.63	20.6	3.4	146.5	24.4	-1.8	-0.29
01867_17899	289	95-98	1119	0.79	8.0	2.6	94.5	30.8	-1.4	-0.47
6877_17899	115	96-98	770	0.97*	5.0	2.4	52.1	24.7	-0.9	-0.41
6376_22408	374	96-99	1120	0.74	8.4	2.7	72.4	23.6	-0.2	-0.07
					Average	2.8		25.9		-0.31
					Stdev	0.4		3.3		0.18

* These parameters are the outcome of the simulated annealing algorithm. The derivative based method did in this case not improve the result.

attributed to deep magma accumulation. These are simple representations of the short-term response to magma accumulation that takes place well below the brittle-ductile transition, within a viscoelastic regime. Because of its anticipated small effect, the contribution of post-rifting adjustment to the observed uplift was not considered in these models.

The InSAR data were unwrapped and the data size was reduced using a two-dimensional quad-tree partitioning algorithm (Jónsson et al., 2002). An inversion procedure using a simulated annealing algorithm followed by a derivative based method (Cervelli et al., 2001) was then applied. Initially we modelled the observed widespread fringe pattern, assuming one inflating Mogi source in an elastic half-space (Mogi, 1958), with loose initial model bounds. The four modelled interferograms showed similar source locations, 65.87 ± 0.18 °N, 16.71 ± 0.76 °W with a depth of 21 ± 3 km. A uniformly opening sill model was also tested, but did not yield a better fit. Best results were found considering the three suggested deformation processes: two Mogi point sources and an opening dislocation aligned along the rift axis.

First we modelled the interferogram with the longest time-span (6 years), leaving all model bounds loose. It displays the strongest deformation signals and hence the best signal to noise ratio. Resulting model parameters (see caption Table 3-1) are well constrained and the model (Figure 3-2e) reduces the RMS of the data from 2.97 cm for a null-model to 0.63 cm (Figure 3-2i & Table 3-1). The parameters found for the deflating Mogi source agree with those found by previous studies (Henriot et al., 2001; Sigmundsson et al., 1997). The opening dislocation is a simplified model reproducing the effects of plate spreading and superimposed post-rifting deformation. We fix the source location parameters from the inversion of the 1993-1999 interferogram, during inversion of the other three data sets, and optimise only for the two Mogi volumes and

the opening of the dislocation source. The residual signal is less than 1 cm for all interferograms.

The results of the inversion are displayed in Figure 3-2e-h and summarized in Table 3-1. The yearly opening decays from 3.4 cm/yr from 1993 to 1999 to an average of 2.5 cm/yr from 1996 to 1999. Post-rifting relaxation is expected to decay with time. The deflating Mogi source, representing a shallow magma chamber, has a depth of 2.4 km and an average volume change of -0.31×10^6 m3/yr, corresponding to surface subsidence of 8.6 mm/yr. This subsidence can be caused by cooling/contraction of the chamber, magma drainage from the chamber or geothermal exploitation of the Krafla area (Sigmundsson et al., 1997; Rymer et al., 1998). The inflating Mogi source has a depth of 21 km and an accumulation rate of 25.9×10^6 m^3/yr, which is two magnitudes larger than the yearly volume change of the deflating Mogi source. The depth of it is close to the crust-mantle boundary where we visualise magma to be accumulating.

3.5 Discussion and conclusions

We take the relatively good fit of our simple models as an indication that magma accumulation is responsible for the widespread uplift, and suggest that post-rifting deformation and plate movements are mostly mimicked by the opening dislocation. The deep Mogi source then suggests that from 1993 to 1999 a total of ~ 0.15 km^3 magma accumulated at 21 km depth beneath the Krafla area. This volume may be a low estimate because elasticity is assumed, rather than rheological properties appropriate for ductile crust. The lower crust is likely to accommodate part of the magma accumulation by ductile flow, limiting the effect on the surface. The volume inferred to have accumulated from 1993-1999 is already a significant fraction of the 1 km^3 volume thought to have moved from a deeper source during the Krafla fires (Tryggvason, 1995).

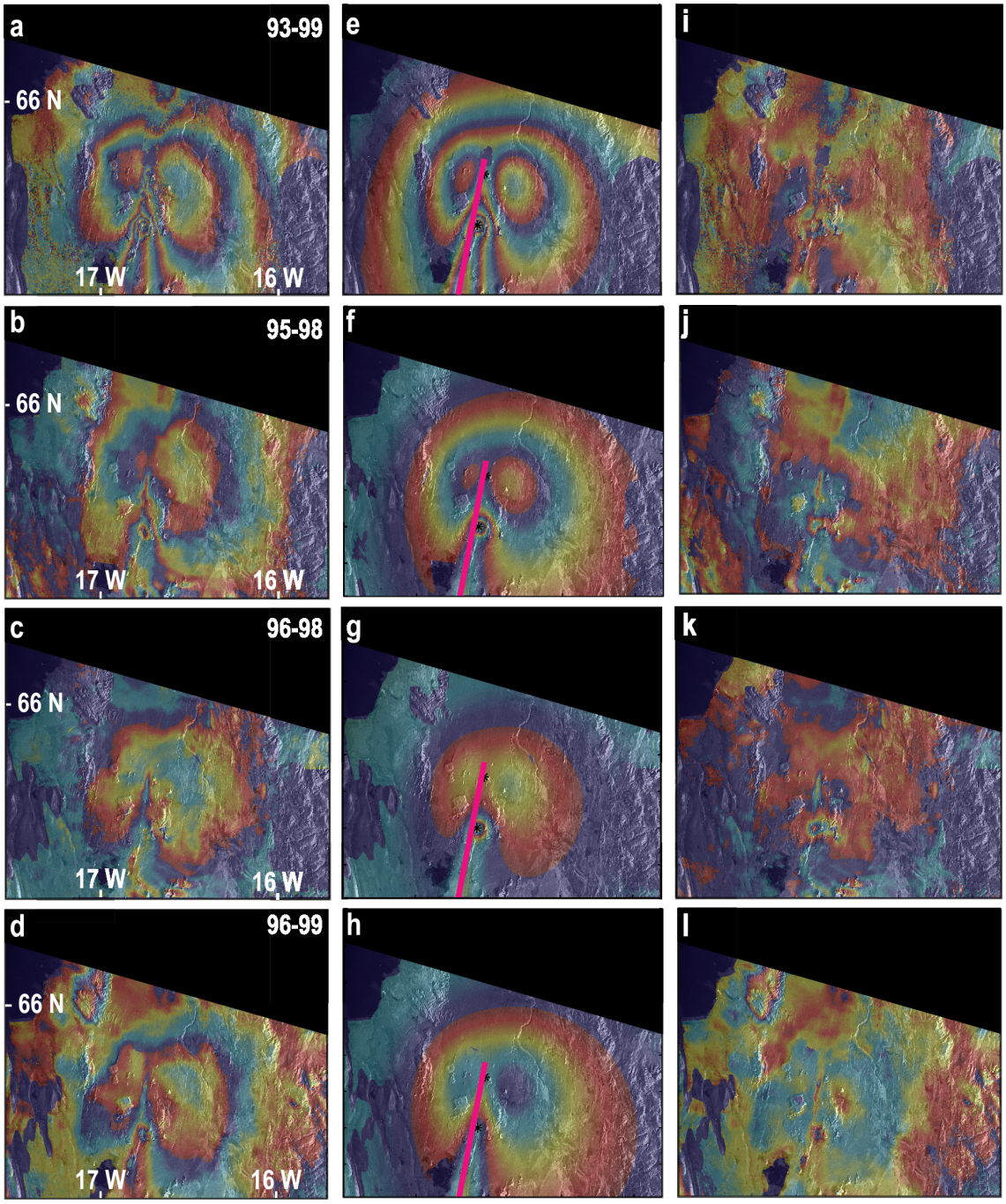

Figure 3-2 Interferograms, models and residuals draped on amplitude image for reference. Interferograms listed in Table 3-1 (panels a-d). For location of frame see outline in Figure 3-1 The best-fit models including location of the tensile dislocation (purple line) and the two Mogi sources (black stars) are displayed in panels e-h). Panels (i-l) show residuals after model subtraction.

Our results suggest accumulation of magma at deep levels under Krafla in the decades after termination of a rifting episode. We suggest that co-rifting pressure decrease of the deeper source stimulates this subsequent inflow of magma. The density contrast between the lower crust and mantle may trap magma there, regardless of the lower than average contrast of 90 ± 10 kg/m^3 (Gudmundsson, 2003). The shallowing of the Moho towards the Krafla rift axis (Brandsdóttir et al., 1997) may focus magma flow towards it. When pressure in the deep source reaches a critical value, magma migrates to the shallow magma chamber from where it can eventually erupt. This complex magma plumbing system is consistent with long periods of dormancy (200-1000 yr) between rifting events.

Our results derive from a relatively simple model. Another simple model would consider the deep magma source as a pressure source at the base of a thin elastic plate. This we consider, however, not suitable in our case as the "plate" overlying the magma source is thick (~21 km) and its lower half is viscoelastic, as well as the mantle beneath it. A more sophisticated earth model would use brittle and ductile layers which might modify the results. Another improvement would be to use existing GPS data (Völksen, 2000) to calibrate the interferograms. Further studies should also consider whether post-rifting adjustment may eventually contribute to the observed signal.

This paper demonstrates the feasibility of investigating deep accumulation of magma using InSAR, despite minimal expressions of such sources at the surface. Our observations are consistent with a deep magma source beneath Krafla, as suggested by previous tilt studies (Tryggvasson, 1986). Such deep sources may play a major role at Icelandic volcanic systems and elsewhere, and have to be considered to fully understand the dynamics of magmatic systems.

3.6 Acknowledgements

We thank Sverrir Gudmundsson for providing the unwrapping tools, Zhong Lu for providing the image filter algoritm, and Fred Pollitz for calculating the postseismic velocity field. EdZvD thanks Jean-Luc Froger for providing the first steps in working with InSAR and John Taylor for help with Figure preparation. EdZvD´s work was supported by the Peter Francis Travel Bursery. ESA provided the raw ERS SAR data, to which they hold the copyright, through Envisat grant A03-212. EU grant RETINA EVG1-CT-2001-00046 supported this project. The manuscript was improved by discussion with Dave Rothery and Hazel Rymer and reviews by Claude Jaupart and Pall Einarsson.

3.7 References

Árnadóttir, T., F. Sigmundsson, and P.T. Delaney, Sources of crustal deformation associated with the Krafla, Iceland, eruption of September 1984, *Geophys. Res. Lett.*, *25* (7), 1043-1046, 1998.

Brandsdóttir, B., W. Menke, P. Einarsson, R.S. White, and R.K. Stapels, Färoe-Iceland ridge experiment 2. Crustal structure of the Krafla central volcano, *J. Geophys. Res.*, *102* (B4), 7867-7886, 1997.

Cervelli, P., M.H. Murray, P. Segall, Y. Aoki, and T. Kato, Estimating source parameters from deformation data, with an application to the March 1997 earthquake swarm off the Izu Peninsula, Japan., *J. Geophys. Res.*, *106* (B6), 11217-11237, 2001.

Einarsson, P., and K. Saemundsson, Earthquake epicenters 1982-1985 and volcanic systems in Iceland (map), in "I Hlutarins Edli", edited by T. Sigfusson, Menningarsjodur, Reykjavik, 1987.

Foulger, G.R., C.H. Jahn, G. Seeber, P. Einarsson, B.R. Julian, and K. Heki, Post-Rifting Stress-Relaxation at the Divergent Plate Boundary in Northeast Iceland, *Nature*, *358* (6386), 488-490, 1992.

Gudmundsson, Ó. The dense root of the Iceland crust., *Earth and Planetary Science Lett.*, *206*, 427-440, 2003.

Henriot, O., T. Villemin, and F. Jouanne, Long period interferograms reveal 1992-1998 steady rate of deformation at Krafla volcano (North Iceland), *Geophys. Res. Lett.*, *28* (6), 1067-1070, 2001.

Massonnet, D., and K. Feigl, Radar interferometry and its application to changes in earth's surface, *Rev. geophys.*, *36* (4), 441-500, 1998.

Menke, W., M. West, B. Brandsdóttir, and D. Sparks, Compressional and shear velocity structure of the lithosphere in northern Iceland, *Bull. Seismol. Soc. Am.*, *88* (6), 1561-1571, 1998.

Mogi, K., Relations between the eruptions of various volcanoes and the deformations of the ground surfaces around them, *Bulletin Earthquake Res. Inst. Univ. Tokyo*, *36*, 99-134, 1958.

Pollitz, F.F., and I.S. Sacks, Viscosity structure beneath northeast Iceland, *J. Geophys. Res.*, *101* (B8), 17771-17793, 1996.

Rymer, H., J. Cassidy, C.A. Locke, and F. Sigmundsson, Post-eruptive gravity changes from 1990 to 1996 at Krafla volcano, Iceland, *J. Volc. Geotherm. Res.*, *87* (1-4), 141-149, 1998.

Sigmundsson, F., H. Vadon, and D. Massonnet, Readjustment of the Krafla spreading segment to crustal rifting measured by satellite radar interferometry, *Geophys. Res. Lett.*, *24* (15), 1843-1846, 1997.

Tryggvason, E., Multiple Magma Reservoirs in a Rift-Zone Volcano - Ground Deformation and Magma Transport During the September 1984 Eruption of Krafla, Iceland, *J. Volc. Geotherm. Res.*, *28* (1-2), 1-44, 1986.

Tryggvason, E., Surface deformation at the Krafla volcano, North Iceland, 1982-1992, *Bull. Volc.*, *56*, 98-107, 1994.

Tryggvason, E., Optical levelling tilt stations in the vicinity of Krafla and the Krafla fissure swarm. Observations 1976 to 1994., *Internal report 9505, NVI, Reykjavik, Iceland*, 1995.

Völksen, C., Die Nutzung von GPS für die Deformationanalyse in regionalen Netzen am Beispiel Islands, *PhD thesis, Universität Hannover, Germany*, 2000.

Welstead, S.T., Fractal and wavelet image compression techniques, SPIE Optical Engineering Press, Bellingham, Washington, 232 p., 1999

Chapter 4: The integration of micro-gravity and geodetic data to constrain shallow system mass changes at Krafla Volcano, N Iceland

This chapter was submitted to Bulletin of Volcanology in September 2004. It contains the results of extensive micro-gravity and geodetic surveys at the Krafla volcano and discusses the impact of water drainage by the geothermal power plant. The location of the stations is described in Appendix A and the original data are displayed in Appendix C.

4.1 Abstract.

New and previously published micro-gravity data are combined with InSAR data, precise levelling and GPS measurements to produce a model for the processes operating at Krafla volcano, 20 years after its most recent eruption. The data have been divided into two periods: from 1990 to 1995 and from 1996 to 2003 and show that the rate of deflation at Krafla is decaying exponentially. The net micro-gravity change at the centre of the caldera is shown, using the measured Free Air Gradient, to be -85 μGal for the first and -100 μGal for the second period. After consideration of the effects of water extraction by the geothermal power station within the caldera, the net gravity decreases are -73 ± 17 μGal for the first and -65 ± 17 μGal for the second period. These decreases are interpreted in terms of magma drainage. Following a Mogi point source model we calculate the mass decrease to be ~2 x 10^{10} kg/yr reflecting a drainage rate of ~0.23 m^3/s, similar to the ~0.13 m^3/s drainage rate previously found at Askja volcano, N-Iceland. Based on the evidence for deeper magma reservoirs and the similarity between the two volcanic systems, we suggest a pressure-link between Askja and Krafla at deeper levels (at the lower crust or the crust-mantle boundary). After the Krafla fires,

co-rifting pressure decrease of a deep source at Krafla stimulated the subsequent inflow of magma, eventually affecting conditions along the plate boundary in N-Iceland, as far away as Askja. We anticipate that the pressure of the deeper reservoir at Krafla will reach a critical value and eventually magma will rise from there to the shallow magma chamber, possibly initiating a new rifting episode. We have demonstrated that by examining micro-gravity and geodetic data sets, our knowledge of active volcanic systems can be significantly improved.

4.2 Introduction

The Northern Volcanic Zone north of the Vatnajokull ice cap in iceland, consists of five NNE-SSW elongated volcanic systems, Theistareykir, Krafla, Fremri-Namur, Askja, and Kverkfjöll, (Figure 4-1; inset). They are arranged en echelon along the plate boundary which is ~50-80 km wide. Each volcanic system consists of a fissure swarm transecting a central volcano.

The Krafla Volcanic system comprises a fissure swarm, which is 100 km long and ~10 km wide, more than 1000 tectonic fractures, and a central volcano (Figure 4-1). The Krafla central volcano forms a low, broad shield some 20 km in diameter with a caldera in the centre. The topographically indistinct caldera has an elliptical shape and stretches 10 km in the east-west direction and 8 km north-south. It formed during an explosive eruption in the last interglacial period about 0.1 Ma ago and has since been filled almost completely with lavas and ash (Brandsdóttir et al., 1997).

Two geothermal areas, Krafla and Námafjall (Figure 4-1) are located in the Krafla Volcanic System. Námafjall is located just south of the Krafla caldera on the eastern part of the Krafla fissure swarm. Its 3-4 km^2 surface expression is characterized by mud pools and fumaroles and three active wells, with a maximum temperature of 320˚C, which supply a 3 MW back-pressure turbine unit. The larger Krafla geothermal

area, ~ 7 km^2, is located in the centre of the caldera and is elongated in the NW-SE direction. At present, 18 wells are used to operate a 60 MW power generator and geothermal fluid temperatures reach 350 ˚C (Gudmundsson and Arnórsson, 2002).

The activity at the Krafla volcanic system is characterised by rifting episodes separated by long periods of dormancy (Árnadóttir et al., 1998). Two historical rifting episodes, the so called Mývatn and Krafla fires, occurred from 1724 to 1729 and 1975 to 1984, respectively. During the Mývatn fires, the crater Víti was formed (Figure 4-2) although most of the other activity manifested itself south of the Krafla caldera (Ewart et al., 1991). Activity resumed in 1975, when seismicity increased and deformation data suggested inflow of magma to the shallow Krafla reservoir, causing inflation, followed by rapid deflation and an initial diking event (Tryggvason, 1994). A rifting episode from 1975 to 1984 was then characterised by ~21 such cycles of which 9 culminated in basaltic fissure eruptions (Björnsson, 1985; Brandsdóttir et al., 1997). During each cycle, the reservoir pressure exceeded a critical value, reservoir walls failed, dykes were injected into the fissure swarm and rifting occurred. The largest and most voluminous eruption of this period occurred over two weeks in September 1984 during which a 8.5 km long volcanic fissure erupted a pahoehoe lava field with a total area of 24 km^2 (Rossi, 1997).

Krafla is one of the few calderas in the world (others include Askja in Iceland (Rymer and Tryggvason, 1993), Masaya in Nicaragua (Williams-Jones et al., 2003), Poas in Costa Rica (Rymer et al., 2000) and Campi Flegrei in Italy (Gottsmann et al., 2003)) with a long-term micro-gravity data set. The area has also been studied extensively using a variety of geophysical techniques (Árnadóttir et al., 1998; Sigmundsson et al., 1997; Tryggvason, 1986). Here we present Interferometric Synthetic Aperture Radar data (InSAR; 1993-1999) and micro-gravity data (1997-2003). Results of these techniques are combined to produce an integrated model for the

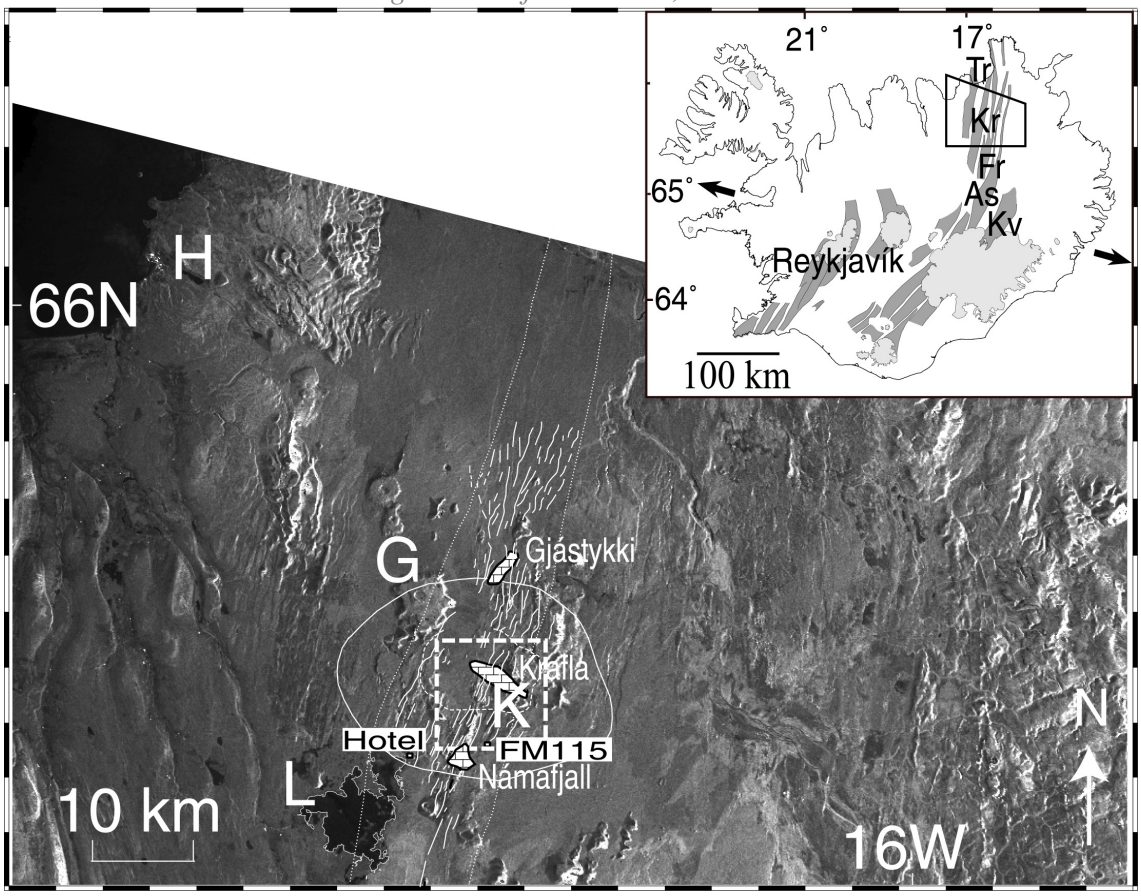

Figure 4-1 Overview of the Krafla volcanic system, inset shows location of Krafla in Iceland. The locations of the main ice caps are depicted with light grey and the volcanic zones are depicted with dark grey. The inset also shows the five NNE-SSW elongated volcanic systems of the Northern Volcanic Zone, Tr is Theystareykir, Kr is Krafla, Fr is Fremri-Namure, As is Askja and Kv is Kverkfjöll (Einarsson, 1991). The black box marked on the inset shows the area covered by the enlargement given in the main Figure. The larger Figure shows the Krafla Rift Zone (dotted), the outline of the Krafla central volcano (solid white line), the caldera (white dashed line), the geothermal areas (blocked), the town of Husavik (H), lake Mývatn (L) and Krafla mountain (K) with A SAR amplitude image for reference in the background. Note the location of micro-gravity stations Hotel and FM115. White dashed box shows outline of Figure 4-1.

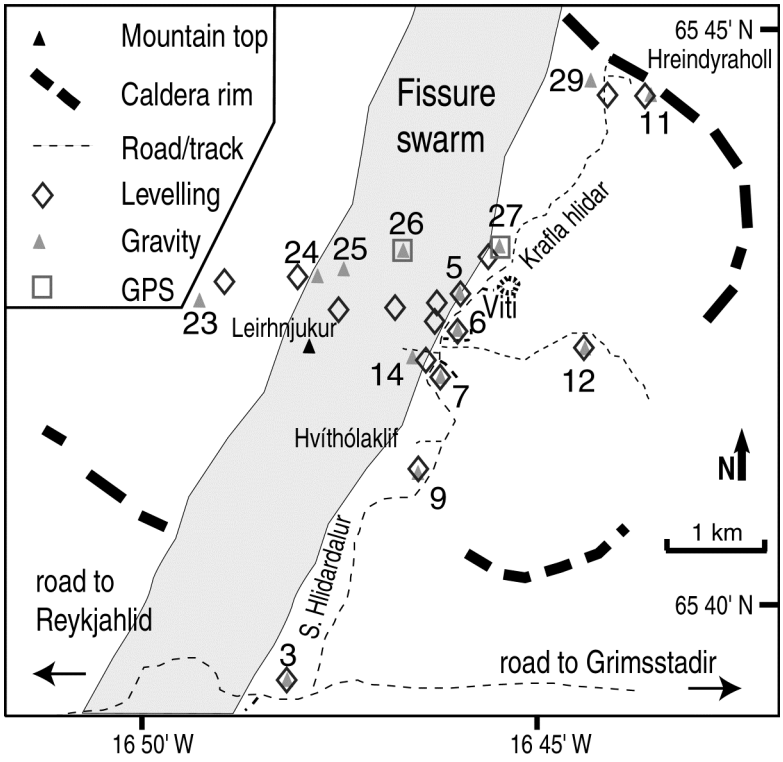

Figure 4-2 Sketch of the location of the main micro-gravity, levelling and GPS stations at Krafla. Numbers refer to station names: 3=FM115, 5=OS5595, 6=5596; 7=OS5596, 9=5599A, 11=5672, 12=OS5684, 14=OS5688, , 23=A001, 24=A002, 25=A003, 26=A004, 27=A005 and 29=A012.

the processes operating at Krafla today, 20 years after the most recent eruption.

4.3 Methods

4.3.1 Geodetic methods

Previously published and new precise levelling, Global Positioning System (GPS) and InSAR data were combined to calculate the height change at each gravity station. InSAR allows the measurement of change in range from ground to satellite at a high spatial resolution by combining pairs of Satellite Aperture Radar (SAR) images acquired at different acquisition times (Massonnet and Feigl, 1995; Massonnet and Feigl, 1998). Interferograms were produced with the use of the DIAPASON software (CNES, 2000) following an approach similar to that used by Sigmundsson et al. (1997). Topographic fringes were removed with the help of a Digital Elevation Model (DEM) from the Icelandic Geodetic Survey and orbital corrections were performed utilising post-computed orbits from the European Space Agency (ESA). Residual orbital effects were removed by subtracting a linear range-change gradient. The remainder of the processing was done using sub-sections of the complete interferograms covering the Krafla area. These sections were filtered using an algorithm developed by Z. Lu (personal communication 2002) and unwrapped using deformation tools developed by Gudmundsson et al. (2001). After unwrapping, the interferograms provide an unambiguous measure of the change in range whereas the original interferograms show deformation as fringes, each corresponding to a vertical displacement of 28 mm. The precise levelling technique measures the vertical deformation, with respect to reference station FM115, with millimetre precision (Figure 4-1). Differential GPS measurements are referred to station NE9301 and have accuracy in the vertical component of ~1-2 cm.

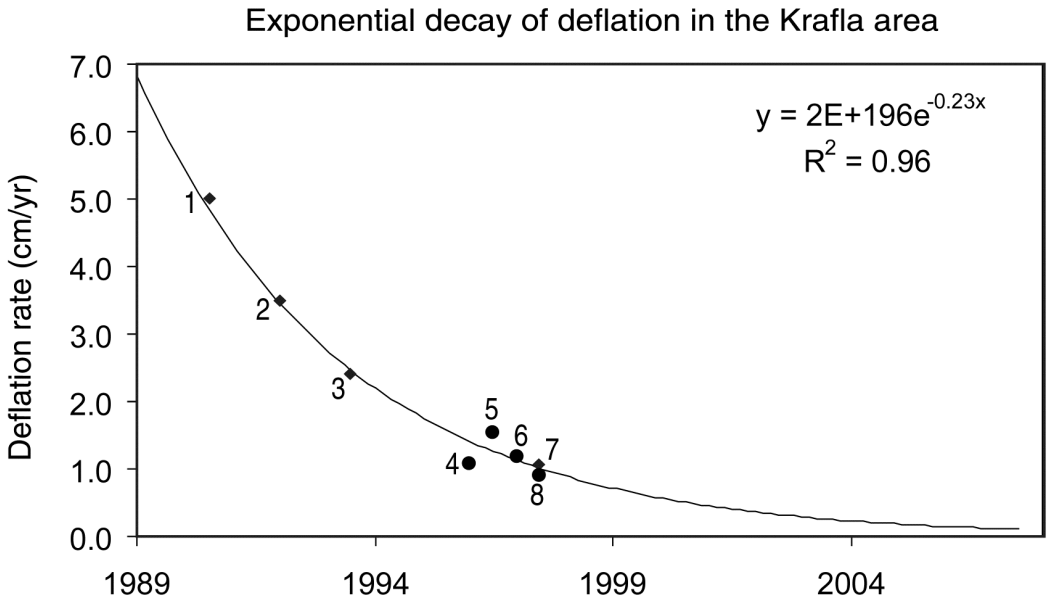

Figure 4-3 Exponential decay of deflation in cm in the area of maximum deflation at Krafla. Numbers refer to publications: 1 (Tryggvason, 1994), 2 (Björnsson and Eysteinsson, 1998), 3 (Sigmundsson et al., 1997), 4-6 and 8 (this paper) and 7 (Ágústsson, 2001).

4.3.2 Micro-gravity methods

All the micro-gravity measurements discussed in this paper were acquired with the use of LaCoste & Romberg instruments following standard techniques as described by Rymer (1996). Meter G-513 has been used for all surveys since 1990 and its calibration characteristics are well known (Carbone and Rymer, 1999); meter G-403 has been used in addition since 1997. The micro-gravity network traditionally uses station Hotel (Figure 4-1) as reference, because it is located outside the main zone of deformation (Rymer et al., 1998a). Station FM115 has also been measured on a regular basis. Although its location, near the central axis of the plate boundary, is not ideal, it has been used here, as an alternative reference station to better coordinate with the deformation network. The uncertainty expected for this type of micro-gravity survey considering the climate, time delay between readings, and jolting of the instruments during transport is 10-20 μGal (Rymer, 1989). Repeat measurements have been made during this study and the uncertainties for the newly acquired data are displayed in Table 4-2. Before we can interpret the micro-gravity data in terms of mass movements they need to be corrected for height with the use of geodetic data. The Free Air Gradient (FAG) is the change of gravity with elevation and is used to calculate the expected gravity change at each station due to the height changes alone. The FAG varies depending on the local sub-surface mass distribution. The local value of the FAG can easily be determined in the field following the methodology of Rymer (1996) and is used here to calculate net gravity changes.

4.4 Data and results

4.4.1 Deformation data

The Krafla system is subject to deformation because of the stresses associated with the divergent plate boundary, the effects of magma movements and geothermal

processes. The recent extensive geothermal exploitation and production at the Krafla power station also influences the system. Any deformation data collected will necessarily reflect the complex interaction between all these processes.

4.4.1.1 Previous results

No significant ground deformation changes were observed in data from the 1938 to 1965 period (Björnsson et al., 1979). Between 1965 and 1971 apparent contraction took place followed by extension and uplift between 1970 and 1975 (Moller and Ritter, 1980; Rymer et al., 1998a). The Krafla power plant was under construction at that time and geodetic surveys and exploration drillings had started in 1974. Levelling profiles crossing the caldera region were available from the very beginning of the 1975-1984 rifting episode. Ground deformation was monitored extensively during the episode (Ewart et al., 1991), using a wide range of techniques such as Electronic Distance Measurements (EDM; (Tryggvason, 1994), precise levelling (Björnsson, 1985), tilt and lake level measurements (Tryggvason, 1986; Tryggvason, 1994). Deformation during the rifting episode was characterised by steady inflation interrupted by rapid subsidence (Tryggvason, 1994). After the last eruption in September 1984, slow inflation was observed from 1985 to 1989. This was followed by subsidence, initially at a rate of ~5 cm/yr, declining to ~2.5 cm/yr in 1992-1995 (Árnadóttir et al., 1998; Rymer et al., 1998a; Sigmundsson et al., 1997; Tryggvason, 1994).

Radar interferometry (InSAR) has also been used successfully in the Krafla region to monitor deformation (de Zeeuw-van Dalfsen et al., 2004a; Henriot et al., 2001; Sigmundsson et al., 1997). Sigmundsson et al. (1997) observed 2.4 cm/yr of subsidence in the centre of the Krafla area and ~0.7 mm/yr along axis subsidence of the spreading segment whilst studying interferograms covering the 1992-1995 period. Henriot et al. (2001) analysed interferograms from the 1992-1998 period and found steady subsidence at Krafla and the fissure swarm of 1.9 cm/yr (2.1 cm/yr in the ground

to satellite direction). Based on interferometric data from 1993 to 1999, de Zeeuw-van Dalfsen et al. (2004a) showed the existence of a wide inflating area in addition to the already suggested subsiding zones.

4.4.1.2 New data

Integration of the new GPS and InSAR data with previously published geodetic data is complicated by the fact that different groups acquired the data, using different reference stations and with several temporal gaps in the data set. To alleviate this problem, all data are first normalised to the same base station (FM115; Figure 4-1 & Figure 4-2) and yearly height changes are calculated for each gravity station (Table 4-1), interpolating and extrapolating where necessary.

First order levelling surveys conducted in the Krafla area in 1989, 1995 and 2000 (Björnsson and Eysteinsson, 1998; Magnússon, 2003) form the basis of our deformation model. The data exceed the requirements for height correction of the gravity data as they have a standard deviation of less than 1.5 cm and the levelling stations are equivalent or close to the micro-gravity stations (Rymer, 1996). We consider two distinct periods, 1990-1995 and 1996-2003, in order to take into account change in productivity of the geothermal power plant from 30 MW to 60 MW between 1995 and 1996 (Hauksson and Benjamínsson, 2003).

Twelve SAR images from European Remote Sensing (ERS) satellites 1 and 2 (track 9, frame 2277), acquired during the period 1993-2000, allowed the formation of twelve interferograms, with reasonable coherence. The four with the best coherence were selected for modelling and the average subsidence rate over the time period (spanning from 2 to 6 years) was acquired. Overall, the subsidence rate calculated from these data decays from ~1.5 cm/yr in late 1996 to ~1.1 cm/yr in late 1997.

Previous work indicates that the deformation rate at Krafla has been decaying rapidly since 1989 (Tryggvason, 1994). In order to extrapolate the deformation data at

Krafla, from 2000 to 2003, it is important to know the trend of this decay. The vertical change over a time period obtained from different measurements by several authors is expressed as a rate (cm/yr) in Figure 4-3. The points may be fitted by two straight lines or by an exponential curve. We prefer an exponential fit because the subsidence is expected to show exponential behaviour like the subsidence at other Icelandic Volcanoes (Sturkell and Sigmundsson 2000). A good fit through the data, with a root mean square of 0.96, is found using estimates for average maximum subsidence from published data (Ágústsson, 2001; Björnsson and Eysteinsson, 1998; Henriot et al., 2001; Sigmundsson et al., 1997; Tryggvason, 1994) together with the newly acquired results from InSAR (Figure 4-3). Since the micro-gravity stations do not coincide with the assumed location of maximum subsidence caused by the shallow magma chamber, the extrapolated height change data (for the period post 2000) also need to be interpolated (spatially). This is done by noting the distribution of measured elevation changes in the 1997-1998 period (middle of the 1995-2000 levelling period) compared to the predicted maximum deformation from the decay curve (Figure 4-3). The same decay curve is also used to interpolate data for those stations lacking levelling data from 1990 to 1995. Finally, the curve is used to extract the 1990 to 1995 deformation from the 1989 to 1995 levelling data. Estimated deformation in 1989 has been subtracted from the 1989-1995 measured value. The total deformation (Table 4-1) at each levelling station relative to base station FM115 is then calculated by adding the results from the levelling (or interpolated values) from 1990 to 2000 and the extrapolated values from 2000 to 2003. Because each micro-gravity station is the same or close to a levelling station, these values are used to interpret the micro-gravity data. The standard deviation is estimated, based on repeated measurements, to be 1.5 cm for the vertical component. In summary, results from geodetic surveys in the Krafla region after 1998, show that the Krafla volcanic system is still deflating. The deflation at Krafla follows an exponential decay

trend and, assuming there is no change in activity, is expected to reach the detection limit by 2007.

The total volume change at the surface, ΔV_e, can be calculated from the deformation data most simply by assuming a Mogi model (Mogi, 1958) where the deformation is caused by a pressure change of a point source within an elastic half-space, (Johnson, 1987):

$$\Delta V_e = 2\pi\Delta h \frac{(r^2 + d^2)^{3/2}}{d} \qquad \text{(eq. 4-1)}$$

The maximum subsidence, Δh, at the centre of the deformation relative to station FM115 is -0.085 m from 1990 to 1995 and -0.024 m from 1996 to 2003. The average depth to the source, d, is 2800 m as inferred from previous geodetic modelling (Árnadóttir et al., 1998; Rymer et al., 1998; Sigmundsson et al., 1997). The horizontal distance from the centre of deformation to this source, r, is 1300 m in the 1990-1995 period and 2000 m in the 1996-2003 period. FM115 is located within the deformation zone and any estimates for ΔV_e are therefore minimum values. InSAR data covering most of this period (de Zeeuw-van Dalfsen et al., 2004a) indicate that the subsidence does not extend beyond this region and therefore the volume calculated for ΔV_e is considered to be realistic. ΔV_e is calculated to be -0.006 km^3 for the 1990 to 1995 period and -0.002 km^3 for the 1996 to 2003 period.

4.4.2 Micro-gravity

The first micro-gravity measurements in the Krafla region were made in 1965 (Björnsson et al., 1979) and extensive work was done during the beginning of the 1975-1984 rifting episode (Johnsen et al., 1980). Since then, micro-gravity measurements have been made yearly at Krafla from 1990 to 1997, with the exception of 1993 (Rymer et al., 1998a) and again in 2002 and 2003.

Table 4-1 Total height change data for 1990 to 2003 based on the precise levelling surveys reported by Björnsson and Eysteinsson (1998) and Ágústsson (2001). Numbers refer to location of station, for coordinates see Table 4-2 (also partly displayed on Figure 4-2). An 'a' in the first column means the levelling station is close to but not identical to the gravity station with that number, but height change data from the a-station are used to correct for height changes at the corresponding gravity station. Method of estimation described in text. Note that the negative numbers here reflect deflation. These should not be confused with the decreasing rate of deflation shown in Figure 4-3. The standard deviation on the data is 1.5 cm which corresponds to ~5 μGal (based on the average FAG ~310 ±12 μGal/m).

No.	Levelling Station	Estimated height change 1990-1995 [m]	Levelling 1995-2000 Águstsson [m]	Estimated height change 2000-2003 [m]	Total height change 1990-2003 [m]
3	FM115	0.000	0.000	0.000	0.000
5	OS5595	-0.074	-0.019	-0.005	-0.097
6	5596	-0.086	-0.041	0.001	-0.126
7	OS5597	-0.061	-0.022	0.001	-0.083
8	5599	-0.013	-0.003	0.000	-0.015
9	5599A	-0.013	-0.003	0.000	-0.015
10	OS5600	-0.002	0.004	0.000	0.002
11	5672	0.013	0.037	0.000	0.049
12	OS5684	-0.052	-0.000	0.001	-0.052
13	OS5685	-0.054	0.007	0.001	-0.046
15	OS5697	-0.000	0.004	0.000	0.004
16	OS5698	0.002	0.003	0.000	0.005
17	OS5699	0.001	0.003	0.000	0.004
1a	KONGSP	0.017	0.014	0.000	0.032
14a	KB08	-0.075	-0.032	0.001	-0.106
14a	KB11	-0.088	-0.030	0.001	-0.117
23a	KV08	-0.079	-0.007	0.001	-0.085
24a	KV12	-0.097	-0.025	0.001	-0.120
25a	KV02	-0.111	-0.028	0.002	-0.137
26a	LV956104	-0.085	-0.028	0.001	-0.112
27a	FM5670	-0.054	-0.011	0.001	-0.064
29a	LV956107	0.108	0.035	-0.001	0.141

The twenty-nine main micro-gravity stations (partly displayed in Figure 4-2, Table 4-2) at Krafla can be grouped according to location: Hreindýrahóll (5672, A008 and A012), Leirhnjúkur (A001, A002, A003 and A004), Hlídar Krafla (OS5595, 5596, 5597, OS5688, NE79077 and A005), Hvíthólaklif (5599, 5599a, OS5843, NE9301 and NE80051) and South Hlídardalur (NE220, OS5697, OS5698, OS5699 and OS5600). There are four control or base stations (Hotel, FM115, Hellahraun and 2313) and two stations that fall outside these groups (OS5684 and OS5685).

4.4.2.1 Previous results

Rymer et al. (1998) investigated post-eruptive gravity changes from 1990 to 1996 inclusively. After corrections for elevation change, significant net gravity decreases, on the order of -50 μGal, were observed over the modelled Mogi-type deflation source. Net gravity increases up to 60 μGal were observed 1-3 km from the centre of deformation. In addition to this, here the effect of water extraction has been taken into account for the 1990-1996 period.

Gottsmann and Rymer (2002) analysed $\Delta g/\Delta h$ gradients for all available data from 1977 to 1996. Their theory suggests that the relationship between the measured gradient, the Free Air Gradient (FAG) and the Bouguer Corrected Free Air Gradient (BCFAG) predicts which process is responsible for caldera unrest.

4.4.2.2 New results

The micro-gravity network at Krafla (Figure 4-2, Table 4-2) was re-measured during the summers of 1997, 2002 and 2003 using station FM115 as a reference and the results are presented here. The average standard deviation of all measurements is 14 and 12 μGal in 2002 and 19 and 18 μGal in 2003 (Table 4-2), for meters G-403 and G-513, respectively.

During the 2002 survey the FAG was measured at several key stations as suggested by Gottsmann and Rymer (2002). The results show a FAG close to the theoretical value for the reference station (FM115) and the South Hlídardalur stations. Across the rift, the FAG differs considerably, with values of -386 ± 12 μGal/m in the Leirnjúkur area and -280 ± 12 μGal/m in the Hreindýrahóll area (Figure 4-3i and Table 4-3). This difference is caused by topographic variations and the local Bouguer anomalies. The measured FAG values were then contoured to allow the FAGs at the unmeasured stations to be estimated.

A comparison of the 2002 and 2003 data with earlier surveys (Figure 4-4) reveals that there has been a micro-gravity increase at the Leirhnúkur, Hlídar Krafla and South Hlídardalur stations from 1990 to 1996 averaging to about ~25 μGal. This is followed by a relative micro-gravity decrease of ~45 μGal from 1996 to 2002 and a small increase of ~10 μGal from 2002 to 2003. At the Hreindýrahóll and Hvíthólarklif stations, micro-gravity data show an increase of ~20 μGal from 1990 to 1994, followed by a steep decrease of 80 μGal from 1994 to 1997. No change occurred from 1997 to 2002 and from 2002 to 2003 these stations show a micro-gravity increase of ~10 μGal. The average of all gravity stations is also depicted in Figure 4-4 (broken line). For gravity changes to be considered significant, they need to exceed 15 μGal. There is some (non-linear) trend in the gravity change signal in Figure 4-4 but before any interpretation can be made, the effects of height changes need to be considered.

4.4.2.3 Calculation of net micro-gravity

The net micro-gravity changes were calculated using the measured values of the FAG where possible (Table 4-3) or with estimates derived from the contoured FAG values. The vertical motion at each station is multiplied by the FAG to calculate the expected micro-gravity change. Subtraction of the expected changes due to vertical

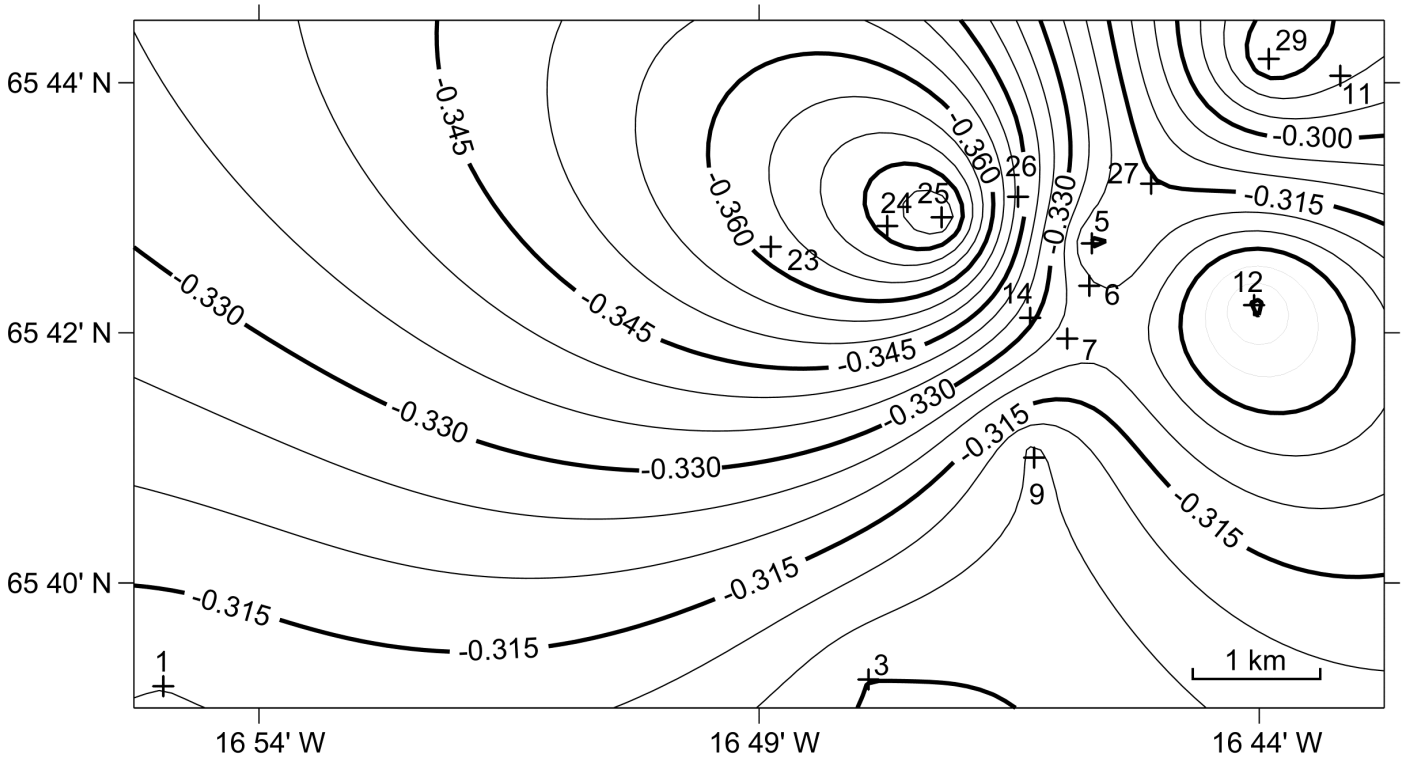

Figure 4-3 i: FAG contour map based on measurements at Krafla in 2002 and 2003. Values in mGal/m. Crosses depict station locations and numbers refer to station names in Tables 4-1, 4-2 and 4-3.

Table 4-2. Coordinates and micro-gravity data for stations in the monitoring network. Numbers refer to location on map (partly displayed in Figure 4-2). Station names starting with A and NE were installed by the Nordic Volcanological Institute, stations Hotel and Hellahraun by the Open University and the remainder by the National Energy Authority of Iceland.

				2002		2003	
No.	Station Name	Latitude	Longitude	Meter G-403	Meter G-513	Meter G-403	Meter G-513
1	Hotel	N65°38'42.0''	W016°54'55.1''	15.436(9)	15.501(7)	15.412(25)	15.518(35)
2	Hellahraun	N65°38'31.1''	W016°54'28.2''	13.311(22)	13.367(1)	13.279(18)	13.395(7)
3	FM115	N65°38'40.6''	W016°48'08.8''	0.000	0.000	0.000	0.000
4	2313	N65°38'40.8''	W016°48'08.9''	13.311(-)	-0.014(5)	-0.021(-)	-0.032(7)
5	OS5595	N65°42'51.5''	W016°45'59.7''	-30.667(8)	-30.761(18)	-30.688(21)	-30.770(16)
6	5596	N65°42'27.2''	W016°46'01.5''	-14.740(1)	-14.769(10)	-14.757(16)	-14.766(0)
7	OS5597	N65°41'56.7''	W016°46'14.2''	-13.222(5)	-13.274(20)	-13.239(16)	-13.260(35)
8	5599	N65°40'54.8''	W016°46'30.9''	-0.179(22)	-0.172(5)	-0.241(-)	-0.184(-)
9	5599A	N65°40'53.2''	W016°46'35.8''	-0.186(21)	-0.211(12)	-0.228(33)	-0.220(18)
10	OS5600	N65°40'20.4''	W016°47'02.4''	-0.479(17)	-0.492(14)	-0.507(-)	-0.455(20)
11	5672	N65°44'28.1''	W016°43'36.9''	-52.051(11)	-52.215(10)	-52.137(-)	
12	OS5684	N65°42'16.1''	W016°44'26.3''	-45.946(-)	-46.078(-)	-45.932(-)	-46.087(-)
13	OS5685	N65°42'08.2''	W016°43'38.0''	-48.230(-)	-48.382(-)	-48.266(-)	-48.382(-)
14	OS5688	N65°42'08.6''	W016°46'35.9''	-13.669(31)	-13.688(2)	-13.662(10)	-13.706(5)
15	OS5697	N65°39'51.5''	W016°47'33.5''	-0.378(16)	-0.358(14)	-0.385(12)	-0.337(34)
16	OS5698	N65°39'30.7''	W016°47'38.4''			-0.127(39)	-0.103(38)
17	OS5699	N65°39'00.8''	W016°47'31.0''	0.152(2)	0.144(3)	0.150(6)	0.168(23)
18	OS5843	N65°41'12.9''	W016°46'41.8''	-15.402(10)	-15.46(21)	-15.435(20)	-15.478(-)
19	NE220	N65°38'13.8''	W016°48'33.6''	-1.377(24)	-1.380(-)	-1.398(21)	-1.338(22)
20	NE9301	N65°41'24.8''	W016°46'31.0''	-13.027(1)	-13.074(18)	-13.061(-)	-13.036(-)
21	NE80051	N65°41'34.5''	W016°45'25.6''	-35.776(-)	-35.864(-)	-35.790(-)	
22	NE79077	N65°42'34.3''	W016°46'34.5''	-34.424(29)	-34.496(4)	-34.445(6)	-34.498(7)
23	A001	N65°42'42.8''	W016°49'14.7''	-31.580(20)	-31.664(43)	-31.669(-)	-31.644(-)
24	A002	N65°43'01.5''	W016°47'46.5''	-39.750(18)	-39.861(27)	-39.794(-)	-39.876(-)
25	A003	N65°43'06.5''	W016°47'26.9''	-39.053(27)	-39.161(17)	-39.121(-)	-39.181(-)
26	A004	N65°43'18.3''	W016°46'42.9''	-28.013(13)	-28.055(7)	-28.056(13)	-28.028(16)
27	A005	N65°43'21.1''	W016°45'29.5''	-31.030(25)	-31.113(29)	-31.088(57)	-31.097(-)
28	A008	N65°44'12.7''	W016°44'54.3''	-34.510(-)	-34.659(-)	-34.628(-)	
29	A012	N65°44'37.7''	W016°44'18.5''	-58.327(8)	-58.487(4)	-58.373(-)	15.518(-)
Average STD				14	12	19	12

motion from the measured micro-gravity changes yields the net micro-gravity change due to changes in sub-surface mass. The net micro-gravity changes for the two periods under consideration are most easily visualised on contour maps (Figure 4-5). Station 5596 was excluded from the contouring during the 1996-2003 period because the net gravity decrease found at this location is small (-20 μGal) compared to that found at nearby gravity stations (~-75 μGal). A reason for this could be that this gravity station is closest to the drill hole site where, in 2002, 1400 KTon of water was injected into the system.

There is an important contrast between the 1990-1995 and 1996-2003 data. During the 1990 to 1995 period a net gravity decrease of -85 μGal was concentrated around the Leirhnúkur stations. This coincides with the location of the latest activity during the Krafla fires and suggests it may have been caused by magmatic processes. During the 1996 to 2003 period almost all stations show a net micro-gravity decrease. An east-west elongated feature, with a maximum net gravity decrease of -100 μGal can be identified. This area correlates well with the location of the drill hole sites. Processes responsible for the observations could be: i) influences of the geothermal power plant: water mass extraction and the increased cooling rate of the shallow magma body (causing contraction) caused by the increased water circulation; ii) drainage of magma from a shallow magma body.

4.4.2.4 Influence of the geothermal power plant

Water extraction (dotted line in Figure 4-4) has been increasing steadily since 1992 (Hauksson and Benjamínsson, 2003). The average yearly water extraction of ~6000 KTon for the 1990-1996 period, increased to ~11000 KTon for the 1998-2003 period (Figure 4-6). There is a clear inverse correlation between the average gravity and the water extraction (Figure 4-4).

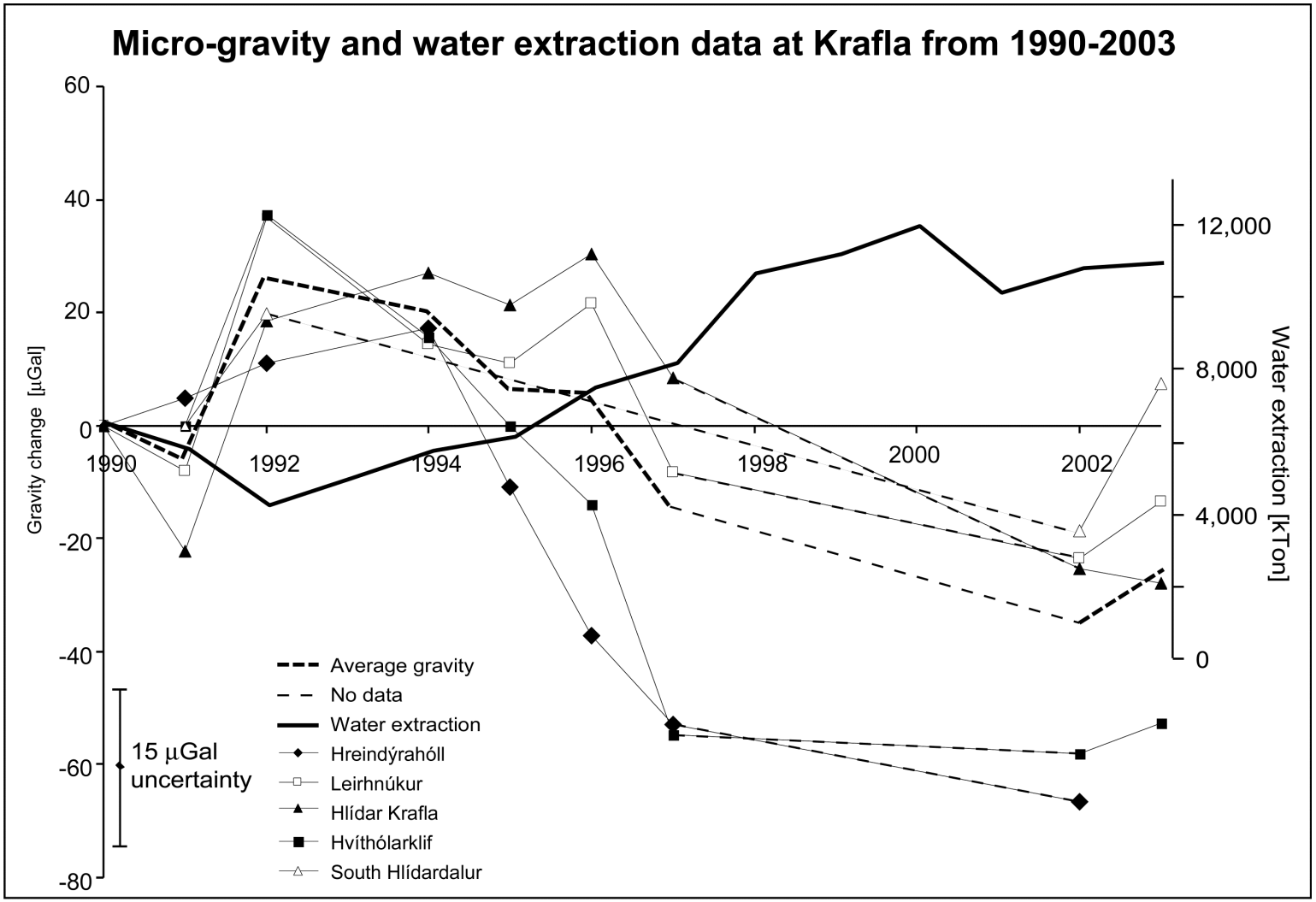

Figure 4-4 Micro-gravity and water extraction data for Krafla between 1990 and 2003. Micro-gravity data are referred to base station FM115 and relative to 1990. The names of the station groups refer to locations plotted in Figure 4-2. The dotted line shows the average gravity. The average standard deviation on all data through all years is 15 µGal. Total yearly water extraction data are taken from the National Energy Authority of Iceland (Hauksson and Benjamínsson, 2003).

Table 4-3 Calculation of the net micro-gravity change for the 1990-1995 and 1996-2003 periods. Numbers refer to location on map (Figure 4-2). FAG values without a star are values measured at that station (±12 μGal/m); values with a star have been estimated from contours. Numbers in bold represent net gravity decreases.

No.	Name	FAG [μGal/m]	1990 to 1995				1996 to 2003			
			Height change [cm]	Expected Δg [μGal]	Measured Δg [μGal]	Net Δg [μGal]	Height change [cm]	Expected Δg [μGal]	Measured Δg [μGal]	Net Δg [μGal]
1	Hotel (kongsp)	-0.310	4.482	-14	35	49	1.720	-5	19	25
3	FM115	-0.300	0.000	0	0	0	0.000	0	0	0
5	OS5595	-0.314	-6.082	19	-1	-20	-2.334	7	-73	-81
6	5596	-0.322*	-13.125	42	35	-7	-5.036	16	-3	-20
7	OS5597	-0.322*	-7.043	23	72	49	-2.702	9	-62	-71
9	5599A	-0.304	-0.960	3	30	27	-0.369	1	-55	-56
11	5672	-0.290*	11.844	-34	-5	29	4.545	-13	-33	-20
12	OS5684	-0.347	0.480	-2	15	17	0.184	-1	-104	-104
14	OS5688 (kb08&11)	-0.330*	-10.244	34	52	19	-3.931	13	-48	-61
23	A001 (kv08)	-0.365*	7.683	-28	41	69	2.948	-11	-42	-31
24	A002 (kv12)	-0.375*	1.921	-7	15	22	0.737	-3	-61	-58
25	A003 (kv02)	-0.386	0.960	-4	12	16	0.369	-1	-77	-75
26	A004 (LV956104)	-0.348*	-8.963	31	-55	-86	-3.439	12	5	-7
27	A005 (FM5670)	-0.315*	-3.521	11	-23	-34	-1.351	4	-14	-19
29	A012 (LV956107)	-0.280	11.204	-31	-13	19	4.299	-12	-53	-41

The fact that there are net micro-gravity changes suggest sub-surface mass changes are occurring. Sub-surface mass decrease could be caused by movement of the steam-water interface, drainage of magma from a reservoir or extraction of geothermal water at the Krafla power plant. Movement of the steam-water interface can not be excluded but its influence will be too small to explain the observed mass changes (Gottsmann and Rymer, 2002). We suggest the two alternative explanations are more likely causes. In order to better understand the non magmatic influence on the gravity signal we consider in more detail the extraction of water at the geothermal power plant (Figure 4-6).

From 1990 to 2002, a total of 7.94 $x10^3$ kTon (7.94 x 10^{10} kg) water was extracted at the various drill holes (Hauksson and Benjamínsson, 2003). The drill holes are co-located with the micro-gravity network (Figure 4-5) and are concentrated at five sites: i) south of the caldera in Bjarnarflag, ii) at Hvíthólaklif, iii) in the centre of the caldera (near the power plant), vi) at Leirbotnar, and v) south of the Krafla mountain at Suðurhlíðar Krafla. The extraction of water was more or less constant from 1981 to 1996 but subsequently almost doubled due to the increased demand caused by the installation of the second turbine in 1996. To complicate the mass balance picture even further, injection of water into the system was initiated in 1999. This did not contribute considerably until 2002 when injection amounted to 1400 kTon a year. This may account for the small increase in raw gravity observed from 2002 to 2003.

The Krafla geothermal system consists of two separate geothermal zones at different depths (Stefánsson, 1981). The shallower of the two is avoided during exploitation of the field because of its lower temperature and association with calcite deposition. The top of the ~1000 m thick deeper zone is located around the 1100-1300 m.

The gravitational effect of the water extraction in the Krafla area can be simulated by a cylinder with changing density, in the same way as used by Hunt (1970) for the Wairakei geothermal field in New Zealand. The density change, σ, can be calculated as follows:

$$\sigma = \frac{\Delta m}{(\pi r^2 h)} \quad \text{(eq. 4-2)}$$

The mass change in kg, Δm, in the centre of the caldera (excluding Bjarnarflag), is -2.28 x 10^{10} kg from 1990 to 1995 and -6.57 x 10^{10} kg from 1996 to 2003. The radius of the cylinder or the effected area, *r,* varies from 1000 to 10,000 m. The height of the cylinder or the thickness of the aquifer, *h,* is 1000 m.

The gravitational effect, Δg, on the surface above the centre of this cylinder can then be calculated as follows (Parasnis, 1979):

$$\Delta g = 2\pi G\sigma\left[h_2 - z + \sqrt{r^2 + z^2} - \sqrt{r^2 + h_2{}^2} \right] \quad \text{(eq. 4-3)}$$

where *G*, is the gravitational constant, of 6.67 x 10^{-11} Nkg^2/m^2. The depth of the cylinder, *z,* from the surface to the top of the aquifer, varies from 1100 to 1300 m. h_2 is the depth to the bottom of the cylinder, in m. Equation 3 is empirical and variations in g will be caused by variations in z, h_2 and *r*.

The results of the calculations are shown in Figure 4-7. The average estimate of the gravitational effect of the water extraction from 1990 to 1995 is approximately -12 μGal assuming the extraction affects an area with a radius of 4 km. This is the approximate radius of the caldera and the aquifer is known to exist as a broad layer within this region (Stefánson, 1981). This effect is smaller than the average standard deviation on the data set and may therefore not be detectable. For the period 1996 to 2003, the estimated gravitational effect is approximately -35 μGal assuming the same area is affected. This effect is larger than the average standard deviation and should

therefore be measurable and visible in the data set. Since we ignore the flow of water into the area from the surroundings to accommodate the water extraction, the estimated gravitational effects are maximum values.

4.5 Interpretation

4.5.1 Geodetic data

Over the years several deformation models have been developed using data acquired with a range of geodetic techniques (Table 4-4, Figure 4-2). All of these models include a Mogi point source sometimes referred to as the Krafla magma reservoir. Its location varies only slightly between models, although depth is less well constrained. Analysis of local earthquakes (Einarsson, 1978) defined two regions of shear wave attenuation, which were inferred as a shallow magma reservoir, although this study did not define the magma reservoir in any detail. Brandsdóttir and Menke (1992) showed the presence of a low velocity zone that is interpreted as the shallow magma reservoir, less than 1 km thick with its top at a depth of approximately 3 km. However, it is not possible to explain all the observed deformation with this one point source, especially at increased distance from the source. Therefore, several types of additional sources have been suggested to complement the model (Table 4-4). All micro-gravity stations lie within the zone mostly influenced by the point source and by the extraction of the geothermal resources, and therefore for the context of this work, only the Mogi source and geothermal field will be considered.

Subsidence observed in interferograms spanning the 1993-1999 period (de Zeeuw-van Dalfsen et al., 2004a), is consistent with a Mogi source deflating at a rate of ~0.3 x 10^6 m^3/yr. This process is envisaged as deflation of the shallow Krafla magma

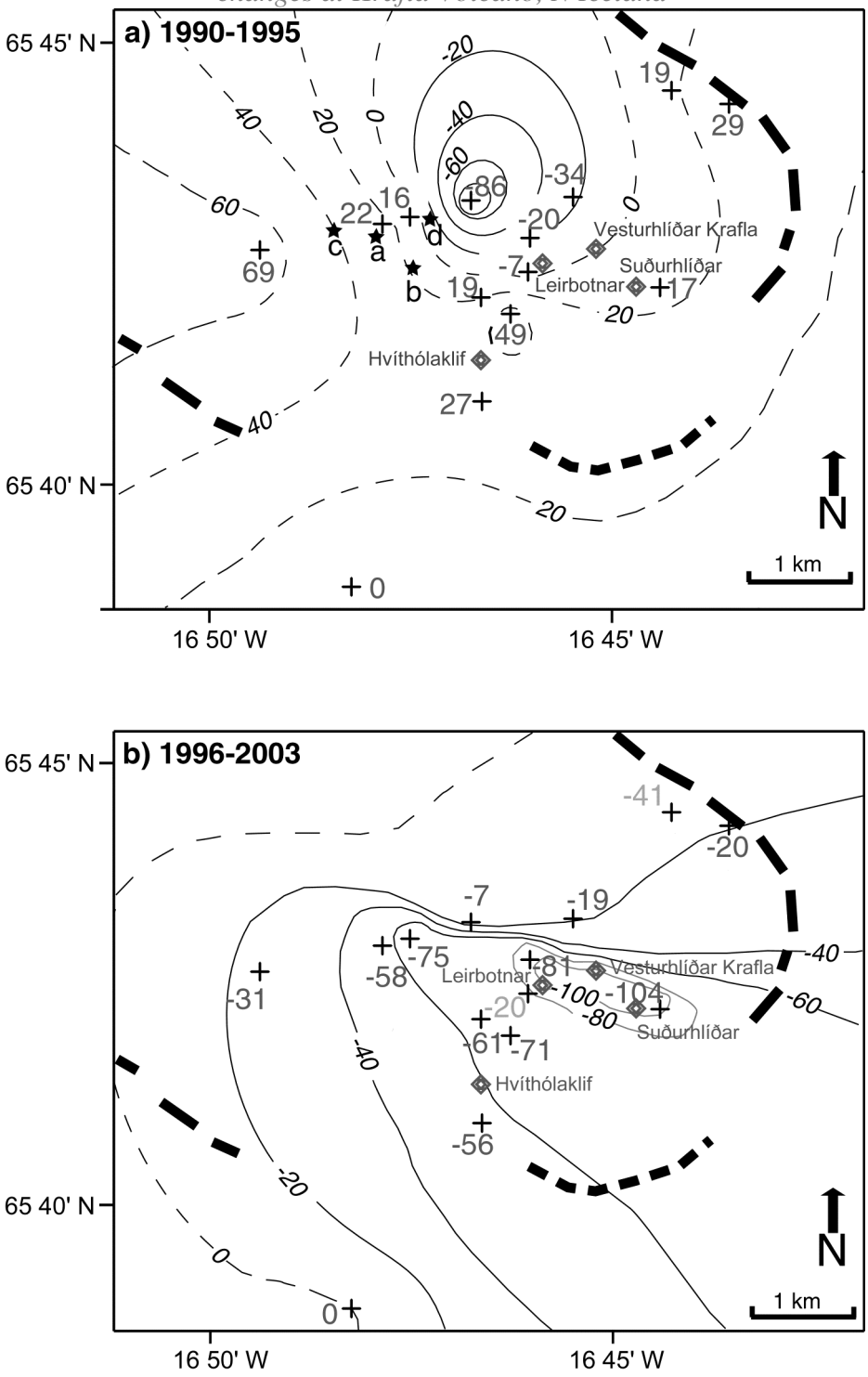

Figure 4-5a) Net micro-gravity contours (in µGal) at Krafla from 1990 to 1995 following data from Table 4-3. Gravity stations are represented by a cross and numbers refer to values as noted in Table 4-3. Diamonds represent drill holes for water extraction. Positive contours are dashed while negative contours are solid lines. Thick dashed line shows the caldera rim. The area of net gravity decrease is located in the centre of the caldera. Suggested locations of possible shallow magma chamber (see Table 4-4) are depicted with black stars a, b, c and d. b) Net micro-gravity contours (in µGal) at Krafla from 1996 to 2003 following data from Table 4-3 and same symbols as Figure 4-5a. Note that the anomalous data points FM5596 and A012 have not been taken into account during the contouring. Area of net gravity decrease is concentrated around the drill hole sites.

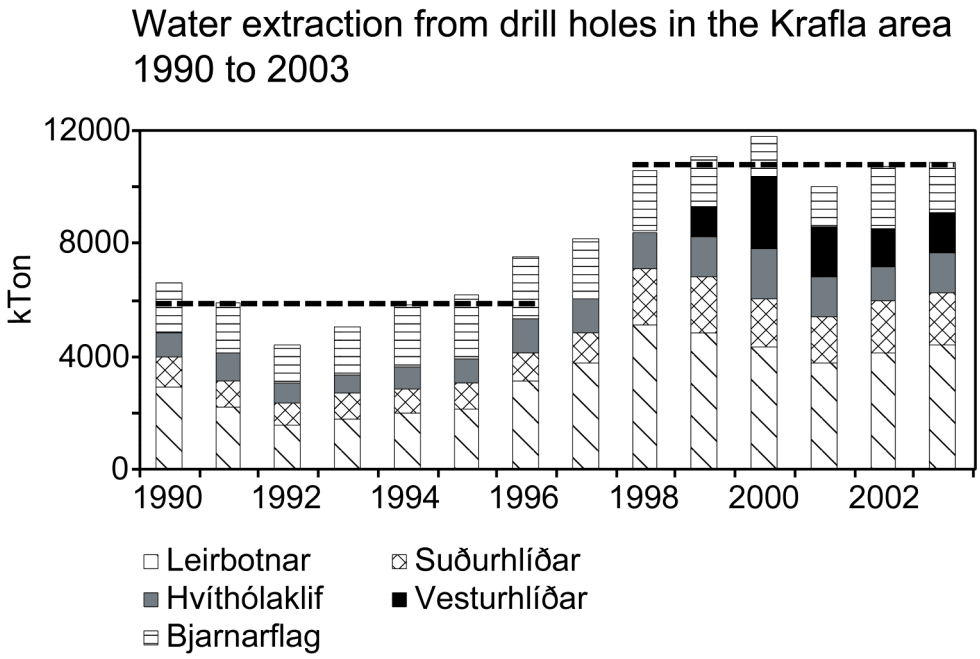

Figure 4-6 Water extraction from drill holes in the Krafla area from 1990 to 2003 (Hauksson and Benjamínsson, 2003). Note that extraction has doubled since 1998 compared to the 1990-1996 period. Names refer to locations of drill sites as used in Figure 4-5.

reservoir. Over the same period, a deeper inflating Mogi source, further north and at 21 km depth, inflated at a rate of ~26 x 10^6 m^3/yr. The inflating source is at or near the crust-mantle boundary as identified by seismic studies and is interpreted as accumulating magma (de Zeeuw-van Dalfsen et al., 2004a).

4.5.2 Gravity data

Rymer et al. (1998) interpreted the observed (1990-1996) net gravity decrease at Krafla as magma drainage of at least 4 x 10^{10} kg and the net gravity increases as the result of a migrating steam-water interface and/or closure of micro-fractures during post-eruptive cooling and contraction. Gottsmann and Rymer (2002) emphasised, however, that the net gravity increases were not only associated with a density increase but also accompanied by a mass increase of ~10^{10} kg. They suggested that magma moved laterally out of the reservoir into dykes.

The inverse correlation between micro-gravity and water extraction data (Figure 4-4) suggests water extraction has an important influence on the mass balance of the system and therefore on the gravity data. Furthermore, the fact that gravity is decreasing in areas of general deflation indicates that sub-surface mass decreases may be occurring. The influence of the water extraction by the geothermal power plant is also obvious in 1996-2003 (Figure 4-5). There may be a volcanic signal hidden within these data, but before this can be observed data should be corrected for the water extraction.

The calculated net gravity decrease from 1990 to 1995 is -85 μGal + 12 μGal (to correct for the influence of water extraction) which leads to a still significant, net gravity decrease of -73 ± 17 μGal (RMS of gravity readings is ± 16 μGal, RMS of deformation data is ± 6 μGal, $\sqrt{16^2 + 6^2} = 17$). Since the effects of water drainage have been taken into account, this mass decrease is most likely caused by magma drainage

a) 1990-1995

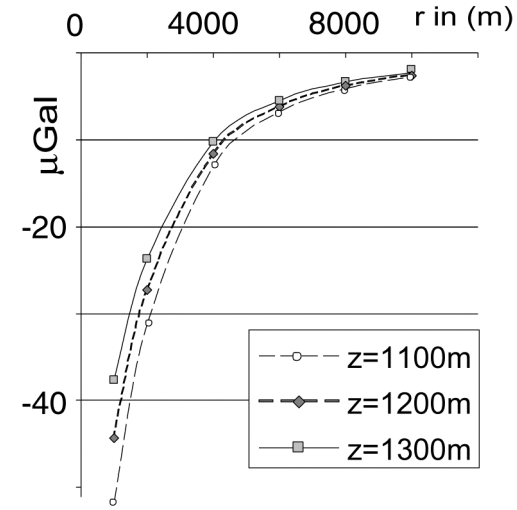

b) 1996-2003

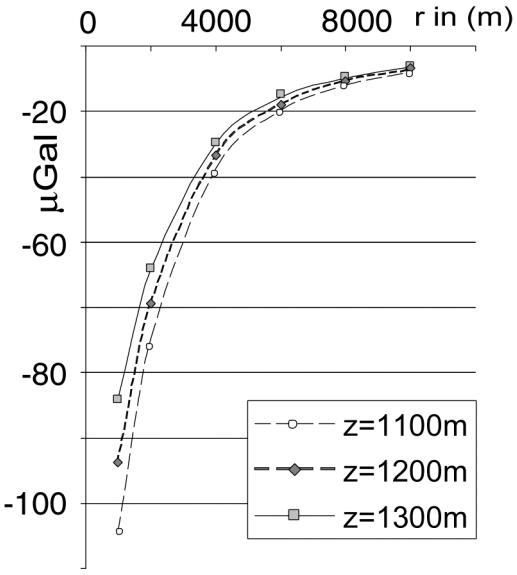

Figure 4-7 Micro-gravity effect of water drainage in µGal for the two periods. *z* is the depth to the top of the cylinder, i.e., the depth to the top of the aquifer, varying from 1100 m to 1300 m. The thickness of the aquifer is 1000 m and *r* is the radius of the cylinder.

Table 4-4 Model data for a Mogi point source as reported by various authors throughout the years.

Reference	Parameters of Mogi Source			Additional source	Input data
	Lat. ˚	Long. ˚	Depth (km)		
Björnsson (1985)	-	-	-	Molten layer 5-7 km feeding shallow reservoir.	magneto-telluric
Trygvasson (1986) see a, Fig. 4-5	65.715	16.797	2.6	3 more stacked reservoirs, at 5-10 km, >20 km and deeper	EDM*, lake level, tilt
Rymer et al.(1996) same as a, Fig. 4-5	65.715	16.797	~2.5		EDM, lake level, tilt
Sigmundsson et al. (1997) see b, Fig. 4-5	65.71	16.79	3	Line source	InSAR
Árnadottir et al. (1998) see c, Fig. 4-5	65.715	16.806	~3	Dike	EDM, tilt, height differences
De Zeeuw-van Dalfsen et al. (2004a) see d, Fig. 4-5	65.72	16.78	~2.4	Mogi 2 at 65.83˚N, 16.73˚ W, Line source	InSAR

*EDM = Electronic Distance Measurements; InSAR = Interferometric Syntethic Aperture Radar.

over the 6 year period. From 1996 to 2003 the calculated net gravity decrease is -100 μGal + 35 μGal (to correct for the influence of water extraction) which culminates in a significant net gravity decrease of -65 ± 17 μGal over the 8 year period.

The mass change (ΔM) within a spherical (point source) body, whose depth is much greater than its radius, causes a gravitational effect on the surface (Δg) that relate by:

$$\Delta M = \frac{\Delta g (r^2 + d^2)^{3/2}}{Gd} \qquad \text{(eq. 4-4)}$$

where G is the Universal gravitational constant of 6.67 x 10^{-11} Nm^2/kg^2. The depth to the point source, d, is 2800 m as estimated by geodetic modelling (Tryggvason 1986; Sigmundsson et al. 1997; Árnadóttir et al. 1998; Rymer et al. 1998). The horizontal distance to this source, r, is 1300 m from 1990-1995 and 2000 m from 1996-2003 (i.e., the horizontal distance from the point source to the area with maximum net gravity change).

In the following text we refer to edifice volume changes (ΔV_e) and relate them to sub-surface magma volume changes (ΔV_m) and magma chamber volume changes (ΔV_{ch}). Following Equation 4-4, a mass decrease of 1.1 x 10^{11} kg occurred from 1990-1995, followed by a decrease of 1.4 x 10^{11} kg from 1996 to 2003. This is equivalent to magma drainage of ~2 x 10^{10} kg/yr visualised as a continuous ongoing process. After correction for the water extraction, the two periods show very similar drainage rates and because drainage is visualized as a continuous process it makes more sense to interpret the data in terms of volume changes for the whole period at once. Assuming a density of 2700 kg/m^3 for the sub-surface magma body, the total mass decrease represents a minimum change in magma outflow volume (ΔV_m) of -0.09 km^3 for the whole period.

Earlier (see section 4.4.1.2), we calculated the total volume change at the surface (ΔV_e) from 1990 to 2003 to be -0.008 km^3. This volume change comprises a

combination of volume change caused by water extraction, cooling/contraction of the magma reservoir and/or magma drainage from the magma reservoir. Because ΔV_e is dependent on the maximum subsidence at the centre of the caldera (h in Equation 4-1), the curve following the decay of deformation is also representative for ΔV_e. This suggests that ΔV_e was not significantly influenced by water extraction as data would not follow a smooth line if influenced by a significant change in water extraction between 1995 and 1996. Therefore we argue that there is no need to correct ΔV_e for water extraction. Following Johnson et al. (2000), the corresponding sub-surface volume change of the Mogi source (ΔV_{ch}) is two thirds of the surface deflation volume or -0.005 km^3. InSAR modelling (de Zeeuw-van Dalfsen et al., 2004a) at Krafla suggests a total volume change of the deflating Mogi source of the same order of magnitude (-0.002 km^3 for the 1993-1999 period).

Comparing this value with the calculated total change in Mogi source volume (ΔV_m) we find that the magma drainage volume is actually seventeen times larger than the Mogi source volume. It has been suggested that volumetric decompression of stored magma may be caused by the variation in reservoir pressure accompanying magma drainage (Johnson, 1992; Johnson et al., 2000). The net volume change of the stored magma, ΔV_c, changes because of this decompression. A combination of reduction of the reservoir size, ΔV_{ch}, and decompression of the stored magma, ΔV_c would accommodate the magma drainage. Although not our preferred explanation, part of the volume discrepancy could also be explained by boiling in the geothermal system and density decrease in excess of that suggested only from extracted water.

4.6 Discussion and conclusions

The results from this work show significant mass decreases at the Krafla caldera which we interpret in terms of magma drainage. The Krafla caldera is located on the

northern volcanic zone in Iceland and as such is part of a larger volcanic system. It is therefore important to extend our interpretation and discussion beyond the Krafla area. In the past three years, more and more data covering the northern volcanic zone have been analysed. To advance our knowledge of volcanic processes it is important to use all available information.

The Askja volcanic centre in the Dyngjufjöll central volcano (Sigvaldason, 2002) hosts three calderas, the largest one being the circular Askja caldera. Askja volcano is located 80 km south of the Krafla volcanic system but is also located on the divergent spreading plate boundary in N-Iceland. The most recent eruption began there in October 1961 and continued into early December of the same year. de Zeeuw-van Dalfsen et al. (2004b) found a net micro-gravity decrease of 115 μGal at Askja caldera corresponding to a sub-surface mass decrease of 1.6 $x10^{11}$ kg between 1988 and 2003. They suggested the mass decrease of 0.125 m^3 s^{-1} was due to magma drainage from a shallow reservoir. They suggest extensional tectonic forces generate space in the ductile lower crust to accommodate drainage (of degassed magma) from the shallow magma chamber to deeper levels. The work presented here, suggests a mass decrease of 2.5 x 10^{11} kg, implying a drainage rate of 0.23 m^3 s^{-1} at Krafla from 1990 to 2003, which is of the same order of magnitude as that at Askja. We suggest that pressure reduction along the plate boundary due to the plate spreading process can accommodate this ongoing magma drainage from the shallow magma chamber. Links between the two volcanoes have been suggested by several authors (Rymer and Tryggvason, 1993; Sturkell et al., 2004 - submitted; Tryggvason, 1986).

Deflation at both Askja and Krafla volcano is decaying through time. However, while Askja has been deflating with an average rate of 5 cm/yr between 1988 and 2003, Krafla deflated at only 1 cm/yr between 1990 and 2003. Also, the $\Delta V_m / \Delta V_{ch}$ ratio at Askja for the 1988-2003 period is 3, roughly five times smaller then the ratio estimated

for Krafla (17) for the 1990-2003 period. A possible explanation for this difference might be the existence of the extensive geothermal system at Krafla cooling the volcanic system more rapidly.

Recently, re-evaluation of new and previously published geodetic data at both volcanoes suggests a best fit for models with two stacked magma reservoirs. For Askja, Sturkell et al. (2004) suggested two magma reservoirs at 3 and 16 km depth while at Krafla, de Zeeuw-van Dalfsen et al. (2004a) suggested the existence of deep magma accumulation at 21 km depth in addition to a magma reservoir at 2.8 km depth. It is possible a pressure-link between these volcanoes exists along the ductile lower crust in Iceland. We suggest that after the Krafla fires, co-rifting pressure decrease of the deeper source stimulated the subsequent inflow of magma. This inflow might influence conditions along the plate boundary as far away as Askja, 70 km to the south. The pressure of the deeper reservoir at Krafla will reach a critical value and eventually magma will rise to the shallow magma chamber, possibly initiating a new rifting episode. The last significant eruptive period at Krafla before 1974 was in 1724-1729 and this may indicate the timescale for replenishment of the upper magma chamber.

It is possible that not only Icelandic but also other volcanoes located on a constructive plate boundary are interconnected at depth. Several authors have suggested connections between volcanoes in other parts of the world in all types of tectonic settings, but the suggested connections are mostly shallow in nature. At Mauna Loa and Kilauea in Hawaii, the possible connection between the two volcanoes remains controversial. Recently, Miklius and Cervelli (2003) suggested a crustal-level interaction between the two magma systems based on a short timescale correlation found in continuous deformation data.

This paper has demonstrated the power of using a range of techniques simultaneously to study volcanoes. We have shown it can improve the understanding of

the ongoing processes at the studied volcano as well as to offer constraint on the dynamics of, and linkages through, the volcanic system at a broader scale. We anticipate that using a range of techniques concurrently will considerably increase our knowledge of volcanic systems in the future.

4.7 Acknowledgements

This work was supported by The Geological Society, London and an Open University studentship. H.R.'s work on this project (1990-2003) was supported by the Royal Society. We would like to thank all the people that have participated in collection of the data at Krafla, especially Ton de Zeeuw, Andrew J. Ball and Halldór Ólafsson who helped during the most recent surveys. The geodetic work on this project was supported by a grant from the Icelandic Research Council RANNÍS and F.S.'s work on this project has been supported by the Retina project (EVG1-CT-00046). An earlier version of the manuscript was greatly improved by discussion with Dave Rothery and reviews by J.T. Freymueller and an anonymous reviewer.

4.8 References

Ágústsson, S., 2001. Landhæðarbreytingar á Kröflusvæðinu (in Icelandic), Háskóli íslands, Reykjavik.

Árnadóttir, T., Sigmundsson, F. and Delaney, P.T., 1998. Sources of crustal deformation associated with the Krafla, Iceland, eruption of September 1984. Geophysical Research Letters, 25(7): 1043-1046.

Björnsson, A., 1985. Dynamics of crustal rifting in NE Iceland. Journal of Geophysical Research, 90: 10151-10162.

Björnsson, A. and Eysteinsson, H., 1998. Breytingar á landhæð við Kröflu 1974-1995 samantekt á landhæðar-mælingum (in Icelandic). Nat. Energy Auth., Reykjavík, OS-98002.

Björnsson, A., Johnsen, G., Sigurdsson, S. and Thorbergsson, G., 1979. Rifting of the plate boundary in north Iceland 1975-1978. Journal of Geophysical Research, 84(B6): 3029-3038.

Brandsdóttir, B. and Menke, W., 1992. Thin low-velocity zone within the Krafla caldera, NE Iceland attributed to a small magma chamber. Geophysical Research Letters, 19: 2381-2384.

Brandsdóttir, B., Menke, W., Einarsson, P., White, R.S. and Stapels, R.K., 1997. Färoe-Iceland ridge experiment 2. Crustal structure of the Krafla central volcano. Journal of Geophysical Research-Solid Earth, 102(B4): 7867-7886.

Carbone, D. and Rymer, H., 1999. Calibration shifts in a LaCoste-and-Romberg gravimeter: comparison with a Scintrex CG-3M. Geophysical Prospecting, 47(1): 73-83.

CNES, 2000. Installation guide for DIAPASON, Centre National d'etudes spatial, Toulouse.

de Zeeuw-van Dalfsen, E., Pedersen, R., Sigmundsson, F. and Pagli, C., 2004a. Satellite Radar Interferometry 1993-1999 suggests deep accumulation of magma near the crust-mantle boundary at the Krafla volcanic system, Iceland. Geophysical Research Letters, 31,L13611, doi:10.1029/2004GL020059.

de Zeeuw-van Dalfsen, E., Rymer, H., Sigmundsson, F., Sturkell, E., 2004b. Net gravity decrease at Askja Volcano, Iceland: constraints on processes responsible for continuous caldera deflation, 1988-2003. Journal of Volcano and Geothermal Research, 139:227-239.

Einarsson, P., 1978. S-wave shadows in the Krafla caldera in NE-Iceland, evidence for a magma chamber in the crust. Bulletin of Volcanology, 41: 1-9.

Einarsson, P., 1991. Earthquakes and present day tectonism in Iceland. Tectonophysics, 189: 261-279.

Ewart, J.A., Voight, B. and Björnsson, A., 1991. Elastic deformation models of Krafla Volcano, Iceland, for the decade 1975 through 1985. Bulletin of Volcanology, 53: 436-459.

Gottsmann, J., Berrino, G., Rymer, H. and Williams-Jones, G., 2003. Hazard assessment during caldera unrest at the Campi Flegrei, Italy: a contribution from gravity-height gradients. Earth and Planetary Science Letters, 211: 295-309.

Gottsmann, J. and Rymer, H., 2002. Deflation during caldera unrest: constraints on subsurface processes and hazard prediction from gravity -height data. Bulletin of Volcanology, 64(5): 338-348.

Gudmundsson, B.T. and Arnórsson, S., 2002. Geochemical monitoring of the Krafla and Námafjall geothermal areas, N-Iceland. Geothermics, 31: 195-243.

Gudmundsson, S., Carstensen, J.M. and Sigmundsson, F., 2001. Unwrapping ground displacement signals in satellite radar interferograms with aid of GPS data and MRF regularization. Transactions of Geosciences and Remote Sensing, 40(8), 1743-1754.

Hauksson, T. and Benjamínsson, J., 2003. Krafla og Bjarnarflag Afköst borhola og efnainnihald vatns og gufu í borholum og vinnslurás árið 2002 (in Icelandic). Rep. Landsvirkjun, Kröflustöð: 1-70.

Henriot, O., Villemin, T. and Jouanne, F., 2001. Long period interferograms reveal 1992-1998 steady rate of deformation at Krafla volcano (North Iceland). Geophysical Research Letters, 28(6): 1067-1070.

Hunt, T.M., 1970. Net mass loss from the Wairakei geothermal field, New Zealand. Geothermics, 2(1): 487-491.

Johnsen, G.V., Björnsson, A. and Sigurdsson, S., 1980. Gravity and elevation changes caused by magma movement beneath krafla caldera, northeast Iceland. Journal of Geophysics, 47: 132-140.

Johnson, D., 1987. Chapter 47: Elastic and inelastic magma storage at Kilauea volcano. In Volcanism in Hawaii, 2, 1297-1306 pp.

Johnson, D.J., 1992. Dynamics of magma storage in the summit reservoir of Kilauea volcano, Hawaii. Journal of Geophysical Research, 97(B2): 1807-1820.

Johnson, D.J., Sigmundsson, F. and Delaney, P.T., 2000. Comment on 'Volume of magma accumulation or withdrawal estimated from surface uplift or subsidence, with application to the 1960 collapse of Kilauea volcano' by P.T. Delaney and D.F. McTigue. Bulletin of Volcanology, 61: 491-493.

Massonnet, D. and Feigl, K., 1995. Discrimination of geophysical phenomena in satellite radar interferograms. Geophysical Research Letters, 22(12): 1537-1540.

Massonnet, D. and Feigl, K., 1998. Radar interferometry and its application to changes in earth's surface. Review of geophysics, 36(4): 441-500.

Miklius, A. and Cervelli, P., 2003. Interaction between Kilauea and Mauna Loa. Nature, 421: 229.

Mogi, K., 1958. Relations between the eruptions of various volcanoes and the deformations of the ground surfaces around them. Bulletin of the earthquake research institute, 36: 99-134.

Moller, D. and Ritter, B., 1980. geodetic measurements and horizontal crustal movements in the rift zone of NE Iceland. Journal of Geophyscs, 47(1-3): 110-119.

Rossi, M.J., 1997. Morphology of the 1984 open-channel lava flow at Krafla volcano, northern Iceland. Geomorphology, 20: 95-112.

Rymer, H., 1989. A contribution to precision microgravity data-analysis using Lacoste and Romberg gravity meters. Geophysical Journal, 97(2): 311-322.

Rymer, H., 1996. Microgravity monitoring. In Monitoring and mitigation of volcano hazards. Springer-Verslag, Berlin, 169-198 pp.

Rymer, H. et al., 2000. Geophysical studies of the recent 15-year eruptive cycle at Poas Volcano, Costa Rica. Journal of Volcanology and Geothermal Research, 97(1-4): 425-442.

Rymer, H., Cassidy, J., Locke, C.A. and Sigmundsson, F., 1998. Post-eruptive gravity changes from 1990 to 1996 at Krafla volcano, Iceland. Journal of Volcanology and Geothermal Research, 87(1-4): 141-149.

Rymer, H. and Tryggvason, E., 1993. Gravity and elevation changes at Askja, Iceland. Bulletin of Volcanology, 55(5): 362-371.

Sigmundsson, F., Vadon, H. and Massonnet, D., 1997. Readjustment of the Krafla spreading segment to crustal rifting measured by satellite radar interferometry. Geophysical Research Letters, 24(15): 1843-1846.

Sigvaldason, G.E., 2002. Volcanic and tectonic processes coinciding with glaciation and crustal rebound: an early Holocene rhyolitic eruption in the Dyngjufjoll volcanic centre and the formation of the Askja caldera, north Iceland. Bulletin of Volcanology, 64(3-4): 192-205.

Stefánsson, V., 1981. The Krafla geothermal field, northeast Iceland. geothermal systems: principles and case histories. John Wiley & Sons Ltd.

Sturkell, E., Sigmundsson, F. and Slunga, R., 2004 – submitted to Bulletin of Volcanology. 1983-2003 decaying rate of deflation at Askja caldera: Pressure decrease in an extensive magma plumbing system at a spreading plate boundary.

Tryggvason, E., 1986. Multiple Magma Reservoirs in a Rift-Zone Volcano - Ground Deformation and Magma Transport During the September 1984 Eruption of Krafla, Iceland. Journal of Volcanology and Geothermal Research, 28(1-2): 1-44.

Tryggvason, E., 1994. Surface deformation at the Krafla volcano, North Iceland, 1982-1992. Bulletin of Volcanology, 56: 98-107.

Williams-Jones, G., Rymer, H. and Rothery, D.A., 2003. Gravity changes and passive SO_2 degassing at the Masaya caldera complex, Nicaragua. Journal of Volcanology and Geothermal Research, 123: 137-160.

Chapter 5: Ups and downs at Stromboli volcano

This Chapter describes analyses and interprets the data aquired during fieldwork at Stromboli volcano. The original micro-gravity data are included on CD and a description of the analysis can be found in Appendix C.

5.1 Introduction

Stromboli Volcano, also known as the lighthouse of the Mediterranean (Rossi et al., 2000), has been active for at least 2000 years. The persistent activity is characterised by ongoing degassing and regular mild explosions emitting ejecta to average heights of 300 m. Various geophysical data can be collected safely from the Pizzo Sopra la Fossa, a rim 150 m above the active crater complex. This makes Stromboli an ideal location at which to test hypotheses regarding conduit and eruptive processes.

5.2 Location

The Aeolian magmatic arc (Figure 5-1), which consists of seven major islands (Alicudi, Filicudi, Salina, Volcano, Lipari, Panarea and Stromboli) and several seamounts, is situated in the southern Tyrrhenian Sea in Italy. Five of the islands (Alicudi, Filicudi, Salina, Panarea and Stromboli) and some of the seamounts form a curving structure extending east-west for about 80 km. Lipari and Vulcano are situated along a NW-SE trend, which transversely intersects the arc. The overall age trend in sub-aerial volcanism is a shift from west (Filicudi) to east (Panarea, Stromboli). However, on each individual island, the volcanic activity has developed a more complex trend (Santo, 2000). The origin of the volcanic arc is the subject of some controversy. Over the past 70 Ma, collision between the African and Eurasian plates in the

Mediterranean area created a complex geodynamic situation. Barberi et al. (1973) suggested active subduction of the African plate beneath the Eurasian plate as the source of volcanism (Inset-Figure 1-1), whereas others (Carminati et al., 1998) believe that the subduction process finished about 1 Ma ago when a general uplift and extension affected the Tyrrhenian area. Thus volcanism would be due to the post-subduction extensional strain caused by the slab detachment beneath the Calabrian Arc and the south-eastern opening of the Tyrrhenian basin.

Stromboli, the northernmost island, is the sub-aerial part of a stratovolcano, which rises from the ocean floor at ~2000 m depth to an elevation of 924 m above sea level (a.s.l.). In the past few years, the 12.6 km^2 island (Figure 5-2) has had less then 500 inhabitants, living in the villages of Stromboli in the NE and Ginostra in the SW. Tourism is their principal source of revenue and during the summer months the island's usual population is increased significantly.

Stromboli volcano is part of a late Quaternary (0.2 Ma – recent) volcanic complex of mostly basaltic-andesitic composition (Tibaldi et al., 2002). Other parts of the complex are Strombolicchio and Cavoni (Hornig-Kjarsgaard et al., 1993). Strombolicchio, a small island to the NW, is a volcanic neck or plug, whereas Cavoni, to the south, is a submerged centre. Alternating building and destructive phases laid the foundation for a complex volcanic structure. Several unconformities, created by the destructive phases, have helped to define a series of lithostratigraphic units representing the main volcanic cycles. They are from old to young: Paleostromboli, Scari complex and Vancori volcano, Neostromboli, and recent Stromboli (Tibaldi et al., 2002). In the last 13 ka, four lateral collapses took place (Pasquarè et al., 1993), the most recent forming the Sciara del Fuoco (Figure 5-2), a horseshoe shaped depression embedding today's active craters at the NW of the island.

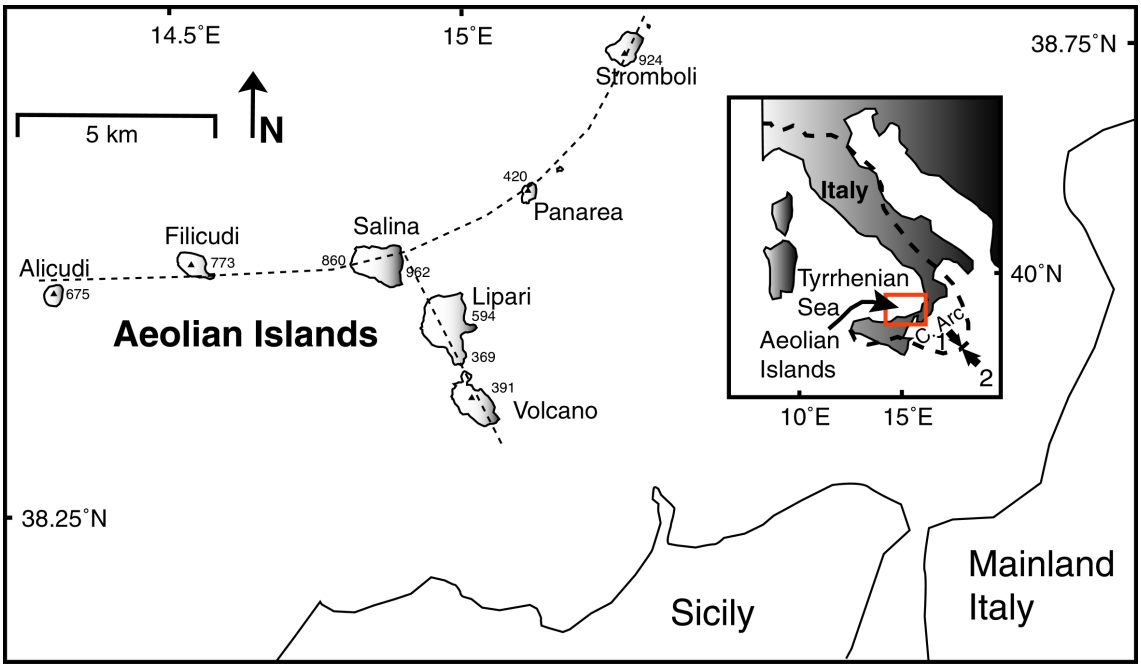

Figure 5-1 Overview of the Aeolian Islands. Inset shows the location of the Aeolian Islands in the Tyrrhenian Sea in Italy. The dashed line in the inset shows the location of the plate boundary, with the Eurasian plate to the north (1) and the African plate to the south (2). The arrows show subduction as suggested by Barberi et al. (1973). Note the location of the Calabrian Arc (C. Arc).

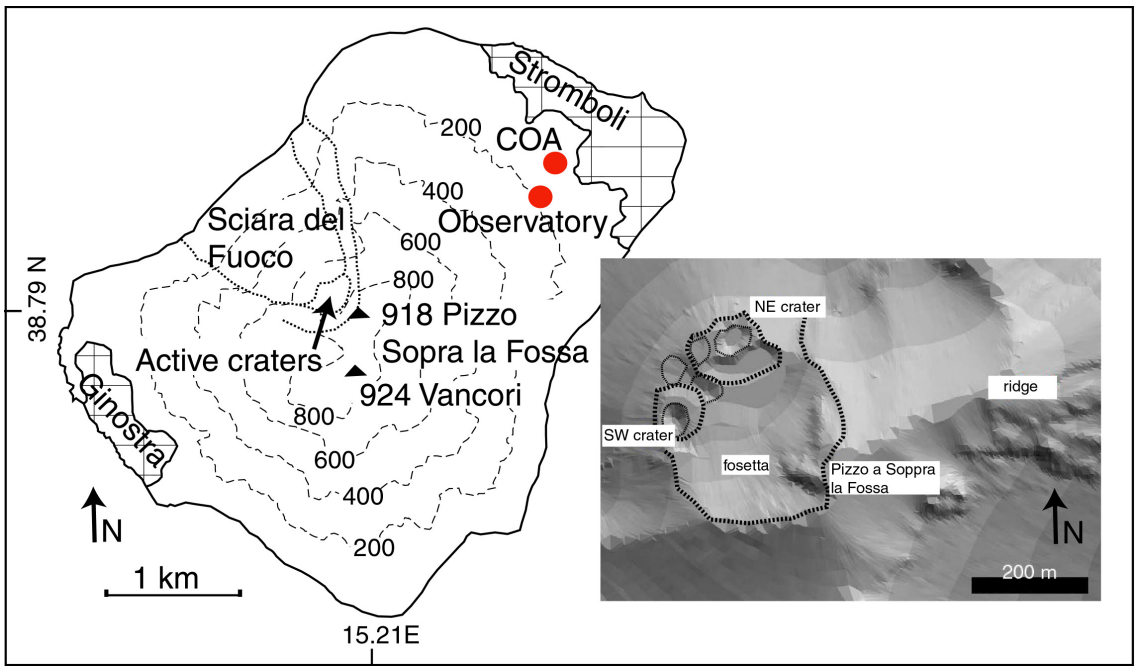

Figure 5-2 Overview of Stromboli island showing the villages of Ginostra and Stromboli, the location of COA: Centro Operativo Avanzato and the observatory. Note the horse-shoe shaped depression of the Sciara del Fuoco, the position of the active craters and the Pizzo Sopra la Fossa and the Vancori. Inset shows the summit area in more detail, depicting the area of instrument location: a ridge 400-500 m away from the craters.

5.3 Current activity

The current (June 2004) activity takes place at three main craters located 750 m a.s.l. within the Sciara del Fuoco (*http://www.educeth.ch/stromboli/).* The activity can be observed from the Pizzo Sopra la Fossa (Figure 5-2), an old crater rim ~150 m above the active craters. 'Normal' Stromboli activity (Figure 5-3) consists of Strombolian explosions at irregular intervals lasting from a few seconds up to several minutes (Barberi et al., 1993). Each burst throws incandescent lava fragments, ash, or both, to heights varying between a few tens to hundreds of metres. This explosive activity is associated with persistent degassing. (*http://www.volcano.si.edu/gvp/world/volcano.cfm?vnum=0101-04=&VErupt=Y&VSources=Y&VRep=Y&VSub=N*)

Activity departing from 'normal' is defined as prolonged Strombolian bursts or fountaining (>1 minute), strong explosions with block and bomb ejection onto the Pizzo Sopra la Fossa or beyond, pyroclastic flows, and emission of lava flows (Barberi et al., 1993). Strong explosions occur on average three times per year, and the most recent fatal one occurred in October 2001 when a German tourist was killed. The most recent large explosion took place on 5 April 2003 (Figure 5-3b), when a mushroom cloud rose to 1 km above the crater rim. The summit was covered with a blanket of pyroclastic products, and bombs damaged houses and roads in both villages.

The latest lava flow was active from 28 December 2002 to 22 July 2003 (Figure 5-3c), and reached a thickness of ~50 m. At the start, an eruptive fissure opened at the base of the NE crater and lava reached the sea within 30 minutes. A week later, vents were located at different heights below the craters and different branches of the flow ran down the Sciara del Fuoco. On the 30 of December 2002, detachment of these lava flow deposits from the slope caused landslides which in turn triggered a tsunami (Bonaccorso et al., 2003; Pino et al., 2004). The waves reached several metres in height (Figure 5-3d) and damaged buildings, boats and roads and injured several people in the villages of

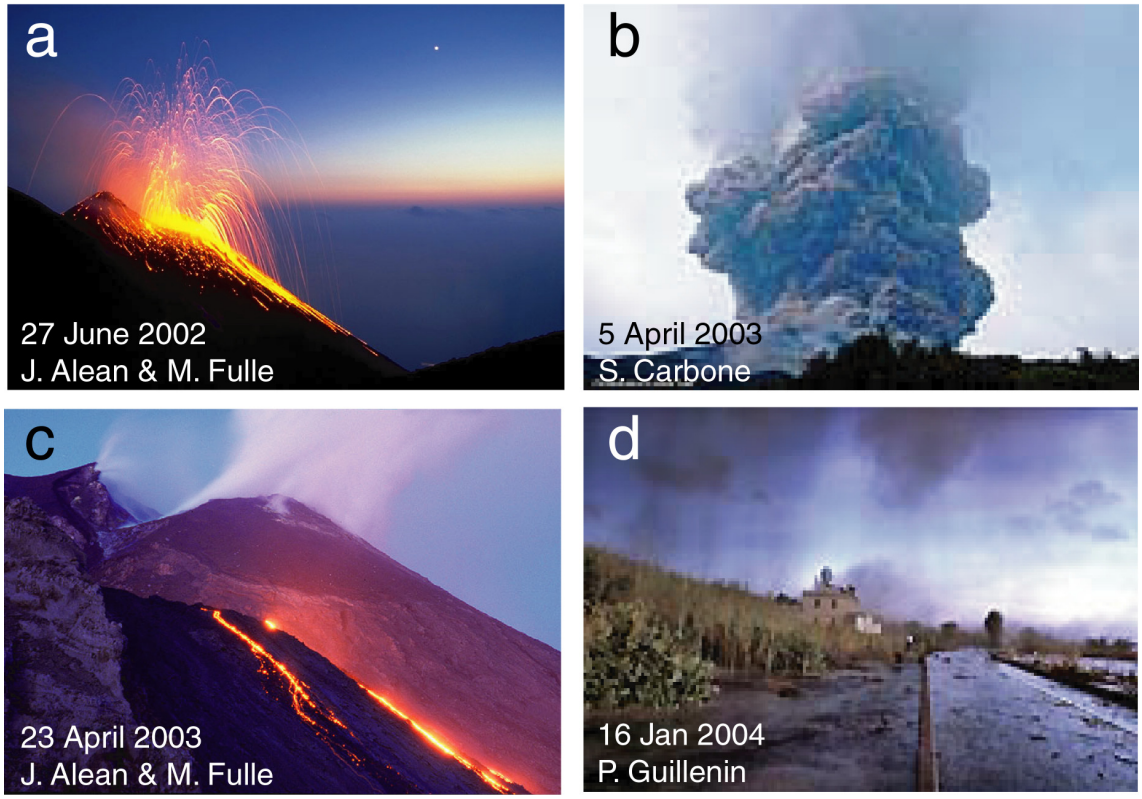

Figure 5-3 Different kinds of activity at Stromboli. The upper left panel (a) shows 'normal' Strombolian activity, lava fountaining. 'Normal' Strombolian activity can be gas or ejecta dominated. The lava fountaining is gas dominated. The upper right panel (b) shows a paroxysmal event, generating an eruption column which reached 1 km above the crater. The lower left panel (c) shows the most recent lava flow, with the NE crater in the background. The lower right panel (d) shows the chaos caused by a tsunami, which resulted from collapse of the poorly attached new lava.

Ginostra and Stromboli. The lave effusion ceased on 22 July 2003 and soon after 'normal' activity resumed.

5.4 Previous work

A team of scientists mainly from the University of Florence, the University of Hawaii, the Alaska Volcano Observatory and the Open University set up a collaborative experiment in 1999 to collect seismic, infrasonic, thermal, meteorological and continuous gravity data. The purpose of this project was to improve the understanding of the dynamics of explosive volcanism.

Activity at Stromboli has been described by two different models. In the first model, rising bubbles collect at a physical boundary, forming a "foam" layer. This boundary may be, for example, a chamber roof or a constriction at the dyke to conduit transition (Ripepe et al., 2002). When this layer reaches a certain thickness it becomes unstable and collapses. This generates a gas slug, which ascends the conduit and causes a Strombolian explosion. In the second model, in slowly rising magma, large bubbles overtake and coalesce with small bubbles and generate a gas slug (Ripepe et al., 2002; Stevenson and Blake, 1998).

The persistent activity at Stromboli must be underlain by efficient conduit convection (Stevenson and Blake, 1998). Gas-rich magma ascends, degasses and sinks within the main conduit either as discrete batches or as a continuous cycle. In addition to strong infrasonic pulses coinciding with the Strombolian explosions, Ripepe and Gordeev (1999) discovered small infrasonic pulses occurring once per second. Visible as 'puffing' at the active vents and associated with shallow volcanic tremor, they are thought to develop as a result of the rising of bubble rich layers as discrete batches. Discrete batches of gas-rich magma layers can be generated from constant gas exsolution, as a consequence of differential gas bubble velocity, which induces

instability waves in magma (Manga, 1996). Alternatively, they could be explained by natural variation in the coalescence of the foam (Vergniolle et al., 1996). If convection occurs in a stable continuous style, then explosive activity should remain fairly regular.

Several cycles are visible in the data collected at Stromboli during the past few years (Harris and Stevenson, 1997; Ripepe et al., 2002). Most prominent are the changes from vigorous to weak explosive activity at minute to hour scale (Figure 5-4). During vigorous phases, bubble layers reach the free surface with a frequency of 0.5-1 sec^{-1}, generating gas puffs. The foam layer builds up rapidly, resulting in frequent foam layer collapse and thus enhanced explosive activity. During weak phases, bubble layers ascend at a rate of 0.25-0.3 sec^{-1}, generating less frequent gas puffs. The foam layer grows more slowly resulting in less frequent foam collapse and thus weaker activity. This cycle is most likely superimposed on longer-term trends (weekly scale) of high- and low-level activity. During high-level activity explosions are ejecta-dominated whereas during low-level activity they are dominated by gas output.

5.5 Working hypothesis

Since the setup of the project at Stromboli in 1999, it has evolved significantly. A permanent thermal, infrasonic and seismic station has now been installed. Data are transmitted to the observatory (COA) on the lower flanks of the volcano and logged using PC's.

By measuring the time delay (Δt) between the arrival at the observation point of thermal and infrasonic pulses, we can get an estimate of the depth of the free surface (h), assuming a constant gas velocity (V_{gas}). Alternatively, assuming a constant depth of the free surface, an estimate of the variation in gas velocities can be achieved.

$$\Delta t = \frac{h}{V_{gas}} - \left(\frac{h}{C_{conduit}} + \frac{x}{C_{air}} \right) \quad \text{(eq.5-1)}$$

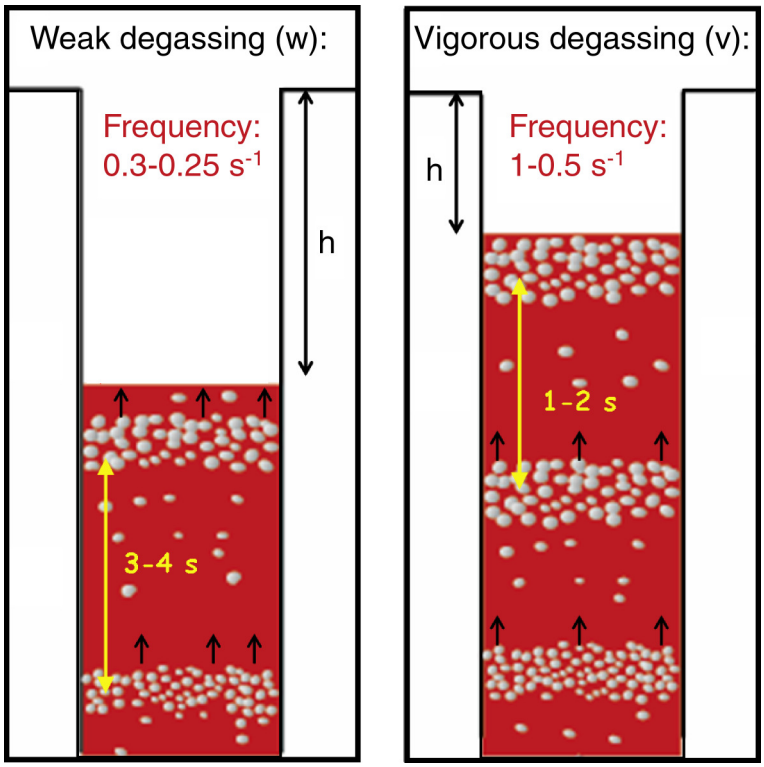

Figure 5-4 Different cycles of Strombolian activity. Variations from weak to vigorous degassing, are visible at minute to hour scale. This is caused by the different frequency at which gas-rich batches of magma arrive at the free surface. The depth of the free surface (h) may be determined with the use of a micro-gravity data. Figure adapted from Ripepe et al. (2002).

With: $C_{conduit}$ = 708 m/s (Weill et al., 1992), C_{air} = 340 m/s and x is the distance from the vent to the detector in m.

Measurements show that time delays are largest during periods of high activity (Ripepe et al., 2002). This suggests the model with batched supply applies in this case. It remains unclear, however, if this results from changes in the free surface level and/or from changes in gas jet velocity.

With the use of Doppler radar measurements, we should be able to see variations in the gas speed during explosions. Continuous micro-gravity measurements may possibly provide estimates of the depth of the free surface (h in Figure 5-4).

5.5.1 Model

Locke et al. (2003) modelled the gravitational effect of mass change in the upper conduit system of persistently active volcanoes (Figure 5-5). The results show that within ~200 m of the active crater, gravity effects will be measurable, e.g., the expected signal is higher than the instrumental noise level (>20 μGal). Micro-gravity variations may be caused by changes in bubble content of the magma, movement of the level of the magma column or change of foam layer thickness. Unlike at most volcanoes, mass changes at Stromboli may occur over relatively short periods, at the minutes to hour scale. To have a chance to record these changes, measurements have to be made at intervals of a few minutes or even more frequently. Continuous micro-gravity measurements have been made at Etna (Carbone et al., 2003), Vesuvius (Berrino et al., 2000), Merapi (Jousset et al., 2000) and Karymsky Volcano (pers. comm., Brodsky, 2002).

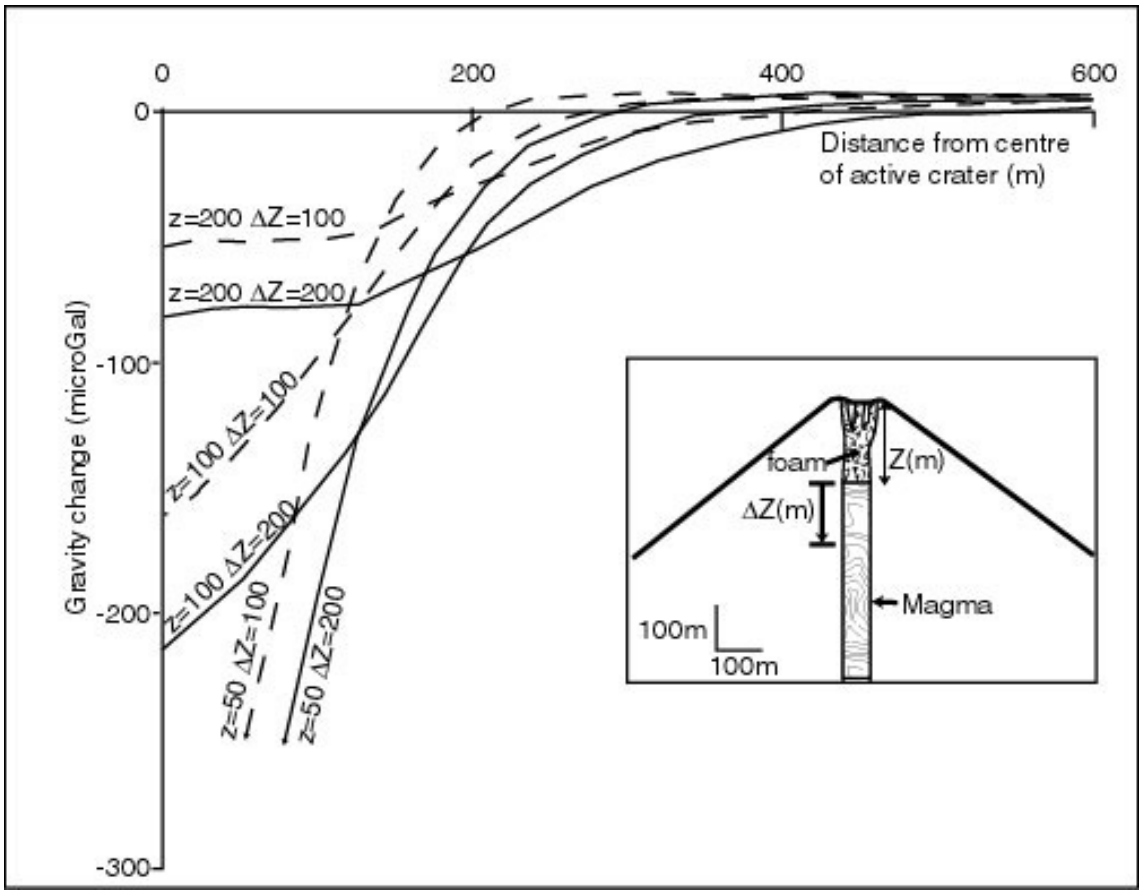

Figure 5-5 The gravitational effect of vertical magma movement in a shallow conduit system based on Stromboli volcano (Harris et al., 1996). The modelled conduit is 50 m wide and the assumed density contrast between magma and foam is 2000 kg/m^3. These calculations suggest that within 200 m of the crater, it is possible to detect micro-gravity changes related to vertical magma movement, whereas further away it will be much more difficult. Figure adapted from Locke et al. (2003).

5.6 D-meters

During this study, gravity was measured using LaCoste & Romberg instruments (http://www.lacosteromberg.com), D41 and D61 with the automatic Aliod 100 feedback system (see APPENDIX B). The instrument displays the gravity (mGal), internal temperature (°C) and battery voltage (volts) directly on an LCD display which is updated every 2 seconds. The data are also sent from a serial port to the PC at 2 Hz as a stream of ASCII data (gravity, long level, cross level, meter temp, battery volts).

Both meters are equipped with two pendulum-type electronic levels, in cross and level direction, with galvanometer output. Unfortunately, the digital level output works only if the meter is set up with levels of the liquid type and the instruments used here are not equipped with those. The 'gravity' is measured using a capacitance bridge with a capacitance plate on the beam and a fixed plate above and below the beam. The Capacitance-beam Position Indicator (CPI) is used to sense the position of the beam. The resulting voltage is then converted to mGal. A 40 second digital FIR low pass filter is applied to the gravity data before they are displayed. A low-pass filter passes relatively low frequency components in the signal but stops the high frequency components. This is necessary to average out the natural background seismic noise.

5.7 Instrument setup

During this study, continuous micro-gravity records (see APPENDIX C) were made at Stromboli volcano, using instrument D41, from 27 July to 14 October 2003. A new bunker was purpose built on a ridge 400-500 m from the summit (Figure 5-2) This location was chosen because it was in line-of-sight with the newly built observatory San Vincenzo (Also called COA: Centro Operativo Avanzato, the operation base from the civil defence at Stromboli, see Figure 5-2) enabling radio telemetry of

data. The concrete box (38.795N 15.22 E) was 0.8 x 0.8 x 0.8 m in size with a drainage hole in the bottom. D41 was installed with its X-level perpendicular to the radial towards the craters and inside a cool-box for thermal insulation (see Figure 5-6). Cables connected the instrument with the antenna and solar panels just 5 m to the N. A transmitter box and software (written in LABVIEW®) were designed (Pasquale Poggi and Maurizo Ripepe, 2003) to enable radio transmission of gravity data, which received the same 'time-stamp' as the other data. Data were stored on a computer at the COA.

5.8 Data Analysis & discussion

All raw data must be corrected for the effects of solid Earth tide. This visco-elastic deformation of the Earth due to the gravitational attraction of the Sun and the Moon may introduce an error of ~ 200 μGal into a single reading. Here we have used computer predicted values calculated with the use of QUICKTIDE®, developed by Micro-g solutions http://www.microgsolutions.com/quicktide.htm). The gravimetric factor (to account for the yield of the Earth in response to tide) used was always 1.16. The tide correction itself was done automatically using scripts written in MATLAB® (see APPENDIX C). Automatic scripts were also used to remove anomalous spikes, caused by transmission problems and re-sampling of the data to one second intervals.

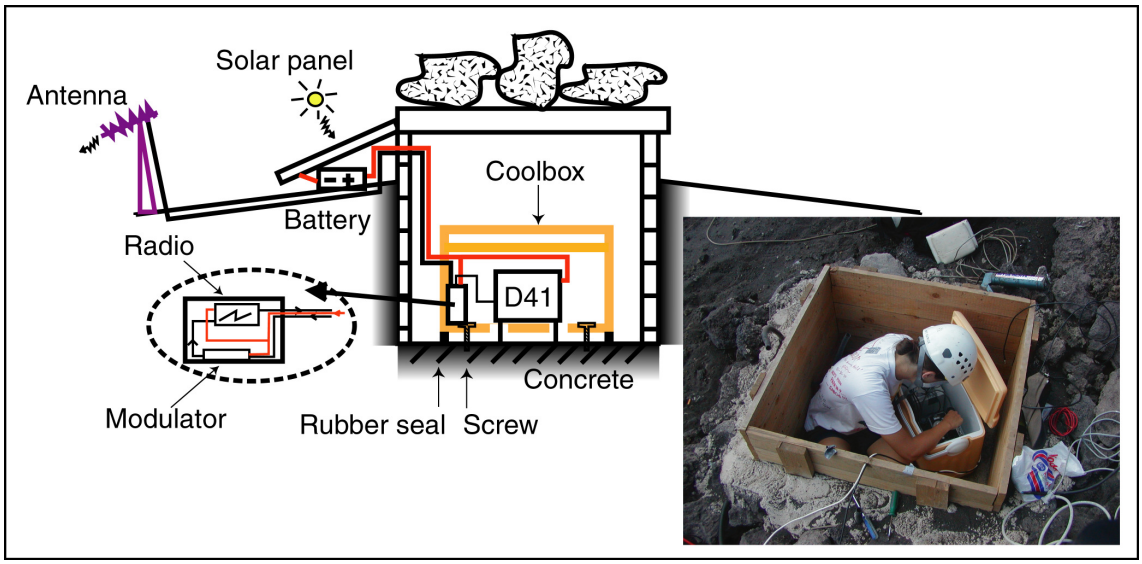

Figure 5-6 Instrument setup at the summit of Stromboli volcano. Data were send to COA by radio-transmission

5.8.1 Long term trends-I

To analyse the long term trends of the data set (Figure 5-7), the data were smoothed using a script written by M. Ripepe (see APPENDIX C). After all corrections were applied, the data still show a more or less linear trend caused by instrumental drift. Instrumental drift is caused by creep in the spring and lever system (Carbone et al., 2003). It is impossible to correct for this drift since the supposedly linear trend shows too many changes in slope. Another remaining effect visible in the data has a daily period and an amplitude of ~100 μGal (Figure 5-7). I suggest this last effect is caused by atmospheric perturbations as suggested by other authors (Andò and Carbone, 2001; Carbone et al., 2003; El Wahabi et al., 2000). The most likely atmospheric interference responsible for the observed effect is temperature, although humidity, which is dependent on temperature, could be directly responsible for gravity changes correlating with temperature (Bastien and Goodacre, 1985; El Wahabi et al., 2000).

For the above reasons, it was impossible to analyse the long term trend of this data set. However, a previously unnoticed signal, with a half-period ranging from ~8 to~43 minutes and an amplitude of ~20 μGal, was observed (Figure 5-7). The 'wiggle' signal, from now on called a Low Frequency Oscillation (LFO) shows both gravity decreases and increases and ends at a similar, but not exactly the same, level compared to where it started. The period of this signal is too short to be influenced significantly by temperature variations and/or instrumental drift. The signal could be caused by: i) movement of the internal instrument mass unrelated to gravity changes, ii) tilt of the volcano iii) 'breathing' of the volcano iv) another instrumental effect or v) change of magma column height/foam thickness. Movement of the internal instrument mass unrelated to gravity changes is caused by seismic displacement. Seismic displacement causes unbalance of the mass on the spring resulting in apparent gravity changes while the instrument is stabilising. The half-period of such a process must be short and is

unlikely to be 15-30 minutes. Volcanic tilt is an ongoing process, however it seems unlikely the tilt would change direction (to give the apparent gravity decreases and increases) in such a short time period, and tilt is a more continuous process. Volcanic 'breathing' as suggested for Monteserrat analysing semi-continuous SO_2 flux and continuous seismic data (Young et al., 2003) has a period of a few hours and a varying amplitude. This contradicts our Strombolian observations and 'breathing' is therefore discarded as the most logical explanation for our observations. If the signal was caused by an instrumental effect, its occurrence would be expected to be more regular.

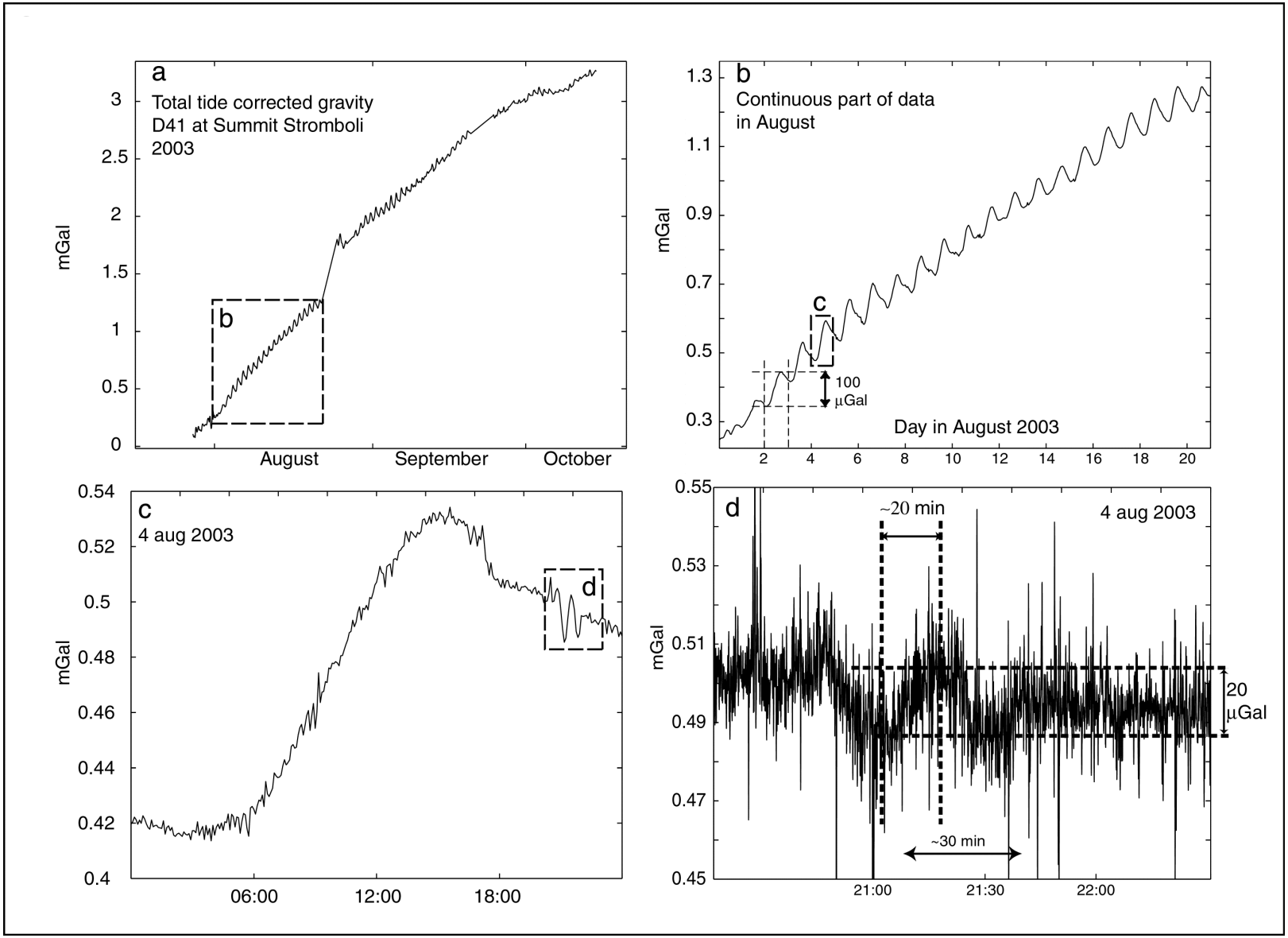

Figure 5-7 D41 recording at the summit of Stromboli volcano. a) All tide corrected data acquired during this survey. The linear trend is caused by instrumental drift. b) Longest continuous part of the data set, covering 1-21 August 2003. The daily oscillations may be related to atmospheric influences. c) Results for one day in August. Note the occurrence of the LFO.d) Close up of LFO, with a half-period of ~20 minutes and an amplitude of 20 µGal.

The most plausible explanation is that the LFOs represent real gravity changes which may be caused by changes in magma column height and/or foam thickness.

Assuming that the entire observed gravity signal is related to magma column height changes then we can calculate the point mass change responsible for a 20 μGal, variation:

$F_v = ma$ (eq.5-2)

$F = \frac{m_1 m_2}{r^2} G$ (eq. 5-3)

and $F_v = F\cos\theta$ (eq. 5-4)

result in: $g = G\frac{m_2}{r^2}\cos\theta$ (eq. 5-5)

with: F is the force in N = kgm/s^2, F_v is the vertical force in N = kgm/s^2 (only vertical Force is measured by a gravity meter), m is the mass in kg, G is the Gravitational constant of 6.67 x 10^{-11} Nm^2/kg^2, r is the line-of-sight distance between instrument and craters in m, g is the gravity caused by mass m in μGal = 10^{-8} m/s^2 and θ is the angle between F_v and F in degrees.

If we assume the craters are located 150 m below and 450 m line-of-site distance away from the Pizzo Soppra la Fossa, θ is calculated to be 70°. Following equation 5-5, a micro-gravity change of 20 μGal at a distance of 450 m from the craters could be caused by a point mass change of 1.8 x 10^9 kg (see Figure 5-8a).

To visualise the extent and likelihood of such a mass change at Stromboli, we assume a density of 2700 kg/m^3 and calculate the volume the mass would occupy to be ~6.6 x 10^5 m^3. We then visualise this volume change by a height or radius change in a cylinder (e.g., the conduit of Stromboli) with a volume V_c of :

$V_c = \pi r^2 h$ (eq. 5-6)

with: r is the radius of the cylinder in m, h is the height change of the cylinder in m.

From equation 5-6, it follows that the volume change could be represented by a column height change of 60 m in a conduit with a radius of 60 m (Figure 5-8b). Other combinations of height change and radius can also produce the same volume and thus mass change.

During periods of 'normal' activity, several different vents within the three craters at Stromboli are active throughout the day. Sub-surface linking of these vents has been suggested by several authors, based on statistics of visual observations (Settle and McGetchin, 1980), thermal data (Harris et al., 1996) and seismic data (Ntepe and Dorel, 1990). Harris et al. (1996) envisaged this vent linking in the form of i) a wide conduit which branches into several narrow conduits which connect to each vent or ii) a wide conduit culminating at a shallow magma chamber which branches into several narrow conduits branching which connect to each vent. From a gravity point of view, we are especially interested in two parameters of these possible models: the diameter of the wide conduit/magma chamber and the depth of the magma free surface. Estimates for the diameter of the conduit/chamber vary from 50-100 m (Harris and Stevenson, 1997; Locke et al., 2003). The 60 m radius suggested in this work is on the high end of this spectrum but in the same order of magnitude. All authors agree that the depth of the magma free surface and/or the depth of the linking shallow magma chamber is 100-600 m. They base their estimates on photoballistic (Chouet et al., 1974), seismic (Chouet et al., 1999; Neuberg et al., 1994; Ripepe et al., 2001) and/or thermal (Harris and Stevenson, 1997; Ripepe and Braun, 1994) observations. These observations suggest the depth of the magma-free surface is sufficient to allow for a 60 m height changes as suggested by our model. Magma column height fluctuations from ~30-150 m have been suggested previously, based on arrival times of seismic waves and air waves (Ripepe and Braun, 1994; Ripepe et al., 2002). Maybe a slightly smaller conduit diameter (~80 m) and a higher magma column change (135 m) are more realistic. If the observed

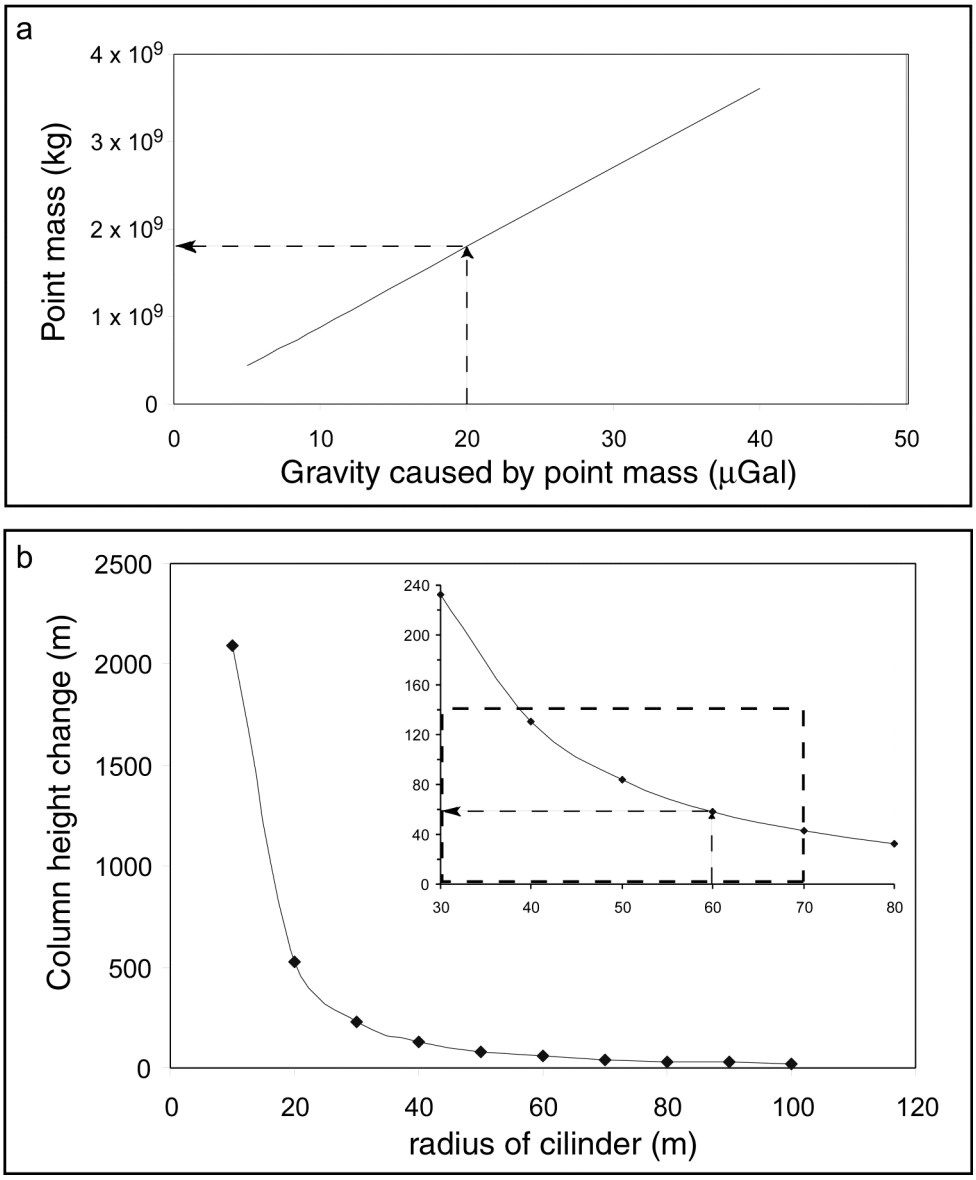

Figure 5-8 Modelling of point source mass responsible for the observed micro- gravity change and its relationship to magma column height change and conduit radius, following equations 5 and 6. a) Calculated values for the point mass able to cause certain gravity changes. r = 450 m, g = 20 μGal, G = 6.67 x 10-11 Nm2/kg2, θ = 70°.b) The size of a cylinder in which a point mass of 1.8 x 109 kg could be 'fitted' assuming a density of 2700 kg/m3. The inset shows a zoomed in section of the same graph depicting the area with physically realistic values with a dashed box.

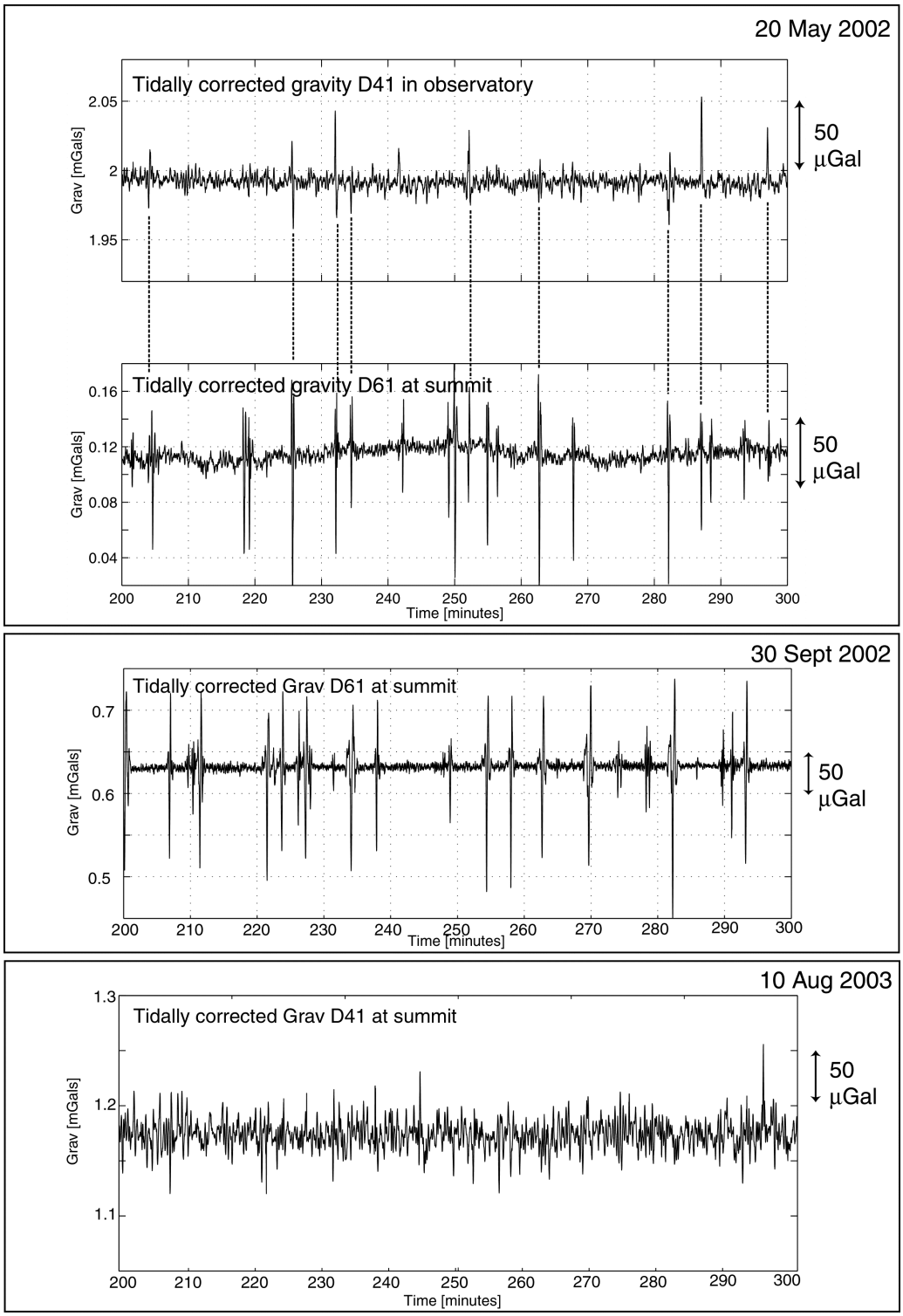

Figure 5-9 HFOs recorded with micro-gravity instrument. The pilot study showed that HFOs recorded at the summit may be picked up at the observatory on the lower flanks. The amplitude of the 'spikes' during this survey was ~100-150 µGal. The 'spikes' picked up during this period had a higher amplitude, ~150-250 µGal which correlates with the increased activity at the summit and the increased height of the explosions at the summit. This survey shows D41 is also able to detect HFOs at the summit, but they are less obvious due to increased background noise. Activity had just resumed after the flank eruption ceased and explosions were relatively small. Amplitude of HFOs at this time is ~100 µGal.

signal represents magma column height changes, a height change of ~135 m was established in 8 to 43 minutes. In other words the column rose with 5-28 cm per second. These values, especially those to the lower side of the range, seem feasible in an open conduit system were the magma has an easy way of passage.

5.8.2 Short term spikes, High Frequency Oscillations (HFOs)

An interesting short term feature are the 100-150 μGal HFOs, which occur on average ~15 times per hour (Figure 5-9) and have a period of 30-60 seconds. These short term HFOs were registered by both gravimeters when installed at the summit, and also at the observatory when events were fairly large. They were first observed during a pilot study in May 2002 when D61 was installed at the summit. It was a revelation to discover these as we did not anticipate any such signal in the data set.

If we compare the HFOs with the time of the sound of the explosion observed at the summit, they correlate very well (Figure 5-10a). There is also a strong correlation between the crater origin of the explosion and the amplitude and shape of the signal. The bigger explosions from the SW crater all have a similar waveform shape. The central crater explosions all have an up-down motion with small amplitude and the NE crater shows a similar 'tooth-shape' in all its explosions. This is an interesting observation as it may enable definition of the source crater when it is not possible to observe this visually, e.g., because of cloud cover. The waveform of the HFO may be controlled by the geometry of the upper part of the conduit, before the rising bubble reaches the surface. When the geometry of the conduit changes, the characteristic shape for the crater may also change. The shape of the waveform may be used to identify which crater exploded but one has to understand that the dynamics of the system mean it changes and it therefore can not be used through time.

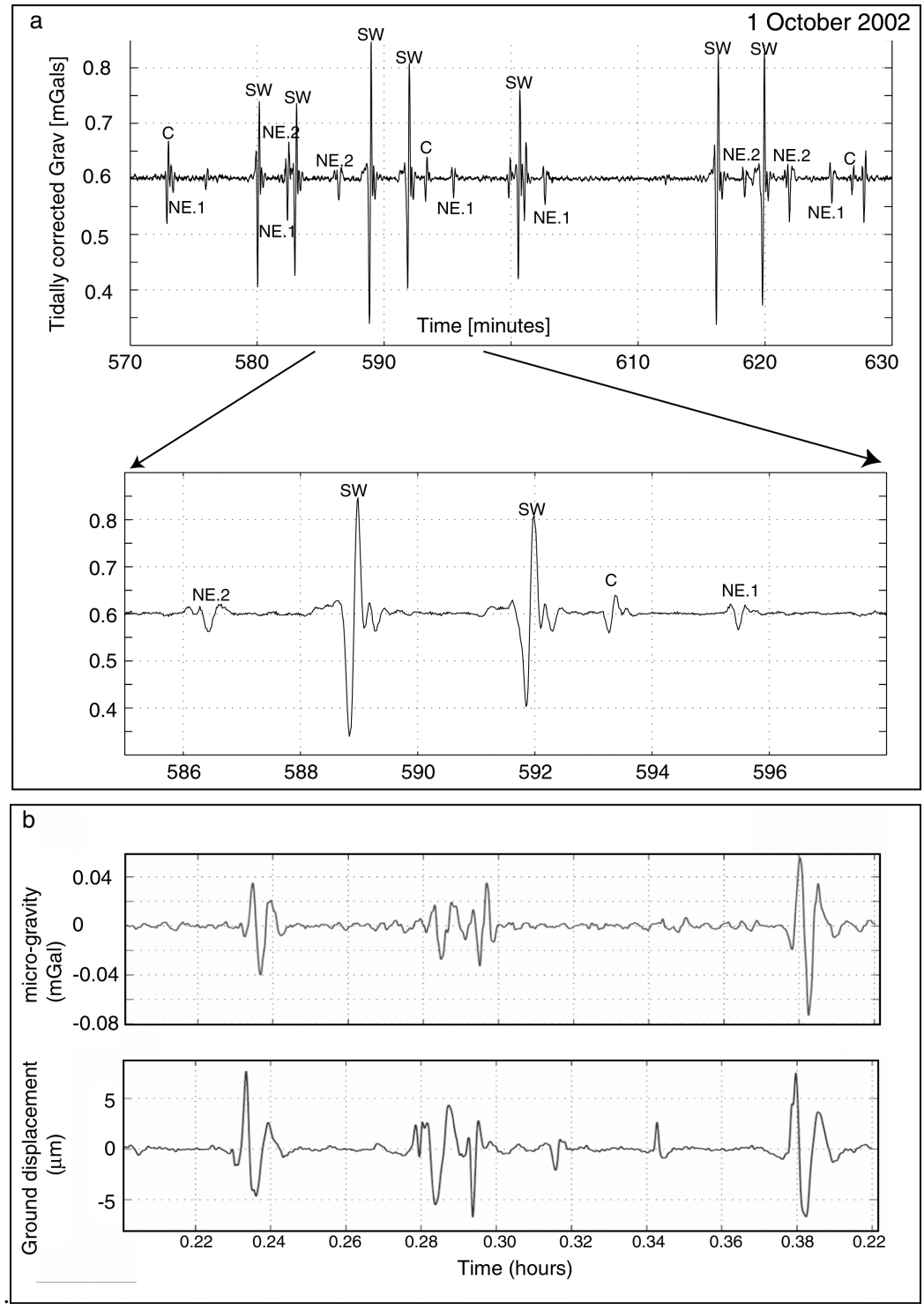

Figure 5-10 a) Correlation between HFOs recorded with micro-gravity instrument and visual observation from Pizzo Soppra la Fossa (Figure 5-2). SW stands for southwest crater, C stands for central crater and NE.1 and NE.2 stand for northeast crater vents 1 and 2. Timing of the visual observation (noted with a letter code on the signal trace) correlates exactly with the observed HFOs. Note that shape of the HFO seems to be consistent with the crater in which the explosion occurs (see zoomed in section of Figure). The shape of the HFO might be controlled by the geometry of the upper part of the conduit, before the bubble reaches the surface. b) Correlation between micro-gravity and ground displacement acquired from a broadband seismometer. See text for discussion.

However, it seems highly unlikely that this signal represents a real gravity change. The period of the signal is too short to explain the amplitude in terms of sub-surface mass changes. Also, we would not expect such a large sub-surface mass change at the location of the instruments, e.g., away from the active vents, nor would we expect sub-surface mass change to reverse within the period of the signal. Another explanation of the gravity change is by ground deformation. However, to create the observed amplitude, the ground would have to have moved by 30-50 cm (using the theoretical change of gravity with elevation of 308.6 μGal/m) in less than 1 minute. This is unlikely since no ground disturbance, like fracturing, was observed. Furthermore to reverse the signal ground movement would have to be in the opposite direction which in such a short time span is impossible. The final possibility is that the signal was caused by an instrumental effect. Strong sudden movements of the internal mass might overwhelm the damping system and cause the gravimeter to respond like a conventional seismometer. This movement could be translated into 'apparent' gravity changes which are meaningless.

To check the last hypothesis, the gravity signal was compared with that from a broadband seismometer, running less than 5 m away from the gravimeter for most of the time. When we compare the gravimeter signal with the integrated data collected by the broadband seismometer (displacement) we observe a good, i.e., more or less perfect, correlation (Figure 5-10b). This suggests our gravity meter is indeed functioning as a seismometer which is understandable if we realise the broadband seismometer also uses a mass on a spring. It should be pointed out that since the costs of a micro-gravity instrument are tenfold compared to those for a broadband seismometer, it does not seem wise to use the gravity meter solely to detect the signals described above.

The above observations suggest that the short term HFOs are caused by the seismic vibrations during an explosion and represent foam collapse resulting in

degassing or even a Strombolian explosion. This means they do not represent a real micro-gravity change. One should realise that in fact these signals may be a source of error during continuous micro-gravity surveys, i.e., a reading at the peak or through of a HFO is not representative. This problem could be overcome, for example, by generating 1 data point a minute by taking the median of 60 data points sampled with a 1 second interval.

Another observation made in the data set collected during the pilot study was the transition from low to high level of activity on 30 September 2002 at ~08:30 GMT (Figure 5-11). This transition is most obvious from the increase amplitude of the HFOs. It correlates with the visual observation that around that time explosions reached higher above the crater rim (700 m compared to earlier 200 m) and became ejecta-dominated rather than gas-dominated. This type of change may take place at a weekly scale (Ripepe et al., 2002). There are also periods of 'pausing' between the HFOs, when the HFO density is lower (Figure 5-11). This may relate to changes in degassing rate at a minute to hour scale as suggested by Ripepe et al. (2002).

5.9 Summary and recommendations

- Modelling (Locke et al., 2003) shows that micro-gravity changes may be picked up at Stromboli volcano if the instrument is installed less than 300 m away from the active craters.
- However, utmost care should be taken when preparing the instrument. The level setup should be checked and the gravity difference over a known height difference should be measured and compared to the expected gravity change over that height difference.

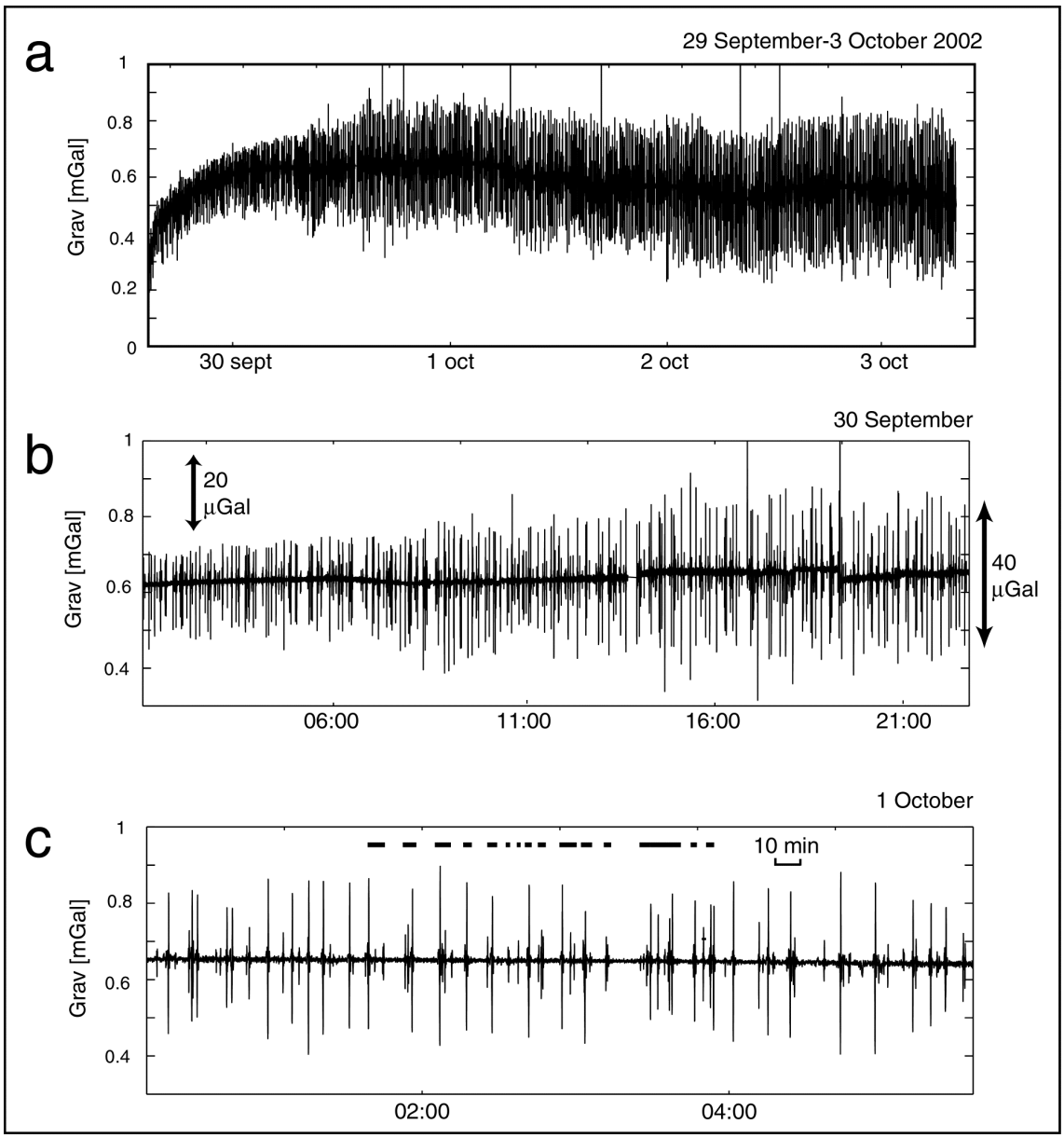

Figure 5-11 Cycles of activity as observed during the pilot study. Change in style of activity is visible in the middle panel (b) when the amplitude of the HFOs doubles in size. This change is thought to take place at a weekly scale. Possible change in degassing rate is visible in the lower panel (c), where the line above the data indicates active periods as registered by D61, followed by quiet periods indicated by gaps. Changes in degassing rate are thought to take place at minute to hour scale.

- Temperature, pressure and humidity should be measured at the site, to allow for possible correction. Variations in these parameters should be kept to a minimum.
- Radio-transmission of data allows for real-time monitoring of changes and is favoured above data logging at the site.
- Interpretation of long-term trends may be possible, but more extensive data are needed to be able to control the instrumental drift. Also the site should be stable enough to prevent the instrument from drifting off level.
- The data collected so far at Stromboli volcano show High Frequency Oscillations (HFOs) and Low Frequency Oscillations (LFOs).
- LFOs may represent real gravity changes. Their amplitude coincides with a mass change of ~1.8 x 10^9 kg which could be caused by a column height change of 60 m in a conduit with a radius of 60 m.
- HFOs do not represent 'real' gravity changes; they are caused by movements of the mass inside the instrument caused by vibrations. They correlate with visual observations and broadband seimic data, change waveform depending on the crater of origin and can be envisaged as foam collapses related to degassing events and/or Strombolian explosions.
- LFOs and HFOs are caused by different volcanic processes with different time scales. HFOs have a very high frequency and even though observed gravity changes are not 'real' they are caused by a very fast rate volcanic process (degassing/Strombolian explosions). LFOs have a lower, but still relatively high frequency, and are caused by a volcanic process with a slightly slower rate (possible movement of magma). Both of these volcanic processes are however very fast (second to minute scale) compared to volcanic processes at Askja and Krafla (decades).

Chapter 6: Conclusions and recommendations

6.1 Broader implications

6.1.1 Introduction

Volcanic processes are the common thread used throughout this project. I have used a range of geophysical techniques to try and learn more about the volcanic processes at the chosen 'example' settings of Stromboli, Italy and Askja and Krafla in Iceland. I analysed stand-alone data sets but also combined them to improve the understanding of the volcanic processes at work at each volcano. I have used a range of geodetic techniques, although micro-gravity measurements, either as a dynamic survey or continuous, have played a major role. I combined these micro-gravity measurements with precise levelling, GPS, EDM, tilt and InSAR measurements.

Rates of volcanic processes vary from fast, represented by our Stromboli setting, to slow, symbolised by our Icelandic volcanoes. The aim of this project was to improve our understanding of volcanic processes at each end of the spectrum. Any of the findings at our 'example' locations might be applicable to similar volcanoes worldwide.

6.1.2 Volcanic processes at persistently active volcanoes (Stromboli)

A combined effort to acquire an extensive data set of activity at Stromboli was started in 1999. The data set consists of seismic, infrasonic, thermal, FLIR, micro-gravity, Flyspec, FTRI, ash-chemistry and visual data collected simultaneously whenever possible. It has been possible to combine the thermal, seismic and infrasonic data to improve our understanding of the conduit system. Our expectation was that by adding micro-gravity data we might be able to learn even more, especially about the movement of magma or foam in the shallow conduit. Unfortunately we encountered

technical problems, which we did not anticipate. Only part of the data turned out to be of high enough quality to interpret, and interpretation in terms of volcanic processes was very difficult. However, the project did not fail completely, as we did learn about the abilities of the micro-gravity instrument and the installation of a continuous micro-gravity instrument (see sections 6.2 and 6.3).

6.1.3 Volcanic processes at calderas in a state of unrest (Askja and Krafla)

Askja and Krafla volcano are both located within the extensional regime of the North Volcanic Zone, approximately 70 km apart (Figure 1-1 and Figure 6.1). Both volcanoes have developed at least one caldera, and magma is thought to be supplied by a shallow magma chamber at ~3 km depth (Árnadóttir et al., 1998; Rymer et al., 1998a; Rymer and Tryggvason, 1993; Sigmundsson et al., 1997; Sturkell and Sigmundsson, 2000; Sturkell et al., 2004 - submitted; Tryggvason, 1986). The location of these shallow magma chambers has been well established at both volcanoes using a diversity of techniques. At Krafla, Tryggvasson (1989) proposed a series of stacked magma chambers at 2.6 km, < 10 km, > 20 km and an undetermined depth, based on tilt data. De Zeeuw-van Dalfsen et al. (2004a) showed the likely existence of at least one deeper reservoir, at 21 km depth, using InSAR data. At Askja, the existence of a deeper reservoir at ~16 km depth was suggested by Sturkell et al. (2004) based on GPS and tilt data.

A N-S seismic reflection profile (Brandsdóttir et al., 1997) of 21 km length, indicates the location of the Moho underneath the Krafla area. The location of the Moho coincides with the proposed location of the 21 km deep magma reservoir. The shallowing of the Moho towards the Krafla rift axis may even focus magma flow towards it. There are no data available that can determine the depth of the Moho at Askja. I suggest that the deeper reservoir at Askja is probably also located close to the crust-mantle boundary.

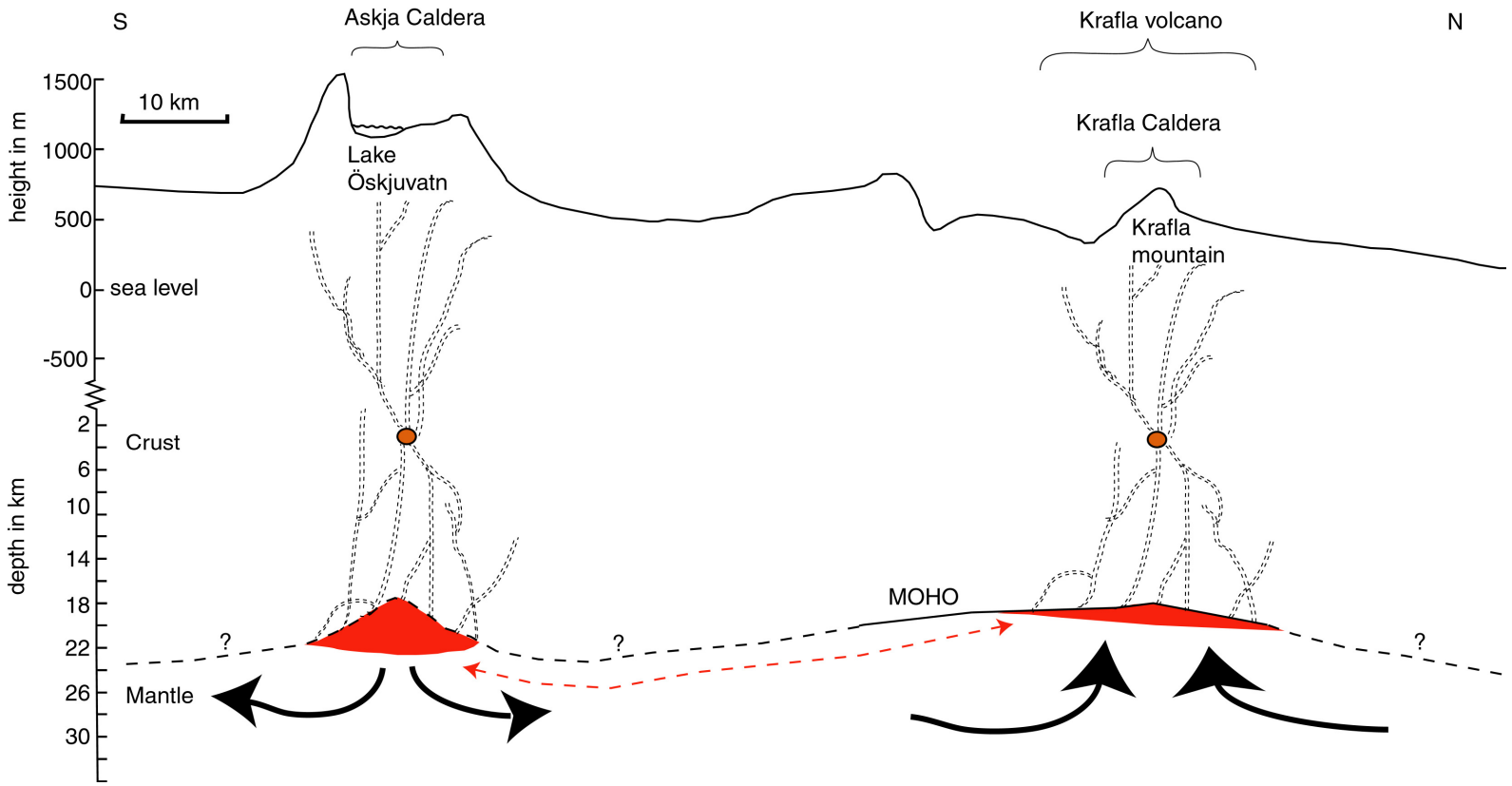

Figure 6-1 NS Profile and cross section across Krafla and Askja caldera. Note that this is a schematic drawing based on data wherever possible but relying on interpretation as well. Also note the change in vertical scale. Krafla caldera is not easily recognisable in the field because it is completely filled with lava. The profile crosses the Krafla caldera at the location of Krafla mountain, making it look like a mountain rather than a caldera. The small circular features at ~ 3 km represent the shallow magma chambers. The Moho is a solid line when data are available and dashed when its location is inferred. The dotted red line between the two volcanic systems represents the suggested pressure-link

Micro-gravity observations at Askja (de Zeeuw-van Dalfsen et al., 2004b) suggest that a combination of magma drainage and cooling and contraction of the shallow magma reservoir at 3 km depth is responsible for the observed surface deformation. They suggest that extensional tectonic forces generate space in the ductile part of the crust to accommodate on-going magma drainage from the shallow magma chamber to the deeper reservoir. Micro-gravity observations at Krafla also suggest the occurrence of magma drainage (de Zeeuw-van Dalfsen et al., submitted Aug 2004) although observations are hampered by water extraction at the geothermal power plant. I suggest that the process of magma drainage at Krafla is similar to that proposed for Askja. Magma drainage from the shallow magma chamber towards the deeper reservoir is visualised as an ongoing process, facilitated by the creation of space in the ductile part of the crust generated by extensional forces. It is possible a pressure-link between these volcanoes exists along the ductile lower crust in Iceland.

Recent InSAR data from the 1993 to 1999 period (de Zeeuw-van Dalfsen et al., 2004a) suggest that the 21 km deep reservoir at Krafla is actually inflating. Magma might accumulate at deep levels under Krafla in the decades after termination of a rifting episode. Co-rifting pressure decrease of the deeper source stimulates the subsequent inflow of magma. This inflow might influence conditions along the plate boundary as far away as Askja, 70 km to the south of Krafla. The density contrast between the lower crust and mantle at Krafla may trap magma, regardless of the lower than average contrast of 90 ± 10 kg/m^3 (Gudmundsson, 2003). When pressure in the deep source reaches a critical value, magma migrates to the shallow magma chamber from where it can eventually erupt during a new rifting episode. This complex magma plumbing system is consistent with long periods of dormancy (200-1000 yr) between rifting events.

Sturkell et al. (2004) estimated the volume decrease of the deeper Mogi source to be 0.412 km^3 during the 1973-2003 period or 0.014 km^3/yr assuming constant drainage. Even though this volume change is very uncertain, as it is based on the assumption that 20% of the inferred subsidence is due to the deeper source, it is in the same order of magnitude as the volume increase of the deeper Mogi source at Krafla of 0.026 km^3/yr as inferred by de Zeeuw-van Dalfsen et al. (2004a) using InSAR. The same volume decrease as increase would be found if, for instance, the deeper source at Askja contributes more than expected (40% instead of 20%) or if the source was deeper (22 km instead of 16.2 km). Of course any combination of the two is also possible.

The process described here (a pressure-link at the level of the lower crust) may be common at thin constructive plate boundaries. Possible links between other Icelandic volcanoes (see Figure 1, Chapter 1) have been implied previously. Eyjafjallajökull and Katla in south Iceland have a history of simultaneous activity suggesting a possible link (Sturkell et al., 2003) and in 1996, earthquakes at Bardarbunga cumulated in eruptive activity at Grimsvötn a day later (Einarsson, 1996).

It is possible that not only Icelandic but also other volcanoes are interconnected, although the already suggested connections are mostly shallow in nature. In Alaska, connections between Katmai volcano and Novarupta have been suggested by Hildreth (1987) based on geochemical and structural relationships. Magma drainage from Katmai Volcano to Novarupta resulted in the collapse of the summit area, forming the caldera. At Mauna Loa and Kilauea in Hawaii the possible connection between the two volcanoes remains a controversy. Recently, Miklius and Cervelli (2003) suggested a crustal-level interaction between the two magma systems based on a short timescale correlation found in continuous deformation data.

Active volcanoes around the world can be divided into three types: spreading centre volcanism, subduction volcanism and intraplate volcanism. In this thesis I have

suggested, based on observations at Askja and Krafla volcanoes, that volcanoes near a spreading centre might be connected at deep levels. This connection is facilitated by the ongoing spreading, allowing space to be generated in the ductile part of the crust and by the linear character of the setting. Volcanoes in a subduction and intraplate setting do not follow these characteristics and are therefore less likely to be connected at deep levels in a similar manner.

6.2 General conclusions (answers to questions posed in Chapter 1)

This study has shown that the combination of geophysical techniques can be a very powerful tool in understanding the complexity of volcanic processes in active volcanoes. Specific conclusions following from this work are:

1) Deflation observed at the surface of Askja caldera is caused by a combination of cooling and contraction of the shallow magma chamber and by magma drainage. The extensional regime generates space in the ductile part of the crust allowing the drained magma to flow to deeper levels. A pressure-link between volcanoes along the spreading plate boundary in north Iceland may effect conditions along that boundary. Activity at Krafla may influence that as far away as Askja thereby increasing the rate of deflation there.

2) Analysis of InSAR data of Krafla indicates the existence of a magma reservoir at 21 km depth, close to the crust-mantle boundary. This reservoir has been inflating at least since 1993, at a rate of ~ 26 x 10^6 m^3/yr, suggesting magma is accumulating at this depth. When the reservoir reaches a certain pressure limit, magma will move to the shallow magma chamber from where it may eventually erupt during a fissure eruption. This fits in well with the long periods of dormancy of 100-200 years, between rifting episodes.

More surprisingly, the effect of such deep sources is recordable at the surface! This suggests that deep sources at other volcanoes may also have detectable effects at the surface.

3) The net micro-gravity changes at Krafla for the 1990-2003 period have been calculated taking into account the water extraction by the geothermal power plant. A net micro-gravity decrease was found and magma drainage is suggested as the most likely cause of this decrease.

4) It may be possible to observe magma column or foam height changes in the open conduit system of Stromboli volcano (or similarly active systems) with the use of continuous micro-gravity techniques, but advances have to be made to improve the control on the diverse factors (such as humidity) influencing the data.

5) Based on observations at Askja and Krafla volcanoes, I suggest that volcanoes in a spreading centre may be connected at deep levels (around the crust-mantle boundary) allowing magma to move from one deep reservoir to another as stimulated by the local pressure differences between the reservoirs. This connection is facilitated by the ongoing spreading, allowing space to be generated in the ductile part of the crust and by the linear character of the setting.

6.3 Recommendations for future work

6.3.1 at Askja

1) The nature of the micro-gravity network as it stands now only allows for minimum estimates for mass and volume changes because deformation is known to continue beyond the current network. A new station (DYNG) further away from the caldera, unfortunately still on the edge but within the deformation zone, has been measured in 2002 and 2003. Continuation of these measurements will provide better estimates for the mass and volume changes in the future once this station can be used as

a reference point. It is feasible to use this station as a reference because it is close to the location of the overnight hut and measurements can be taken each day before setting off and upon return. Furthermore this station also serves as a reference station for the current GPS network and accurate height control is therefore readily available. It is logistically not feasible to construct a base station outside the deformation zone.

2) Three more stations (NE0205, NE0206 and 430 on the levelling line), located within the deformation field, have been added to the micro-gravity network. They should be measured during the upcoming field campaigns, which we advise to be held at least once every two years, following the current activity. Measurements at these stations increase the 'spread' of the stations possibly allowing for more advanced modelling, using sources with shapes other than a point source.

3) Choosing the right reference point is of utmost importance. However, it is impossible to know where will be the best location at the start of a long time series of data collection. Therefore it is unavoidable to have to change to a more suitable reference station throughout the study. It is therefore advisable to measure more than one station on a daily basis, so that in the future data can be referred to this second station and are not 'lost'.

4) I recommend that geodetic data are taken simultaneously with the micro-gravity readings to improve height corrections. This way unnecessary interpolation and extrapolation can be avoided, improving the quality of the resulting values. This would have the added advantage that height changes would no longer be model dependent.

6.3.2 at Krafla

1) At Krafla the same recommendations apply as for Askja. The reference station situation at Krafla is even worse then at Askja because the GPS measurements are referred to a station in the middle of the deformation field. It should be possible to

compromise and decide on a station suitable for use by both the micro-gravity network and the geodetic network in the future.

2) Values for the water extraction and injection at the Krafla geothermal power plant (from the National Energy Authority) should be requested each year to be able to correct the micro-gravity data. To improve the correction, more detailed information is necessary about the characteristics of the producing aquifer, especially about the extent of the area from where the aquifer is replenished.

3) InSAR data have suggested an inflating source at 21 km depth north of Krafla mountain. This inflation is also detected by geodetic measurements in that area. Unfortunately the current micro-gravity network does not continue into the area which is inflating. I therefore suggest expansion of the micro-gravity network to the north. This expansion should be done by taking into consideration the currently measured geodetic stations in this area because correction for height changes remains essential. As the area comprises several previously established (geodetic) stations, I would suggest using two or three of those.

4) The InSAR images generated during this study can be modelled taking into account more factors. A more sophisticated Earth model would use brittle and ductile layers which may modify the results. Another improvement would be to use existing GPS data (Völksen, 2000) to calibrate the interferograms. Further studies should also consider if post-rifting adjustment may eventually contribute to the observed signal.

5) A problem with the ESR-2 satellite in 2001 resulted in the failure of the production of good quality interferograms overlapping this period (combining an image before the failure with one from after the failure). It should, however, be possible to combine radar images from after the failure so a continuous interferometric data set of the Krafla area can be established. This is important to evaluate if the inflation is

ongoing and how it is progressing. Also in the near future, it may be possible to complement the data set with ENVISAT InSAR data.

6) Try to find evidence for other (Icelandic) volcanoes with a deep magma reservoir by looking at previously recorded geodetic data.

7) Track the Moho further south towards Askja, building upon the work by Brandisdottir et al (1997).

6.3.3 at Stromboli

1) Make sure levels are set correctly and instruments are properly sealed before installing them at the volcano. Also make sure the legs of the instrument have an equal length. This minimises the problem with the instruments becoming off level during the survey.

2) Record meteorological parameters such as temperature, pressure and humidity, at the same frequency as the continuous micro-gravity. This enables corrections for these parameters if necessary and allows you to observe if the micro-gravity data correlate with any of these parameters.

3) A major campaign would use at least six instruments set up in pairs. Two set up at the summit, two at the flanks and two in the observatory. The reason for using two instruments at the same location is to exclude individual instrumental factors. The reason for setting up instruments at different distances from the active craters, and thus from the magma and or foam column movements, is to establish that the observed signature is indeed caused by a magmatic process (it should not be recordable further away from the active craters).

Bibliography

Ágústsson, S., 2001, Landhæðarbreytingar á Kröflusvæðinu (in Icelandic): Reykjavik, Thesis, Háskóli íslands.

Allard, P., Carbonnelle, J., Métrich, N., Loyer, H., and Zettwoog, P., 1994, Sulphur output and magma degassing budget of Stromboli volcano: Nature, v. 369, p. 326-329.

Allen, R.M., Nolet, G., Morgan, W.J., Vogfjörd, K., Bergsson, B.H., Erlendsson, P., Foulger, G., Jakobsdóttir, S., Julian, B.R., Pritchard, M.J., Ragnarsson, S., and Stefánsson, R., 1999, The thin hot plume beneath Iceland: Geophysical Journal International, v. 137, p. 51-63.

Allen, R.M., Nolet, G., Morgan, W.J., Vogfjörd, K., Bergsson, B.H., Erlendsson, P., Foulger, G., Jakobsdóttir, S., Julian, B.R., Pritchard, M.J., Ragnarsson, S., and Stefánsson, R., 2002a, Imaging the mantle beneath Iceland using integrated seismological techniques: Journal of Geophysical Research-Solid Earth, v. 107, p. 2325.

Allen, R.M., Nolet, G., Morgan, W.J., Vogfjörd, K., Nettles, M., Ekström, G., Bergsson, B.H., Erlendsson, P., Foulger, G., Jakobsdóttir, S., Julian, B.R., Pritchard, M.J., Ragnarsson, S., and Stefánsson, R., 2002b, Plume-driven plumbing and crustal formation in Iceland: Journal of Geophysical Research, v. 107, p. 101029.

Amelung, F., Jonsson, S., Zebker, H., and Segall, P., 2000, Widespread uplift and 'trapdoor' faulting on Galapagos volcanoes observed with radar interferometry: Nature, v. 407, p. 993-996.

Amelung, F., and Day, S., 2002, inSAR observations of the 1995 Fogo, Cape Verde, eruption: implications for the effects of collapse events upon island volcanoes: Geophysical Research Letters, v. 29, p. 101029.

Anderson, D.L., 2000, The thermal state of the upper mantle: No role for mantle plumes: Geophysical Research Letters, v. 27, p. 3623-3626.

Andò, B., and Carbone, D., 2001, A methodology for reducing the effect of meteorological parameters on a continuously recording gravity meter: IEEE transactions on instrumentation and measurements, v. 50, p. 1248-1254.

Andò, B, 2004, A test ona nEuro-Fuzzy algorithm used to reduce continuous gravity records for the effect of meteorological parameters: Physics of the Earth and planetary interiors, v. 142, p. 37-47.

Árnadóttir, T., Sigmundsson, F., and Delaney, P.T., 1998, Sources of crustal deformation associated with the Krafla, Iceland, eruption of September 1984: Geophysical Research Letters, v. 25, p. 1043-1046.

Árnadóttir, T., Jónsson, S., Pedersen, R., and Gudmundsson, G.B., 2003, Coulomb stress changes in the South Iceland Seismic zone due to two large earthquakes in June 2000: Geophysical Research Letters, v. 30, p. 1205.

Arnórsson, S., 1995, Geothermal systems in Iceland: structure and conceptual models-I. high-temperature areas: Geothermics, v. 24, p. 561-602.

Avallone, A., Zollo, A., Briole, P., Delacourt, C., and Beauducel, F., 1999, Subsidence of Campi Flegrei (Italy) detected by SAR interferometry: Geophysical Research Letters, v. 26, p. 2303-2306.

Ballu, V., Diament, M., Briole, P., and Ruegg, J.-C., 2003, 1985-1999 gravity field variations across the Asal Rift: insights on vertical movements and mass transfer: Earth and Planetary Science Letters, v. 208, p. 41-49.

Barberi, F., Gasparini, P., Innocenti, F., and Villari, L., 1973, Volcanism of the southern Tyrrhenian Sea and its geodynamic implications: Journal of Geophysical Research, v. 78, p. 5221-5232.

Barberi, F., Rosi, M., and Sodi, A., 1993, Volcanic hazard assesment at Stromboli based on review of historical data: Acta Vulcanologica, v. 3, p. 173-187.

Bastien, R., and Goodacre, A.K., 1985, The effect of humidity variations on long-term tidal gravity recordings: Contribution of the Geological Survey of Canada, v. No. 43188, p. 7506-7510.

Battaglia, M., Roberts, C., and Segall, P., 1999, Magma intrusion beneath Long Valley Caldera confirmed by temporal changes in gravity: Science, v. 285, p. 2119-2122.

Battaglia, M., Segall, P., and Roberts, C., 2003, The mechanics of unrest at Long Valley caldera, California. 2. Constraining the nature of the source using geodetic and micro-gravity data: Journal of Volcanology and Geothermal Research, v. 127, p. 219-245.

Beauducel, F., Briole, P., and Froger, J.L., 2000, Volcano-wide fringes in ERS synthetic aperature radar interferograms of Etna (1992-1998): deformation or tropospheric effect? : Journal of Geophysical Research, v. 105, p. 16391-16402.
Berrino, G., Rymer, H., Brown, G.C., and Corrado, G., 1992, Gravity Height Correlations for Unrest at Calderas: Journal of Volcanology and Geothermal Research, v. 53, p. 11-26.
Berrino, G., 1994, Gravity changes induced by height-mass variations at the Campi Flegrei caldera: Journal of Volcanology and Geothermal Research, v. 61, p. 293-309.
Berrino, G., 2000a, Combined gravimetry in the observation of volcanic processes in Southern Italy: Journal of Geodynamics, v. 30, p. 371-388.
Berrino, G., Corrado, G., Magliulo, R., and Riccardi, U., 2000b, Continuous gravity record at Mount Vesuvius: A tool to monitor its dynamics: Physics and Chemistry of the Earth Part a-Solid Earth and Geodesy, v. 25, p. 713-717.
Bertagnini, A., Metrich, N., Landi, P., and Rosi, M., 2003, Stromboli volcano (Aeolian Archipelago, Italy): An open window on the deep-feeding system of a steady state basaltic volcano: Journal of Geophysical Research, v. 108, p. 2336.
Björnsson, A., Johnsen, G., Sigurdsson, S., and Thorbergsson, G., 1979, Rifting of the plate boundary in north Iceland 1975-1978: Journal of Geophysical Research, v. 84, p. 3029-3038.
Björnsson, A., 1985, Dynamics of crustal rifting in NE Iceland: Journal of Geophysical Research, v. 90, p. 10151-10162.
Björnsson, A., and Eysteinsson, H., 1998, Breytingar á landhæð við Kröflu 1974-1995 samantekt á landhæðar-mælingum (in Icelandic): Nat. Energy Auth., Reykjavík, OS-98002.
Bonaccorso, A., 1998, Evidence of a dyke-sheet intrusion at Stromboli volcano inferred through continuous tilt: Geophysical Research Letters, v. 25, p. 4225.
Bonaccorso, A., Campisi, O., Consoli, O., Falzone, G., Gambino, S., Laudani, G., Mattia, M., Puglisi, B., Rossi, M., and Velardita, R., 2000, Discrete (EDM and GPS) and continuous (tilt and GPS) deformation monitoring (Vulcano and Stromboli): Acta Vulcanologica, v. 12, p. 111-114.
Bonaccorso, A., 2002a, Ground deformation of the southern sector of the Aeolian islands volcanic arc from geodetic data: Tectonophysics, v. 351, p. 181-192.
Bonaccorso, A., Calvari, S., Garfì, G., Lodato, L., and Patanè, D., 2003, Dynamics of the Decmber 2002b flank failure and tsunami at Stromboli volcano inferred by volcanological and geophysical observations: Geophysical Research Letters, v. 30.
Bonafede, M., and Mazzanti, M., 1998, Modelling gravity variations consistent with ground deformation in the Campi Flegrei caldera (Italy): Journal of Volcanology and Geothermal Research, v. 81, p. 137-157.
Bonforte, A., Ferretti, A., Prati, C., Puglisi, G., and Rocca, F., 2001, Calibration of atmospheric effects on SAR interferograms by GPS and local atmosphere models: first results: Journal of Atmospheric and Solar-Terrestrial Physics, v. 63, p. 1343-1357.
Bonvalot, S., Diament, M., and Gabalda, G., 1998, Continuous gravity recording with Scintrex CG-3M meters: a promising tool for monitoring active zones: Geophysical Journal International, v. 135, p. 470-494.
Branca, S., Carbone, D., and Greco, F., 2003, Intrusive mechanism of the 2002 NE-rift eruption at Mt. Etna (Italy) inferred through continuous microgravity data and volcanological evidences: Geophysical Research Letters, v. 30.
Brandsdóttir, B., and Menke, W., 1992, Thin low-velocity zone within the Krafla caldera, NE Iceland attributed to a small magma chamber: Geophysical Research Letters, v. 19, p. 2381-2384.
Brandsdóttir, B., Menke, W., Einarsson, P., White, R.S., and Stapels, R.K., 1997, Färoe-Iceland ridge experiment 2. Crustal structure of the Krafla central volcano: Journal of Geophysical Research, v. 102, p. 7867-7886.
Briole, P., Massonnet, D., and Delacourt, C., 1997, Post-eruptive deformation associated with the 1986-87 and 1989 lava flows of Etna detected by radar interferometry: Geophysical Research Letters, v. 24, p. 37-40.
Brodsky, E., 2002, Continuous micro-gravity measurments at Karymsky volcano, personal communication.
Brown, G.C., and Rymer, H., 1986, New light on volcano summit evolution from gravity-data: Geophysical Journal of the Royal Astronomical Society, v. 85, p. 251-251.
Brown, G., Rymer, H., Dowden, J., Kapadia, P., Stevenson, D., Barquero, J., and Morales, L.D., 1989, Energy Budget Analysis for Poas Crater Lake - Implications for Predicting Volcanic Activity: Nature, v. 339, p. 370-373.

Brown, G.C., Everett, S.P., Rymer, H., McGarvie, D.W., and Foster, I., 1991a, New Light on Caldera Evolution - Askja, Iceland: Geology, v. 19, p. 352-355.
Brown, G.C., Rymer, H., and Stevenson, D., 1991b, Volcano Monitoring by Microgravity and Energy Budget Analysis: Journal of the Geological Society, v. 148, p. 585-593.
Budetta, G., and Carbone, D., 1997, Potential application of the Scintrex CG-3M gravimeter for monitoring volcanic activity: Results of field trials on Mt Etna, Sicily: Journal of Volcanology and Geothermal Research, v. 76, p. 199-214.
Budetta, G., and Carbone, D., 1998, Temporal variations in gravity at Mt Etna (Italy) associated with the 1989 and 1991 eruptions: Bulletin of Volcanology, v. 59, p. 311-326.
Budetta, G., Carbone, D., and Greco, F., 1999, Sub-surface mass redistribution at Mount Etna (Italy) during the 1995-1996 explosive activity detected by microgravity studies: Geophysical Journal International, v. 138, p. 77-88.
Bürgmann, R., Rosen, P.A., and Fielding, E.J., 2000, Synthetic Aperture Radar interferometry to measure earth's surface topography and its deformation: Annual review of Earth and Planetary Science., v. 28, p. 169-209.
Camitz, J., Sigmundsson, F., Foulger, G., Jahn, C.H., Volksen, C., and Einarsson, P., 1995, Plate boundary deformation and continuing deflation of the Askja volcano, North Iceland, determined with GPS, 1987-1993: Bulletin of Volcanology, v. 57, p. 136-145.
Carbone, D., and Rymer, H., 1999, Calibration shifts in a LaCoste-and-Romberg gravimeter: comparison with a Scintrex CG-3M: Geophysical Prospecting, v. 47, p. 73-83.
Carbone, D., Budetta, G., and Greco, F., 2003a, Possible mechanisms of magma redistribution under Mt Etna during the 1994-1999 period detected through microgravity measurements: Geophysical Journal International, v. 153, p. 187-200.
Carbone, D., Budetta, G., Greco, F., and Rymer, H., 2003b, Combined discrete and continuous gravity observations at Mount Etna: Journal of Volcanology and Geothermal Research, v. 123, p. 123-135.
Carminati, E., Wortel, M.J.R., Spakman, W., and Sabadini, R., 1998, The role of slab detachment processes in the opening of the Western-Central MEditerranean basins: some geological and geophysical evidence: Earth and Planetary Science Letters, v. 160, p. 651-665.
Carn, S.A., 1999, Application of synthetic aperture radar (SAR) imagery to volcano mapping in the humid tropics: a case study in East Java, Indonesia: Bulletin of Volcanology, v. 61, p. 92-105.
Cervelli, P., Murray, M.H., Segall, P., Aoki, Y., and Kato, T., 2001, Estimating source parameters from deformation data, with an application to the March 1997 earthquake swarm off the Izu Peninsula, Japan: Journal of Geophysical Research, v. 106, p. 11217-11237.
Chouet, B., Hamisevicz, N., and McGetchin, T.R., 1974, Photoballistics of volcanic jet activity at Stromboli, Italy: Journal of Geophysical Research, v. 79, p. 4961-4976.
Chouet, B., Saccorotti, G., Dawson, P., Martini, M., Scarpa, R., De Luca, G., Milana, G., and Cattaneo, M., 1999, Broadband measurements of the sources of explosions at Stromboli volcano, Italy: Geophysical Research Letters, v. 26, p. 1937-1940.
Clifton, A.E., Sigmundsson, F., Feigl, K.L., Guðmundsson, G., and Árnadóttir, T., 2002, Surface effects of faulting and deformation resulting from magma accumulation at the Hengill triple junction, SW Iceland, 1994-1998: Journal of Volcanology and Geothermal Research, v. 115, p. 233-255.
Clifton, A., Pagli, C., Jónsdóttir, J.F., Eythorsdóttir, K., and Vogfjörd, K., 2002, Surface effects of triggered fault slip on Reykjanes peninsula, SW Iceland: Tectonophysics, v. 369, p. 145-154.
CNES, 2000, Installation guide for DIAPASON: Toulouse, Centre National d'etudes spatial.
Coltelli, M., Del Carlo, P., and Pompílio, M., 2000, Eruptive activity (Stromboli): Acta Vulcanologica, v. 12, p. 93-95.
Courtillot, V., Davaille, A., Besse, J., and Stock, J., 2002, Three types of hotspots in the earth's mantle, v. Earth and Planetary science letters, p. 295-308.
de Zeeuw-van Dalfsen, E., Pedersen, R., Sigmundsson, F., and Pagli, C., 2004a, Satellite Radar Interferometry 1993-1999 suggests deep accumulation of magma near the crust-mantle boundary at the Krafla volcanic system, Iceland: Geophysical Research Letters, v. 31, no. 13.
de Zeeuw-van Dalfsen, E., Rymer, H., Sigmundsson, F., and Sturkell, E., 2004b, Net gravity decrease at Askja volcano, Iceland: constraints on processes responsible for continuous caldera deflation, 1988-2003: Journal of Volcanology and Geothermal Research, 139:227-239.

de Zeeuw-van Dalfsen, E., Rymer, H., Williams-Jones, G., Sturkell, E., and Sigmundsson, F., submitted 2004c, The intergration of micro-gravity and geodetic data at Krafla volcano, N Iceland: Bulletin of Volcanology.
Delacourt, C., Briole, P., and Achache, J., 1998, Tropospheric corrections of SAR interferograms with strong topography. Application to Etna: Geophysical Research Letters, v. 25, p. 2849-2852.
DeMets, C., Gordon, R.G., Argus, D.F., and Stein, S., 1994, Effect of recent revisions to the geomagnetic reversal time scale on estimates of current plate motions: Geophysical Research Letters, v. 21, p. 2191-2194.
Einarsson, P., 1978, S-wave shadows in the Krafla caldera in NE-Iceland, evidence for a magma chamber in the crust: Bulletin of Volcanology, v. 41, p. 1-9.
Einarsson, P., 1991, Earthquakes and present day tectonism in Iceland: Tectonophysics, v. 189, p. 261-279.
Einarsson, P., 1996, Bardarbunga/Grimsvotn Volcanoes, Iceland, Smithsonian's Global Volcanism Network, p. 1.
El Wahabi, A., Dittfeld, H.-J., and Simon, Z., 2000, Meteorological influence on tidal gravimeter drift: Bull. Inf. Marées Terrestres, v. 133, p. 10403-10414.
Emter, D., Zurn, W., Schick, R., and Lombargo, G., 1986, Search for tidal effects on volcanic activities at Mt. Etna and Stromboli: Proc. Tenth Int. Symp. Earth Tides, p. 765-774.
Everett, S., Brown, G.C., and Rymer, H., 1988, Investigation of the Static Gravity-Field at Askja Volcano, Iceland: Geophysical Journal-Oxford, v. 92, p. 556-556.
Ewart, J.A., Voight, B., and Björnsson, A., 1991, Elastic deformation models of Krafla Volcano, Iceland, for the decade 1975 through 1985: Bulletin of Volcanology, v. 53, p. 436-459.
Falsapera, S., 1991, Stromboli: Acta Vulcanologica, v. 1, p. 272-274.
Falsapera, S., and Schick, R., 1993, Geophysical studies on Stromboli volcano- a review: Acta Vulcanologica, v. 3, p. 153-162.
Falsapera, S., Privitera, E., Chouet, B., and Dawson, P., 2002, Analysis of long-period events recorded at Mount Etna (Italy) in 1992, and their relationship to eruptive activity: Journal of Volcanology and Geothermal Research, v. 114, p. 419-440.
Feigl, K.L., Gasperi, J., Sigmundsson, F., and Rigo, A., 2000, Crustal deformation near Hengill volcano, Iceland 1993-1998: Coupling between magmatic activity and faulting inferred from elastic modeling of satellite radar interferograms: Journal of Geophysical Research-Solid Earth, v. 105, p. 25655-25670.
Fernández, J., Yu, T.-T., Rodríguez-Velasco, G., González-Matesanz, J., Romero, R., Rodríguez, G., Quirós, R., Dalda, A., Aparicio, A., and Blanco, M.J., 2003, New geodetic monitoring system in the volcanic island of Tenerife, Canaries, Spain. Combination of InSAR and GPS techniques: Journal of Volcanology and Geothermal Research, v. 124, p. 241-253.
Foulger, G.R., Jahn, C.H., Seeber, G., Einarsson, P., Julian, B.R., and Heki, K., 1992, Post-Rifting Stress-Relaxation at the Divergent Plate Boundary in Northeast Iceland: Nature, v. 358, p. 488-490.
Foulger, G., Pritchard, M.J., Julian, B.R., Evans, J.R., Allen, R.M., Nolet, G., Morgan, W.J., Bergsson, B.H., Erlendsson, P., Jakobsdóttir, S., Ragnarsson, S., Stefansson, R., and Vogfjörd, K., 2000, The seismic anomaly beneath Iceland extends down to the mantle transition zone and no deeper: Geophysical Journal International, v. 142, p. F1-F5.
Foulger, G., Du, Z., and Julian, B.R., 2003, Icelandic-type crust: Geophysical Journal International, v. 155, p. 567-590.
Fournier, N., 2003, Shallow volcanic processes at persistently active volcanoes: multidisciplinary study at Poas Volcano, Costa Rica [PhD thesis]: Milton Keynes, The Open University.
Francis, P., Oppenheimer, C., and Stevenson, D., 1993, Endogenous growth of persistently active volcanoes: Nature, v. 366, p. 554-557.
Franzson, H., Gudlaugsson, S., and Fridleifsson, G., 2001, Petrophysical properties of Icelandic Rocks: Proceedings of the 6th Nordic Symposium on Petrophysics, Trondheim, Norway.
Froger, J.L., Merle, O., and Briole, P., 2001, Active spreading and regional extension at Mount Etna imaged by SAR interferometry: Earth and Planetary Science Letters, v. 187, p. 245-258.
Furman, T., Meyer, P.S., and Frey, F., 1992, Evolution of Icelandic Central Volcanos - Evidence from the Austurhorn Intrusion, Southeastern Iceland: Bulletin of Volcanology, v. 55, p. 45-62.
Gens, R., 2003, Two-dimensional phase unwrapping for radar interferometry: developments and new challenges: International journal of remote sensing, v. 24, p. 703-710.

Gottsmann, J., and Rymer, H., 2002b, Deflation during caldera unrest: constraints on subsurface processes and hazard prediction from gravity -height data: Bulletin of Volcanology, v. 64, p. 338-348.
Gottsmann, J., Berrino, G., Rymer, H., and Williams-Jones, G., 2003, Hazard assesment during caldera unrest at the Campi Flegrei, Italy: a contribution from gravity-height gradients: Earth and Planetary Science Letters, v. 211, p. 295-309.
Gudmundsson, A., 1995, Infrastructure and Mechanics of Volcanic Systems in Iceland: Journal of Volcanology and Geothermal Research, v. 64, p. 1-22.
Gudmundsson, A., 2000, Dynamics of volcanic systems in Iceland: Example of tectonism and volcanism at juxtaposted hot spot and Mid-Ocean ridge systems: Annual review of Earth and Planetary Science, v. 28, p. 107-140.
Gudmundsson, B.T., and Arnórsson, S., 2002, Geochemical monitoring of the Krafla and Námafjall geothermal areas, N-Iceland: Geothermics, v. 31, p. 195-243.
Gudmundsson, Ó. 2003, The dense root of the Iceland crust: Earth and Planetary Science Letters, v. 206, p. 427-440.
Gudmundsson, S., Carstensen, J.M., and Sigmundsson, F., 2001, Unwrapping ground displacement signals in satellite radar interferograms with aid of GPS data and MRF regularization: IEEE Transactions of Geosciences and Remote Sensing, 40(8), 1743-1754.
Gudmundsson, S., and Sigmundsson, F., 2002, Three-dimensional surface motion maps estimated from combined interferometric synthetic aperature radar and GPS data: Journal of Geophysical Research, v. 107, p. 2250.
Harris, A.J.L., Stevens, N.F., Maciejewski, A.J.H., and Rollin, P.J., 1996, Thermal evidence for linked vents at Stromboli: Acta Vulcanologica, v. 8, p. 57-61.
Harris, A.J.L., and Stevenson, D.S., 1997a, magma budgets and steady-state activity of Vulcano and Stromboli: Geophysical Research Letters, v. 24, p. 1043-1046.
Harris, A.J.L., 1997b, Thermal observations of degassing open conduits and fumerols at Stromboli and Vulcano using remotely sensed data: Journal of Volcanology and Geothermal Research, v. 76, p. 175-198.
Harris, A.J.L., Murray, J.B., Aries, S.E., Davies, M.A., Flynn, L.P., Wooster, M.J., Wright, R., and Rothery, D.A., 2000, Effusion rate trends at Etna and Krafla and their implications for eruptive mechanisms: Journal of Volcanology and Geothermal Research, v. 102, p. 237-270.
Harris, A.J.L., and Neri, M., 2002, Volumetric observations during paroxysmal eruptions at Mount Etna: pressurized drainage of a shallow chamber or pulsed supply? Journal of Volcanology and Geothermal Research, v. 116, p. 79-95.
Hauksson, T., and Benjamínsson, J., 2003, Krafla og Bjarnarflag Afköst borhola og efnainnihald vatns og gufu í borholum og vinnslurás árið 2002 (in Icelandic): Rep. Landsvirkjun, Kröflustöð, 1-70
Henriot, O., Villemin, T., and Jouanne, F., 2001, Long period interferograms reveal 1992-1998 steady rate of deformation at Krafla volcano (North Iceland): Geophysical Research Letters, v. 28, p. 1067-1070.
Henriot, O., 2003, La deformation actuelle au nord de l'islande, a la jonction entre un rift et une transformante: mesure par insar et modelistation d'un system volcano-tectonique actif: PhD thesis, universite de Savoie.
Hildreth, W., 1987, New perspectives on the eruption of 1912 in the valley of ten thousand smokes, Katmai National PArk, Alaska: Bulletin of Volcanology, v. 49, p. 680-693.
Hochstein, P., and Hunt, T.M., 1970, Seismic, gravity and magnetic studies, broadlands geothermal field, New Zealand: Geothermics, v. 2, p. 333-346.
Hofton, M.A., and Foulger, G., 1996, Postrifting anelastic deformation around the spreading plate boundary, north Iceland. 2. Implications of the model derived from the 1987-1992 deformation field: Journal of Geophysical Research, v. 101, p. 25423-25436.
Hornig-Kjarsgaard, I., Keller, J., Koberski, U., Stadlbauer, E., Francalanci, L., and Lenhart, R., 1993, Geology, stratigraphy and volcanological evolution of the island of Stromboli, Aeolian arc, Italy: Acta Vulcanologica, v. 3, p. 21-68.
Hreinsdottir, S., Einarsson, P., and Sigmundsson, F., 2001, Crustal deformation at the oblique spreading Reykjanes Peninsula, SW Iceland: GPS measurements from 1993 to 1998: Journal of Geophysical Research, v. 106, p. 13803-13816.
Hunt, T.M., 1970a, Net mass loss from the Wairakei geothermal field, New Zealand: Geothermics, v. 2, p. 487-491.
Hunt, T.M., 1970b, Net mass loss from the Wairakei geothermal fiels, New Zealand: Geothermics, v. 2, p. 487-491.

Hunt, T.M., 1992, Gravity Anolomies, caldera structure, and subsurface geology in the rotorua area, New Zealand: Geothermics, v. 21, p. 65-74.
Johnsen, G.V., Björnsson, A., and Sigurdsson, S., 1980, Gravity and elevation changes caused by magma movement beneath krafla caldera, northeast Iceland: Journal of Geophysics., v. 47, p. 132-140.
Johnson, D.J., 1992, Dynamics of magma storage in the summit reservoir of Kilauea volcano, Hawaii: Journal of Geophysical Research, v. 97, p. 1807-1820.
Johnson, D.J., Sigmundsson, F., and Delaney, P.T., 2000, Comment on 'Volume of magma accumulation or withdrawal estimated from surface uplift or subsidence, with application to the 1960 collapse of Kilauea volcano' by P.T. Delaney and D.F. McTigue: Bulletin of Volcanology, v. 61, p. 491-493.
Johnson, D., 1987, Chapter 47: Elastic and inelastic magma storage at Kilauea volcano. In Volcanism in Hawaii, Volume 2, United States Government Printing Office, Washington, 1297-1306 p.
Jónasson, K., 1994, Rhyolite volcanism in the Krafla central volcano, north-east Iceland: Bulletin of Volcanology, v. 56, p. 516-528.
Jónsson, Ó. 1942, Öskjuvatn (in Icelandic), Náttúrufræðingurinn v. 12, p. 56-72.
Jónsson, S., Einarsson, P., and Sigmundsson, F., 1997, Extension across a divergent plate boundary, the eastern Volcanic Rift Zone, south Iceland, 1967-1994, observed with GPS and electronic distance measurements: Journal of Geophysical Research, v. 102, p. 11913-11929.
Jónsson, S., Zebker, H., Segall, P., and Amelung, F., 2002, Fault slip distribution of the 1999 Mw 7.2 Hector mine earthquake, California,estimated from Satellite radar and GPS measurements: Bulletin of the Seismological Society of America, v. 92.
Jousset, P., Dwipa, S., Beauducel, F., Duquesnoy, T., and Diament, M., 2000a, Temporal gravity at Merapi during the 1993-1995 crisis: an insight into the dynamical behaviour of volcanoes: Journal of Volcanology and Geothermal Research, v. 100, p. 289-320.
Jousset, P., and Mori, H.O.H., 2000b, Possible magma intrusion revealed by temporal gravity, ground deformation and ground temperature observations at Mount Komagatake (Hokkaido) during the 1996-1998 crisis: Geophysical Journal International, v. 143, p. 557-574.
Jousset, P., Mori, H., and Okada, H., 2003, Elastic models for the magma intrusion associated with the 2000 eruption of Uso volcano, hakkaido, Japan: Journal of Volcanology and Geothermal Research, v. 2607, p. 1-26.
Keller, W.R., Anderson, D.L., and Clayton, R.W., 2000, Resolution of tomographic models of the mantle beneath Iceland: Geophysical Research Letters, v. 27, p. 3993-3996.
Klees, R., and Massonnet, D., 1998, Deformation measurements using SAR interferometry: potential and limitations: Geologie en Mijnbouw, v. 77, p. 161-176.
LaCoste, and Romberg, 2000, Model G and D meter Manual.
Locke, C.A., Rymer, H., and Cassidy, J., 2003, Magma transfer processes at persistently active volcanoes: insights from gravity observations: Journal of Volcanology and Geothermal Research, v. 127, p. 73-86.
Lundgren, P., Berardino, P., Coltelli, M., Fornaro, G., Lanari, R., Puglisi, G., Sansosti, E., and Tesauro, M., 2003, Coupled magma chamber inflation and sector collapse slip observed with syntehtic aperature radar interferometry on Mt. Etna volcano: Journal of Geophysical Research, v. 108, p. 2247.
M.P.Hochstein, and T.M.Hunt, 1970, Seismic, gravity and magnetic studies, broadlands geothermal field, New Zealand: Geothermics, v. 2, p. 333-346.
Maclennan, J., Jull, M., McKenzie, D., Slater, L., and Grönvold, K., 2002, The link between volcanism and deglaciation in iceland: Geochemistry, Geophysics, Geosystems, v. 3, p. 1-25.
Magnússon, I., 2003, Þyngdarmælingar vid Kröflu árid 2000 (in Icelandic): Internal report Landsvirkjun, Orkustofnun, OS-2003/06.
Malengreau, B., Lenat, J.F., and Froger, J.L., 1999, Structure of Reunion island (Indian ocean) inferred from interpreation of gravity anomalies: Journal of Volcanology and Geothermal Research, v. 88, p. 131-146.
Manga, M., 1996, Waves of bubbles in basaltic magmas and lavas: Journal of Geophysical Research, v. 101, p. 17457-17465.
Massonnet, D., Rossi, M., Carmona, C., Adragna, F., Peltzer, G., Feigl, K., and Rabaute, T., 1993, The displacement field of the Landers earthquake mapped by radar interferometry: Nature, v. 364, p. 138-142.
Massonnet, D., and Feigl, K., 1995, Discrimination of geophysical phenomena in satellite radar interferograms: Geophysical Research Letters, v. 22, p. 1537-1540.

Massonnet, D., and Feigl, K., 1998, Radar interferometry and its application to changes in earth's surface: Review of geophysics, v. 36, p. 441-500.
McTigue, D.F., 1987, Elastic stress and deformation near a finite spherical magma body: resolution of the point source paradox: Journal of Geophysical Research, v. 92, p. 12934-12940.
Menke, W., West, M., Brandsdóttir, B., and Sparks, D., 1998, Compressional and shear velocity structure of the lithosphere in northern Iceland: Bulletin of the Seismological Society of America, v. 88, p. 1561-1571.
Miklius, A., and Cervelli, P., 2003, Interaction between Kilauea and Mauna Loa: Nature, v. 421, p. 229.
Mogi, K., 1958, Relations between the eruptions of various volcanoes and the deformations of the ground surfaces around them: Bulletin of the earthquake research institute, v. 36, p. 99-134.
Moller, D., and Ritter, B., 1980, geodetic measurements and horizontal crustal movements in the rift zone of NE Iceland: Journal of Geophysics, v. 47, p. 110-119.
Morgan, W.J., 1971, Convection plumes in the lower mantle: Nature, v. 230.
Mörner, S.A., 1981, Crustal movements and geodynamics in fennoscandia: Tectonophysics, v. 71, p. 241-251.
Mouginis-Mark, P., Garbeil, H., 1993, Digital topography of volcanoes from radar interferometry: an example from Mt Vesuvius, Italy: Bulletin of Volcanology, v. 55, p. 566-570.
Nairn, I.A., McKee, C.O., Talai, B., and Wood, C.P., 1995, Geology and eruptive history of the Rabaul Caldera area, Papua New Guinea: Journal of Volcanology and Geothermal Research, v. 69, p. 255-284.
Neuberg, J., Luckett, R., Ripepe, M., and Braun, T., 1994, Highlights from a seismic broadband array on Stromboli Volcano: Geophysical Research Letters, v. 21, p. 749-752.
Newhall, C.G., and Dzurisin, D., 1988, Historical unrest at large calderas of the world: Reston, Virginia, US Geol Surv, 1855 p.
Newman, A.V., Dixon, T.H., Ofoegbu, G.I., and Dixon, J.E., 2001, Geodetic and seismic constraints on recent activity at Long valley caldera, California: evidence for viscoelastic theology: Journal of Volcanology and Geothermal Research, v. 105, p. 183-206.
Nielsen, G., Maack, R., Gudmundsson, Á., and Gunnarsson, G.I., 2000, Completion of the Krafla geothermal powerplant: Proceedings world geothermal congress, p. 3259-3264.
Ntepe, N., and Dorel, J., 1990, Observations of seismic volcanic signals at Stromboli volcano (Italy): Journal of Volcanology and Geothermal Research, v. 43, p. 235-251.
NVI, 2001, Volcanic geology of Krafla, Nordic Volcanological Institute website: http://www.norvol.hi.is/.
Okubo, S., and Watanabe, H., 1989, Gravity change caused by a fissure eruption: Geophysical Research Letters, v. 16, p. 445-448.
Opheim, J.A., and Gudmundsson, A., 1989, Formation and Geometry of Fractures, and Related Volcanism, of the Krafla Fissure Swarm, Northeast Iceland: Geological Society of America Bulletin, v. 101, p. 1608-1622.
Óskarsson, N., Sigvaldason, G.E., and Steinthórsson, S., 1982, A dynamic model of rift zone petrogenesis and the regional petrology of Iceland: Journal of Petrology, v. 23, p. 28-74.
Pagli, C., Pedersen, R., Sigmundsson, F., and Feigl, K., 2003, Triggered fault slip on June 17, 2000 on the Reykjanes Peninsula, SW Iceland captured by radar interferometry: Geophysical Research Letters, v. 30, p. 1273.
Parasnis, D.S., 1979. Chapter 3: Gravitational methods, Principles of Applied Geophysics. Chapman and Hall.
Pasquarè, G., Francalanci, L., Garduño, V.H., and Tibaldi, A., 1993, Structure and geologic evolution of the Stromboli volcano, Aeolian islands, Italy: Acta Vulcanologica, v. 3, p. 79-89.
Pedersen, R., Sigmundsson, F., Feigl, K.L., and Arnadottir, T., 2001, Coseismic interferograms of two M-S=6.6 earthquakes in the South Iceland Seismic Zone, June 2000: Geophysical Research Letters, v. 28, p. 3341-3344.
Pingue, F., Berrino, G., Capuano, p., Obrizzo, F., De Natale, G., Esposito, T., Serio, C., Tammaro, U., De Luca, G., Scarpa, R., Troise, C., and Corrado, G., 2000, Ground deformation and gravimetric Monitoring at Somma-Vesuvius and in the Campanian Volcanic Arc (Italy). Physics and Chemistry of the Earth Part a-Solid Earth and Geodesy, v. 25, p. 747-754.
Pino, N.A., Ripepe, M., and Cimini, G.B., 2004, The Stromboli Volcano landslides of December 2002: A seismological description: Geophysical Research Letters, v. 31.
Pliny, t.y., 80, Letters of the younger Pliny.

Pollitz, F.F., and Sacks, I.S., 1996, Viscosity structure beneath northeast Iceland: Journal of Geophysical Research, v. 101, p. 17771-17793.
Pritchard, M.J., Simons, M., Rosen, P., Hensley, S., and Webb, F.H., 2002, Co-seismic slip from the 1995 July 30 Mw=8.1 Antofagasta, Chili, earthquakes as constrained by InSAR and GPS observations: Geophysical Journal International, v. 150, p. 362-376.
Puglisi, G., and Coltelli, M., 2001, SAR Interferometry applications on active volcanoes: state of the art and perspectives for volcano monitoring: Nuovo Cimento Della Societa Italiana Di Fisica C-Geophysics and Space Physics, v. 24, p. 133-145.
Ripepe, M., and Braun, T., 1994, Air-wave phases in Strombolian explosion-quake seismographs: a possible indicator for the magma level? : Acta Vulcanologica, v. 5, p. 201-206.
Ripepe, M., Poggi, P., Braun, T., and Gordeev, E., 1996, Infrasonic waves and volcanic tremor at Stromboli: Geophysical Research Letters, v. 23, p. 181-184.
Ripepe, M., and Gordeev, E., 1999, Gas bubble dynamics model for shallow volcanic tremor at Stromboli: Journal of Geophysical Research, v. 104, p. 10,639-10,654.
Ripepe, M., Ciliberto, S., and Della Schiava, M., 2001, Time constraint for modelling source dynamics of volcanic explosions at Stromboli: Journal of Geophysical Research, v. 106, p. 8713-8727.
Ripepe, M., Harris, A.J.L., and Carniel, R., 2002a, Thermal, seismic and infrasonic evidences of variable degassing rates at Stromboli volcano: Journal of Volcanology and Geothermal Research, v. 118, p. 285-297.
Ripepe, M., and Marchetti, E., 2002b, Array tracking of infrasonic sources at Stromboli volcano: Geophysical Research Letters, v. 29.
Rossi, M., Sbrana, A., and Principe, C., 1983, The phlegraen files: Structural evolution, volcanic history and eruptive mechanisms: Journal of Volcanology and Geothermal Research, v. 17, p. 273-288.
Rossi, M.J., 1996, Morphology and mechanism of eruption of postglacial shield volcanoes in Iceland: Bulletin of Volcanology, v. 57, p. 530-540.
Rossi, M.J., 1997, Morphology of the 1984 open-channel lava flow at Krafla volcano, northern Iceland: Geomorphology, v. 20, p. 95-112.
Rossi, M., Bertagnini, A., and Landi, P., 2000, Onset of the persistent activity at Stromboli Volcano (Italy): Bulletin of Volcanology, v. 62, p. 294-300.
Rothery, D.A., Coltelli, M., Pirie, D., Wooster, M.J., and Wright, R., 2001, Documenting surface magmatic activity at Mount Etna using ATSR remote sensing: Bulletin of Volcanology, v. 63, p. 387-397.
Rymer, H., and Brown, G.C., 1984, Periodic Gravity Changes at Poas Volcano, Costa-Rica: Nature, v. 311, p. 243-245.
Rymer, H, 1985, Causes of Microgravity Change over Active Volcanos: Geophysical Journal of the Royal Astronomical Society, v. 81, p. 318-318.
Rymer, H., 1988, How Precise Is a Lacoste and Romberg Gravity Meter: Geophysical Journal-Oxford, v. 92, p. 537-537.
Rymer, H, 1989a, A contribution to precision microgravity data-analysis using Lacoste and Romberg gravity meters: Geophysical Journal, v. 97, p. 311-322.
Rymer, H., and Brown, G., 1989b, Gravity Changes as a Precursor to Volcanic-Eruption at Poas Volcano, Costa-Rica: Nature, v. 342, p. 902-905.
Rymer, H, 1991, Under the Volcano - a Tale of Some Gravity: New Scientist, v. 130, p. 40-44.
Rymer, H., 1992, Report on workshop in Iceland on deformation of volcanoes, IAVCEI news, p. 307-308.
Rymer, H., and Tryggvason, E., 1993, Gravity and elevation changes at Askja, Iceland: Bulletin of Volcanology, v. 55, p. 362-371.
Rymer, H, 1994, Microgravity Change as a Precursor to Volcanic Activity: Journal of Volcanology and Geothermal Research, v. 61, p. 311-328.
Rymer, H, 1996, Microgravity monitoring: in Monitoring and Mitigation of Volcano Hazards, Berlin, Springer-Verslag, 169-198 p.
Rymer, H., Cassidy, J., Locke, C.A., and Sigmundsson, F., 1998a, Post-eruptive gravity changes from 1990 to 1996 at Krafla volcano, Iceland: Journal of Volcanology and Geothermal Research, v. 87, p. 141-149.
Rymer, H., de Vries, B.V., Stix, J., and Williams-Jones, G., 1998b, Pit crater structure and processes governing persistent activity at Masaya Volcano, Nicaragua: Bulletin of Volcanology, v. 59, p. 345-355.
Rymer, H., Cassidy, J., Locke, C.A., Barboza, M.V., Barquero, J., Brenes, J., and Van der Laat, R., 2000a, Geophysical studies of the recent 15-year eruptive cycle at Poas Volcano, Costa Rica: Journal of Volcanology and Geothermal Research, v. 97, p. 425-442.

Rymer, H., and Williams-Jones, G., 2000b, Volcanic eruption prediction: Magma chamber physics from gravity and deformation measurements: Geophysical Research Letters, v. 27, p. 2389-2392.
Rymer, H, 2003, Introduction: Journal of Volcanology and Geothermal Research, v. 123, p. vii-viii.
Salichon, J., Delouis, B., Giardini, D., Costantini, M., and Rosen, P., 2003, Joint inversion of broadband teleseismic and interferometric synthetic aperature radar (InSAR) data for the slip history of the Mw = 7.7, Nazca ridge (Peru) earthquake of 12 November 1996: Journal of Geophysical Research, v. 108, p. 2085.
Santo, A.P., 2000, Volcanolgical and geochemical evolution of Filicudi (Aeolian Islands, south Tyrrhenian Sea, Italy): Journal of Volcanology and Geothermal Research, v. 96, p. 79-101.
Schleusener, A., and Torge, W., 1971, Investigations of secular gravity variations in Iceland: Z. Geophys., v. 37, p. 679-701.
Settle, M., and McGetchin, T.R., 1980, Statistical analysis of persistent explosive activity at Stromboli, 1971: implications for eruption prediction: Journal of Volcanology and Geothermal Research, v. 8, p. 45-58.
Shen, Y., Solomon, S.C., Bjarnason, I.T., Nolet, G., Morgan, W.J., and Allen, R.M., 2002, Seismic evidence for a tilted mantle plume and north-south mantle flow beneath Iceland: Earth and Planetary Science Letters, v. 197, p. 261-271.
Sigmundsson, F., Einarsson, P., and Bilham, R., 1992, Magma Chamber Deflation Recorded by the Global Positioning System - the Hekla 1991 Eruption: Geophysical Research Letters, v. 19, p. 1483-1486.
Sigmundsson, F., Einarsson, P., Bilham, R., and Sturkell, E., 1995, Rift-Transform Kinematics in South Iceland - Deformation from Global Positioning System Measurements, 1986 to 1992: Journal of Geophysical Research, v. 100, p. 6235-6248.
Sigmundsson, F., Vadon, H., and Massonnet, D., 1997, Readjustment of the Krafla spreading segment to crustal rifting measured by satellite radar interferometry: Geophysical Research Letters, v. 24, p. 1843-1846.
Sigmundsson, F., Durand, P., and Massonnet, D., 1999, Opening of an eruptive fissure and seaward displacement at Piton de la Fournaise volcano measured by RADARSAT satellite radar interferometry: Geophysical Research Letters, v. 26, p. 533-536.
Sigurdsson, H., and Sparks, R.S.J., 1978, Rifting episode in north Iceland in 1874-1875 and the eruption of Askja and Sveinagja: Bulletin of Volcanology, v. 41, p. 149-167.
Sigvaldason, G.E., 2002, Volcanic and tectonic processes coinciding with glaciation and crustal rebound: an early Holocene rhyolitic eruption in the Dyngjufjoll volcanic centre and the formation of the Askja caldera, north Iceland: Bulletin of Volcanology, v. 64, p. 192-205.
Speranza, F., Pompílio, M., and Sagnotti, L., 2004, Paleomagnetism of spatter lavas from Stromboli volcano (Aeolian Islands, Italy): Implications for the age of paroxysmal eruptions: Geophysical Research Letters, v. 31.
Stefánsson, V., 1981, The Krafla geothermal field, northeast Iceland, in Geothermal systems: principles and case histories, John Wiley & Sons Ltd.
Stevenson, D., and Blake, S., 1998, Modelling the dynamics and thermodynamics of volcanic degassing: Bulletin of Volcanology, v. 60, p. 307-317.
Sturkell, E., and Sigmundsson, F., 2000, Continuous deflation of the Askja caldera, Iceland, during the 1983-1998 noneruptive period: Journal of Geophysical Research, v. 105, p. 25671-25684.
Sturkell, E., Sigmundsson, F., and Einarsson, P., 2003, Recent unrest and magma movements at Eyjafjallajökull and Katla volcanoes, Iceland: Journal of Geophysical Research, v. 108.
Sturkell, E., Sigmundsson, F., and Slunga, R., 2004 – submitted to Bull of Volc., 1983-2003 decaying rate of deflation at Askja caldera: Pressure decrease in an extensive magma plumbing system at a spreading plate boundary.
Sutton, A.J., Elias, T., Gerlach, T.M., and Stokes, J.B., 2001, Implications for eruptive processes as indicated by sulfur dioxide emissions from Kilauea Volcano, Hawaii, 1979-1997: Journal of Volcanology and Geothermal Research, v. 108, p. 283-302.
Symonds, R.B., Gerlach, T.M., and Reed, M.H., 2001, Magmatic gas scrubbing: implications for volcano monitoring: Journal of Volcanology and Geothermal Research, v. 108, p. 303-341.
Thordarson, T., and Hoskuldsson, A., 2002, Classic geology in Europe 3, Iceland: Chapter 7, the northeast.
Tiampo, K.F., Rundle, J.B., FErnandez, J., and Langbein, J.O., 2000, Spherical and ellipsoidal volcanic sources at Long Valley caldera, California, using a genetic algorithm inversion technique: Journal of Volcanology and Geothermal Research, v. 102, p. 189-206.

Tibaldi, A., 2001, Multiple sector collapses at Stromboli volcano Italy: how they work: Bulletin of Volcanology, v. 63, p. 112-125.
Tibaldi, A., 2004, Major changes in volcano behaviour after a sector collapse: insights from Stromboli, Italy: Terra Nova, v. 16, p. 2-8.
Tibaldi, A., Corazzato, C., Apuani, T., and Cancelli, A., 2002, Deformation at Stromboli Volcano (Italy) revealed by rock meachanisms and structural geology: Tectonophysics, v. 6790, p. 1-18.
Tinti, S., Bortulucci, E., and Romagnoli, C., 2000, Computer simulations of tsunamis due to sector collpase at Stromboli, Italy: Journal of Volcanology and Geothermal Research, v. 96, p. 103.
Tryggvason, E., 1986, Multiple Magma Reservoirs in a Rift-Zone Volcano - Ground Deformation and Magma Transport During the September 1984 Eruption of Krafla, Iceland: Journal of Volcanology and Geothermal Research, v. 28, p. 1-44.
Tryggvason, E, 1989a, Ground deformation in Askja, Iceland: its source and possible relation to flow of the mantle plume: Journal of Volcanology and Geothermal Research, v. 39, p. 61-71.
Tryggvason, E 1989b, Measurement of ground deformation in Askja 1966 to 1989: Nordic Volcanological Institute Report 8904.
Tryggvason, E, 1994, Surface deformation at the Krafla volcano, North Iceland, 1982-1992: Bulletin of Volcanology, v. 56, p. 98-107.
Tryggvason, E., 1995, Optical levelling tilt stations in the vicinity of Krafla and the Krafla fissure swarm. Observations 1976 to 1994: Internal report 9505, NVI, Reykjavik, Iceland.
Vadon, H., and Sigmundsson, F., 1997, Crustal deformation from 1992 to 1995 at the Mid-Atlantic Ridge, southwest Iceland, mapped by satellite radar interferometry: Science, v. 275, p. 193-197.
Vergniolle, S., Brandeis, G., and Mareschal, J.-C., 1996, Strombolian explosions 2. Eruption dynamics determined from acoustic measurements: Journal of Geophysical Research-Solid Earth, v. 101, p. 20.449-20.466.
Völksen, C., 2000, Die Nutzung von GPS für die Deformationanalyse in regionalen Netzen am Beispiel Islands: PhD thesis, Universität Hannover, Germany.
Wallace, P.J., 2001, Volcanic SO2 emmisions and the abundance and distribution of exsolved gas in magma bodies. Journal of Volcanology and Geothermal Research, v. 108, p. 85-106.
Weill, A., Brandeis, G., Vergniolle, S., Baudin, F., Bilbille, J., Fevre, J., Piron, B., and Hill, X., 1992, Acoustic sounder measurements of the vertical velocity of volcanic jets at Stromboli volcano: Geophysical Research Letters, v. 19, p. 2357-2360.
Welstead, S.T., 1999, Fractal and wavelet image compression techniques: Bellingham, Washington, SPIE Optical Engineering Press, 232 p.
Widiwijayanti, C., Mikhailov, V., Diament, M., Deplus, C., Louat, R., Tikhotsky, S., and Gvishiani, A., 2003, Structure and evolution of the Molucca Sea area: constraints based on interpretation of a combined sea-surface and satellite gravity dataset. Earth and Planetary Science Letters, v. 215, p. 135-150.
Williams, C.A., and Wadge, G., 1998, The effects of topography on magma chamber deformation models: Application to Mt Etna and radar interferometry: Geophysical Research Letters, v. 25, p. 1549-1552.
Williams-Jones, G., Stix, J., Heiligmann, M., Barquero, J., Fernandez, E., and Gonzalez, E.D., 2001, A model of degassing and seismicity at Arenal Volcano, Costa Rica: Journal of Volcanology and Geothermal Research, v. 108, p. 121-139.
Williams-Jones, G., and Rymer, H., 2002, Detecting volcanic eruption precursors: a new method using gravity and deformation measurements. Journal of Volcanology and Geothermal Research, v. 113, p. 379-389.
Williams-Jones, G., Rymer, H., and Rothery, D.A., 2003, Gravity changes and passive SO_2 degassing at the Masaya caldera complex, Nicaragua: Journal of Volcanology and Geothermal Research, v. 123, p. 137-160.
Young, S.R., Voight, B., and Duffell, H.J., 2003, Magma extrusion dynamics revealed by high-frequency gas monitoring at Soufrière Hills volcano, Montserrat., in Oppenheimer, C., Pyle, D.M., and Barclay, J., eds., Volcanic degassing: London, Geological Society, p. 219-230.
Zhao, D., 2001, Seismic structure and origin of hotspots and mantle plumes: Earth and Planetary Science Letters, v. 192, p. 251-265.

APPENDIX A: Gravity stations locations

This description of stations is based on observations made in the field in 2002 and 2003. Coordinates are measured using a handheld GPS and where possible they have been checked with those obtained by colleagues during the Icelandic GPS surveys. The station numbers and names are those already assigned by bodies such as the Icelandic meteorological office (4 letter codes), the National Energy Authority (NE codes) and Orkustofnun (OS codes).

A.1 Askja

TABLE A - 1 Coordinates and description of micro-gravity stations at Askja.

No.	Station name	Coordinates	Monumen-tation	Marker	Description
1	NE84011/ DYNG	N65º03′22.8″ W016º39′05.8″	Y/NE84011	Cairn/ yellow paint	300 m N of Dyngja/NVI hut, look for car trails, walk ~300 m N over pumice to 1961 lava flow. Station on horizontal top of flow ~2.5 m above ground level.
2	83009	N65º03′56.5″ W016º41′07.7″	Y/83009	Cairn/ yellow paint	From Dreki follow the road W to the Askja parking lot for 5.5 km (or 2.4 km from the intersection with the road leading to the Dyngja hut). After 90° wiggle in road look for 100 m^2 flat phh surface 10 m S of road (left) surrounded by aa flow (both 1961). S view towards gully.
3	83001 /VIKR	N65º04′05.8″ W016º43′26.7″	Y/83001	Cairn/ yellow paint	Drive up to car park at Askja.Walk back towards Dreki along the road for 100 m (3rd yellow stick). Then walk onto the lava flow towards NW for 400 m. Watch for cairn on phh lava.
4	430	N65º04′08.9″ W016º43′39.2″	Y/430	Cairn/ yellow paint	This station is end of the levelling line, which also contains 412 and 405. From 83001 follow the yellow paint levelling signs across small aa flow for ~200m until you get to phh lava.
5	412	N65º03′48.6″ W016º44′06.1″	Y/412	Cairn/ yellow paint	This station is also part of levelling line. Follow the line from 430, looking for yellow paint and cairns. The line follows the middle of the 1961 lava flow into the caldera curving around the base of the spatter cones. Stations will have nails and cairns and paint. In between stations there are yellow painted T signs. Alternatively follow the tourist trail starting at the car park, over the spatter cones for 700 m. Start heading NW looking for signs of the levelling line. Once on the line look at the nail number to decide which way to follow the line.

No.	Station name	Coordinates	Monumen-tation	Marker	Description
6	405	N65º03′35.6″ W016º43′55.8″	Y/405	Two cairns/ Yellow paint	If on the levelling line at 412, follow line towards E for ~300 m until large area ~200 m^2 of flat phh surrounded by large tumuli. Alternatively walk 1 km along tourist trail before heading 200 m NW towards the 1961 lava flow.
7	Von Knebel	N65º02′47.3″ W016º43′54.7″	N/ Measure at S base of cairn on muddy ground	Large cairn, metal plate in memory of VonKnebel/ Rudloff	Follow tourist trail to Viti. When you spot large cairn head SW for it or follow the trail to it from Viti. The memorial/cairn is close to the edge of cliff of lake Öskjuvatn in muddy surroundings. Put base plate S of cairn and push it firm into mud.
8	IV16	N65º02′49.4″ W016º43′10.9″	N/ Measure N side of big boulder	Lonely boulder with yellow paint IV16.	From Cairn at Von Knebel walk E towards Viti. Keep walking E around Viti. Then Head S to large blocks and boulders from rockslide from Askja caldera wall. This is going down in elevation slightly and you might have to cross some snow. IV16 is lonely boulder (1.5 m^3) about 80 m from caldera wall and has a flat surface slightly tilting towards S. IV16 is painted on E side boulder with yellow paint. It is a little smaller and further away from wall then the other large boulders. In July 2002 it was still covered in snow. In August 2003 only top 0.5 m of boulder was visible above the loose gravel and mud!

No.	Station name	Coordinates	Monumen-tation	Marker	Description
9	D-18 /BATS	N65º02′36.9″ W016º43′08.8″	Y/ Darthmouth 18	Two cairns/S one larger then N one. Cairns contain golden pumice.	From IV16 or Viti, walk towards old (1929) aa lava flow in SE, slight descend. Climb onto the flow just W of small pit 4 m across. Look for big cairn containing golden pumice locks on lava flow. Station ~middle aa flow with 20 m S a 3m higher lava wall and 20 m W (towards the lake) a drop of ~ 20 m.
10	NE200200 5 /MASK	N65º02′48.2″ W016º45′58.4″	Y/NE2002 005	Troll shaped lava rocks	Walk along the shore of lake towards NW for 1.5 km. Do not mistake the big boulders in aa flow N of pumice field for trolls. Trolls is further ahead and consists of a unit of 4 blocks of lava sticking up in the air ~ 1 m high within the pumice field. Nail is S of highest Troll, close to crack. Station ~400 m from lake. Base plate is placed with 2 legs E of crack and one W of leg.
11	NE200200 6	N65º02′32.9″ W016º46′52.6″	Y/NE2002 006	Cairn	From trolls follow the shoreline for ~850m, past pumice field until you reach lava flow. Look for small tumuli ~100m from shoreline with cairn. Nail is 5m W of cairn.
12	NE82005 /005 /OLAF	N65º02′32.6″ W016º46′58.1″	Y/82005	Cairn	~80 m West of LOO, ~100 m from lake. On tumuli in aa field covered with golden pumice. Is part of dry tilt station/ GPS station OLAF.
13	D-19	N65º02′30.3″ W016º46′58.0″	Y/ Dartmouth 19	Cairn	Cross pumice field ~80 m towards SSW from 005. 20 m N of lake at corner with ‘beech’ below cliff. Station on flat phh. Nail 5 m S of cairn.

A.2 Krafla

TABLE A - 2 Coordinates and description of micro-gravity stations at Krafla volcano.

No.	Station name	Coordinates	Nail	Marker	Description
1	Hotel	N65º38′42.0″ W016º54′55.1″	N/base plate on NE side concrete.	Old concrete flag post	Hotel Reynihlid. Measurement is taken on old concrete flag post 20 m W of hotel building, close to line of new flag posts.
2	Hellahraun	N65º38′31.1″ W016º54′28.2″	N/base plate on concrete.	House	NVI House at Hellahraun 1, grey house opposite post office. Measurement on concrete doorstep between door and gate to garden.
3	FM115	N65º38′40.6″ W016º48′08.8″	Y/No number	Cairn/ Yellow wooden stick	Drive from Reykjahlid towards Krafla (direction Grimsstadir). 100 m past intersection with road to boiling mud pools, 200 m before road to N towards Krafla, station 3 m N of road on flat phh lava.
4	2313	N65º38′40.8″ W016º48′08.9″	Y/2313	Cairn/ pink paint	5 m North of FM115 on phh lava.
5	5843	N65º41′12.9″ W016º46′41.8″	Y/OS5843	Cairn/ Wooden stick	~4.5 km from intersection, just after road ascends, turn W on gravel road towards bore hole. Walk up Southern most hill. Station on top of hill on S side at exposure.
6	5699	N65º39′00.8″ W016º47′31.0″	Y/OS5699	Cairn/ Wooden stick	Past mudpools turn N onto road to Krafla. Station after 780 m, 40 m E of road on flat phh. Station is part of line installed by Trygvasson and is last of line of cairns before land turns grassy without exposures.

No.	Station name	Coordinates	Nail	Marker	Description
7	5698	N65º39′30.1″ W016º47′38.0″	Y/OS5698	Cairn/ Wooden stick /red paint	~1.7 km from intersection, past the grassy area E of the road. Station is ~50 m E of road. Walk to the edge of the green area with isolated lava blocks. Station ~50 m S of main rubbly lava flow on sloping block. Measurement taken 0.1 m towards the road.
8	5697	N65º39′51.5″ W016º47′33.5″	Y/OS5697	Cairn/ Wooden stick	~2.4 km from intersection (or 1.6 km from 5699), 20 m W of road on first elevated phh block. ~1m above ground.
9	5688	N65º42′08.6″ W016º46′35.9″	Y/OS5688	Cairn	~6.3 km from intersection, turn W towards visitor centre at geothermal power plant. Walk W towards horse shoe shaped lava wall. Station on floor of S side of wall.
10	5685	N65º42′08.2″ W016º43′38.0″	Y/OS5685	Cairn	Continue driving E on road passed 5684 up to last bore hole. Look for car tracks turning N, follow this trail to East lying exposure of yellow tuff.
11	5684	N65º42′16.1″ W016º44′26.3″	Y/OS5684	Cairn/ Paint	~6.5 km from intersection, 2nd turn E after geothermal power plant turn into gravel road, pass the chain and continue driving up hill, past 2 active bore holes. Road runs roughly EW, parallel to valley. Station on exposure S of road on slight hill. Cairn might be difficult to spot from road!
12	5672	N65º44′28.1″ W016º43′36.9″	Y/5672	Cairn/ 2 wooden sticks/ paint	Follow the gravel road going N passed A008, ascend ‘plateau’. Just before (S of) track leading up hill to A012, take track turning E, when track bends to North look for lava wall, W of trail, station ~20 m W of lava wall, ~10 m E of track.
14	5599	N65º40′54.8″ W016º46′30.9″	Y/ No number	2 cairns	~4.39 km from intersection, just before road ascends, 5 m W of road in very open phh lava field. Just N of 5599A. 70 m South of little parking spot/start hiking trail.

No.	Station name	Coordinates	Nail	Marker	Description
15	5599A	N65º40′53.2″ W016º46′35.8″	Y/5599A	Cairn/ Wooden stick	~3.55 km from intersection 45 m W of road in very open phh lava field. Just S of 5599.
13	5600	N65º40′20.4″ W016º47′02.4″	Y/OS5600	Wooden stick/ Paint.	~2.5 km from intersection at ridge 50 m East of road, cross stream ~100 m S of station look for tracks, station at first exposure of rock, at big boulder 1.5 m above ground.
16	5597	N65º41′56.7″ W016º46′14.2″	Y/OS5597	Cairn/ Wooden stick	~5 km from intersection at geothermal power plant take 1st turn SE. Follow the road for ~300m. Stop just before crossing the river. Now walk 120 m S past lava ‘ice sheets’. Station on flat phh.
17	5596	N65º42′27.2″ W016º46′01.5″	Y/No number	Cairn/ Wooden stick/ orange tag	~6.49 km from intersection, past ‘3 pipes tunnel’, turn E on last gravel road towards bore hole before steep ascend. After ~100m take first road N and park after 30 m. Station on E side of pipes and W side of stream.
18	5595	N65º42′51.5″ W016º45′59.7″	Y/OS5595 or SO5595	5 m N of plastic pipe	Take road to Krafla towards Viti. After steep climb road turns E. Take gravel road to N (left) after ~400 m passing the crater formed after an explosion in bore hole, Station is on plateau covered with gravel W of road. Look for bigger rocks on plateau and plastic pipe.
19	NE220	N65º38′42.0″ W016º48′33.6″	Y/NE220	Two cairns	From Reykjahild drive towards Krafla (direction Grimstaddir). Turn South towards boiling mud pools car park. From car park walk ~470 m S on path past active steam vent and old steam vent. ~30 m E of path dry tilt station (circular) with many cairns on flat phh. Station measured is central one between two cairns.

No.	Station name	Coordinates	Nail	Marker	Description
20	9301	N65º41′24.8″ W016º46′31.0″	Y/NE9301	Cairn/ Wooden stick	~4.5 km from intersection, just after road ascends, turn W on gravel road towards bore hole. Look for cairn on 5m high lava hill just N of pipes. Climb over pipes. Measure S of nail on same rock. GPS station.
21	80051	N65º41′34.5″ W016º45′25.6″	Y/NE80051	Cairn	~*5* km from intersection, just after road ascends, turn E on gravel road towards ski lift and park. Station is steep 20 min climb away on top of escarpment SE of lift. You have to pass few deep gullies. Station S side of escarpment, big rock. Take camera, nice view!!
22	79077	N65º42′34.3″ W016º46′34.5″	Y/NE79077	Cairn	~6.65 km from intersection, notice reddish hill W of road, after steep climb turn W to car park. Before car park turn S onto track leading to hill. Park at base and walk up to lower peak at S side of hill. GPS station.
23	A001	N65º42′42.8″ W016º49′14.7″	N	Iron spike	From A002 walk WSW down hill until intersecting tourist trail marked by white wooden sticks. Follow the tourist trail through lava tunnel than cuts across the lava field (NNW) towards the northerly hill of the two. Ascend the hill on SW side. Station at top, bigger boulder.
24	A002	N65º43′01.5″ W016º47′46.5″	N	Iron spike/ Small cairn	Walk E down from hill with A003 at summit, past small (10 m across) explosion pit, cross young lava flow (mostly aa), climb up hill. Station at top, group of bigger boulders, steaming, muddy.
25	A003	N65º43′06.5″ W016º17′26.9″	N/but hole from previous nail	Some paint remains	Follow tourist trail past the boiling mud pools up the hill (Colourful hill that you can see W of car park) to end of trail. Station on S side hill, ignimbrite exposure, lowest flat rock of group of 6. Used to be GPS station. Alternatively: follow the trail to base of hill, ascend following grassy bits. Station is 20 m W of metal pipes.

No.	Station name	Coordinates	Nail	Marker	Description
26	A004	N65º43′18.3″ W016º46′42.9″	N	Iron spike/ Two wooden sticks/ White paint	From main Krafla car park follow tourist trail heading W. At intersection of trail with 2nd (newer) lava flow (~300 m before mud pools) turn N following the sheep trail at base of this 'ice sheet' lava flow. Look for two wooden sticks 5 m onto flow.
27	A005	N65º43′21.1″ W016º45′29.5″	Y/No number	Cairn/ Wooden stick/ Iron stick	Follow road to Viti from Krafla main car park. At Viti car park take the gravel road towards N, pass the chain follow it for ~300 m. Go past two? small explosion craters to your W and park the car. Walk 80 m to WSW over flat overgrown lava, look for cairn with iron rod and wooden sticks. GPS point.
28	A008	N65º44′12.7″ W016º44′54.3″	N/small iron pin	~0.5 m iron stick, Two big boulders	Follow gravel road going N from Viti, pass chain, pass A005, drive to where road starts to ascend steeply before right hand turn, park car, Walk towards W for 500m, Look for two big (2 m^2) boulders (not visible from road) just W of fault, to get there you have to cross two 'fault line' gullies. One boulder has 0.5 m iron stick, other small iron pin. Measure at boulder with small pin.
29	A012	N65º44′37.7″ W016º44′18.5″	N/slightly bend iron pin	Cairn/ Wooden stick	Follow the gravel road going N passed A008, ascend 'plateau', Look for track going W up main hill in area. You can turn car up the hill just before summit. Station is at summit of this hill. Previously used as GPS point.

APPENDIX B: Micro-gravity methodology

B.1 LaCoste and Romberg micro-gravity meters

Two types of LaCoste and Romberg instruments were used during this study; a G-meter in Iceland and a D-meter at Stromboli, Italy. Both instruments function like long-period seismographs. They consist of a mass on the end of a beam which is supported by a 'zero length' spring (Figure A-1). A 'zero length' spring has a real length which equals its extension. The gravity is measured as a function of the amount of adjustment required to balance the torque on the mass (caused by gravity force) and the torque on the spring. The material of which the spring is made is sensitive to pressure and temperature changes and the instrument is therefore insulated and controlled by a thermostat powered by a 12 V DC gel-cell battery (for more details see http://www.lacosteromberg.com/). The main difference between the G and D-meter is that the D-meter is typically 10 times more sensitive making it possible to read it with an accuracy of up to 0.1 μGal. The D-meter used during this study (D41) has been retrofitted with the aliod100 system (http://www.lacosteromberg.com/newprod.htm). Of the G-meters, G513 has been retrofitted with a galvanometer readout, but not feedback and G403 has no modifications.

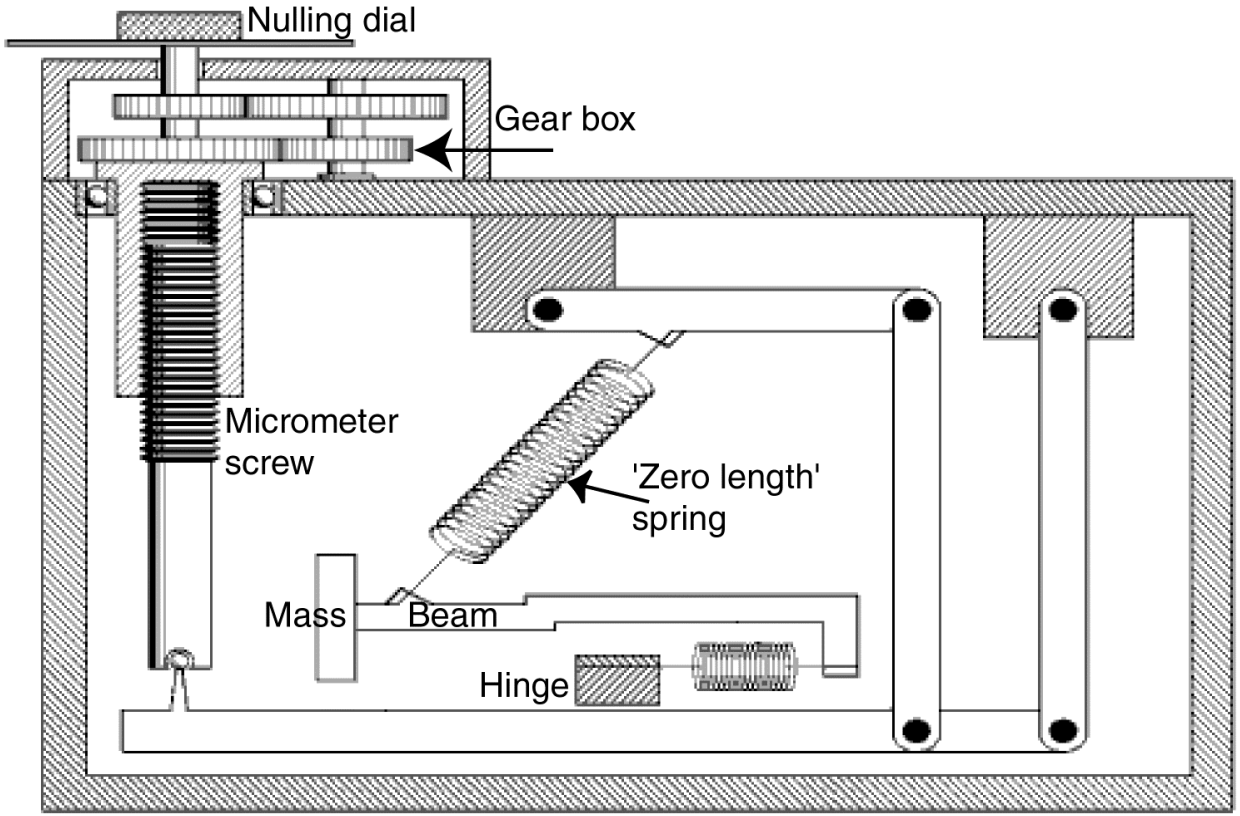

A - 1 Mechanism of the LaCoste & Romberg gravity meter. LaCoste & Romberg Manual, 2000.

B.2 Network set-up and reading of the instrument

G-meters

Utmost care should be taken while transporting the instrument as it is very sensitive to knocks. The same instrument should be used throughout the survey and preferably the reading is done by the same operator using the same procedures (Rymer, 1996). The same instrument, LaCoste and Romberg meter G-513, has been used during micro-gravity surveys at Askja since 1988 and at Krafla since 1990. LaCoste and Romberg meter G-403 has been used in addition since 1997.

A dynamic gravity survey uses a network of stations which are re-measured on a regular basis. To enable repeat measurements, stations should be clearly marked with a pin or paint and consist of a purpose built concrete block or an existing stable rock outcrop. When installing or choosing new stations, ensure they are relatively easy to reach and can accommodate a metal base plate. At Askja, the network comprises mainly stations established previously for geodetic purposes. The thirteen stations were set-up by Eysteinn Tryggvason while he was working at the University of Tulsa (3), by scientists from the Nordic Volcanological Institute (NVI) (4), by scientists from The Open University (2) and scientists from Darthmouth College (2). Most of them are of the 'outcrop' type, and two stations have been added in 2002 by NVI in collaboration with the OU (see Chapter 2). At Krafla, the regularly measured network consists of twenty-nine stations set-up by scientists from the National Energy Authority of Iceland (17), the Nordic Volcanological Institute (11) and the Open University (1). Most of these were also built for geodetic purposes.

Dynamic gravity measurements are always referred to a base station which should be located outside the area of gravity variation. Unfortunately, recent geodetic measurements (de Zeeuw-van Dalfsen et al., 2004a; Sturkell and Sigmundsson, 2000) have shown that base stations used for Askja and Krafla are located inside the deformation field. This results in a minimum estimate of any sub-surface mass change observed.

A base plate is placed accurately over the station. The instrument is placed on the plate and levelled. The internal temperature and the level are checked before a reading is made. A reading should always be approached from the same direction to avoid hysterisis effects within the spring (Rymer, 1996). The average of a few repeat readings is taken and noted down together with the exact time of the reading (to correct for earth tides). The network should be measured following a multiple cross-looping method (Rymer, 1996). At Askja, it is feasible to measure the network in one day; at Krafla a minimum of three days is needed.

D-meters

A continuously recording D-meter was installed at Stromboli volcano, Italy (see Chapter 5 for details of the installation). Important considerations in the installation were to protect the instrument from the weather, passing tourists and eruptions.

The power switch for the Aliod100 should be left on at all times during the survey. The instrument is levelled using the electronic levels and the reading appears in the LCD screen. Data can be sent via the serial port and transferred to a computer where they can be stored.

B.3 Data reduction

Raw data must be corrected using the calibration factors supplied by the manufacturer. For G-meters, this calibration results from the fact that the spring does not behave in a perfectly linear fashion across the range of the instrument. For D-meters, the manufacturer has most often assigned a single calibration factor. This means the assumption is made the calibration is linear which is reasonable because only about 62% of the full range of the lever and micrometer system is used (LaCoste and Romberg, 2000). Furthermore, data should be corrected for solid Earth tides, the deformation of the Earth as a response to the gravitational attraction of the Sun and Moon. Jolting of the instrument can result in 'tares' which should also be taken into account. Anomalous points caused by transmission problems during continuous recording, are removed and data are re-sampled to one data point per second. (see Chapter 5).

B.4 Data Interpretation

Before any dynamic gravity data can be interpreted in terms of sub-surface mass or density changes, they have to be corrected for vertical movements e.g., the net micro-gravity changes must be calculated. The necessity of this calculation is illustrated in Figure A - 2. The calculation is done by correcting for the change of gravity with height above ground level using the Free Air Gradient. The FAG is the change of gravity with elevation which has a theoretical value of -308.6 μGal m^{-1}. The use of a measured FAG (Rymer, 1996) however, is more accurate then the use of the theoretical value for the FAG and is therefore favoured. The local value of the FAG can easily be determined by subtracting the micro-gravity

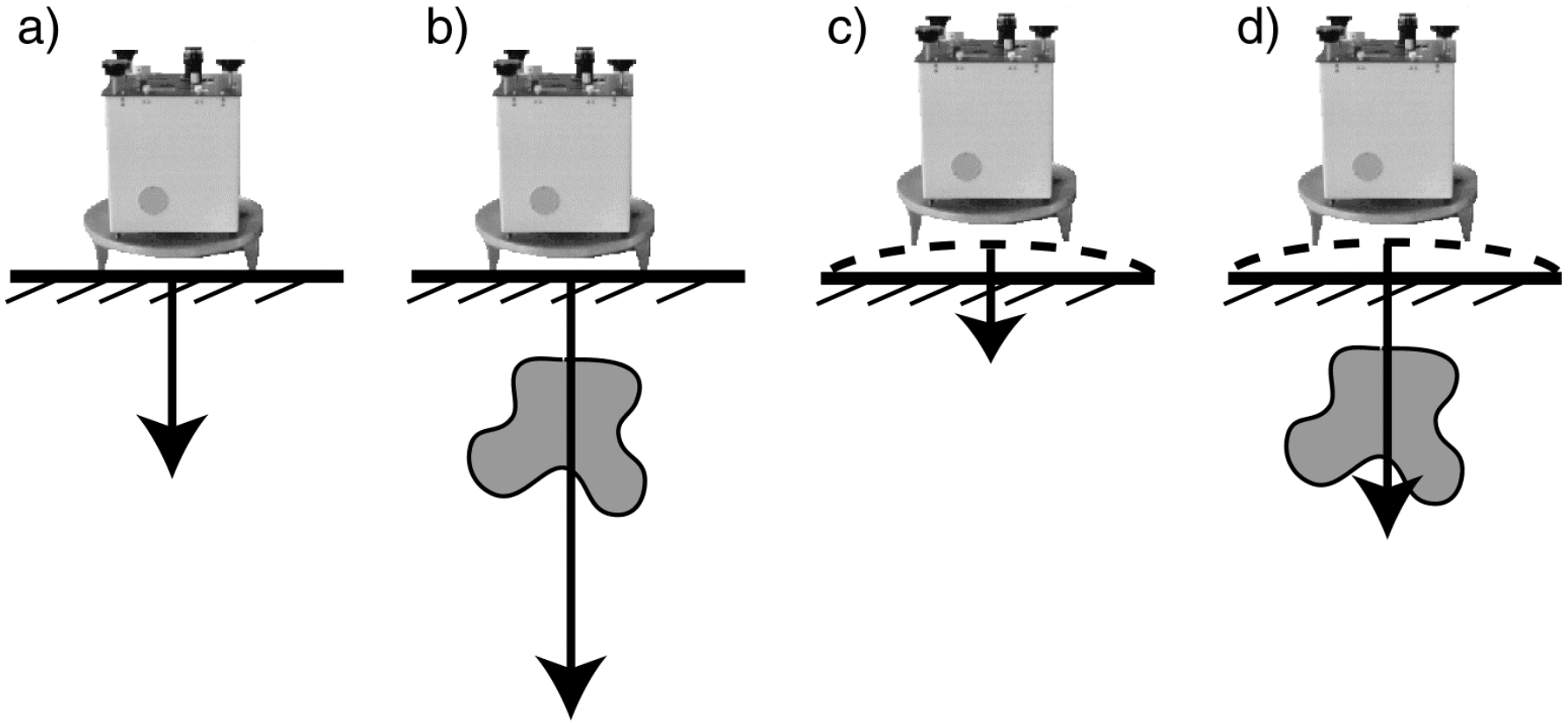

A - 2 The effect of gravity change with sub-surface mass change and/or elevation change. Solid line depicts the surface, arrow the gravitational force experienced by the LaCoste & Romberg gravity meter. Elevation change is shown with a dashed line; sub-surface mass change is represented by the sub-surface "blob".a) The gravitational effect at the surface.b) The gravitational effect of sub-surface mass change, in this case increase. Compared to a, the gravitational force has increased. c) The gravitational effect of elevation change, in this case inflation. Compared to a, the gravitational force has decreased because the instrument is further away from the attracting body. d) The gravitational effect of sub-surface mass change and elevation change, in this case mass increase and inflation. The gravitational force has increased, compared to a, but not as much as expected if there was no inflation (compared to b). This illustrates the importance of accurate height correction before interpretation in terms of sub-surface mass changes is attempted.

measured at the top of a tripod from that at the ground and dividing it by the tripod height (Rymer, 1996). Measurements of the FAG at Askja, completed in 2002 and 2003, resulted in a range from -240 μGal/m in the southeast, to -360 μGal/m in the centre. These deviations from the theoretical value are due to the caldera-centred Bouguer negative gravity anomaly (Brown et al., 1991), and a positive anomaly in the east associated with a fissure swarm (Rymer and Tryggvason, 1993). During the 2002 survey at Krafla, the FAG was measured at several key stations as suggested by previous workers (Gottsmann and Rymer, 2002). The results show a FAG close to the theoretical value for the reference station (FM115) and the South Hlídardalur stations (seeFigure 4-3i). Across the rift the FAG differs considerably, with values of -386 μGal/m in the Leirnjúkur area and -280 μGal/m in the Hreindýrahóll area (Table 4-3).

The total deformation at a station in a period of interest, relative to the same base station as used for the micro-gravity survey, is multiplied by the FAG measured at that station. Subtraction from the measured micro-gravity change in that period at that station results in the net micro-gravity change in the period of interest at that station. This change can then be explained by a sub-surface mass change, providing it is larger then the errors on the gravity data.

B.5 Geodetic Measurements

For the purpose of this study, data generated by collaborating groups and of several geodetic techniques have been used. The techniques used here are precise levelling, GPS and InSAR. The first two data sets have been generated by colleagues from the Meteorological Office of

Iceland and of the Nordic Volcanological Institute (Rymer et al., 1998a; Sturkell and Sigmundsson, 2000), the latter have been generated by scientists from the Nordic Volcanological Institute and the Open University (de Zeeuw-van Dalfsen et al., 2004a). The standard deviation on the total geodetic data set is thought to be within 2 cm for the vertical measurements. This generates a maximum error of ~6 μGal which is acceptable for the long time periods (13-15 year) we have looked at.

APPENDIX C: Data

C.1 Dynamic gravity and geodetic data from Askja and Krafla

Micro-gravity data measured with meter G-513, G-105 and G-403 at each station in mGal are relative to station 83001 at Askja and station FM115 at Krafla. These data have been corrected for Earth tides, calibration factors and tares but need to be corrected for geodetic changes before interpretation is done. Data were collected by Geoff Brown (1985-1992), Hazel Rymer (1985-2002), Corinne Locke (1994-1997) and Elske de Zeeuw-van Dalfsen (2002-2003) all from the Open University. Meter G-105 was destroyed in 1993 and the last data set collected using this instrument was obtained in 1992. Numbers refer to locations of stations depicted in Figure 2-2 for the Askja data and Figure 4-2 for the Krafla data. Abbreviations in the station names stand for: D is Darthmouth College, NE is Norræna Eldfjallastöðin (Nordic Volcanological Institute), OS is Orkustofnun (National Energy Authority of Iceland), FM is Fallmælingar Raforkumálaskriftstofu (today National Energy Authoroty of Iceland), LV is Landsvirkjun (the National Power Company), LM is Landmælingar Íslands (National land survey of Iceland) and KV is Kröfluvirkjunar (Krafla power station).

Askja

Micro-gravity data

TABLE C - 1 G-105 data for Askja, 1988-1992

No.	Station	1988	1989	1990	1991	1992
1	DYNG	-	-	-	-	-
2	83009	-	-	-	-	14.289
3	83001	0.000	0.000	0.000	0.000	0.000
4	430	-	-	-	-	-
5	412	-3.573	-3.575	-3.552	-3.549	-3.564
6	405	-3.531	-3.495	-3.519	-3.518	-3.536
7	Von Knebel	-9.190	-9.204	-9.183	-9.182	-9.202
8	IV16	-3.050	-3.040	-3.022	-3.046	-3.030
9	D-18	-0.238	-0.219	-0.220	-0.202	-0.231
10	NE2002005	-	-	-	-	-
11	NE2002006	-	-	-	-	-
12	NE82005	-15.487	-15.462	-15.455	-15.447	-15.488
13	D-19	-15.255	-15.262	-15.225	-15.223	-

TABLE C - 2 G-403 data for Askja, 1997, 2002 and 2003.

No.	Station	1997	2002	2003
1	DYNG	-	23.539	23.567
2	83009	14.113	14.124	14.125
3	83001	0.000	0.000	0.000
4	430	-	-	0.637
5	412	-3.547	-3.536	-3.548
6	405	-3.474	-3.476	-3.480
7	Von Knebel	-9.166	-9.127	-9.120
8	IV16	-2.985	-	-3.059
9	D-18	-0.204	-0.199	-0.235
10	NE2002005	-	-14.707	-14.757
11	NE2002006	-	-15.455	-15.466
12	NE82005	-15.421	-15.368	-15.400
13	D-19	-15.223	-15.185	-15.173

TABLE C - 3 G-513 data for Askja, 1988 to 2003.

No.	Station	1988	1989	1990	1991	1992	1994	1995	1997	2002	2003
1	DYNG	-	-	-	-	-	-	-	-	23.600	23.584
2	83009	14.174	14.206	14.173	14.168	14.172	-	-	14.225	14.167	14.142
3	83001	0.000	0.000	0.000	0.000	0.000	0.000	0.000	0.000	0.000	0.000
4	430	-	-	-	-	-	-	-	-	0.692	0.650
5	412	-3.561	-3.567	-3.562	-3.550	-3.536	-3.533	-3.530	-3.518	-3.560	-3.547
6	405	-3.507	-3.521	-3.516	-3.510	-3.503	-3.526	-3.504	-3.498	-3.503	-3.491
7	Von Knebel	-9.197	-9.198	-9.193	-9.189	-9.160	-9.151	-9.176	-9.167	-9.144	-9.103
8	IV16	-3.047	-3.025	-3.043	-3.042	-3.007		-3.002	-3.063	-3.035	-3.015
9	D-18	-0.226	-0.205	-0.236	-0.215	-0.187	-0.224	-0.200	-0.798	-0.175	-0.174
10	NE2002005	-	-	-	-	-	-	-	-	-14.756	-14.779
11	NE2002006	-	-	-	-	-	-	-	-	-15.478	-15.490
12	NE82005	-15.470	-15.479	-15.458	-15.480	-15.445	-15.465	-15.512	-15.448	-15.434	-15.432
13	D-19	-15.253	-15.246	-15.245	-15.235	-15.219	-15.240	-15.246	-15.262	-15.212	-15.209

Geodetic data

The total vertical displacement in meters (Table 2-2) is calculated for each year following the two point Mogi model suggested by Sturkell et al. (2004). This model is based on precise levelling, GPS and tilt data. The standard deviation on the total geodetic data set is thought to be within 2 cm for the vertical measurements. This generates a maximum error of ~6 μGal which is acceptable for the long time period we have looked at.

TABLE C - 4 geodetic data for Askja, 1989 to 2003.

	Station	1989	1990	1991	1992	1993	1994	1995	1996	1997	1998	1999	2000	2001	2002	2003
1	DYNG	0.0099	0.0096	0.0094	0.0091	0.0089	0.0087	0.0085	0.0082	0.0080	0.0078	0.0076	0.0074	0.0073	0.0071	0.0069
2	83009	0.0065	0.0064	0.0062	0.0061	0.0059	0.0058	0.0056	0.0055	0.0053	0.0052	0.0051	0.0049	0.0048	0.0047	0.0046
3	83001	0.0000	0.0000	0.0000	0.0000	0.0000	0.0000	0.0000	0.0000	0.0000	0.0000	0.0000	0.0000	0.0000	0.0000	0.0000
4	430	-0.0003	-0.0003	-0.0003	-0.0003	-0.0003	-0.0003	-0.0003	-0.0003	-0.0003	-0.0003	-0.0003	-0.0003	-0.0002	-0.0002	-0.0002
5	412	-0.0059	-0.0057	-0.0056	-0.0054	-0.0053	-0.0052	-0.0050	-0.0049	-0.0048	-0.0047	-0.0045	-0.0044	-0.0043	-0.0042	-0.0041
6	405	-0.0073	-0.0071	-0.0069	-0.0067	-0.0066	-0.0064	-0.0062	-0.0061	-0.0059	-0.0058	-0.0056	-0.0055	-0.0053	-0.0052	-0.0051
7	Von Knebel	-0.0124	-0.0121	-0.0118	-0.0115	-0.0112	-0.0110	-0.0107	-0.0104	-0.0101	-0.0099	-0.0096	-0.0094	-0.0092	-0.0089	-0.0087
8	IV16	-0.0062	-0.0060	-0.0059	-0.0057	-0.0056	-0.0055	-0.0053	-0.0052	-0.0051	-0.0049	-0.0048	-0.0047	-0.0046	-0.0044	-0.0043
9	D-18	-0.0059	-0.0057	-0.0056	-0.0054	-0.0053	-0.0052	-0.0050	-0.0049	-0.0048	-0.0047	-0.0045	-0.0044	-0.0043	-0.0042	-0.0041
10	NE2002005	-0.0340	-0.0331	-0.0323	-0.0315	-0.0307	-0.0299	-0.0292	-0.0284	-0.0277	-0.0270	-0.0263	-0.0257	-0.0250	-0.0244	-0.0238
11	NE2002006	-0.0369	-0.0360	-0.0351	-0.0342	-0.0333	-0.0325	-0.0317	-0.0309	-0.0301	-0.0294	-0.0286	-0.0279	-0.0272	-0.0265	-0.0258
12	NE82005	-0.0368	-0.0359	-0.0350	-0.0341	-0.0333	-0.0324	-0.0316	-0.0308	-0.0300	-0.0293	-0.0285	-0.0278	-0.0271	-0.0264	-0.0258
13	D-19	-0.0364	-0.0354	-0.0346	-0.0337	-0.0328	-0.0320	-0.0312	-0.0304	-0.0297	-0.0289	-0.0282	-0.0275	-0.0268	-0.0261	-0.0254

Krafla

Micro-gravity data

TABLE C - 5 Micro-gravity data G-513 acquired at Krafla 1990-2003.

	Station	1990	1991	1992	1994	1995	1996	1997	2002	2003
1	Hotel	15.463	15.457	15.477	15.474	15.498	15.493	15.506	15.501	15.956
2	Hellahraun	-	-	-	-	-	-13.026	-13.063	-13.0743	-13.036
3	FM115	0.000	0.000	0.000	0.000	0.000	0.000	0.000	0.000	0.000
4	2313	-	-	-	-	0.001	-0.035	-0.026	-0.014	-0.032
5	OS5595	-30.696	-30.703	-30.708	-30.692	-30.697	-30.684	-30.689	-30.761	-30.770
6	5596	-14.798	-14.810	-14.746	-14.757	-14.763	-14.776	-14.753	-14.769	-14.766
7	OS5597	-13.270	-13.282	-13.220	-13.218	-13.198	-13.239	-13.255	-13.274	-13.260
8	5599	-	-	-	-	-0.113	-0.159	-0.174	-0.172	-0.184
9	5599a	-	-0.194	-0.172	-0.170	-	-0.159	-0.206	-0.211	-0.220
10	OS5600	-	-0.468	-0.445	-	-	-	-	-0.492	-0.455
11	5672	-	-52.177	-52.166	-	-52.181	-52.192	-52.223	-52.215	-
12	OS5684	-45.998	-	-	-	-45.982	-	-	-46.078	-46.087
13	OS5685	-	-	-	-	-	-	-	-48.382	-48.382
14	OS5688	-13.710	-13.731	-13.697	-13.686	-13.658	-13.669	-13.704	-13.688	-13.706
15	OS5697	-	-	-	-	-	-0.310	-	-0.358	-0.337
16	OS5698	-	-0.117	-	-	-	-	-	-	-0.102
17	OS5699	-	0.149	-	-	-	-	-	0.144	0.168
18	OS5843	-	-15.437	-	-	-	-	-	-15.462	-15.478
19	NE220	-	-	-	-	-	-	-	-1.380	-1.338
20	NE9301	-	-	-	-	-	-13.026	-13.063	-13.074	-13.036
21	NE80051	-	-35.777	-35.739	-	-	-	-	-35.864	-34.498
22	NE79077	-	-34.442	-34.424	-34.381	-	-	-	-34.496	-34.498
23	A001	-31.643	-31.668	-31.605	-31.638	-31.602	-31.616	-31.658	-31.664	-31.644
24	A002	-39.830	-39.811	-39.798	-39.849	-39.815	-39.847	-39.844	-39.861	-39.876
25	A003	-39.116	-39.125	-39.106	-39.080	-39.104	-39.141	-39.155	-39.161	-39.181
26	A004	-28.026	-28.045	-28.030	-28.046	-28.033	-28.014	-28.051	-28.055	-28.028

	Station	1990	1991	1992	1994	1995	1996	1997	2002	2003
27	A005	-31.060	-31..75	-31.057	-31.038	-31.083	-31.050	-31.055	-31.113	-31.097
28	A008	-34.570	-	-	-	-	-	-	-34.659	-
29	A012	-58.421	-58.413	-	-58.383	-	-58.484	-	-58.487	-
a	KONGSP	-	-	-	-	-	-	-	-	15.956

TABLE C - 6 Micro-gravity data G-105 acquired at Krafla 1990-1992.

	Station	1990	1991	1992
1	Hotel	15.457	15.461	15.460
2	Hellahraun	-	-	-
3	FM115	0.000	0.000	0.000
4	2313	-	-	-
5	OS5595	-30.553	-30.589	-30.647
6	5596	-14.658	-14.770	-14.774
7	OS5597	-13.166	-13.206	-13.168
8	5599	-0.163	-0.141	-
9	5599a	-0.176	-	-0.136
10	OS5600	-0.466	-0.457	-0.455
11	5672	-	-51.913	-51.969
12	OS5684	-45.762	-	-
13	OS5685	-	-	-
14	OS5688	-13.582	-13.702	-13.624
15	OS5697	-	-	-
16	OS5698	-	-0.103	-
17	OS5699	0.144	0.152	-
18	OS5843	-	-	-
19	NE220	-	-	-
20	NE9301	-	-	-
21	NE80051	-	-	-
22	NE79077	-	-	-
23	A001	-31.497	-31.501	-31.578
24	A002	-39.662	-39.661	-39.661
25	A003	-38.956	-38.993	-39.005
26	A004	-27.903	-27.929	-27.979
27	A005	-30.902	-30.929	-30.969
28	A008	-34.387	-	-
29	A012	-58.152	-58.171	-
a	KONGSP	-	-	-

TABLE C - 7 Micro-gravity data G-403 aquired at Krafla 1997,2002 and 2003.

	Station	1997	2002	2003
1	Hotel	-	15.436	15.412
2	Hellahraun	13.331	13.311	13.279
3	FM115	0.000	0.000	0.000
4	2313	-0.013	-0.004	-0.021
5	OS5595	-30.612	-30.667	-30.688
6	5596	-14.618	-14.740	-14.757
7	OS5597	-13.080	-13.222	-13.239
8	5599	-0.181	-0.179	-0.241
9	5599a	-0.208	-0.186	-0.228
10	OS5600	-	-0.479	-0.507
11	5672	-51.924	-52.051	-52.137
12	OS5684	-	-45.946	-45.932
13	OS5685	-	-48.230	-48.266
14	OS5688	-13.567	-13.669	-13.662
15	OS5697	-	-0.378	-0.385
16	OS5698	-	-	-0.127
17	OS5699	-	0.152	0.150
18	OS5843	-	-15.402	-15.435
19	NE220	-	-1.377	-1.398
20	NE9301	-13.019	-13.027	-13.061
21	NE80051	-	-35.776	-35.790
22	NE79077	-	-34.424	-34.445
23	A001	-31.632	-31.580	-31.669
24	A002	-39.724	-39.750	-39.794
25	A003	-39.013	-39.053	-39.121
26	A004	-27.984	-28.013	-28.056
27	A005	-30.905	-31.030	-31.088
28	A008	-	-34.510	34.628
29	A012	-	-58.327	-58.373
a	KONGSP	-	-	15.925

Geodetic data

To calculate the total vertical deformation in the Krafla area, several steps have been taken.

I) The average yearly deflation at Krafla is estimated by the various authors using several geodetic methods (Table C-8). The resulting decay curve is displayed in Figure 4-3. The curve follows the equation: deformation = $2E + 196e^{-0.23*year}$.

TABLE C - 8 Average yearly deflation at Krafla.

from	to	average yr	sub./yr [cm]	references
1989	1992	1990.5	5.0	Tryggvason, 1994
1989	1995	1992.0	3.5	Björnsson & Eysteinsson, 1998
1992	1995	1993.5	2.4	Sigmundsson et al., 1997
1992	1998	1995.0	2.3	Henriot et al., 2001*
1993	1999	1996.0	1.1	InSAR 11677_22408
1995	1998	1996.5	1.5	InSAR 01867_17899
1996	1998	1997.0	1.2	InSAR 6877_17899
1995	2000	1997.5	0.9	Agustsson, 2001**
1996	1999	1997.5	1.1	InSAR 6376_22408

* Number reported in paper is ground to satellite displacement, 23° from vertical of 2.1 cm.

** The vertical displacement from station KONGSP to the area of maximum deformation between 1995 and 2000.

II) Levelling data from Águstsson (2001) and Bjornsson and Eysteinsson (1998) form the basis of the calculation. Levelling station names marked in bold indicate that the levelling station used is the same as the gravity station.Otherwise, the closest possible levelling station has been used. The data show there has been deflation in the centre of the area, no deformation to the S and inflation to the N and far E.

TABLE C - 9 Levelling data for Krafla acquired in 1989, 1995 and 2000.

Gravity name	Levelling name	Bjornsson & Eysteinsson 1989	Águstsson 1995	Águstsson 2000	WRTFM115 1989	WRTFM115 1995	WRTFM115 2000	[m] 1995-2000	[m] 1989-1995
FM115	**FM115**	359.4317	359.4317	359.4317	0.0000	0.0000	0.0000	0.0000	0.0000
KONGSP	**LM1420**	279.4577	279.4816	279.4960	-79.9740	-79.9501	-79.9357	0.0144	0.0239
A004	LV956104		533.13338	533.1059	-359.4317	173.70168	173.6742	-0.0275	
A008	LV956106		612.3992	612.4275	-359.4317	252.9675	252.9958	0.0283	
A012	LV956107		648.6332	648.6679	-359.4317	289.2015	289.2362	0.0347	
NE9301	**NE9301**		451.2651	451.2537	-359.4317	91.8334	91.822	-0.0114	
5843	NE9301		451.2651	451.2537	-359.4317	91.8334	91.822	-0.0114	
OS5595	**OS5595**	551.7777	551.6760		192.346	192.2443	-359.4317	-0.0190	-0.1017
OS5596	**OS5596**	469.6477	469.5292	469.4882	110.216	110.0975	110.0565	-0.0410	-0.1185
OS5597	**OS5597**	458.0207	457.9363	457.9139	98.5890	98.5046	98.4822	-0.0224	-0.0844
OS5598	**OS5598**	443.7797	443.7381	443.7276	84.3480	84.3064	84.2959	-0.0105	-0.0416
OS5599	**OS5599**	394.6597	394.6421	394.6394	35.2280	35.2104	35.2077	-0.0027	-0.0176
OS5599a	OS5599	394.7877	394.7704	394.7674	35.3560	35.3387	35.3357	-0.0030	-0.0173
OS5600	**OS5600**	389.6017	389.5989	389.6027	30.1700	30.1672	30.171	0.0038	-0.0028
A005	OS5670	547.6157	547.5421	547.5310	188.1840	188.1104	188.0993	-0.0111	-0.0736
OS5672	**OS5672**	659.6237	659.6416	659.6782	300.1920	300.2099	300.2465	0.0366	0.0179

Gravity name	Levelling name	Bjornsson & Eysteinsson	Agustsson	Agustsson	WRTFM115			[m] 1995-2000	[m] 1989-1995
		1989	1995	2000	1989	1995	2000		
A005	OS5681	535.0947	534.9749	534.9458	175.6630	175.5432	175.5141	-0.0291	-0.1198
OS5684	**OS5684**	610.5287	610.4574	610.4571	251.0970	251.0257	251.0254	-0.0003	-0.0713
5688	OS-KB11	490.8207	490.7004	490.6701	131.3890	131.2687	131.2384	-0.0303	-0.1203
A003	OS-KV2	530.2857	530.1334	530.1057	170.8540	170.7017	170.674	-0.0277	-0.1523
A001	OS-KV8	526.4657	526.3569	526.3502	167.0340	166.9252	166.9185	-0.0067	-0.1088
A002	OS-KV12	541.0797	540.9467	540.9221	181.6480	181.5150	181.4904	-0.0246	-0.1330
OS5685	OS5685	626.8277	626.7540	626.7612	267.3960	267.3223	267.3295	0.0072	-0.0737
OS5697	OS5697	381.0027	381.0026	381.0069	21.5710	21.5709	21.5752	0.0043	-0.0001
OS5698	OS5698	372.4247	372.4273	372.4303	12.9930	12.9956	12.9986	0.0030	0.0026
OS5699	OS5699	361.2897	361.2908	361.2938	1.8580	1.8591	1.8621	0.0030	0.0011
850051	OS7162		445.9074	445.9087	-359.4317	86.4757	86.477	0.0013	

III) Following the decay equation, the maximum deformation expected in the Krafla area from 1995 to 2000 is:

TABLE C - 10 Maximum deformation expected in the Krafla area 1995-2000.

year	Calculated max deflation [cm]
1995	-1.70
1996	-1.36
1997	-1.09
1998	-0.86
1999	-0.69
Total	**-5.69**

IV) At each station only a percentage of this maximum will be reached, assuming there is only one centre of deformation and deformation is decreasing with distance from this centre.

TABLE C - 11 Percentage of maximum deformation which will be reached at each station.

Gravity name	Levelling name	[m]	percentage from max
FM115	**FM115**	0.0000	0.0000
KONGSP	**LM1420**	0.0144	-0.2530
A004	LV956104	-0.0275	0.4829
A008	LV956106	0.0283	-0.4973
A012	LV956107	0.0347	-0.6098
NE9301	**NE9301**	-0.0114	0.2003
5843	NE9301	-0.0114	0.2003
OS5595	**OS5595**	-0.0190	0.3339
OS5596	**OS5596**	-0.0410	0.7205
OS5597	**OS5597**	-0.0224	0.3936
OS5598	**OS5598**	-0.0105	0.1845
OS5599	**OS5599**	-0.0027	0.0474
OS5599a	OS5599	-0.0030	0.0527
OS5600	**OS5600**	0.0038	-0.0668
A005	OS5670	-0.0111	0.1951
OS5672	**OS5672**	0.0366	-0.6432
A005	OS5681	-0.0291	0.5114
OS5684	**OS5684**	-0.0003	0.0053
OS5685	**OS5685**	0.0072	-0.1265
OS5697	**OS5697**	0.0043	-0.0756
OS5698	**OS5698**	0.0030	-0.0527
OS5699	**OS5699**	0.0030	-0.0527
850051	OS7162	0.0013	-0.0228
5688	OS-KB8	-0.0324	0.5694
5688	OS-KB11	-0.0303	0.5325
A003	OS-KV2	-0.0277	0.4868
A001	OS-KV8	-0.0067	0.1177
A002	OS-KV12	-0.0246	0.4323

V) Following the decay equation, the maximum deformation expected in the Krafla area from 1990 to 1995 is:

TABLE C - 12 Maximum deformation expected from 1990 to 1995.

year	Calculated max deflation [cm]
1990	-5.27
1991	-4.21
1992	-3.35
1993	-2.67
1994	-2.13
Total	**-17.64**

TABLE C - 13 Maximum deformation expected from 2000 to 2003.

year	Calculated max deflation [cm]
2000	-0.55
2001	-0.44
2002	-0.35
total	**-1.34**

VI) The maximum deformation is multiplied with the percentages to estimate the deformation in these time periods at the different stations:

TABLE C - 14 Estimated deformation at the different stations (taking into account the percentage of the maximum).

Gravity name	Levelling name	percentage	1990-95	2000-03
FM115	**FM115**	0.0000	0.0000	0.0000
Kongsp	**LM1420**	-0.2530	0.0446	0.0034
A004	LV956104	0.4829	-0.0852	-0.0064
A008	LV956106	-0.4973	0.0877	0.0066
A012	LV956107	-0.6098	0.1076	0.0081
NE9301	**NE9301**	0.2003	-0.0353	-0.0027
5843	NE9301	0.2003	-0.0353	-0.0027
OS5595	**OS5595**	0.3339	-0.0589	-0.0045
OS5596	**OS5596**	0.7205	-0.1271	-0.0096
OS5597	**OS5597**	0.3936	-0.0694	-0.0053
OS5598	**OS5598**	0.1845	-0.0326	-0.0025
OS5599	**OS5599**	0.0474	-0.0084	-0.0006
OS5599a	OS5599	0.0527	-0.0093	-0.0007
OS5600	**OS5600**	-0.0668	0.0118	0.0009
A005	OS5670	0.1951	-0.0344	-0.0026
OS5672	**OS5672**	-0.6432	0.1135	0.0086
A005	OS5681	0.5114	-0.0902	-0.0068
OS5684	**OS5684**	0.0053	-0.0009	-0.0001
OS5685	**OS5685**	-0.1265	0.0223	0.0017
OS5697	**OS5697**	-0.0756	0.0133	0.0010
OS5698	**OS5698**	-0.0527	0.0093	0.0007
OS5699	**OS5699**	-0.0527	0.0093	0.0007
850051	OS7162	-0.0228	0.0040	0.0003
5688	OS-KB8	0.5694	-0.1004	-0.0076
5688	OS-KB11	0.5325	-0.0939	-0.0071
A003	OS-KV2	0.4868	-0.0859	-0.0065
A001	OS-KV8	0.1177	-0.0208	-0.0016
A002	OS-KV12	0.4323	-0.0763	-0.0058

VII) Following the decay equation, the maximum deformation expected in the Krafla area from 1989 to 1995 is:

TABLE C - 15 Maximum deformation expected at Krfala from 1989 to 1995.

year	Calculated max deflation [m]	Percentage of total
1989	-0.0661	27.2655
1990	-0.0527	21.7437
1991	-0.0421	17.3401
1992	-0.0335	13.8284
1993	-0.0268	11.0278
1994	-0.0213	8.7945
Total	**-0.2426**	**100.0000**

The deformation in 1989 is estimated and subtracted from the 1989-1995 value (II) to get the 1990-1995 value:

TABLE C - 16 Estimated deformation from 1990 to 1995.

Gravity name	**Levelling name**	**Bjornsson 1989-1995 [m]**	**1989**	**1990-1995**
FM115	**FM115**	0.0000	0.0000	0.0000
Kongsp	**LM1420**	0.0239	0.0065	0.0174
A004	LV956104			
A008	LV956106			
A012	LV956107			
NE9301	NE9301			
5843	**NE9301**			
OS5595	**OS5595**	-0.1017	-0.0277	-0.0740
OS5596	**OS5596**	-0.1185	-0.0323	-0.0862
OS5597	**OS5597**	-0.0844	-0.0230	-0.0614
OS5598	**OS5598**	-0.0416	-0.0113	-0.0303
OS5599	**OS5599**	-0.0176	-0.0048	-0.0128
OS5599a	OS5599	-0.0173	-0.0047	-0.0126
OS5600	**OS5600**	-0.0028	-0.0008	-0.0020
A005	OS5670	-0.0736	-0.0201	-0.0535
OS5672	**OS5672**	0.0179	0.0049	0.0130
A005	OS5681	-0.1198	-0.0327	-0.0871
OS5684	**OS5684**	-0.0713	-0.0194	-0.0519
OS5685	**OS5685**	-0.0737	-0.0201	-0.0536
OS5697	**OS5697**	-0.0001	0.0000	-0.0001
OS5698	**OS5698**	0.0026	0.0007	0.0019
OS5699	**OS5699**	0.0011	0.0003	0.0008
850051	OS7162			
5688	OS-KB8	-0.1029	-0.0281	-0.0748
5688	OS-KB11	-0.1203	-0.0328	-0.0875
A003	OS-KV2	-0.1523	-0.0415	-0.1108
A001	OS-KV8	-0.1088	-0.0297	-0.0791
A002	OS-KV12	-0.1330	-0.0363	-0.0967

VIII) Now the total deformation is calculated from 1990 to 2003 and for the two periods, 1990 to 1995 and 1996 to 2003, see Table 4-1.

TABLE C - 17 Estimated total deformation at Krafla from 1990 to 2003.

Gravity name	Levelling name	Estimated 1990-95 [m]	Bjornsson [m]	Difference [cm]	Total 1990-1995 [m]	Agustsson 1995-2000 [m]	Estimated 2000-03 [m]	1995-2003 [m]	1990-2003 [m]
FM115	**FM115**	0.0000	0.0000	0.0000	0.0000	0.0000	0.0000	0.0000	0.0000
Kongsp	**LM1420**	0.0446	0.0174	**2.7261**	0.0174	0.0144	-0.0002	0.0142	0.0316
A004	LV956104	-0.0852			-0.0852	-0.0275	0.0011	-0.0263	-0.1115
A008	LV956106	0.0877			0.0877	0.0283	-0.0012	0.0271	0.1149
A012	LV956107	0.1076			0.1076	0.0347	-0.0014	0.0333	0.1408
NE9301	**NE9301**	-0.0353			-0.0353	-0.0114	0.0005	-0.0109	-0.0463
5843	NE9301	-0.0353			-0.0353	-0.0114	0.0005	-0.0109	-0.0463
OS5595	**OS5595**	-0.0589	-0.0740	1.5062	-0.0740	-0.0190	-0.0045	-0.0235	-0.0974
OS5596	**OS5596**	-0.1271	-0.0862	**-4.0922**	-0.0862	-0.0410	0.0012	-0.0398	-0.1260
OS5597	**OS5597**	-0.0694	-0.0614	-0.8059	-0.0614	-0.0224	0.0008	-0.0216	-0.0830
OS5598	**OS5598**	-0.0326	-0.0303	-0.2296	-0.0303	-0.0105	0.0004	-0.0101	-0.0404
OS5599	**OS5599**	-0.0084	-0.0128	0.4430	-0.0128	-0.0027	0.0002	-0.0025	-0.0153
OS5599a	OS5599	-0.0093	-0.0126	0.3282	-0.0126	-0.0030	0.0002	-0.0028	-0.0154
OS5600	**OS5600**	0.0118	-0.0020	1.3818	-0.0020	0.0038	0.0000	0.0038	0.0018
A005	OS5670	-0.0344	-0.0535	1.9119	-0.0535	-0.0111	0.0007	-0.0104	-0.0639
OS5672	**OS5672**	0.1135	0.0130	**10.0452**	0.0130	0.0366	-0.0002	0.0364	0.0494
A005	OS5681	-0.0902	-0.0871	-0.3083	-0.0871	-0.0291	0.0012	-0.0279	-0.1151
OS5684	**OS5684**	-0.0009	-0.0519	**5.0930**	-0.0519	-0.0003	0.0007	0.0004	-0.0515
OS5685	**OS5685**	0.0223	-0.0536	**7.5927**	-0.0536	0.0072	0.0007	0.0079	-0.0457
OS5697	**OS5697**	0.0133	-0.0001	1.3404	-0.0001	0.0043	0.0000	0.0043	0.0042
OS5698	**OS5698**	0.0093	0.0019	0.7410	0.0019	0.0030	0.0000	0.0030	0.0049
OS5699	**OS5699**	0.0093	0.0008	0.8501	0.0008	0.0030	0.0000	0.0030	0.0038
850051	OS7162	0.0040			0.0040	0.0013	-0.0001	0.0012	0.0053
5688	OS-KB8	-0.1004	-0.0748	**-2.5606**	-0.0748	-0.0324	0.0010	-0.0314	-0.1062
5688	OS-KB11	-0.0939	-0.0875	-0.6440	-0.0875	-0.0303	0.0012	-0.0291	-0.1166
A003	OS-KV2	-0.0859	-0.1108	**2.4896**	-0.1108	-0.0277	0.0015	-0.0262	-0.1370
A001	OS-KV8	-0.0208	-0.0791	**5.8363**	-0.0791	-0.0067	0.0011	-0.0056	-0.0848
A002	OS-KV12	-0.0763	-0.0967	**2.0469**	-0.0967	-0.0246	0.0013	-0.0233	-0.1200

C.2 Continuous gravity data from Stromboli.

The data collected at Stromboli are too extensive to display in graphs (~ 2 samples a second). Therefore the data have been appended in digital format on CD. The CD has a directory called APPENDIX C which is divided into four subdirectories: raw data, corrected data, PTh_data and scripts. The data directories are divided into the three periods during which measurements were made at Stromboli: may 2002, October 2002 and July-October 2003. Raw data are those straight from the instrument in text format. Corrected data, in MATLAB® format, have been corrected for earth tides and unrealistic spikes caused by transmission problems have been taken out. Also data disturbed by storms and those from the initial set up period, when instruments were still settling have been ignored. Data have been manipulated using scripts written with the MATLAB® software. The scripts are printed below to explain how they work, but are also saved on CD. Pressure, Temperature and humidity data are only available during two days in May 2002 and during the October 2002 survey period. The scripts are:

I]	read_all_files.m	=> To read the raw data files and merge them into daily MATLAB® file.
II]	clean.m	=> To clean the merged data files.
III]	resample.m	=> To re-sample the cleaned data.
IV]	daily.m	=> Changing the files so the run for a full day.
V]	tide.m	=> Preparation of the tide data from quicktide.
VI}	tide_corr.m	=> Correction of gravity data, using correction factor and earth tides.
VII]	merge_monthly.m	=> Smoothing and merging of the data into monthly files.
VIII]	smoothing.m	=> The smoothing function.
IX]	detrend.m	=> To de-trend the data.
X]	total.m	=> To add all data.

I] To read the raw data files and merge them into daily matlab files:

```
--------------------------------------------------------------------------
% This is a script which reads in the original raw data and puts them into 1 file for each day.
% Maurizio Ripepe and Elske de Zeeuw-van Dalfsen, April 2004.

% First we close and clear all active programs.
close all
clear all
% We identify the days of each month.
dm=[31 28 31 30 31 30 31 31 30 31 30 31];
ntype=0
% We open the correct directory.
vol='C:\MATLAB6p1\work\Stromboli\microgravity 2003\#D41_merge'
mat=matlabroot;
ind=findstr(mat,':');
root=mat(1:ind(1));
% We read in all folders:
cd(vol)
D=dir(vol);
s=length (D);
D=struct2cell(D);
% We extract the names of the files:
n=0;
for i=1:4:s*4;
  n=n+1;
  foldername(n)=D(i);
              lbyte(n)=D{i+2};
              lbyte(n)=lbyte(n)/15;
end
nlast=length(foldername)+ntype;
for ii=1:nlast
volf=strcat(vol,char(foldername(ii)),':')
cd(char(volf))
D=dir (char(volf));
s=length(D);
D=struct2cell(D);
n=0;
for         i=1:4:s*4;
              n=n+1;
              filename(n)=D(i);
```

```
                lbyte(n)=D{i+2};
                lbyte(n)=lbyte(n)/15;
end
nfile=length(filename)
dt=1/1.85;
% We open the files:
for     i=1:nfile,
                i
                file=char(filename(i))

        fid=fopen((file),'rt');
        dati=fread(fid);
                fclose (fid)
% and address variables we need later:
                j=find(dati==44);
                dati(j(1:length(j)))=46;

                nc=find(dati==13);
                tsec=dati(1:nc(1));
                mgal=dati(nc(1)+1:nc(2));

                % separate the gravity values
                clear j
                j=find(mgal==9);
                j=j';
                l=[1 j+1];
                q=length(l);
                j(q)=length(mgal);
                mgal=mgal';
  for   k=1:q
                                mk(k)=str2num(char(mgal(l(k):j(k))));
                end
                if      i==1
                        mg=mk;
                else
                        mg=[mg mk];
                end
                % separate the time values
                clear j l
                j=find(tsec==9);
                j=j';
```

```
                    l=[1 j+1];
                    w=length(l);
                    j(w)=length(tsec);
                    tsec=tsec';
                    tsA=str2num(char(tsec(l(1):j(1))));
                    tsZ=str2num(char(tsec(l(w):j(w))));
                    i0=findstr(file,'_');
                    i1=findstr(file,'-');
                    i2=findstr(file,'.');
                    dd =file(5:i1(1)-1);
                    mm =file(i1(1)+1:i1(2)-1);
day  =str2num(file(5:i1(1)-1));
month =str2num(file(i1(1)+1:i1(2)-1));
hour =str2num(file(i0(2)+1:i2(1)-1));
min  =str2num(file(i2(1)+1:i2(2)-1));
sec=str2num(file(i2(2)+1:length(file)));
                    T=tsZ-tsA;
                    dt0=dt;
                    dt=T/(q-1);
  if        dt<0
            dt=dt0;
  end
                    dt
                    tg=tsA+dt*(0:q-1);
                    tsec=(sum(dm(1:month-1)))*24*3600;
                    tsec=tsec+(day)*24*3600;
                    ts=tsec+tg;
                    ts=ts./86400;
                    if          i==1
                                tt=ts;
                    else
                                tt=[tt ts];
                    end
                    clear ts tsec tg dati mgal j i0 i1 i2

end
tzero=datenum(2003,1,0);
tt=tzero+tt;
d=datestr(tt(1),1);
% We plot the data:
figure(1), plot(tt,mg)
```

```
datetick('x',15)
title(d)
zoom on
drawnow
% We save the data in the correct directory
volm='C:\MATLAB6p1\work\Stromboli\microgravity 2003\#D41_merge';
cd(volm);
fln=strcat('D41_',d)
save(fln, 'tt', 'mg')
clear tt mg filename
end
return
```

II] To clean the merged data files:

```
---------------------------------------------------------------------------
% This is a script which can be used to clean data for unrealistic spikes.
% It is based on a script written by Emanuelle Marchetti and adapted by Elske de zeeuw-van Dalfsen.
% The program is interactive and asks you what you want to do, do not forget to save data after they have been cleaned!
% First we close and clear all active programs.
close all
clear all
% We open the correct directory
vol='C:\MATLAB6p1\work\Stromboli\microgravity 2003\Charlotte\august'
 mat=matlabroot;
ind=findstr(mat,':');
root=mat(1:ind(1));
cd(vol)
% We extract the files in the directory
D=dir(vol);
D=struct2cell(D);
D(:,1:2)=[]
s=length (D);
n=0;
for     i=1:4:s*4;
        n=n+1;
        foldername(n)=D(i);
                lbyte(n)=D{i+2};
                lbyte(n)=lbyte(n)/15;
end
filename=foldername;
nfile=length(filename)
% We load the files in the directory
for     i=1:nfile
                file=char(filename(i))
                load(file)
% We plot the gravity data, but without the time:
        figure(1)
        plot (mg)
        grid
        zoom on
        r=input('(c)lear, (n)ext, (e)xit,s(a)ve','s');
```

```
% When r does not equal n:
  while r~='n'
% When r = e exit
   if r=='e'
     return
   end
% When r=a save
   if r=='a',
     save (file,'tt','mg')
   end
% When r=c, start ginput for correction
   if r=='c'
     [nn aa]=ginput(2);
     n1=nn(1);
     n2=nn(2);
     n=length(tt);
     tt2=[tt(1:n1) tt(n2:n)];
     mg2=[mg(1:n1) mg(n2:n)];
     clear tt mg
     tt=tt2;
     mg=mg2;
     figure(1)
     plot (mg)
     grid
     zoom on
   end
   r=input('(c)lear, (n)ext, (e)xit,s(a)ve','s');
 end
end
```

III] Re-sampling of the cleaned data:

```
---------------------------------------------------------------------------
% This program resamples the data so there is exactly one data point per second in each file.
% This is done to simplify the tide correction.
% However, the disadvantage is that this program introduces spikes which might need to be corrected for using an adapted version of clean.
% Elske de Zeeuw-van Dalfsen April 2003.
% First we close and clear all active programs.
close all
clear all
% We identify the days of each month.
dm=[31 28 31 30 31 30 31 31 30 31 30 31];
ntype=0
% We open the correct directory.
vol='C:\MATLAB6p1\work\Stromboli\microgravity 2003\Charlotte\august'
mat=matlabroot;
ind=findstr(mat,':');
root=mat(1:ind(1));
% We read in all folders:
cd(vol)
D=dir(vol);
s=length (D);
D=struct2cell(D);
D(:,1:2)=[]
s=length (D);
% We extract the names of the files:
n=0;
for i=1:4:s*4;
  n=n+1;
  foldername(n)=D(i);
            lbyte(n)=D{i+2};
            lbyte(n)=lbyte(n)/15;
end
filename=foldername;
nfile=length(filename)
% We open the files:
for i=1:nfile,
            i
            file=char(filename(i))
            load(file)
```

```
% We change the time axis to seconds:
  t1=tt-datenum(2003,1,0);
  min1=min(t1)
  dec=rem(min1,1);
  min2=min1-dec
  t2=t1-min2;
  t3=t2*86400;
% We devide the data into second spacing:
  min3=min(t3);
  max=max(t3);
  xx=min3:1:max;
  [t4 int]=unique(t3);
  mg2=mg(int);
  yy=spline(t4,mg2,xx);
% We view the results and save the data in the correct directory
volm='C:\MATLAB6p1\work\Stromboli\microgravity 2003\#D41_merge\august\resampled';
  cd(volm);
  d=datestr(tt(1),1);
  fln=strcat('D41_',d);
  rtt=xx;
  rmg=yy;
  save(fln, 'rtt', 'rmg')
  plot (rtt,rmg)
end
--------------------------------------------------------------------------------
```

IV] Changing the files so the run for a full day.

```
--------------------------------------------------------------------------------
% This program is designed to make sure each daily file starts at 00:00:00 and ends at 23:59:59.
% This way tide correction is simplified.
% Check to make sure the results of this procedure contains 86399 lines.
% Elske de Zeeuw-van Dalfsen april2004.
% First we close and clear all active programs.
close all
clear all
% We identify the days of each month. dm=[31 28 31 30 31 30 31 31 30 31 30 31];
ntype=0
% We open the correct directory.
vol='C:\MATLAB6p1\work\Stromboli\microgravity 2003\#D41_merge\July\resampled'
mat=matlabroot;
ind=findstr(mat,':');
root=mat(1:ind(1));
% We read in all folders:
cd(vol)
D=dir(vol);
D=struct2cell(D);
D(:,1:2)=[]
s=length (D);
% We extract the names of the files:
n=0;
for i=1:4:s*4;
  n=n+1;
  foldername(n)=D(i);
            lbyte(n)=D{i+2};
            lbyte(n)=lbyte(n)/15;
end
filename=foldername;
nfile=length(filename)
% We load the data:
for i=1:nfile,
            i
            file=char(filename(i))
  load(file);
% change the time so it is a complete day, check with plots, to make sure there are no odd jumps in the
data. Save the data
```

```
figure,plot(rtt,rmg)
i1=find(rtt<=86400);
rtt2=rtt(i1);
rmg2=rmg(i1);
figure,plot(rtt2,rmg2)
save(strcat('rttday',strvcat(D(1,i))),'rtt2','rmg2')
i2=find(rtt>86400);
rttnext=rtt(i2)-86400;
rttnext(1)=0;
rmgnext=rmg(i2);
save(strcat('rttnext',strvcat(D(1,i))),'rttnext','rmgnext')
 if i==1
                        tday=rtt2;
                        mday=rmg2;
  volm='C:\MATLAB6p1\work\Stromboli\microgravity 2003\#D41_merge\July\Day';
  cd(volm);
  save(strvcat(D(1,i)), 'tday', 'mday')
  figure,plot(tday,mday)
  cd(vol)
          else
  i=i-1;
  file2=strcat('rttnext',strvcat(D(1,i)))
  load(strcat('rttnext',strvcat(D(1,i))));
                        tday=[rttnext rtt2];
                        mday=[rmgnext rmg2];
  volm='C:\MATLAB6p1\work\Stromboli\microgravity 2003\#D41_merge\July\Day';
  cd(volm);
  i=i+1;
  file3=strvcat(D(1,i))
  save(strvcat(D(1,i)), 'tday', 'mday')
  figure,plot(tday,mday)
  cd(vol)
          end
end
```

V] Preparation of the tide data from quicktide:

```
---------------------------------------------------------------------------
% This program prepares the tide files calculated by quicktide to be used for correction of gravity data in MATLAB.
% It needs input from quicktide, files exported as texfile, 1 second spacing, lat & long 38.79 N 15.21 E (for Stromboli)!!!
% Also remove the first 'text' line as it interferes with the processing.
% Elske de Zeeuw-van Dalfsen, april 2004.
% First we close and clear all active programs.
close all
clear all
% We identify the days of each month.
dm=[31 28 31 30 31 30 31 31 30 31 30 31];
ntype=0
% We open the correct directory.
vol='C:\MATLAB6p1\work\Stromboli\microgravity 2003\tide\august'
mat=matlabroot;
ind=findstr(mat,':');
root=mat(1:ind(1));
% We read in all folders:
cd(vol)
D=dir(vol);
s=length (D);
D=struct2cell(D);
D(:,1:2)=[]
s=length (D);
% We extract the names of the files:
n=0;
for i=1:4:s*4;
  n=n+1;
  foldername(n)=D(i);
        lbyte(n)=D{i+2};
        lbyte(n)=lbyte(n)/15;
end
filename=foldername;
nfile=length(filename)
% We load the file and extract the tide data, we generate time data.
for i=1:nfile,
        i
        file=char(filename(i))
```

```
        Q=load(file);
  d=datestr(file,7)
  time=[0:1:86399];
  time=time';
  tide=Q(:,4);
  tide=tide/1000;
    % We plot the data to ensure they are correct:
  figure, plot(time,tide)
    % We save the data in the correct directory:
  volm='C:\MATLAB6p1\work\Stromboli\microgravity 2003\tides\august';
  cd(volm);
  fln=strcat('tide',d,'aug');
  save(fln, 'time', 'tide')
  cd(vol)
end
```

VI] Correction of gravity data, using correction factor and earth tides:

```
%This is a program to correct the cleaned resampled daily gravity data with a factor between 1.9 and 2.5
and correct for tides
% Elske de Zeeuw-van Dalfsen,april 2004.
% First we close and clear all active programs.
close all
clear all
% We identify the days of each month.
dm=[31 28 31 30 31 30 31 31 30 31 30 31];
ntype=0
% We open the folder with the data and the folder with the tide files
vol='H:\Stromboli\microgravity 2003\#D41_merge\october\day'
vol2='H:\Stromboli\microgravity 2003\tides\october'
mat=matlabroot;
ind=findstr(mat,':');
root=mat(1:ind(1));
% We Find all the file names in the data folder
cd(vol)
D=dir(vol);
s=length (D);
D=struct2cell(D);
D(:,1:2)=[]
s=length (D);
% We find all the files in the tide folder
cd(vol2)
D2=dir(vol2);
s=length (D2);
D2=struct2cell(D2);
D2(:,1:2)=[]
s=length (D2);
% We read in all folders:
n=0;
for i=1:4:s*4;
  n=n+1;
  foldername(n)=D(i);
  foldername2(n)=D2(i);
            lbyte(n)=D{i+2};
            lbyte(n)=lbyte(n)/15;
end
```

```
filename=foldername;
filename2=foldername2;
nfile=length(filename)
% We open all the files
for i=1:nfile,
            i
 file=char(filename(i))
 cd(vol)
 load(file);
  cd(vol2)
 file2=char(filename2(i))
            load(file2);
  % We change row to column
 mday=mday';
 tday=tday';
 % We calculate the gravity using the correction factor.
 mdayc1_9=mday/1.9;
 mdayc2_0=mday/2;
 mdayc2_1=mday/2.1;
 mdayc2_2=mday/2.2;
 mdayc2_3=mday/2.3;
 mdayc2_4=mday/2.4;
 mdayc2_5=mday/2.5;
 % We calculate the corrected gravity
 [i3 int]=unique(tday);
  if min(i3)==0
    i3=i3+1;
  end
 time2=time(i3);
 tide2=tide(i3);
 gravc=mday-tide2;
 gravc1_9=mdayc1_9-tide2;
 gravc2_0=mdayc2_0-tide2;
 gravc2_1=mdayc2_1-tide2;
 gravc2_2=mdayc2_2-tide2;
 gravc2_3=mdayc2_3-tide2;
 gravc2_4=mdayc2_4-tide2;
 gravc2_5=mdayc2_5-tide2;
 % We plot the results
 figure,subplot (5,1,1),plot(time2,tide2)
 subplot(5,1,2),plot(tday,mday)
```

```
 subplot(5,1,3),plot(tday,gravc)
 subplot(5,1,4),plot(tday,gravc2_0)
 subplot(5,1,5),plot(tday,gravc2_5)
  tday2_3=tday;
 % We save the data
 volm='H:\Stromboli\microgravity 2003\#D41_merge\october\Corrected';
 cd(volm);
 save(strvcat(D(1,i)), 'tday', 'tday2_3', 'gravc', 'gravc1_9', 'gravc2_0', 'gravc2_1', 'gravc2_2', 'gravc2_3',
'gravc2_4', 'gravc2_5')
end
```

VII] Smoothing and merging of the data into monthly files:

```
--------------------------------------------------------------------------------
% This script merges all the daily data of the same month.
% It also calls for the script smooth, written by Maurizio Ripepe.
% Elske de Zeeuw-van Dalfsen
% First we close and clear all active programs.
close all
clear all
% We identify the days of each month.
dm=[31 28 31 30 31 30 31 31 30 31 30 31];
ntype=0
% We open the correct directory.
vol='H:\Stromboli\microgravity 2003\#D41_merge\october\Corrected'
vol2='H:\Stromboli\microgravity 2003\#D41_merge\october\original'
mat=matlabroot;
ind=findstr(mat,':');
root=mat(1:ind(1));
% We read in all folders:
cd(vol)
s=length (D);
D=D(3:s);
s=length (D);
D=struct2cell(D);
cd(vol2)
D2=dir(vol2);
s2=length (D2);
D2=D2(3:s2);
s2=length (D2);
D2=struct2cell(D2);
% We extract the names of the files:
n=0;
for i=1:4:s*4;
  n=n+1;
  foldername(n)=D(i);
  foldername2(n)=D(i);
            lbyte(n)=D{i+2};
            lbyte(n)=lbyte(n)/15;
end
filename=foldername;
filename2=foldername2;
```

```
nfile=length(filename)
% We open the files:
for i=1:nfile,
        i
        file=char(filename(i))
        cd(vol)
 load(file)
 cd(vol2)
 file2=char(filename2(i))
 load(file2)
 gravc2_3=gravc2_3';
 tday2_3=tday2_3';
 t=tday2_3/86400;
 d=datestr(tt(1),1);
 t2=datenum(d);
 tday2=t+t2;
 % Smoothing the data:
        gravcor=smooth(gravc2_3,3000);
        tk=tday2(1:3000:length(tday2));
        mk=gravcor(1:3000:length(gravcor));
          if i==1
                tsec=tk;
                mgal=mk;
          else
                mgal=[mgal mk];
    tsec=[tsec tk];
          end
end
% Plot the data:
figure, plot(tsec,mgal)
datetick('x',1)
zoom on
drawnow
% Save the data
volm='H:\Stromboli\microgravity 2003\#D41_merge\october'
cd(volm)
save october_all tsec mgal
return
```

VIII] The smoothing function:

```
--------------------------------------------------------------------------------
function y=smooth(x,w)
% y=smooth(x,w) this function smoothes the function over the window w
% Maurizio Ripepe, April 2004
wh=round(w/2);
w=wh*2;
n=length(x);
xm=cumsum(x);
xw(1:wh)   =xm(wh+1:w)-xm(1);
xw(wh+1:n-wh)=xm(w+1:n)-xm(1:n-w);
xw(n-wh+1:n) =xm(n)-xm(n-w+1:n-wh);
wl(1:wh)=wh+(0:wh-1);
wl(wh+1:n-wh)=w;
wl(n-wh+1:n) =w-(1:wh);
y=xw./wl;
return
--------------------------------------------------------------------------------
```

IX] To detrend the data:

```
--------------------------------------------------------------------------------
% This program is to detrend the data e.g. to correct for instrumental drift.
% However,I am not sure how usefull this is.
% Elske de Zeeuw van Dalfsen, april 2004
% Close and clear all running programs.
clear all
close all
% Open the data and load them
vol='C:\MATLAB6p1\work\Stromboli\microgravity 2003\#D41_merge\July'
cd(vol)
D=dir(vol);
load july.mat
% Plot the original data
figure,
plot (tsec,mgal);
datetick('x',1);
% detrend the data
mgal2=detrend(mgal);
% Plot the detrended data
figure(2),
plot (tsec,mgal2);
datetick('x',1);
--------------------------------------------------------------------------------
```

X] To add all data

```
% This script adds all data together. Elske de Zeeuw-van Dalfsen, april 2004
% Close and clear all running programs.
close all
clear all
% Open all the needed folders
vol1='H:\Stromboli\microgravity 2003\#D41_merge\July'
vol2='H:\Stromboli\microgravity 2003\#D41_merge\august'
vol3='H:\Stromboli\microgravity 2003\#D41_merge\september'
vol4='H:\Stromboli\microgravity 2003\#D41_merge\October'
% Load all the data.
cd(vol1)
load july_all
julytime=tsec;
julygrav=mgal;
cd(vol2)
load august_all
augtime=tsec;
auggrav=mgal;
cd(vol3)
load september_all
septime=tsec;
sepgrav=mgal;
cd(vol4)
load october_all
octtime=tsec;
octgrav=mgal;
% Add all the data together.
totaltime=[julytime augtime septime octtime];
totalgrav=[julygrav auggrav sepgrav octgrav];
totalgrav2=detrend(totalgrav)
% Plot the data
plot(totaltime,totalgrav)
datetick('x',1);
figure,plot(totaltime,totalgrav2)
datetick('x',1);
% Save the data
save total totaltime totalgrav totalgrav2
```

APPENDIX D: InSAR Methodology

D.1 What is InSAR?

InSAR stands for Interferometric Synthetic Aperture Radar. It is a remote sensing technique that uses radar satellite images acquired by satellites such as ERS1, ERS2 and Radarsat. The technique can be used to monitor ground deformation (Massonnet and Feigl, 1998) and has been applied in this thesis to analyse volcanic deformation (de Zeeuw-van Dalfsen et al., 2004a). The advantages of this technique above conventional geodetic monitoring techniques are that it provides overview, the data have good spatial density, risk to field workers is eliminated and it is possible to analyse data with hindsight and it is possible to analyse data acquired at night.

D.2 How does InSAR work?

A pulse of radar energy is emitted from a satellite, scattered by the Earth's surface and recorded back at the satellite. Because the natural resolution of a radar in orbit is very poor, complex computer processing 'synthesizes' a larger antenna, leading to a better resolution. This is called SAR imaging (Synthetic Aperture Radar). The radar energy received by the satellite consists of two types of information, the amplitude and the phase of the signal. The amplitude depends on the terrain's capacity to send the incident signal back towards the radar. The phase of the radar image is used as a measure of the distance from ground to satellite. The difference between two radar images acquired at different times from the same point in space relates to the movement of the ground surface in that period. Because images are hardly ever

taken from the same point in space geometric corrections are applied to account for the difference. The baseline is the distance between the two satellite positions and can be divided into 'normal' and 'parallel' baselines. The shorter the normal baseline the higher the chances are for good correlation. The inverse of the normal baseline is called the altitude of ambiguity.

D.3 Limits of InSAR

To achieve reasonable coherence in an interferogram the observed surface has to be relatively stable. Lakes and agricultural areas are examples of unstable areas. The difference in orbits of the two images should be less than one kilometre for ERS satellites (Massonnet and Feigl, 1998). Ground movements should not cause too great a physical compression or extension of the ground, exceeding half a wavelength per pixel. Interferograms are ambiguous; they measure the movement of the ground towards satellite by modulus half the wavelength. Spatial continuity is necessary to allow for counting of fringes starting at a reference point.

D.4 The DIAPASON software

DIAPASON stands for Differential Interferometric Automated Process Applied to Survey of Nature. The software developed by CNES (Centre National d'Etudes Spatial, Toulouse, France) consists of so called descriptor files and runs in WINDOWS under a UNIX emulator (CYGWIN). There are three steps to run, called pre-processing, PRISME and DIAPASON. The name of the script used for execution of each step is mentioned in brackets.

D.4.1 Pre-processing:

* *Information extraction and concatenation*: Information is extracted from the header of the raw data file. If necessary, raw data files are added together to form one concatenated file (.c5b). The data format is described in the PAF_<product_origin>.form (EXTRACT_CONCATGB.sh)
* *Compression rate, incidence angle and pixel size:* In preparation for the PRISME software, the compression rate in azimuth at the near and far range and the incidence angles and pixel sizes are calculated. (TAUXGB.sh)
* *Doppler in azimuth:* In preparation for the PRISME software, the average doppler in azimuth is estimated from an extract of the concatenated raw data image. (DOPPLERGB.sh)

D.4.2 PRISME processing:

* *PRISME:* Software which enables transformation of RAW data into a complex focussed image with improved resolution. (PRISMEGB.sh) PRISME generates two images, one of the integer complex type (.ci2) and one of the multilook type (mv_52.byt, see D - 1)

D.4.3 DIAPASON processing:

* *Data installation (descriptor files):* Several files should be available for the DIAPASON software to run correctly. The sensor descriptor file contains information on the angle of viewing, the carrier frequency, the echo distance sampling frequency and the pulse repetition frequency (sar_ERS1.dat). Each orbit is described by an orbit file, containing a list of the radar's successive positions and velocities during imaging (<orbit#>.orb). The radar images are encoded in CI2 format

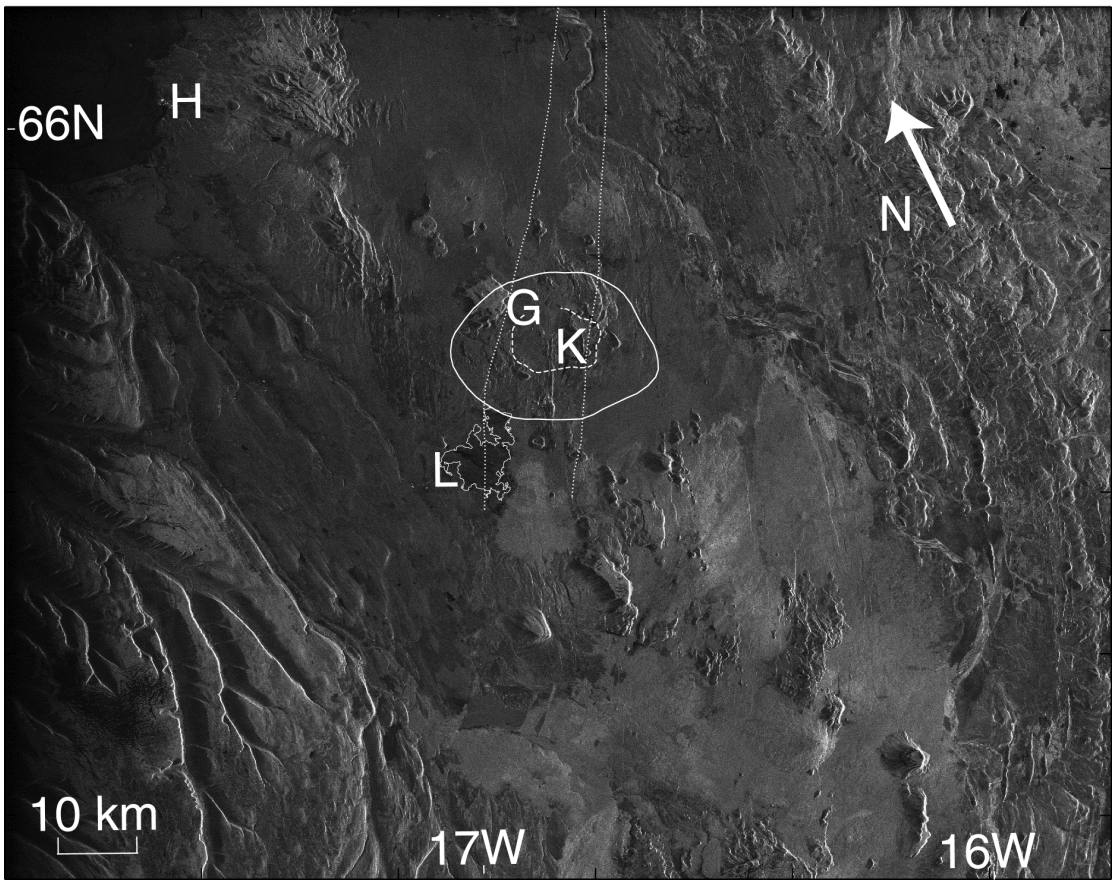

D - 1 SAR Image 22408, H is the town of Húsavik, L is Lake Mývatn, K is Krafla mountain, G is Gæsafjöll. The solid line shows the Krafla volcano outline, the dashed line the Krafla caldera and the dotted line the Krafla fissure swarm. Two of these SAR images are combined to form one radar interferogram. The same outlines and letters will be used throughout the Figures for this APPENDIX.

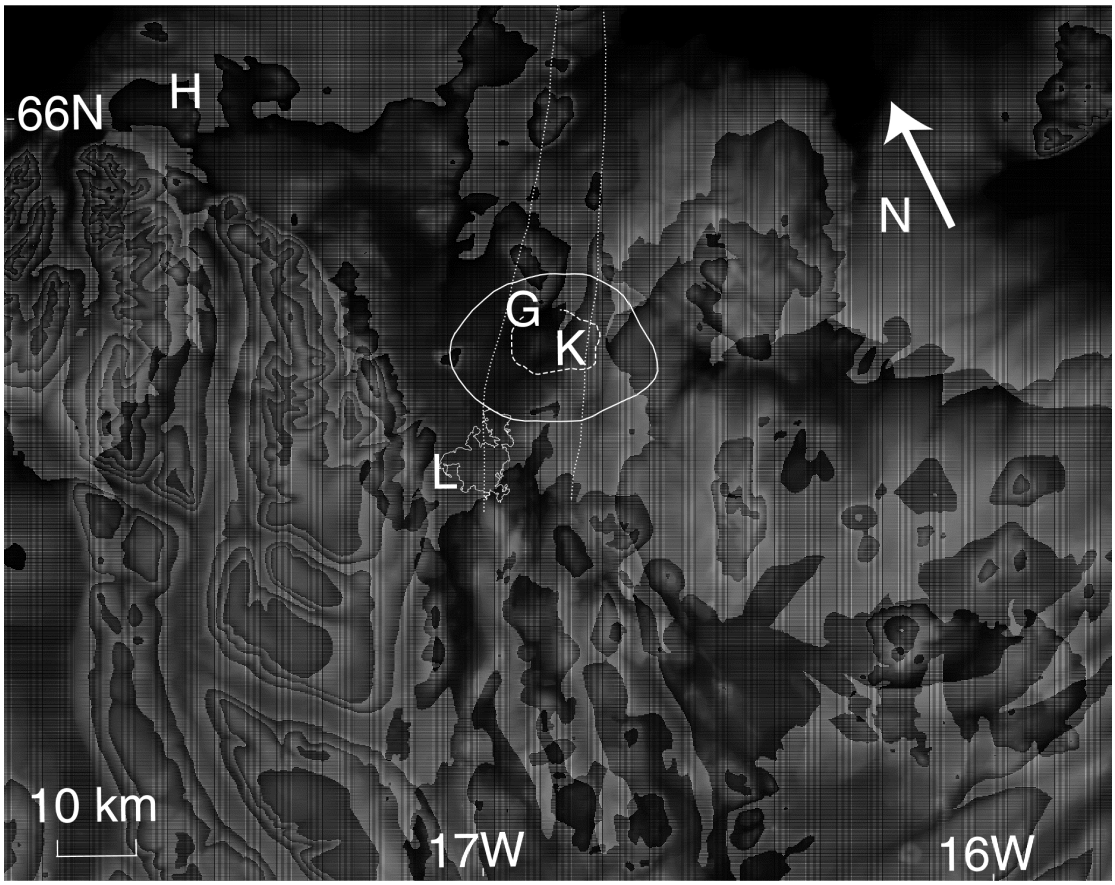

D - 2 The digital elevation map (DEM) which was used for topographic corrections of all interferograms produced for this study. The DEM was produced by the Icelandic geodetic survey and has an accuracy of 30 m.

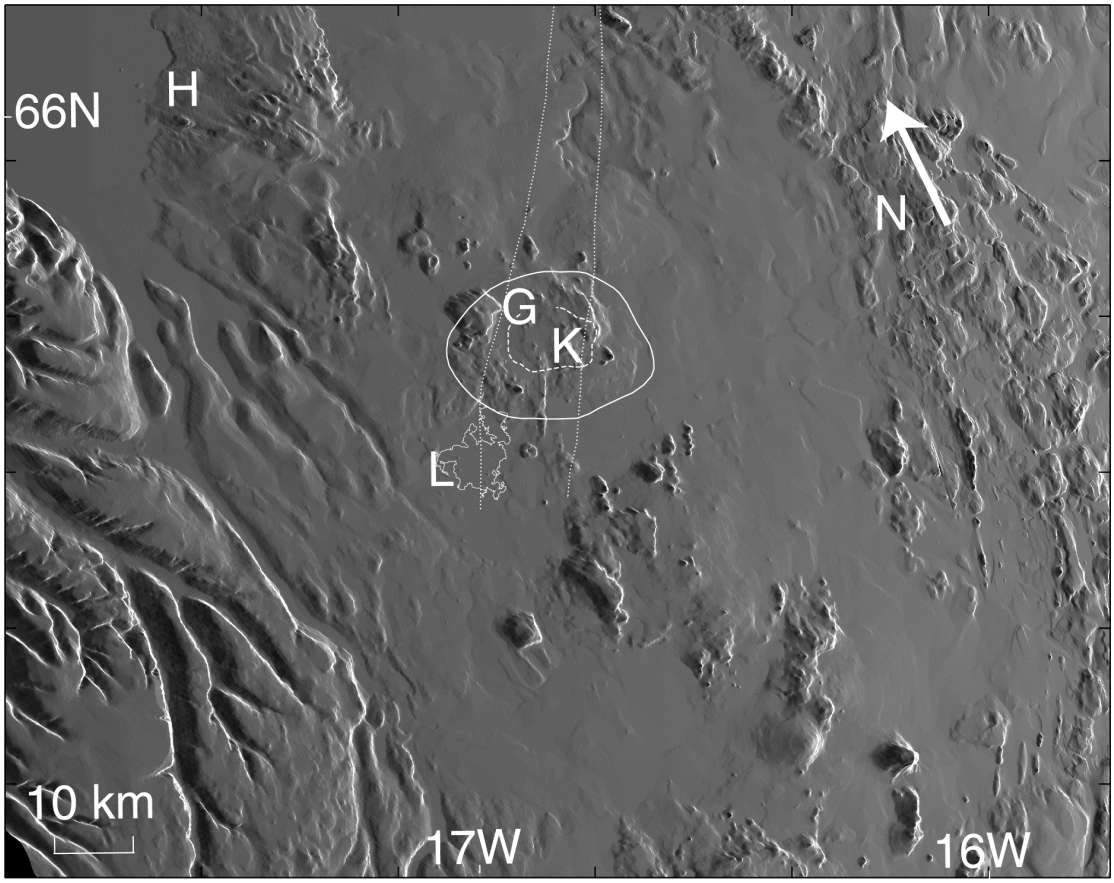

D - 3 The simulated file of the 11677_22408 interferogram, used by the DIAPSON process to line up the master and DEM image so they overlap exactly.

(<orbit#master.ci2 and orbit#slave.ci2). An image description file contains information concerning its geometry: actual dimensions, time of start of acquisition, near range distance, name of orbit file, name of sensor description file, the sub-sampling factors and the geometrical image restitution Doppler (rough_geosar<orbit#master>.dat and rough_geosar<orbit#slave>.dat). Each complex radar image has its associated multi-look image encoded on a byte. A Digital Elevation Model (DEM, see D - 2) is used to correct for existing topography. A DEM descriptor file defines the name and size of the DEM, type of altitude encoding, scale factor and offset, projection used, the zero reference for altitudes and zone extracted (dted_all_3.dat). Once all data have been set-up DIAPSON is started (DIAPASON.sh)

* *Lining up the Master image with the DEM:* this is done by creating a simulated image from the master image (see D - 3), correlating the master image with the simulation, precise setting of the master image and finally verification of the new settings.
* *Geometrical superimposition of the two radar images:* correlation of the two radar images, fine modelling of deformation between radar images, re-sampling of slave radar image to make it super-imposable on the master image and finally verification of the new settings.
* *Interferometric processing:* Calculation of viewing point from orbit data and theoretical phase difference of master and slave, optimizing of pulse responses by filtering of complex master and slave images, creation of raw complex interferogram, the raw complex interferogram is corrected using the theoretical phase to create a compensated complex interferogram,

production of phase image output (D - 4), coherency image output (D - 5) and amplitude image output (D - 6).

* *Automatic correction of residual orbital fringes:*estimates of the average gradient of the interferogram for distance and azimuth are used to generate a network to be substracted from the interferogram.

D.4.3.1 Scripts

Scripts are the files which need to be executed consecutively to successfully complete the DIAPASON processing chain. Part two of the descriptor file might need changing according to the set-up of the computer on which the software is running and depending on the radar images that are used. The variables used here are an example only.

* *EXTRACT_CONCATGB.sh*

Utilisation of the script:
Sh extract_concatGB.sh –d1 d:/scene1/dat_01.001 –f ../../../../FORM/paf_uk.form –c c:/diapason/T9/2277/22408/22408.c5b

```
#!/bin/sh
#=================================================#
# SCRIPT to read ESA RAW data
# Parameters extraction for PRISME software
# Automatic concatenation of ESA Raw data
#=================================================

#=================================================
# usage of the script
#=================================================

usage()
{
echo "
Usage : $1 Extraction of parameters and concatenation of ESA RAW DATA
   -d1 file_data1 -d2 file_data2 ... -dn file_datan
            (path and name of the raw data files)
          -f paf_file
            (name of the file which describe the PAF format
                    THIS NAME IS CASE SENSITIVE AND MUST BE GIVEN
                    WITHOUT USE OF ENVIRONMENT VARIABLE like
                    $DIAPASON_HOME)
          Optional parameters :
          -c output file
            (name of the concatened file)
          -pc
            (Raw file format on the CDROM : PC, default format : SUN)
" >&2
exit 1
}

#=================================================
# Function to extract parameters from a file
# $1 : absolute value of the bytes to extract/ 1
# $2 : number of bytes to extract
# $3 : input file
# $4 record a sauter avant lecture
#=================================================

extract_info
```

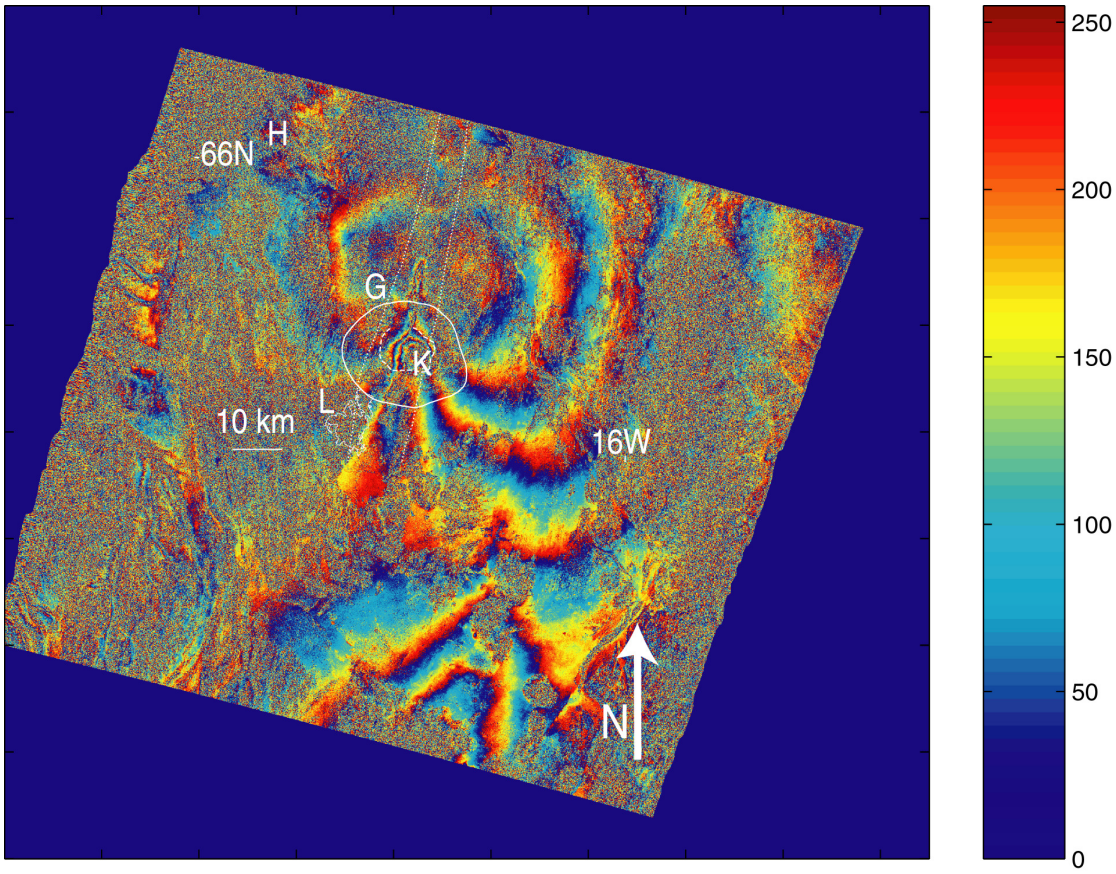

D - 4 Interferometric image produced with images 11677 and 22408. The bar on the right shows the way the colour changes through one cycle of a phase also called a fringe. One fringe represents 2.835 cm of deformation. Deformation is visible in the Krafla area and also further south towards Askja. In the Krafla area the broad fringes move down in the colour cycle counting towards the centre, which means a decrease in satellite to surface distance, suggesting inflation. In the Askja area, fringes move up in the colour cycle counting towards the centre, which means an increase in satellite to surface distance, suggesting deflation. These observations were confirmed with other geodetic data.

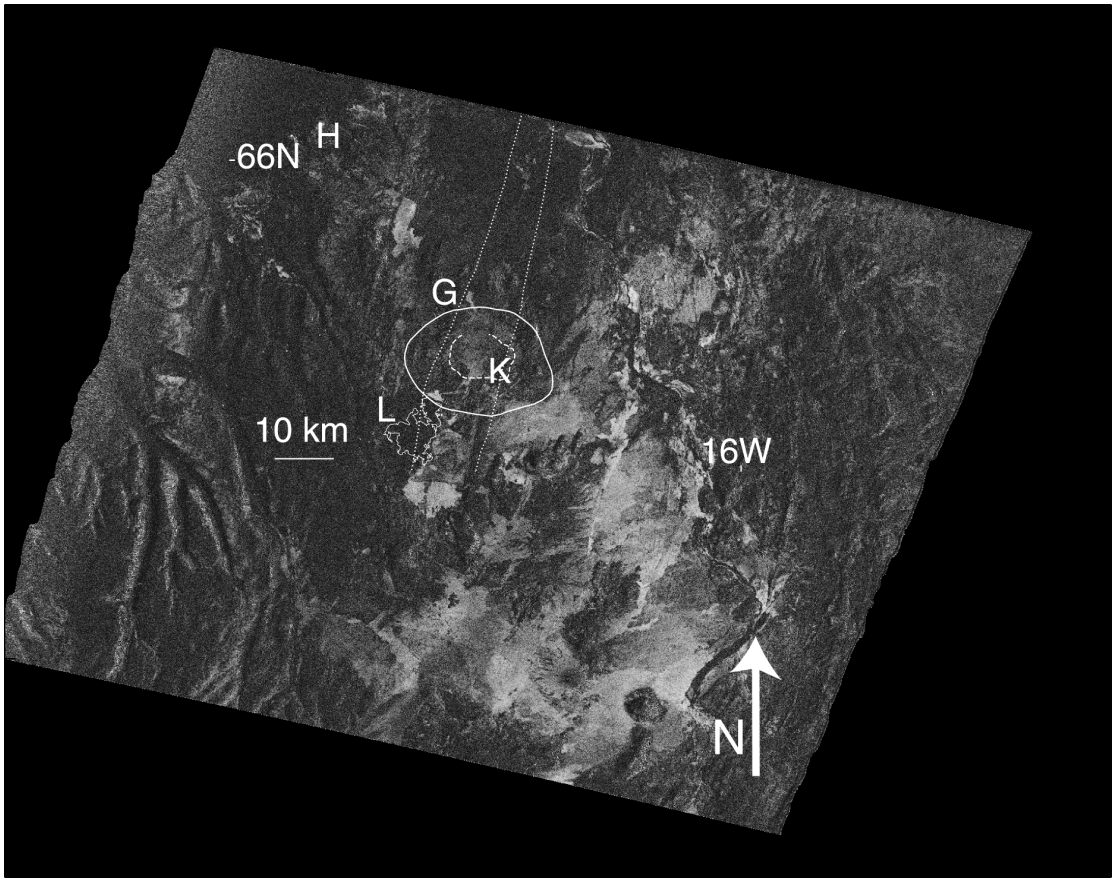

D - 5 Coherence image for the 11677_22408 interferogram. The coherence is a measure for the correlation of the phase information of two corresponding signals and varies from 0 to 1. It can be used as a quality measure because it influences the accuracy of phase differences and height measurements. Bright areas indicate regions of high coherence; dark areas represent areas with low coherence. Factors decreasing the coherence are: local steep slopes, vegetated or moving surfaces, specular reflectors like water (Lake Mývatn is black), long time differences between images and a large baseline. The coherence for the displayed interferogram is amazingly good.

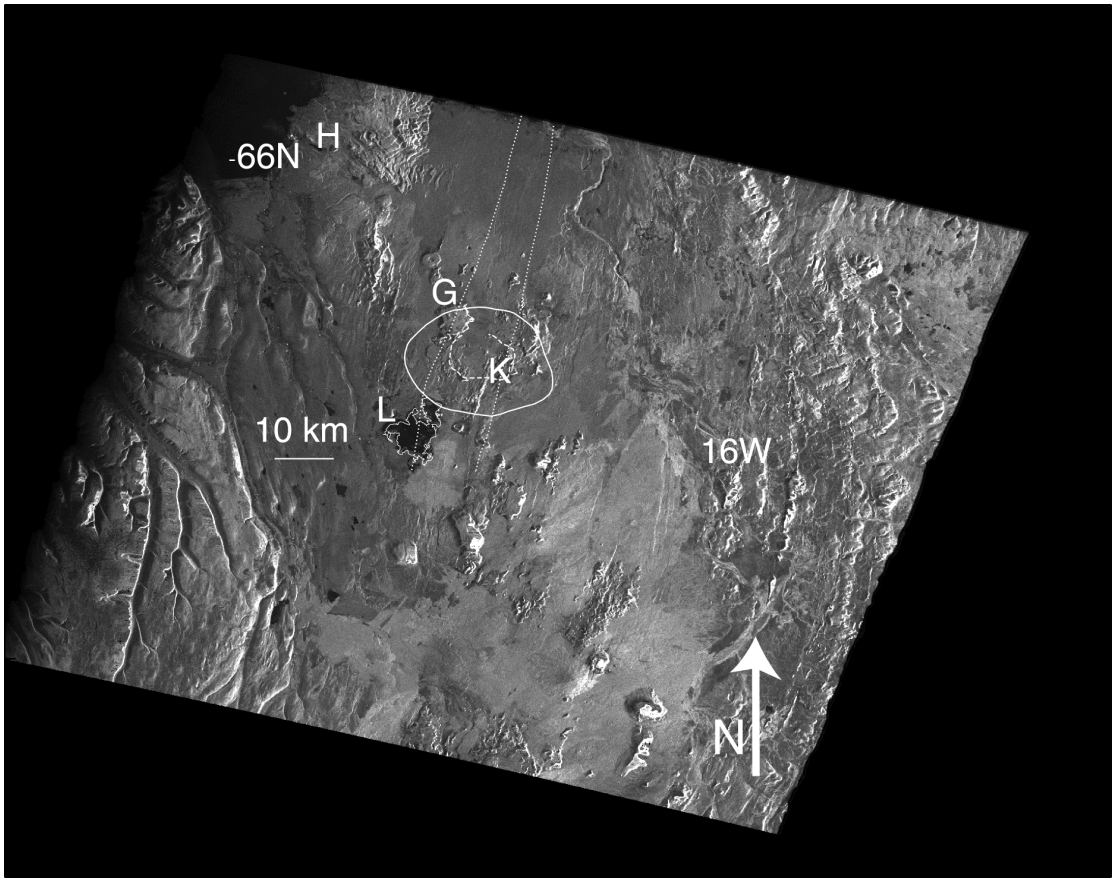

D - 6 Amplitude image of interferogram 11667_22408. An amplitude image shows mountains (K), rivers, lakes (L), cities (H) and other useful information. Also note the effect of foreshortening and shadowing at the sides of mountains and river beds. This effect is caused by the fact that slopes facing the radar are compressed into a shorter difference in range than they truly represent.

```
{
  # On a PC, you have to reverse the bytes from the CDROM produced on a Sun computer.
  if [ $CD = SUN ] ; then
          skip=`expr $1 + $2 - 2 + $4`
          i=`expr $2 - 1`
          val=0
          base=1
          while [ $i -ge 0 ] ; do
            val_byte=`dd if=$3 bs=1 skip=$skip count=1 2>/dev/null | od -t u1 2>&1 | head -1 | cut -c 9-11`
            val=`expr $val + $val_byte \* $base`
            base=`expr $base \* 256`
            i=`expr $i - 1`
            skip=`expr $skip - 1`
    done
          echo $val
   else
          skip=`expr $1 + $2 - 2 + $4`
#         echo "\n skip =",$skip
          i=`expr $2 - 1`
          val=0
          base=1
          while [ $i -ge 0 ] ; do
            val_byte=`dd if=$3 bs=1 skip=$skip count=1 2>/dev/null | od -t u1 2>&1 | head -1 | cut -c 9-11`
            val=`expr $val + $val_byte \* $base`
            base=`expr $base \* 256`
            i=`expr $i - 1`
            skip=`expr $skip - 1`
#                   echo $3
#                   echo $val_byte, $base, $skip, $val
    done
          echo $val
   fi
}

concat1()
{
concat >> extract_concat.log << EOF
$i
$fichier_out
$CONCAT_LOG
$PREFIX_PAF_FORM
$cpt     ! file number(=1)
$nb_lignes  ! output file lines number
$NB_PIXEL  ! output file columns number
$SWST         ! output file reference SWST
EOF
}

concat2()
{
concat >> extract_concat.log << EOF
$i
$fichier_out
$CONCAT_LOG
$PREFIX_PAF_FORM
$cpt     ! file number(=2 or =3)
$nb_lignes  ! output file lines number
$NB_PIXEL  ! output file columns number
$COMPTEUR           ! start counter of lines
$SWST         ! output file reference SWST
EOF
}
#=================================================


#=================================================
#               MAIN PROGRAM
#=================================================

PRG=`basename $0`
[ "$#" -eq 0 ] && usage $PRG

# Extraction of script parameters
CONCAT_LOG=extract_concat
nb_fic=0
files=""

# Binary file format ( SUN type or PC type)
CD=SUN

# Flag to run the concatenation (=0 -> YES)
CONC=0

while [ $# -gt 0 ] ; do
  case $1 in
    -\?) usage $PRG ;;
    -d*) files="$files $2"
            nb_fic=`expr $nb_fic + 1`
            shift ;;
          -f)  PAF_FORM=$2 ; shift ;;
          -c)  fichier_out=$2
             CONC=1
             shift ;;
          -pc) CD=PC
             shift ;;
    *)  echo "\n Error : unknown parameter '$1'"; usage $PRG ;;
  esac
  shift
done

if [ -z "$PAF_FORM" ]; then
          echo "\nError : argument -f mandatory !"
          usage $PRG
fi

if [ ! -f $PAF_FORM ]
```

```
 then
  echo
  echo
  echo "PAF file unfound : "
  echo $PAF_FORM
  exit
 fi

#=================================================
#Reading parameters from the PAF file (paf_XXX.form)
#mandatory keywords: "COUNTER","SWST","NPRI","DATA position",
#"number of columns" and "Number of raw data files".
#=================================================

POS_COMPTEUR=`grep -i "COUNTER" $PAF_FORM | awk '{print $1}'`
POS_SWST=`grep -i "SWST" $PAF_FORM | awk '{print $1}'`
POS_NPRI=`grep -i "NPRI" $PAF_FORM | awk '{print $1}'`
POS_DATA=`grep -i "DATA position" $PAF_FORM | awk '{print $1}'`
NB_PIXEL=`grep -i "number of columns"  $PAF_FORM | awk '{print $1}'`
NB_BANDE=`grep -i "Number of raw data files" $PAF_FORM | awk '{print $1}'`
NB_SKIP=`grep -i "number of records to skip" $PAF_FORM | awk '{print $1}'`
RECORD_SIZE=`grep -i "record size" $PAF_FORM | awk '{print $1}'`

SKIP_SIZE=`expr $RECORD_SIZE \* $NB_SKIP`

echo "*****************************************"
echo "EXTRACTION AND CONCATENATION OF ESA RAW DATA"
echo "*****************************************"
echo
echo "Initialisation..."

# Test if the files exist
i=0
set $files
first_data_file=$1

for file in $*
do
 if [ ! -f $file ]
 then
  echo "This file does not exist : $file "
  echo
  exit 1
 fi
done


#=================================================
#Extraction from the different records of the required parameters
#=================================================

echo

echo "Number of raw data files: $NB_BANDE "
echo

echo "Number of skipped bytes: $SKIP_SIZE"

echo "Line counter position in bytes: $POS_COMPTEUR"
COMPTEUR=`extract_info $POS_COMPTEUR 4 $first_data_file $SKIP_SIZE`
echo "Line counter value for the first line: $COMPTEUR"
echo

echo "SWST position in bytes: $POS_SWST"
SWST=`extract_info $POS_SWST 2 $first_data_file $SKIP_SIZE` echo "SWST value for the first line: $SWST "
echo

echo "NPRI position in bytes: $POS_NPRI"
NPRI=`extract_info $POS_NPRI 2 $first_data_file $SKIP_SIZE`
echo "NPRI value: $NPRI"
echo

echo "DATA position in bytes: $POS_DATA"
echo

echo "Number of raw columns: $NB_PIXEL"
echo

data_size=0
for i in $*
do
 size=`file_size $i`
 data_size=`expr $data_size + $size`
done

record_length=`expr 2 \* $NB_PIXEL + $POS_DATA - 1`

nb_lignes=`expr $data_size / $record_length`
echo "Total number of lines : $nb_lignes"
echo
if [ $NB_BANDE -gt $nb_fic ]
then
 echo "WARNING : Incorrect number of files, wrong number of lines !!!!"
 echo
fi

echo "End of parameters extraction"
echo

PREFIX_PAF_FORM=`echo $PAF_FORM | sed - -e 's/.form//'`
# PREFIX_PAF_FORM=`echo $PREFIX_PAF_FORM | sed - -e 's/.form//'`

echo $PREFIX_PAF_FORM
echo $PAF_FORM

if [ $CONC -eq 1 ]
then
```

```
  echo "Start of concatenation"
  echo
  echo "Please, verify the extract_concat.log and extract_concat.log2 files..."
  cpt=1
  for i in $*
  do
          echo "Concatenation file no : $cpt "
          if [ $cpt -eq 1 ]
          then
            concat1
          else
            concat2
          fi
          cpt=`expr $cpt + 1`
  done
  echo
  echo "End of Concatenation"
  echo
fi
```

Results of the execution are displayed in extract.log:

```
Orbit number                                        : 22408
Valeur du SWST de la premiere ligne                 : 10
Valeur du NPRI                                      : 2820
Total number of columns in file                     : 5822
NCOLD                                               : 5616
PREFIXC                                             : 200
SUFFIXC                                             : 0
Nombre de lignes total                              : 28001
Pays de generation des donnees RAW                  : UK
Lieu et date de creation des donnees RAW            : GENERATED AT UK-PAF 26-AUG-1999 20:35:35.720
Identification de la scene                          : ORBIT 22408 DATE 3-AUG-1999 12:25:55
Localisation de la scene                            : FRAME 2277 LAT: 65.58 LON: 343.18
Near range (m)                                      : 836842.33009650
First pixel (jj-MMM-aaaa hh:mm:ss.ttt)              :
First pixel seconds of day                          : 44755.82600000
Horloge satellite (aaaaMMjjhhmmssttt)               : 19990803122604159
Altitude du satellite (m)                           : 7159555
Position X,Y,Z du satellite (m)                     : 2.976301230000000E+06 -5.341493600000000E+05 6.484706940000000E+06
```

* *TAUXGB.sh*

#!/bin/sh

```
#=================================================
#
#  COMPUTATION OF COMPRESSION RATE IN AZIMUTH
#
#=================================================

#=================================================
#     ATTENTION : DO NOT TOUCH PART 1
#           ONLY MODIFY PART 2!
#=================================================

#=================================================
#         PART ONE
#=================================================

#=================================================
#         usage()
#=================================================
{
echo "
Usage: $1

 Edit taux_ers1.sh and fill in manually between the two EOF...

" >&2

exit 1
}

if [ $TARGET_ARCH != pc ] ; then ulimit -c 0 ;fi

PRG=`basename $0`
[ "$#" -gt 1 ] && usage $PRG

while [ $# -gt 0 ] ; do
  case $1 in
    -\?)            usage $PRG ;;
    -h)             usage $PRG ;;
    -help)          usage $PRG ;;
    *)              echo "unknown argument '$1'" ; exit 1 ;;
  esac
  shift
done

LANGUE=ENGLISH
export LANGUE

#=================================================
#             PART TWO
#  PARAMETERS to assign are between the two EOF...
```

```
#================================================

echo "Execution of taux..."
taux >> tauxGB.log << EOF
          ! sampling frequency
822333.   ! near range
5616      ! number of columns
          ! satellite altitude
          ! target latitude
          ! wavelength
          ! PRF
          ! orbit inclinaison
          ! view side (right=-1, left=1)
-1        ! direction (ascending=1, descending=-1)
EOF
```

Results of the execution are displayed in taux.log:

```
  Messages in English

  +-------------------------------------------+
  | Computation of SAR compression      |
  |       rate in azimuth        |
  |                     |
  +-------------------------------------------+

$Sampling frequency.....................[18962700]       18.9624680e6
$Near range.............................[830000]         836842.33009650
$Number of columns......................[5616]           5616
$Satellite altitude.....................[7159555]        7159555
$Target latitude........................[45]             65.8833
$Wavelength.............................[5.6560000E-02]  0.0566660
$Pulse Repetition Frequency.............[1679.9000]      1679.90239363
$Orbit inclination......................[98.70000000000]  98.5
$Viewing direction (right=-1, left=1)......[-1]          -1
$Orbit direction (Ascend.=1, Descend.=-1)..[-1]          -1

                    Near Range:         Far Range:          by pixel:

Range:              836842.33           881228.29           7.90489027
Compression rate :  1319.20             1387.15             0.01210116
Azimuth pixel size: 3.99                4.00
Ground pixel size:  25.11               17.69
Ground incidence:   18.35               26.55
```

* *DOPPLERGB.sh*

Normal procedure is to run dopplerGB.sh at two locatiations (different lines) and then take the average as the average for that image. PRISME should then be run using the average doppler of both master and slave radar images.

```
#!/bin/sh
#=========================================================================
#
#       COMPUTATION OF MEAN AZIMUTH DOPPLER
#
#=========================================================================

LANGUE=ENGLISH
export LANGUE

#=========================================================================
#
#          PARAMETERS TO INPUT ARE BETWEEN THE TWO "EOF"
#
#=========================================================================

echo "Execution of doppler..."
doppler >> dopplerGB.2.log << EOF
f=F:/22408/22408.c5b,nl=28001,nc=5616,type=c5b    ! input raw data file
extract, column1=1000,nc=1024,line1=1000,nl=1024  ! transformation
EOF
```

Results of the execution are displayed in doppler.log:

```
Messages in English

 +-------------------------------------------------------------+
 |
 |     DOPPLER: computation of mean azimuth doppler
 |
 +-------------------------------------------------------------+

(1) READING : ? lines, ? columns, type CR4 : CR4 Data to analyse
$ File/device.........[None,NL=16,NC=16,type=Cr4]
f=F:/22408/22408.c5b,nl=28001,nc=5616,type=c5b
 28001 lines, 5616 columns, type C5b ( 11232 bytes / line )
 on direct access file F:/22408/22408.c5b
```

```
$ Transformation sequence.................[NONE]
extract, column1=3000,nc=1024,line1=3000,nl=1024
 Transformation number 1 :
 Extraction in azimuth of 1024 lines of C5b from line 3000
 Transformation number 2 :
 Extraction in range of 1024 columns of C5b from column 3000
 Transformation number 3 :
 Conversion of C5b into Cr4 with a gain of 1.000000000000000
100 / 1024
200 / 1024
300 / 1024
400 / 1024
500 / 1024
600 / 1024
700 / 1024
800 / 1024
900 / 1024
1000 / 1024

 CLOSING image 1
 1024 accesses over F:/22408/22408.c5b
Accumulation over points. 1047552 points.
Symbol DOPPLER_AZIMUT = "9.92748961E-02"
Symbol COHERENCE_DOPPLER = "0.308638722"
```

* ***PRISMEGB.sh***

Prisme is run for both images using the average doppler of the two images.

#!/bin/sh

```
#=================================================#
#     RADAR PROCESSING PROGRAM "PRISME"
##================================================

#================================================
#PARAMETERS TO INPUT ARE BETWEEN THE TWO "EOF"
##================================================

LANGUE=ENGLISH
export LANGUE

echo "Execution of prisme..."
echo "Start"
date
date >> prismeGB.log
prisme.exe >> prismeGB.log << EOF
858.5               !Range compression rate
768                 !Chirp length
0.05656   !Wavelength
18.96e6   !Sampling frequency
0.098274  !Mean Doppler in azimuth
0.0                 !Mean Doppler in range
1323.79   !Compression rate at first raw column
0.01311757          !Increase of compression rate / pixel
2                   !Presumming rate
1                   !First processed line
1                   !First processed column
28001               !Number of lines processed
5616                !Number of columns processed
f=C:/DIAPASON/DATA/22408/22408.c5b,nl=28001,nc=5616,type=c5b ! input file (raw data)
none                                                          ! transformation
2                                                             ! number of output files
conv,gain=10.,type=r8; aver,range=2,azim=5! first output (multilook 5 2)
file=22408_mv52, type=byt
conv,gain=100.,type=ci2                                  ! second output (slc)
file=22408.ci2
EOF
echo "END"
date
date >> prismeGB.log
```

Results are displayed in PrismeGB.log:

```
Tue Jul 1 16:32:31 2003

Messages in English
   +-------------------------------------------------------------+
   |                                        |
   |          PRISME: Radar Processing           |
   |                                        |
   +-------------------------------------------------------------+
Range compression rate:.....................[0]          858.5
Chirp length:...............................[0]          768
Wavelength:.................................[0]          0.05656
Sampling Frequency:.....................[1000000]          18.96e6
Average azimuth Doppler:....................[0]          0.098274
Average range Doppler:......................[0]          0.0
Azimuth compression rate at raw data point 1:.[0]          1323.79
Azimuth compression rate slope:.............[0]          0.01311757
Presumming ratio:...........................[1]          2
First processed line:.......................[0]          1
First processed point (column):.............[0]          1
Number of lines processed:..................[10]          28001
Number of points processed:.................[10]          5616
```

```
(1) READING : ? lines, ? columns, type CR4 : Raw data
$ File/device.........[None,NL=16,NC=16,type=Cr4]
f=C:/DIAPASON/DATA/22408/22408.c5b,nl=28001,nc=5616,type=c5b
 28001 lines, 5616 columns, type C5b ( 11232 bytes / line )
 on direct access file C:/DIAPASON/DATA/22408/22408.c5b
$ Transformation sequence..................[NONE]
none
 Transformation number 1 :
 Conversion of C5b into Cr4 with a gain of 1.000000000000000

(2) WRITING : 14000 lines, 5616 columns, type CR4 : Processed radar data
$ Number of files/devices.....................[1]
2
 1 st file/device:
$ Transformation sequence..................[NONE]
conv,gain=10.,type=r8; aver,range=2,azim=5
 Transformation number 2 :
 Conversion of Cr4 into r8 with a gain of 10.00000000000000
 Transformation number 3 :
 Conversion of r8 into r8 with a gain of 1.000000000000000
... ignored because without effect
 Transformation number 3 :
 Averaging in range, grouping of r8 by 2 columns
 Transformation number 4 :
 Averaging in azimuth, grouping of r8 by 5 lines
$ File/device......[None,NL=2800,NC=2808,type=r8]
file=22408_mv52, type=byt
 2800 lines, 2808 columns, type byt ( 2808 bytes / line )
 on direct access file 22408_mv52
 Transformation number 5 :
 Conversion of r8 into byt with a gain of 1.000000000000000
 2 nd file/device:
$ Transformation sequence..................[NONE]
conv,gain=100.,type=ci2
 Transformation number 6 :
 Conversion of Cr4 into Ci2 with a gain of 100.0000000000000
$ File/device....[None,NL=14000,NC=5616,type=Ci2]
file=22408.ci2
 14000 lines, 5616 columns, type Ci2 ( 22464 bytes / line )
 on direct access file 22408.ci2
NUMBER OF PRESUMMING PROCESSING(S) = 225
Normalized Doppler = 9.82740000E-02
Presumming processing 1 / 225 terminated
Presumming processing 2 / 225 terminated
Presumming processing 3 / 225 terminated
Presumming processing 4 / 225 terminated
Presumming processing 5 / 225 terminated
Presumming processing 6 / 225 terminated
Presumming processing 7 / 225 terminated
Presumming processing 8 / 225 terminated
Presumming processing 9 / 225 terminated
Presumming processing 10 / 225 terminated
Presumming processing 11 / 225 terminated
Presumming processing 12 / 225 terminated
Presumming processing 13 / 225 terminated
Presumming processing 14 / 225 terminated
Presumming processing 15 / 225 terminated
Presumming processing 16 / 225 terminated
Azimuth FFT
Writing of processed data
Presumming processing 17 / 225 terminated
Presumming processing 18 / 225 terminated
Presumming processing 19 / 225 terminated
Presumming processing 20 / 225 terminated
Presumming processing 21 / 225 terminated
Presumming processing 22 / 225 terminated
Presumming processing 23 / 225 terminated
Presumming processing 24 / 225 terminated
.
.
.
.etc.
Presumming processing 221 / 225 terminated
Presumming processing 222 / 225 terminated
 iostat = 80
 File/device C:/DIAPASON/DATA/22408/22408.c5b unavailable after 28000 accesses
 Line 28001 of image 1 could not be read
Presumming processing 223 / 225 terminated

 CLOSING image 1

 CLOSING image 2
 2696 accesses over 22408_mv52
 13480 accesses over 22408.ci2
Tue Jul 1 16:43:38 2003
```

* *DIAPASONGB.sh & Descriptor files*

Rough_geosar.dat:

```
DESCRIPTOR FILE OF THE SAR IMAGE GEOMETRY
-----------------------------------------------------
(each line must be an iso-doppler)

LANGUE                          ENGLISH

AREA                            KRAFLA

SAR DESCRIPTOR FILE             C:/DIAPASON/DAT/sar_ers2_2820.dat

ORBITAL FILE                    C:/DIAPASON/ORB/22408.orb

NUMBER OF ROWS                  14000

NUMBER OF COLUMNS               5616

TIME OF THE FIRST LINE          44755.82600

NEAR RANGE                      836842.330

AZIMUTH UNDERSAMPLING           2

RANGE UNDERSAMPLING             1

REDUCED ISO-DOPPLER             0.0
```

Example of part of 22408.orb:

```
-----------------------------------------------------
18111 42900000 22408
-6651.995344  2640.816765   335.387020
 0.930982978  1.385009838  7.369235253
18111 42960000 22408
-6582.899359  2718.449272   776.595838
 1.371213959  1.201255237  7.332923602
18111 43020000 22408
-6487.587955  2784.797025  1214.763334
 1.804531773  1.008984258  7.267889911
18111 43080000 22408
-6366.529313  2839.373454  1648.173119
 2.229162875  0.809018602  7.174384720
```

DEM descriptor file, dted_all_3.dat:

```
-----------------------------------------------------
FICHIER DESCRIPTIF D'UN MNT
DESCRIPTOR FILE OF THE DEM
-----------------------------------------------------

LANGUE                          FRANCAIS

FICHIER BINAIRE                 C:/DIAPASON/DEM/dted_all_3.i2
(BINARY FILE)

NOMBRE DE LIGNES                6001
(NUMBER OF ROWS)

NOMBRE DE COLONNES              7202
(NUMBER OF COLUMNS)

(si fichier mnt effectif/if DEM file exists :)
CODAGE (I2, I4 ou R4)           I2

(si aucun fichier/if not :)
ALTITUDE CONSTANTE
(CONSTANT ELEVATION)

-----------------------------------------------------

EXTRACTION                      OUI
(OUI ou NON)
(si oui :)
PREMIERE LIGNE EXTRAITE         2100
(FIRST EXTRACTED ROW)

PREMIERE COLONNE EXTRAITE       4100
(FIRST EXTRACTED COLUMN)

LIGNES EXTRAITES                1600
(EXTRACTED ROWS)

COLONNES EXTRAITES              1900
```

```
(EXTRACTED COLUMN)

PAS D'EXTRACTION DES LIGNES   1
(NO EXTRACTED ROW)

PAS D'EXTRACTION DES COLONNES 1
(NO EXTRACTED COLUMNS)

-------------------------------------------------
OFFSET D'ALTITUDE             0
(ELEVATION OFFSET)

FACTEUR D'ECHELLE ALTITUDE    1
(ELEVATION SCALE FACTOR)

ELLIPSOIDE ASSOCIE            WGS84
(ASSOCIATED ELLIPSOID : NAD27, NTF, GRS80, ED50, WGS72 ou WGS84)

REFERENCE DES ALTITUDES       GEOIDE
(ELEVATION REFERENCE : GEOIDE ou ELLIPSOIDE)

NATURE DES COORDONNEES        GEOGRAPHIQUES
(SYSTEM OF COORDINATES : GEOGRAPHIQUES ou CARTOGRAPHIQUES)

-------------------------------------------------
       COORDONNEES GEOGRAPHIQUES
-------------------------------------------------

(Si les coordonnees sont geographiques :)
(If it is a geographic system :)

LONGITUDE DU POINT 1          335.00000 (en degres)
(LONGITUDE POINT 1 in degrees)

PAS LONGITUDE                 0.00166666666666(en degres)
(LONGITUDE GRID in degrees)

LATITUDE DU POINT 1           68.000000 (en degres)
(LATITUDE POINT 1 in degrees)

PAS LATITUDE                  -0.00083333333333(en degres)
(LATITUDE GRID in degrees)

-------------------------------------------------
             COORDONNEES CARTOGRAPHIQUES
-------------------------------------------------

(Si les coordonnees sont cartographiques :)
(If it is a cartographic system :)

COORDONNEE X POINT 0          (en metres)
(COORDINATE IN X FOR POINT 0 in meters)

PAS X                         (en metres)
(GRID IN X in meters)

COORDONNEE Y POINT 0          (en metres)
(COORDINATE IN Y FOR POINT 0 in meters)

PAS Y                         (en metres)
(GRID IN Y in meters)


REPRESENTATION UTM    (UTM ou LAMBERT)

(si la representation est Lambert :)
(if it is a Lambert representation :)

LATITUDE ORIGINE EN DEGRES              0
(ORIGIN OF THE LATITUDE IN DEGREES)

LONGITUDE ORIGINE EN DEGRES             0
(ORIGIN OF THE LONGITUDE IN DEGREES)

COORDONNEES EN X DE L'ORIGINE           0
(COORDINATE IN X OF THE ORIGIN)

COORDONNEES EN Y DE L'ORIGINE           0
(COORDINATE IN Y OF THE ORIGIN)

FACTEUR D'ECHELLE LAMBERT               1
(SCALE FACTOR FOR THE LAMBERT REPRESENTATION)

(si la representation est utm :)
(if it is an utm representation :)

NUMERO DU FUSEAU
(NUMBER OF THE TIME ZONE [1:60])

HEMISPHERE
(NORD ou SUD)
-------------------------------------------------
```

SAR_ERS1_2820.dat

```
-------------------------------------------------
FICHIER DE PARAMETRES POUR ERS-1, DANS LE MODE NPRI = 2820
-------------------------------------------------

LANGUE                        FRANCAIS

FREQUENCE D'ECHANTILLONNAGE   18.9627E6
(SAMPLING FREQUENCY)
```

```
PRF                           1679.90239363
(PULSE REPETITION FREQUENCY)

FREQUENCE PORTEUSE            5.300E9
(CARRIER FREQUENCY)

VISEE                         DROITE
(SIDE)
```

* DIAPASONGB.sh

```
#!/bin/sh

#=====================================================
# INTERFEROMETRIC PROCESSING OF A COUPLE OF CI2
#            IMAGES (WITH DEM)"DIAPASON"
#=====================================================

#=====================================================
#     ATTENTION : DO NOT TOUCH PART ONE
#           ONLY MODIFY PART TWO !
#=====================================================

#=====================================================
#              PART ONE
#=====================================================


set -a   # exports the source variables

#=====================================================
#              PART TWO
# PARAMETERS TO ASSIGN ARE HERE BELOW...
#   LINES CONTAINING ## ARE MANDATORY !
#=====================================================

LANGUE=ENGLISH

#=====================================================
#      START AND END OF THE PROCESSING
# Careful, if you change this, also comment out the
#     line at the bottom executing clean_GB.sh
#=====================================================

START=CLEAN_DEM
END=CLEAN_DEM

# Definition of possible value for start parameter REPRISE
# and for end parameter FIN :

# SIMU_SAR   ----> simulation
# CORREL_SIM  ----> correlation between Master image and simulation
# CORRECTION  ----> correction of Near Range and acquisition start time
# CORREL_IMA  ----> correlation between Master image and Slave image
# GRID     ----> computation of deformation grids
# CHANGEO   ----> change of Slave image geometry
# INTERF_SAR  ----> computation of SAR geometry interferogram
# INTERF_DEM  ----> computation of DEM geometry interferogram
# GRADIENT_SAR ----> measurement of SAR geometry interferogram gradient
# CLEAN_SAR  ----> linear cleaning of SAR geometry interferogram
# GRADIENT_DEM ----> measurement of DEM geometry interferogram gradient
# CLEAN_DEM  ----> linear cleaning of DEM geometry interferogram

# START is the first process
# END  is the last process



#=====================================================
#  ASSIGNMENT OF DISK FOR OUTPUT PRODUCTS
#=====================================================

WDIR=.       ## working directory

DK=.        # directory for simulation file


#=====================================================
#    DEFINITION OF THE INPUT COMPLEX IMAGES
#=====================================================

CI2_MASTER=../11677/11677.ci2 ## path and name for the master image SLC
CI2_SLAVE=../22408/22408.ci2 ## path and name for the slave image SLC
DOPPLER_AZIMUT=0.154443   ## azimuth doppler
PRESUMMING_RATE=2      ## presumming rate

NL_CI2_MASTER=14000 ## number of lines of master complex image
NC_CI2_MASTER=5616 ## number of columns of master complex image
NL_CI2_SLAVE=14000 ## number of lines of slave complex image
NC_CI2_SLAVE=5616 ## number of columns of slave complex image
NL_DEM=1600     ## number of lines of DEM
NC_DEM=1900     ## number of lines of DEM


#=====================================================
#    MULTILOOK IMAGES CHARACTERISTICS
#=====================================================

ML_MASTER=../11677/11677_mv52.oct  #name of multilook master image
```

```
ML_SLAVE=../22408/22408_mv52.oct  ## name of multilook slave image
MLazi=5     ## number of looks in azimuth
MLran=2   ## number of looks in range

#=================================================
#   DEFINITION OF DESCRIPTOR FILES
#=================================================

DAT=. ## descriptors directory

ROUGH_DESCRIPTOR_SAR_M=
$DAT/geosar_11677_ci2_rough.dat ##
ROUGH_DESCRIPTOR_SAR_S=
$DAT/geosar_22408_ci2_rough.dat ##
PRECISE_DESCRIPTOR_SAR_M=
$DAT/geosar_11677_ci2_precis.dat ##
DEM_DESCRIPTOR=/data/DEMS/dtedT9.dat ##
SAR_GRAD_DESCRIPTOR=$DAT/gradient_sar.dat ##
DEM_GRAD_DESCRIPTOR=$DAT/gradient_mnt.dat ##

#=================================================
#    DEFINITION OF OUTPUT GENERIC NAMES
#=================================================

# generic names for intermediate and output files :

MASTER=11677                  ##
SLAVE=22408                   ##


#=================================================
#  SIMULATION - MASTER CORRELATION CHARACTERISTICS
#=================================================

DIR_SIM=$DAT          # .dat files directory
DISK_SIM=$DK          # grid disk
NOM_SIM=${MASTER}_simu     # grid generic name

INTER_L_SIM=50         # interval in azimuth of the grid pixels
INTER_C_SIM=50         # interval in range of the grid pixels
THRESH_SIM=0.3         # correlation rate threshold used by "cormoy" program

# rough locking with FFT choice :

ROUGH_LOCKING=YES  # YES or NO         ##

# if ROUGH_LOCKING is NO :

DECazi=0.0         # known azimut shift
DECran=0.0         # known range shift

#=================================================
#    CARACTERISTICS OF CORRELATION BETWEEN
#           MASTER AND SLAVE
#=================================================

# Estimate rough shifts by FFT?
ROUGH_LOCKING_ME=YES       # YES or NO, default = YES

# if the choice is NO:
# offset between master and slave
DECranME=0.0          # shift in range (pixels)
DECaziME=0.0          # shift in azimut (pixels)

#=================================================
#       DEFORMATION GRIDS CHARACTERISTICS
#=================================================

DIR_IMA=$DAT        # .dat files directory
DISK_IMA=$DK_SIM      # grids disk
NOM_IMA=${MASTER}_${SLAVE} # generic grid name

INTER_L_IMA=50       # grid interval in azimuth
INTER_C_IMA=50       # grid interval in range
THRESH_IMA=0.4       # threshold of correlation rate for grillegeo


set +a                    # terminates the exports

# erase files before starting
#. clean_GB.sh

# run with interf_sar
. automatic_GB.sh

# skip interf_sar, proceed to interf_mnt
#. automatic_mntGB.sh
```

Results are displayed in DIAPASONGB.log:

```
   Messages in English

+-------------------------------------------------+
| SIMU_SAR:  Simulation of radar amplitude image |
+-------------------------------------------------+

$Descriptor of Digital Elevation Model.....[]          ./data/DEMS/dtedT9.dat
Geoid file is                                         ./local/diapason/DAT/grille_geoide.dat
Ellipsoid descriptor file is                          ./usr/local/diapason/DAT/ellipsoides.dat
Geographical transformation file is                   ./usr/local/diapason/DAT/transf_sys_geo.dat
$Descriptor of radar image geometry.............[]   ./geosar_11677_ci2_rough.dat

          Average incidence: 23.82512829436533
          DEM and SAR image have same orientation.
```

```
 (1) WRITING : 14000 lines, 5616 columns, type R4 : R4 Simulated radar image

$$ Number of files/devices.............[1]              1
$$ Transformation sequence.............[NONE]
 aver, quad, azi=MLazi, ran=MLran; conv, type=byt
 Transformation number 1 :
 Conversion of r4 into r8 with a gain of 1.000000000000000
 Transformation number 2 :
 Quadratic averaging in range, grouping of r8 by 2 columns
 Transformation number 3 :
 Quadratic averaging in azimuth, grouping of r8 by 5 lines
 Transformation number 4 :
 Conversion of r8 into byt with a gain of 1.000000000000000
$$ File/device.....[None,NL=2800,NC=2808,type=byt]
 file=./sim_11677_ml52.byt
 2800 lines, 2808 columns, type byt ( 2808 bytes / line )
 on direct access file ./sim_11677_ml52.byt

 (2) WRITING : 14000 lines, 5616 columns, type R4 : R4 Incidence image in degrees
$$ Number of files/devices.....................[1]
 0
 1 / 14000
 1001 / 14000
 2001 / 14000
 3001 / 14000
.
. etc.
 12001 / 14000
 13001 / 14000

 CLOSING image 1
 2800 accesses over ./sim_11677_ml52.byt

 CLOSING image 2

 Messages in English

+-------------------------------------------------+
|  CORREL: correlation of two images       |
+-------------------------------------------------+


$Grid Descriptor name..........................[]
 ./grid_cor_11677_simu.dat
$Disk..........................................[]
 ./

 (1) READING : ? lines, ? columns, type R4 : R4 Master Image
$$ File/device..........[None,NL=16,NC=16,type=r4]
 nl=NL_ML_MASTER, nc=NC_ML_MASTER, type=byt, f=../11677/11677_mv52.oct
 2800 lines, 2808 columns, type byt ( 2808 bytes / line )
 on direct access file ../11677/11677_mv52.oct
$$ Transformation sequence.................[NONE]
 none
 Transformation number 1 :
 Conversion of byt into r4 with a gain of 1.000000000000000

 (2) READING : ? lines, ? columns, type R4 : R4 Slave image
$$ File/device..........[None,NL=16,NC=16,type=r4]
 nl=NL_ML_SIMULATION, nc=NC_ML_SIMULATION, type=byt, f=./sim_11677_ml52.byt
 2800 lines, 2808 columns, type byt ( 2808 bytes / line )
 on direct access file ./sim_11677_ml52.byt
$$ Transformation sequence.................[NONE]
 none
 Transformation number 2 :
 Conversion of byt into r4 with a gain of 1.000000000000000
$Automatic calculation of rough shifts.......[NON]
 yes
 Multilook characteristics
 Multilook 5 5
 Master image multilook generation
 Slave Image multilook generation
 CORRELATION by FFT
 Looking for maximum
 Shifts computation
 For information, we find 5 and 10

 Shift Master-Slave = (S coord. - M coord.)

$...in columns (range).........................[10]
$...in lines (azimuth).........................[5]

 Interval between grid points

$...in columns (range).......................[0] 50
$...in lines (azimuth).......................[0] 50
$Correlation rate threshold.................[0] 0

$Multilook in azimuth........................[1] 5
$Multilook in range..........................[1] 2

 First grid point at line 46 , column 20

 Grid: 55 lines, 56 columns

 1        / 55
 2        / 55
 3        / 55
 4        / 55
 5        / 55
 .
 .
 . etc.
 53       / 55
 54       / 55
 55       / 55
```

```
 Messages in English


+-------------------------------------------------+
|    CORMOY: Determination of radar image         |
|       geometry based on simulated radar image   |
+-------------------------------------------------+


$Grid descriptor file name.....................[]
 ./grid_cor_11677_simu.dat
$Disk name.....................................[]
 ./
$Simulated image descriptor file..............[]
 ./geosar_11677_ci2_rough.dat
$Name of the descriptor file to be created.....[]
 ./geosar_11677_ci2_precis.dat
$Correlation rate threshold....................[0]
 0.3
 Number of kept points: 1168

 Estimation of averages in azimuth and range

 Messages in English

+-------------------------------------------------+
|   CORREL: correlation of two images             |
+-------------------------------------------------+


$Grid Descriptor name..........................[]
 ./grid_cor_11677_22408.dat
$Disk..........................................[]
 ./

 (1) READING : ? lines, ? columns, type R4 : R4 Master Image
$$ File/device..........[None,NL=16,NC=16,type=r4]
 nl=NL_ML_MASTER, nc=NC_ML_MASTER, type=byt, f=../11677/11677_mv52.oct
 2800 lines, 2808 columns, type byt ( 2808 bytes / line )
 on direct access file ../11677/11677_mv52.oct
$$ Transformation sequence.................[NONE]
 none
 Transformation number 1 :
 Conversion of byt into r4 with a gain of 1.000000000000000

 (2) READING : ? lines, ? columns, type R4 : R4 Slave image
$$ File/device..........[None,NL=16,NC=16,type=r4]
 nl=NL_ML_SLAVE, nc=NC_ML_SLAVE, type=byt, f=../22408/22408_mv52.oct
 2800 lines, 2808 columns, type byt ( 2808 bytes / line )
 on direct access file ../22408/22408_mv52.oct
$$ Transformation sequence.................[NONE]
 none
 Transformation number 2 :
 Conversion of byt into r4 with a gain of 1.000000000000000
$Automatic calculation of rough shifts.......[NON]
 yes
 Multilook characteristics
 Multilook 5 5
 Master image multilook generation
 Slave Image multilook generation
 CORRELATION by FFT
 Looking for maximum
 Shifts computation
 For information, we find -90 and -10

 Shift Master-Slave = (S coord. - M coord.)

$...in columns (range).....................[-10]
$...in lines (azimuth).....................[-90]

 Interval between grid points

$...in columns (range).....................[0] 50
$...in lines (azimuth).....................[0] 50
$Correlation rate threshold.................[0] 0
$Multilook in azimuth.......................[1] 5
$Multilook in range.........................[1] 2

 First grid point at line 131 , column 40

 Grid: 54 lines, 56 columns

 1        / 54
 2        / 54
 3        / 54
 .
 .
 .etc.
 51       / 54
 52       / 54
 53       / 54
 54       / 54


 Messages in English


+-------------------------------------------------+
|    GRILLEGEO: Deformation grids computation      |
|     to be applied for image change of geometry   |
+-------------------------------------------------+


$Correlation Grids descriptor file.............[]
 ./grid_cor_11677_22408.dat
```

```
$Disk.....................................[]
 ./
$Correlation rate threshold.....................[0]
 0.4
 Number of valid points: 1663
 Grid: 54 lines of 56 columns
 First column: 79.5000000 , Interval between columns: 100.000000
 First line: 653.000000 , Interval between lines: 250.000000
 Average shift in range: -18.8084240
 Average shift in azimuth: -445.363892
 Number of points rectified by interpolation: 1361
 Number of points replaced by averaging: 0
$DEM descriptor file.............................[]
 /data/DEMS/dtedT9.dat
$Master image descriptor.........................[]
 ./geosar_11677_ci2_precis.dat
$Slave image descriptor..........................[]
 ./geosar_22408_ci2_rough.dat
   Geoid file is /usr/local/diapason/DAT/grille_geoide.dat
   Ellipsoid descriptor file is /usr/local/diapason/DAT/ellipsoides.dat
   Geographical transformation file is /usr/local/diapason/DAT/transf_sys_geo.dat
 100 / 1600
 200 / 1600
 300 / 1600
 400 / 1600
 500 / 1600
 600 / 1600
 700 / 1600
 800 / 1600
 900 / 1600
 1000 / 1600
 1100 / 1600
 1200 / 1600
 1300 / 1600
 1400 / 1600
 1500 / 1600
 1600 / 1600
 Correction of the grid in azimuth
 Correction of the grid in range

 Messages in English

+-------------------------------------------------+
|    CHANGEO: Change of radar image geometry      |
+-------------------------------------------------+


$Descriptor file name............................[]
 ./grid_11677_22408.dat

 (3) READING : ? lines, ? columns, type CR4 : Image to be resampled
$$ File/device.........[None,NL=16,NC=16,type=Cr4]
 nl=NL_CI2_SLAVE, nc=NC_CI2_SLAVE, type=ci2, f=../22408/22408.ci2
 14000 lines, 5616 columns, type Ci2 ( 22464 bytes / line )
 on direct access file ../22408/22408.ci2
$$ Transformation sequence..................[NONE]
 none
 Transformation number 1 :
 Conversion of Ci2 into Cr4 with a gain of 1.000000000000000
$Central frequency of range spectrum............[0]
 0.0
$Central frequency of azimuth spectrum.........[0]
 .308886
$Number of lines to be produced.................[1]
 14000
$Number of columns to be produced..............[1]
 5616

 (4) WRITING : 14000 lines, 5616 columns, type CR4 : Resampled Image
$$ Number of files/devices.....................[1]
 2
 1 st file/device:
$$ Transformation sequence..................[NONE]
 conversion, type=ci2
 Transformation number 2 :
 Conversion of Cr4 into Ci2 with a gain of 1.000000000000000
$$ File/device....[None,NL=14000,NC=5616,type=Ci2]
 file=./geo_22408_11677.ci2, type=ci2
 14000 lines, 5616 columns, type Ci2 ( 22464 bytes / line )
 on direct access file ./geo_22408_11677.ci2
 2 nd file/device:
$$ Transformation sequence..................[NONE]
 aver, quad, azi=MLazi, ran=MLran; conv, gain=GAIN_CI2_ML, type=byt
 Transformation number 3 :
 Conversion of Cr4 into r8 with a gain of 1.000000000000000
 Transformation number 4 :
 Quadratic averaging in range, grouping of r8 by 2 columns
 Transformation number 5 :
 Quadratic averaging in azimuth, grouping of r8 by 5 lines
 Transformation number 6 :
 Conversion of r8 into byt with a gain of 0.10000000014901161
$$ File/device.....[None,NL=2800,NC=2808,type=byt]
 file=./geo_22408_11677_ml52.byt
 2800 lines, 2808 columns, type byt ( 2808 bytes / line )
 on direct access file ./geo_22408_11677_ml52.byt
 100 / 14000
 200 / 14000
 300 / 14000
 400 / 14000
 .
 .
 . etc.
 13800 / 14000
 13900 / 14000
 14000 / 14000

 CLOSING image 3
```

```
 13564 accesses over ../22408/22408.ci2

 CLOSING image 4
 14000 accesses over ./geo_22408_11677.ci2
 2800 accesses over ./geo_22408_11677_ml52.byt

 Messages in English

+-------------------------------------------------+
|   INTERF_MNT: Generation of interferograms      |
|       in the DEM geometry                       |
+-------------------------------------------------+


$DEM descriptor file.............................[]
 /data/DEMS/dtedT9.dat
   Geoid file is /usr/local/diapason/DAT/grille_geoide.dat
   Ellipsoid descriptor file is /usr/local/diapason/DAT/ellipsoides.dat
   Geographical transformation file is /usr/local/diapason/DAT/transf_sys_geo.dat
$Descriptor of master image geometry.............[]
 ./geosar_11677_ci2_precis.dat
$Descriptor of slave image geometry..............[]
 ./geosar_22408_ci2_rough.dat
$Filter coefficients filename....................[]
 /usr/local/diapason/DAT/filtre.dat
 DEM Orientation:
 ------------------
 DEM line - DEM column;
 radar line - radar column
   1   1900  !  -4634.06  127.28
  1600    1  !  18536.64 4904.70
  1600   1900  !  13171.69 -1732.26
   1    1  !   403.14 7292.56
 DEM and image have same orientation.

 (1) READING : 14000 lines, 5616 columns, type CR4 : Master image
$$ File/device....[None,NL=14000,NC=5616,type=Cr4]
 nl=NL_CI2_MASTER, nc=NC_CI2_MASTER, type=ci2, f=../11677/11677.ci2
 14000 lines, 5616 columns, type Ci2 ( 22464 bytes / line )
 on direct access file ../11677/11677.ci2
$$ Transformation sequence...................[NONE]
 none
 Transformation number 1 :
 Conversion of Ci2 into Cr4 with a gain of 1.000000000000000

 (2) READING : 14000 lines, 5616 columns, type CR4 : Slave image
$$ File/device....[None,NL=14000,NC=5616,type=Cr4]
 nl=NL_CI2_MASTER, nc=NC_CI2_MASTER, type=ci2, f=./geo_22408_11677.ci2
 14000 lines, 5616 columns, type Ci2 ( 22464 bytes / line )
 on direct access file ./geo_22408_11677.ci2
$$ Transformation sequence...................[NONE]
 none
 Transformation number 2 :
 Conversion of Ci2 into Cr4 with a gain of 1.000000000000000

 (5) WRITING : 1600 lines, 1900 columns, type R4 : R4 Amplitude
$$ Number of files/devices.....................[1]
 1
$$ Transformation sequence...................[NONE]
 conv, gain=GAIN_CI2_ML, typ=byt
 Transformation number 3 :
 Conversion of r4 into byt with a gain of 0.1000000014901161
$$ File/device.....[None,NL=1600,NC=1900,type=byt]
 f=./amp_11677_22408_ort.byt
 1600 lines, 1900 columns, type byt ( 1900 bytes / line )
 on direct access file ./amp_11677_22408_ort.byt

 (6) WRITING : 1600 lines, 1900 columns, type PHA : PHA Interferogram
$$ Number of files/devices.....................[1]
 1
$$ Transformation sequence...................[NONE]
 none
$$ File/device.....[None,NL=1600,NC=1900,type=pha]
 f=./pha_11677_22408_ort.byt
 1600 lines, 1900 columns, type pha ( 1900 bytes / line )
 on direct access file ./pha_11677_22408_ort.byt

 (7) WRITING : 1600 lines, 1900 columns, type BYT : BYT Coherence
$$ Number of files/devices.....................[1]
 1
$$ Transformation sequence...................[NONE]
 none
$$ File/device.....[None,NL=1600,NC=1900,type=byt]
 f=./coh_11677_22408_ort.byt
 1600 lines, 1900 columns, type byt ( 1900 bytes / line )
 on direct access file ./coh_11677_22408_ort.byt

 (8) WRITING : 1600 lines, 1900 columns, type I4 : I4 Counter
$$ Number of files/devices.....................[1]
 0
 1 / 14000
 geocoded output: 1 / 1600
 geocoded output: 101 / 1600
 1001 / 14000
 geocoded output: 201 / 1600
 2001 / 14000
 3001 / 14000
 geocoded output: 301 / 1600
 4001 / 14000
 geocoded output: 401 / 1600
 5001 / 14000
 geocoded output: 501 / 1600
 6001 / 14000
 geocoded output: 601 / 1600
 7001 / 14000
 8001 / 14000
 geocoded output: 701 / 1600
```

```
 9001 / 14000
 geocoded output: 801 / 1600
 10001 / 14000
 geocoded output: 901 / 1600
 11001 / 14000
 geocoded output: 1001 / 1600
 12001 / 14000
 geocoded output: 1101 / 1600
 13001 / 14000

 CLOSING image 1
 14000 accesses over ../11677/11677.ci2

 CLOSING image 2
 14000 accesses over ./geo_22408_11677.ci2
 geocoded output: 1201 / 1600
 geocoded output: 1301 / 1600
 geocoded output: 1401 / 1600
 geocoded output: 1501 / 1600

 CLOSING image 5
 1600 accesses over ./amp_11677_22408_ort.byt

 CLOSING image 6
 1600 accesses over ./pha_11677_22408_ort.byt

 CLOSING image 7
 1600 accesses over ./coh_11677_22408_ort.byt

 CLOSING image 8


 Messages in English



+-------------------------------------------------+
|    GRADIENT_FRANGES: Computation of the mean     |
|     phase gradients in range and azimuth        |
+-------------------------------------------------+


$Gradients descriptor file.....................[]
 ./gradient_mnt.dat
$Initial column interval.....................[10]
 10
$Initial line interval.......................[50]
 50

 (1) READING : ? lines, ? columns, type BYT : Interferogram
$$ File/device.........[None,NL=16,NC=16,type=byt]
 f=./pha_11677_22408_ort.byt, typ=pha, nl=NL_ORTHO_PHASE, nc=NC_ORTHO_PHASE
 1600 lines, 1900 columns, type pha ( 1900 bytes / line )
 on direct access file ./pha_11677_22408_ort.byt
$$ Transformation sequence..................[NONE]
 none
 Transformation number 1 :
 Conversion of pha into byt with a gain of 1.000000000000000

 CLOSING image 1
 1600 accesses over ./pha_11677_22408_ort.byt
 File read


+-------------------------------------------------+
|                  Results in range               |
+-------------------------------------------------+


 Impossible to find gradient direction
 Trial with a larger initial interval
 Too flat histogram. Gradient = 0.0
 Final gradient in range = 0.00000000E+00


+-------------------------------------------------+
|                  Results in azimuth             |
+-------------------------------------------------+


 POSITIVE GRADIENT
 -----------------
 Iteration: 1 azimut : 50 Gradient :  2.58 / 1000 points
 Iteration: 2 azimut : 70 Gradient :  3.40 / 1000 points
 Final gradient in azimuth = 3.40401777E-03
 ------------------------------


 Messages in English

+-------------------------------------------------+
|  PROPRE_LINEAIRE: Linear cleaning of fringes    |
+-------------------------------------------------+


$Gradient descriptor file.....................[]
 ./gradient_mnt.dat
 gradient in range = 0.00000000E+00
 gradient in azimuth = 3.40401777E-03

 (1) READING : ? lines, ? columns, type PHA : pha Original interferogram
$$ File/device.........[None,NL=16,NC=16,type=pha]
 f=./pha_11677_22408_ort.byt, typ=pha, nl=NL_ORTHO_PHASE, nc=NC_ORTHO_PHASE
 1600 lines, 1900 columns, type pha ( 1900 bytes / line )
 on direct access file ./pha_11677_22408_ort.byt
$$ Transformation sequence..................[NONE]
 none
```

```
 (2) WRITING : 1600 lines, 1900 columns, type PHA : pha Cleaned interferogram
$$ Number of files/devices.....................[1]
 1
$$ Transformation sequence..................[NONE]
 none
$$ File/device.....[None,NL=1600,NC=1900,type=pha]
 f=./cln_11677_22408_ort.byt
 1600 lines, 1900 columns, type pha ( 1900 bytes / line )
 on direct access file ./cln_11677_22408_ort.byt

 200 / 1600
 400 / 1600
 600 / 1600
 800 / 1600
 1000 / 1600
 1200 / 1600
 1400 / 1600
 1600 / 1600

 CLOSING image 1
 1600 accesses over ./pha_11677_22408_ort.byt

 CLOSING image 2
 1600 accesses over ./cln_11677_22408_ort.byt
```

D.4.4 Post-processing:

* *Correction of residual orbital fringes:* If the automatic correction fails it is necessary to estimate the average gradient by manually counting the residual fringes. DIAPASON can then be restarted from the CLEAN_DEM point so the manually estimated linear range-change gradient can be subtratced. Results following this method for orbital correction are good (see D - 7).

* *Filtering of interferogram:* A power spectrum smoothing algorithm is used to filter the interferograms (Zhong Lu, personal communication, 2003, D - 8).

* *Unwrapping of interferogram:* The deform toolbox developed for MATLAB (Gudmundsson et al., 2001) was used to unwrap (D - 9) and mask (D - 10) the interferogram.

* *Data size reduction*: The data size of each interferogram was reduced using a two-dimensional quad-tree partitioning algorithm (Jónsson et al., 2002; Welstead, 1999) developed for use in MATLAB (D - 11).

* *Data Modelling:* An inversion procedure using a simulated annealing algorithm followed by a derivative based method (Cervelli et al., 2001) was applied to model the data. Best results were found considering the three suggested deformation processes: two Mogi point sources and an opening

dislocation aligned along the rift axis (D - 12). The residual signal is less than 1 cm for all interferograms (D - 13).

D.5 Interferograms created for this study

In total 12 ESA, ESR images (track 9, frame 2277 covering the Krafla area) were used, to create 26 interferograms with a reasonable altitude of ambiguity (not <30 m) using the DIAPASON software (Table D-1) available at the Nordic Volcanological Institute (NVI) and the Open University. Two interferograms, marked with a * in table 1, were created previously at NVI, but were also analysed during this study. The altitude of ambiguity of those interferograms suitable for unwrapping varied from 115 to 374, the altitude of the unusable interferograms from 35 to 436. It follows that a high altitude of ambiguity is no guarantee for a usable interferogram although it is reasonable to expect better results when the altitude of ambiguity is higher. Some images do not combine well with any of the other images (e.g. 27919, 22909 and 17398); some always seem to suffer from orbital fringes and or atmospheric disturbances (e.g. 16897). Ordering the image which will produce a useful interferogram always partly depends on luck. But ordering those with high altitude of ambiguity (as one can check using the DESCW software: http://pooh.esrin.esa.it/descw/), taken during the same time of year (with no snow cover) might increase your chances of good results.

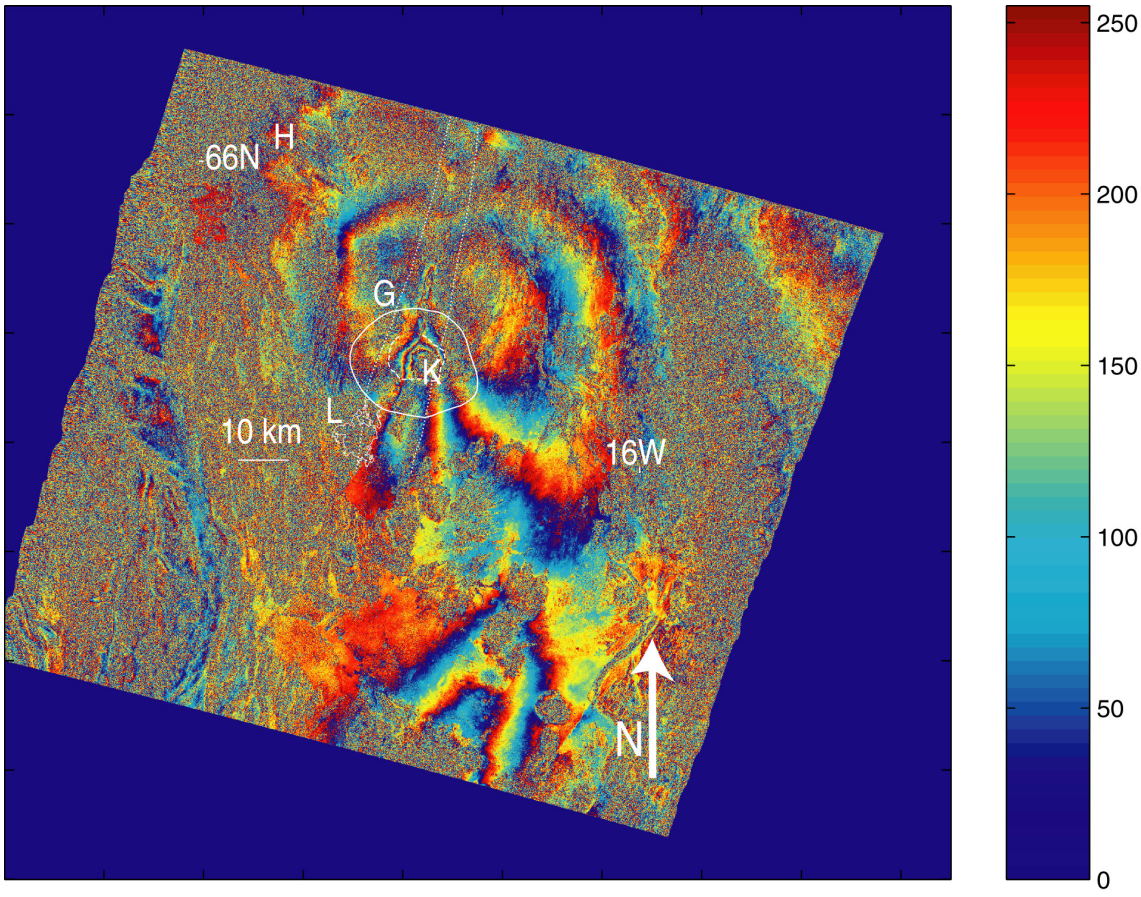

D - 7 The phase image of interferogram 11677_22408 corrected for orbital fringes. Changes are only small but in comparison to D - 4 the image does look more balanced.

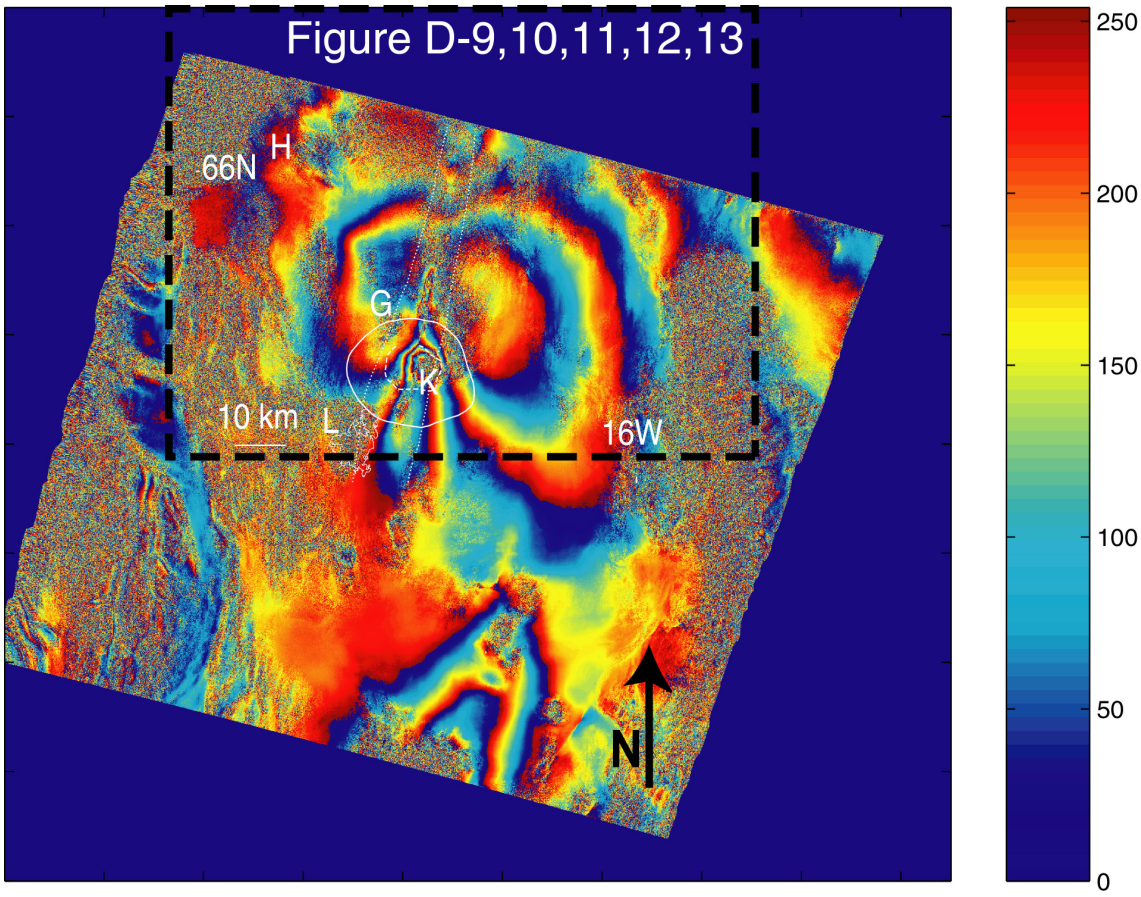

D - 8 Image D7 has been filtered using a power spectrum smoothing algorithm developed by Zhong Lu. The dashed black line shows the outline of D - 9, D - 10, D - 11,D - 12, D - 13.

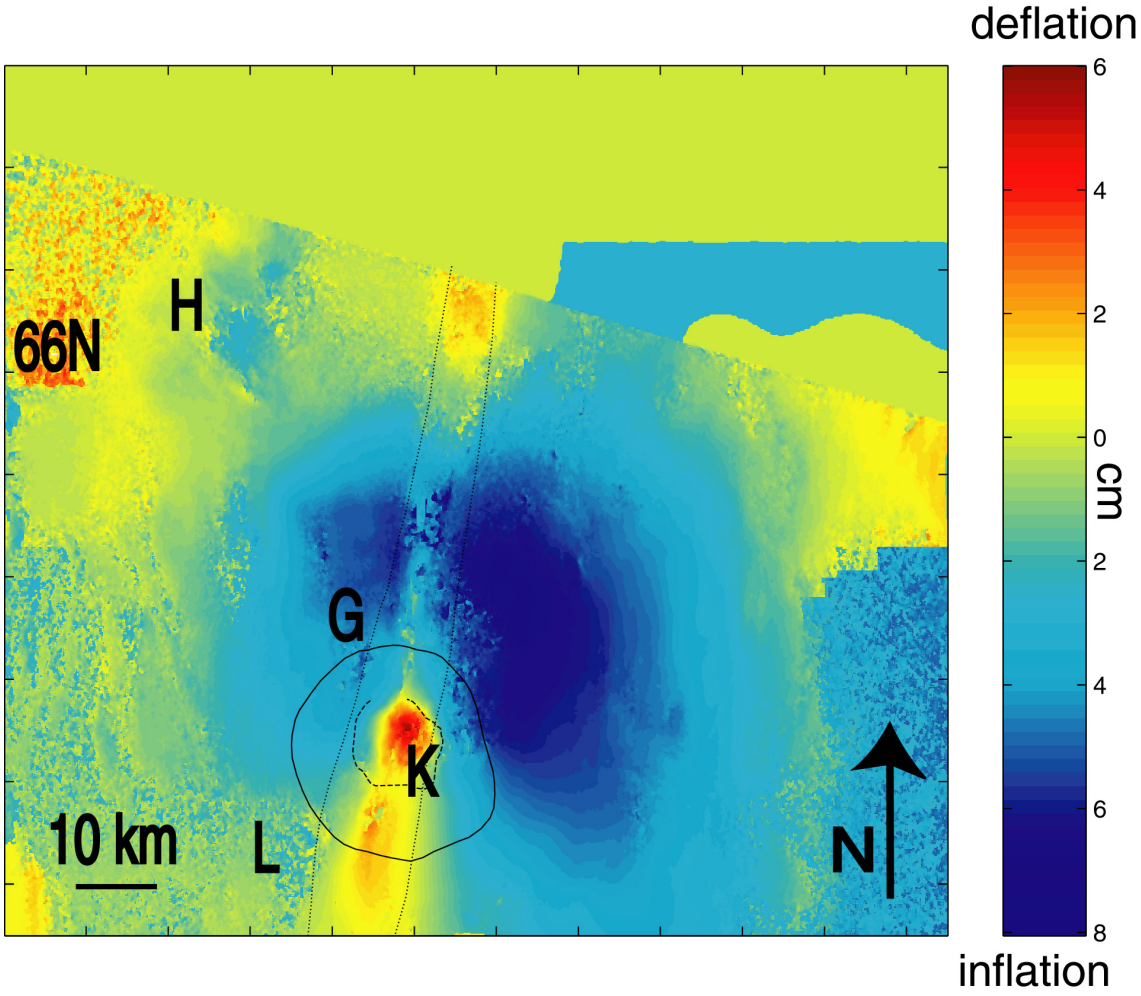

D - 9 Unwrapped interferogram 11677_22408. The unwrapping has been done with the use of a toolbox developed by S. Gudmundsson (2001) in MATLAB. Unwrapping is performed to convert the phase to elevation and involves adding or subtracting of multiples of 2π in the appropriate places. The bar on the right now displays deflation or inflation in cm. The images shows three deformation structures: a broad inflation just N of Krafla, a much smaller scale deflation more or less in the centre of the caldera and a deflating structure along the Krafla rift zone.

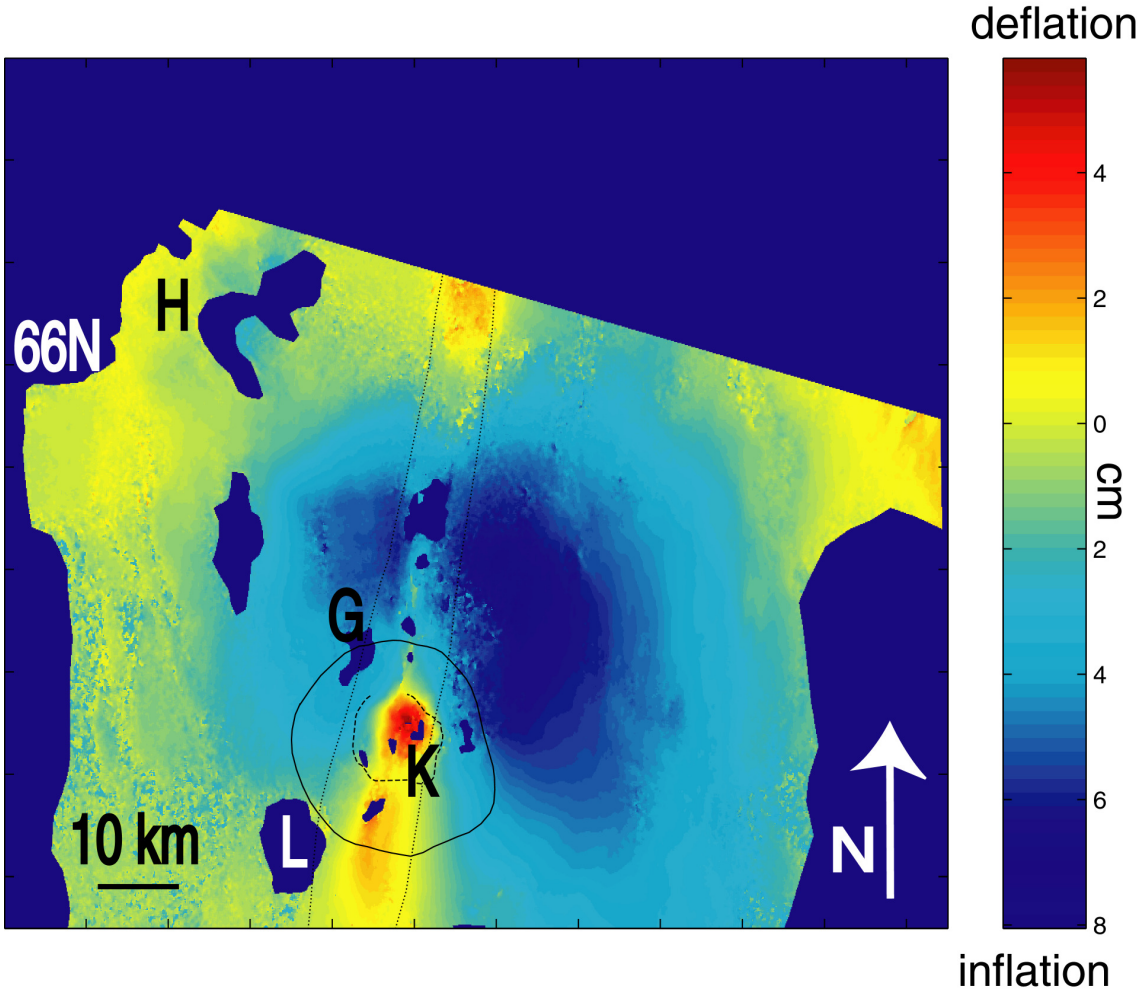

D - 10 Masked version of D - 9. The areas of poor coherence, such as Lake Mývatn, and areas were the phase unwrapping was inaccurate have been masked.

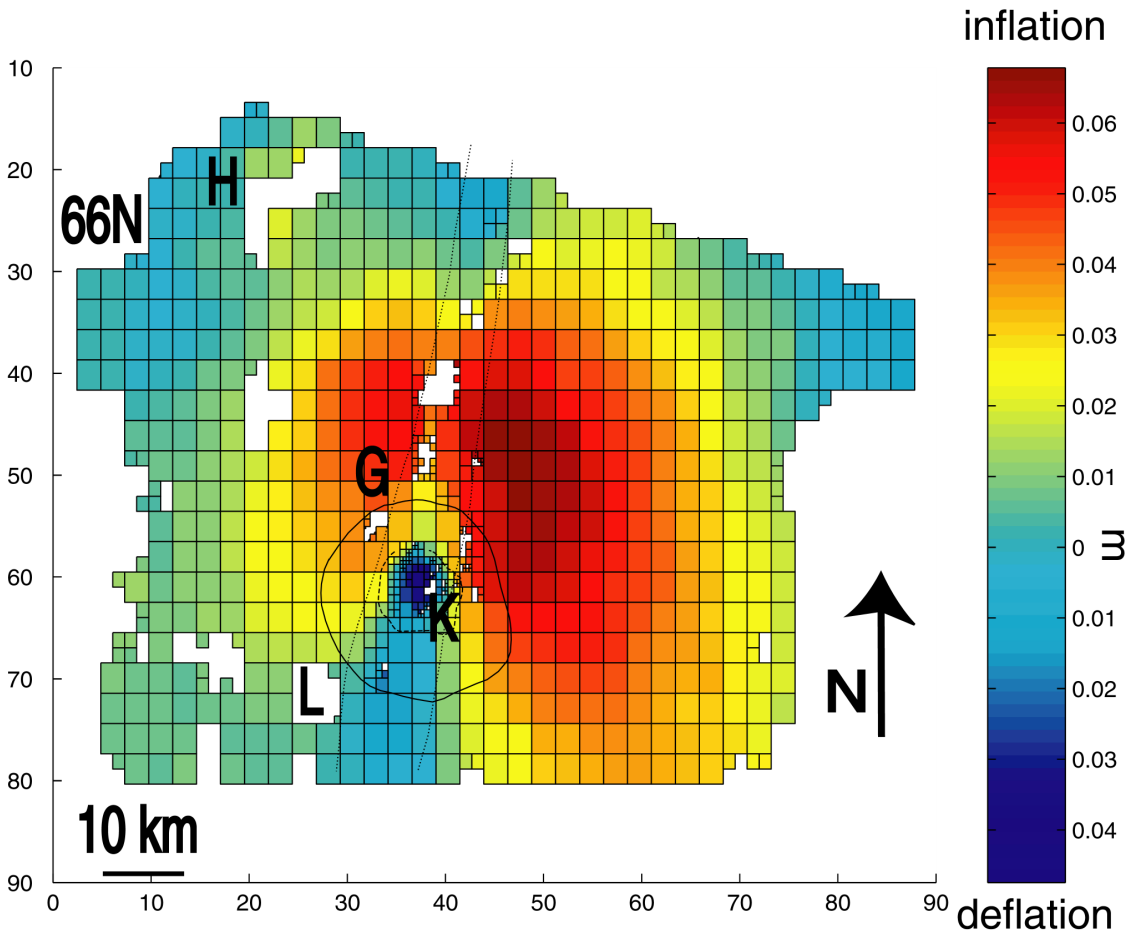

D - 11 Quadtreed image of interferogram 11677_22408. The data size of each interferogram was reduced using a two-dimensional quad-tree partitioning algorithm (Jónsson et al., 2002; Welstead, 1999) developed for use in MATLAB. Note the scale has been converted to m.

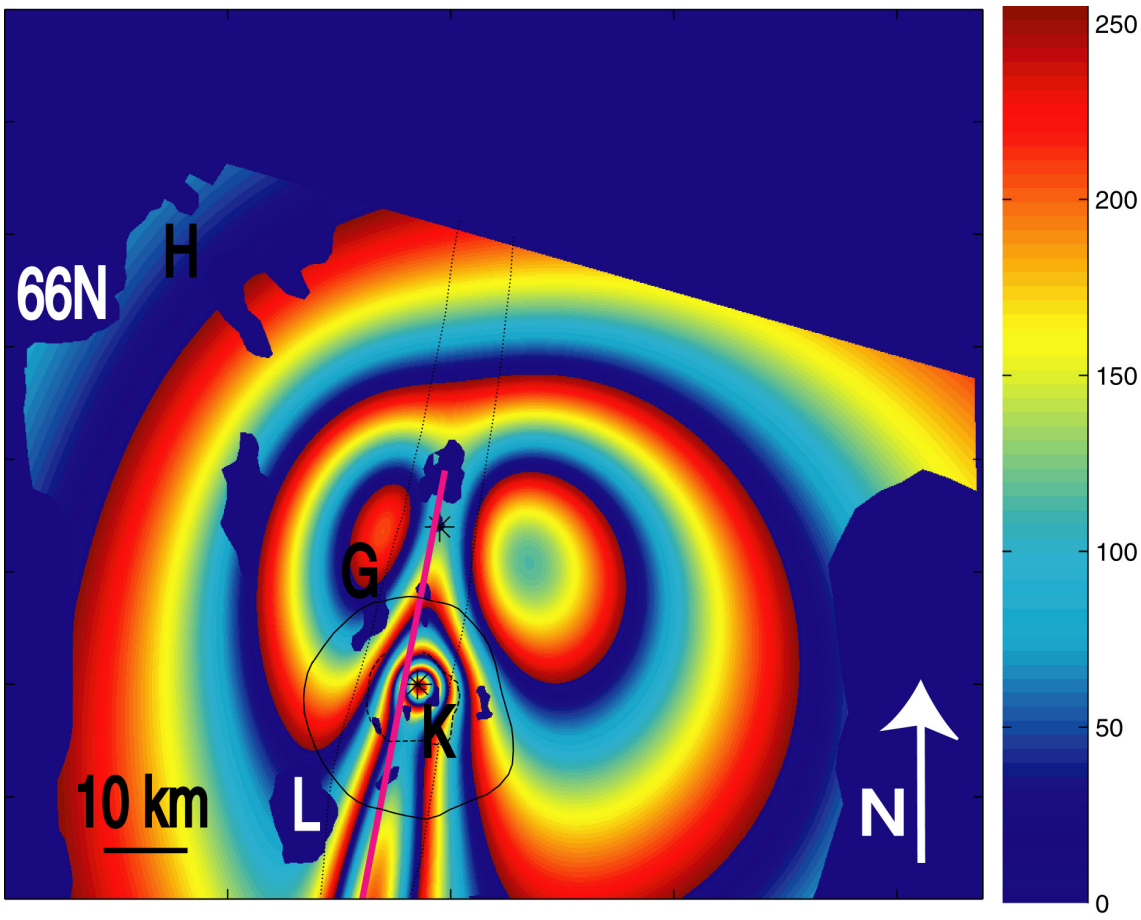

D - 12 Model for interferogram 11677_22408. A best fit model comprises an opening dike, representing plate spreading and post-rifting deformation, and two Mogi sources, one deflating and one inflating. We modelled this interferogram leaving all model bounds loose. Resulting model parameters are well constrained and the model reduces the RMS of the data from 2.97 cm for a null-model to 0.63 cm. The parameters found for the deflating Mogi source agree with those found by previous studies (Henriot et al., 2001; Sigmundsson et al., 1997). The opening dislocation is a simplified model reproducing the effects of plate spreading and superimposed post-rifting deformation.

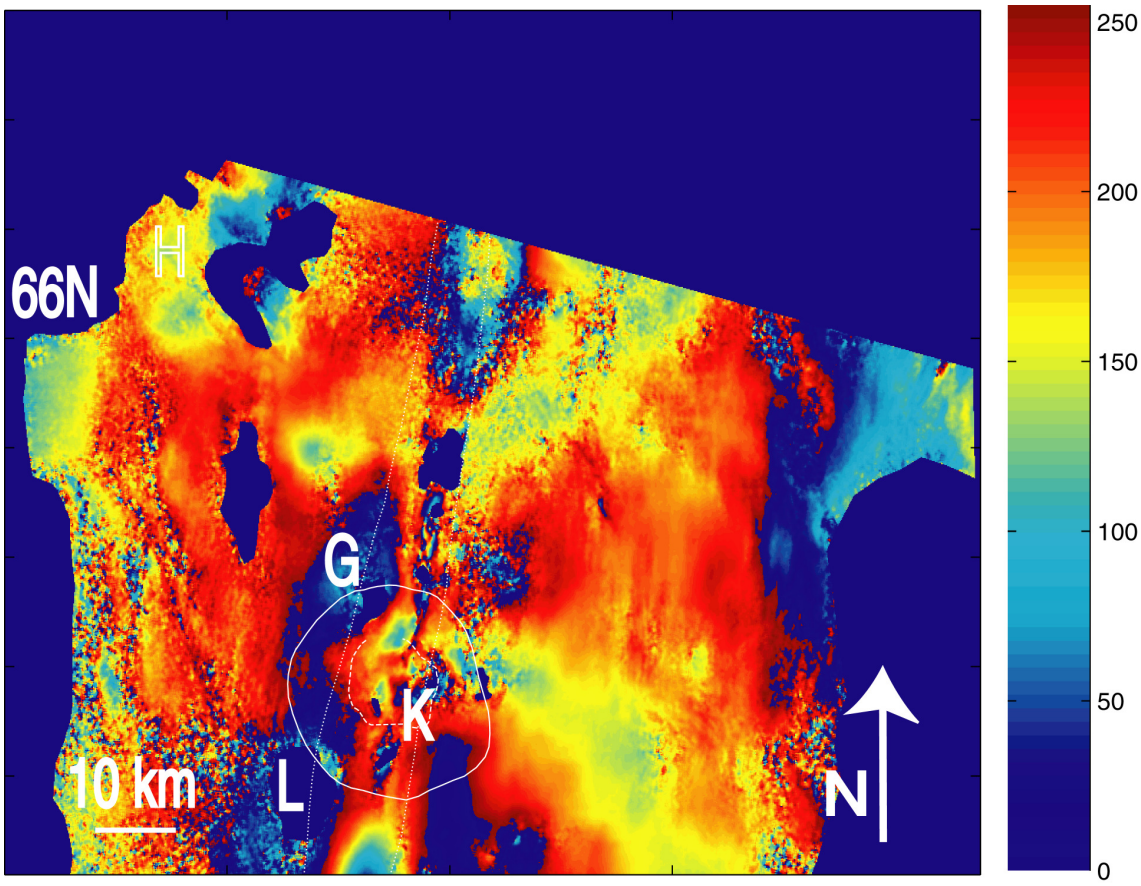

D - 13 Residual after the model has been subtracted from the phase image. The residual is less than 1 cm.

TABLE D - 1 Interferograms analysed for this study.

Image	Dates	Altitude of amb. [m]	Description
In6376_6877	09/07/96-13/08/96	57	No def. visible, time span too short.
In6376_22408	09/07/96-03/08/99	374	All three def. structures visible, unwrapped.
In6376_17899	09/07/96-22/09/98	38	Not good, alt. of amb. too low, no coherence.
In6376_11887	09/07/96-29/07/97	35	Not good, alt. of amb. too low, no coherence.
In6877_11887	13/08/96-29/07/97	93	Usable, rift structure visible, atmospheric disturbance.
In6877_17899	13/08/96-22/09/98	115	All three def. structures visible, unwrapped.
In6877_22408	13/08/96-03/08/99	-68	Usable, rift & deflation visible, broad inflation less clear, atmospheric disturbance.
In6877_27919	13/08/96-22/08/00	77	Not good, no correlation.
In11887_17899	29/07/97-22/09/98	-498	Not good, atmospheric noise.
In11887_27919	29/07/97-22/08/00	436	Not good, no correlation.
In11887_22408	29/07/97-03/08/99	-39	Not good, alt. of amb. too low, no coherence.
In16897_17398	14/07/98-18/08/99	-57	Not good, too many orbital fringes.
In16897_22909	14/07/98-07/09/99	97	Not good, too many orbital fringes.
In17899_22408	22/09/98-03/08/99	-42	Not good, alt. of amb. too low, no coherence.
In17899_27919	22/09/98-22/08/00	233	Not good, no correlation.
In22909_27418	07/09/99-18/07/00	327	Not good, atmospheric noise.
In01867_17899	29/08/95-22/09/98	289	All three def. structures visible, unwrapped.
In01867_27919	29/08/95-22/08/00	128	Not good, no correlation.
In01867_11887	29/08/95-29/07/97	183	Broad inflation & rift clear, deflation less visible, unwrapped.
In01867_6877	29/08/95-13/08/96	-191	Broad inflation & rift clear, deflation less visible, unwrapped.
In11677_01867	09/10/93-29/08/95	58	All thee structures marginally visible, altitude of amb. low.
In11677_22408	09/10/93-03/08/99	-369	All three def. structures visible, unwrapped.
In11677_6376	09/10/93-09/07/96	-186	Not good, poor coherence.
In11677_6877	09/10/93-13/08/96	84	Not good, poor coherence.
In11677_11887	09/10/93-29/07/97	44	Not good, alt. of amb. too low, no coherence.
In11677_27919	09/10/93-22/08/00	40	Not good, no correlation.
In6166_6376*	19/09/92-09/07/96	-317	Usable, deflation & rift visible, broad inflation not clear.
In6166_6877*	19/09/92-13/08/96	70	Usable, deflation & rift visible, broad inflation not clear.

D.6 Use of interfergrams

The initial idea was to use the created interferograms for elevation control of the gravity data. Micro-gravity data can not be interpreted unless corrections are made for elevation changes. The problem is that conventional geodetic data are often made at slightly different sites, and geodetic surveys often use a base station which differs from that used by the micro-gravity network. InSAR data could potentially overcome both these problems. The difficulty using InSAR to get the vertical displacement is that the depicted deformation is a combination of vertical and horizontal displacement and it is impossible to distinguish between the two. Another potential problem is the fact that the

time-span of an interferogram often covers more than a year. To get results for yearly deformation, the assumption would have to be made that deformation was constant over the time-span.

A comparison between levelling and InSAR data for the 1995 to 2000 period shows that for most stations the total difference between the ttwo methods is less than 4 mm. Bigger differences can result from horizontal movement likely caused by rifting (E-W extension) or by contraction towards a deflating mogi source e.g. shallow magma chamber (E-W compression). An increase in range change can be caused by displacement to the west (rifting) or subsidence while a decrease in range change can be caused by displacement to the east (compression towards magma chamber) or inflation. Stations with a bigger positive difference (e.g. InSAR value>levelling value) plot towards the east while those with a bigger negative difference (e.g. InSAR value<levelling value) plot towards the west. From this we conclude that InSAR data were influenced by compression towards the deflating magma chamber.

A comparison between GPS and InSAR for the 1993-2002 period, gives the same result. In summary, almost all stations show less than 4 mm total difference between vertical deformation calculated from InSAR and that calculated using other geodetic methods. However, it is complicated to use InSAR as a source for vertical deformation because some stations do show big differences. In the cases we looked at here, the bigger difference was probably caused by contraction towards the shallow magma chamber. An additional source of horizontal deformation could be extension along the rift zone. For this study we therefore decided to use available levelling data (see APPENDIX C) which have sufficient precision. InSAR data were still used to establish the equation of the decay of deformation at Krafla. InSAR data can be adequate for use with micro-gravity data if ample modelling is done to separate horizontal and vertical deformation.